CALIBRATION AND VERIFICATION OF THE COOLING LAKE MODEL FOR NORTH ANNA POWER STATION

During the Period July 1978 - September 1981

by

Scott A. Wells
E. Eric Adams
Donald R.F. Harleman

RALPH M. PARSONS LABORATORY
AQUATIC SCIENCES AND ENVIRONMENTAL ENGINEERING

Report No. 272

Prepared under the support of
Virginia Electric and Power Company
Richmond, Virginia

March 1982

MIT

DEPARTMENT
OF
CIVIL
ENGINEERING

SCHOOL OF ENGINEERING
MASSACHUSETTS INSTITUTE OF TECHNOLOGY
Cambridge, Massachusetts 02139

R 82-22

CALIBRATION AND VERIFICATION OF THE COOLING LAKE MODEL FOR NORTH ANNA POWER STATION

During the Period July 1978 - September 1981

by

Scott A. Wells

E. Eric Adams

Donald R.F. Harleman

RALPH M. PARSONS LABORATORY

AQUATIC SCIENCES AND ENVIRONMENTAL ENGINEERING

DEPARTMENT OF CIVIL ENGINEERING

MASSACHUSETTS INSTITUTE OF TECHNOLOGY

Report No. 272

Prepared under the support of

Virginia Electric and Power Company
Richmond, Virginia

MARCH 1982

ABSTRACT

The North Anna Power Station (3 proposed nuclear units with a total capacity of 2820MWe) is located in the State of Virginia about 41 miles northwest of Richmond. The plant condenser heat dissipation system consists of a complex geometric arrangement including a Waste Heat Treatment Facility (WHTF), consisting of a series of separate ponds with attached dead-end side arms, and Lake Anna which is a deep reservoir created by impounding the North Anna River.

A segmented mathematical model was used to simulate thermal structure within the Lake Anna system. Initial model development, calibration based on pre-operational data (1977-1976), and predictions under station operation for the historical period 1957-1966 are documented in Jirka et al (1977). Since Unit 1 came on line in the Summer of 1978 and Unit 2 in Fall of 1980, an extensive data collection effort was undertaken to calibrate the model to operational data. Continuous measurements were made of meteorological variables, plant load, water temperature at various points in the system and current speeds in one of the WHTF side-arms. Supplemental data, with greater spatial resolution, were collected at weekly or monthly intervals.

Calibration of the model included examination of assumptions inherent in the model development and refinement of model coefficients. Major areas of investigation included surface heat transfer processes (short wave solar radiation, long-wave atmospheric radiation and evaporation), dilution and entrance mixing, dead end side arm flow dynamics, vertical diffusion of heat below the well-mixed upper layer in the main lake, and linkage of the WHTF calculations with those of the main lake.

Comparison against a three year period of operational data (1978-1981) showed that the model predictions were very accurate. An error analysis detailed explicity the model's strengths and weaknesses, with mean surface errors (prediction-data) ranging from + 0.9^{o}F to - 0.4^{o}F at four diagnostic control points and standard error ranging from 2.8^{o}F to 1.8^{o}F. Excellent agreement was also found in the vertical temperature profiles in the main lake.

After verification, the model was used in a predictive mode to simulate temperatures for 1, 2 and 3 nuclear units under a range of meteorological conditions. Synthetic meteorological data had previously been prepared for the ten year period, 1957-1966, by means of a regionalization procedure. Temperature predictions for this ten year period could then be used to characterize both average and extreme conditions.

During extremely warm periods (e.g., the Summer of 1959), the temperature of water released from Lake Anna to the N. Anna River

downstream would have exceeded the present temperature standard of 89.6°F (32°C). A one-dimensional river temperature model was developed to predict downstream temperatures. Furthermore, several possibilities for reducing downstream temperatures were examined including: (i) dilution reduction in the WHTF, (ii) rerouting of the flow through the WHTF side-arms, (iii) reduction in condenser flow rate, (iv) bubble aerators in the main lake, and (v) a siphon to mix hypolimnetic cool water with warm surface water for discharge into the N. Anna River. For the siphon, which appears to be the most efficient option, simulations were performed to identify the maximum flow rate and the total volume of hypolimnetic water withdrawn, in order to comply with downstream temperature standards in each of the ten years simulated.

ACKNOWLEDGEMENTS

This research on model verification was supported by Virginia Electric and Power Company, Richmond, Virginia under MIT OSP No's 86944, 88328, 89883 and 91560. Previous research on model development was supported by VEPCO through contract with Stone and Webster Engineering Corporation of Boston, Massachusetts. Technical reports which resulted from the earlier development stage, and upon which the present analysis is based, include

Watanable, M., Harleman, D., and Connor, J., "Finite Element Model for Transient Two-Layer Cooling Pond Behavior," Technical Report No. 202, R.M. Parsons Laboratory, Department of Civil Engineering, MIT, 1975.

Brocard, D., Jirka, G., and Harleman, D., "A Model for the Convective Circulation in Side Arms of Cooling Lakes," Technical Report No. 223, R.M. Parsons Laboratory, Department of Civil Engineering, MIT, 1977.

Octavio, K., Jirka, G., and Harleman, D., "Vertical Heat Transport Mechanisms in Lakes and Reservoirs," Technical Report No. 227, R.M. Parsons Laboratory, Department of Civil Engineering, MIT, 1977.

Jirka, G., Brocard, D., Octavio, K., Watanabe, M., and Harleman, D., "Analysis of Cooling Effectiveness and Transient Long-Term Simulations of a Cooling Lake with application to the North Anna Power Station, Technical Report No. 232, R.M. Parsons Laboratory, Department of Civil Engineering, M.I.T., 1977.

We wish to express our profound gratitude to VEPCO for their past and present support and to Dr. Morris Brehmer, Mr. Wally Hadder, Mr. John White and Mr. Robert Rasnic at VEPCO for their personal cooperation with our studies.

This report represents the Masters thesis of Mr. Scott Wells submitted to the MIT Department of Civil Engineering. Thesis supervision was provided by Dr. Eric Adams, Principal Research Engineer in the MIT Energy Laboratory and Lecturer in the Department of Civil Engineering. Overall project guidance was provided by Dr. Donald R.F. Harleman, Ford Professor of Engineering and Director of the Ralph M. Parsons Laboratory.

Appreciation is expressed to past and present students Dr. Peter Shanahan, Mr. Scott Kukshtel and Mr. Kevin Farley who participated in the initial phases of model verification, to Mr. Paul Singarella who drafted many of the figures and to Mrs. Stephanie George who typed the manuscript.

TABLE OF CONTENTS

1. INTRODUCTION

Predictive mathematical models are important for assessing the environmental impact of waste discharges. In dealing with complex predictive "tools", calibration and verification of the model can only be obtained after taking detailed data, undergoing laboratory experiments, and/or making observations of the system or similar systems. At that point, the models' "faithfulness" can be established, and its predictive nature can then be validated.

One such approach was undertaken at North Anna Power Station, operated by Virginia Electric and Power Company, where a cooling lake was designed for the condenser water supply and heat dissipation system. The ability to predict the effect of the heat rejected by the plant on the thermal structure of the resulting reservoir and downstream effects in the river were considered imperative in determining cooling effectiveness, the need for alternative thermal dissipation strategies, and the proper management of the waste heat for minimizing the environmental impact.

1.1 North Anna Power Station Characteristics

The North Anna Power Station is located in Louisa County in central Virginia, 41 miles northwest of Richmond and 40 miles east of Charlottsville (Figure 1.1). The station is situated on the south bank of a lake formed by a dam on the North Anna River (Figure 1.2) which was closed in January of 1972.

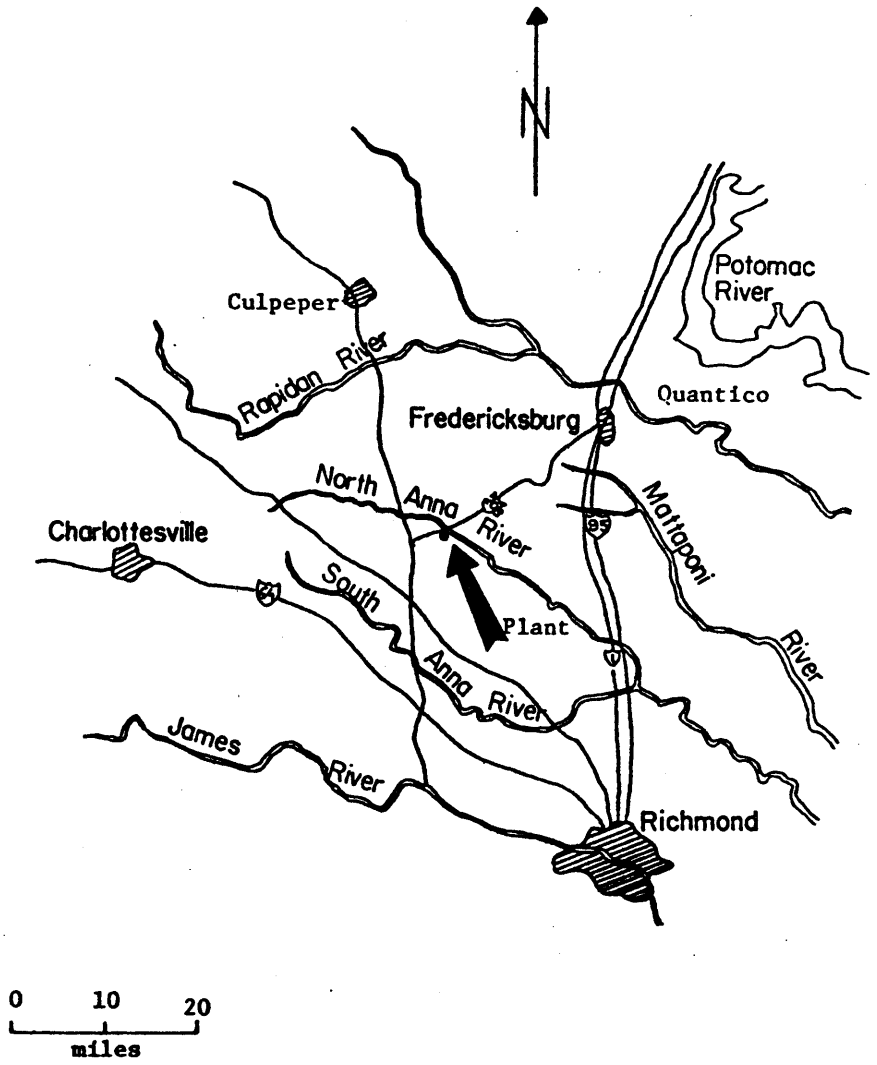

Figure 1.1: Map showing relative location of North Anna Power Station with Respect to Richmond and Charlottesville.

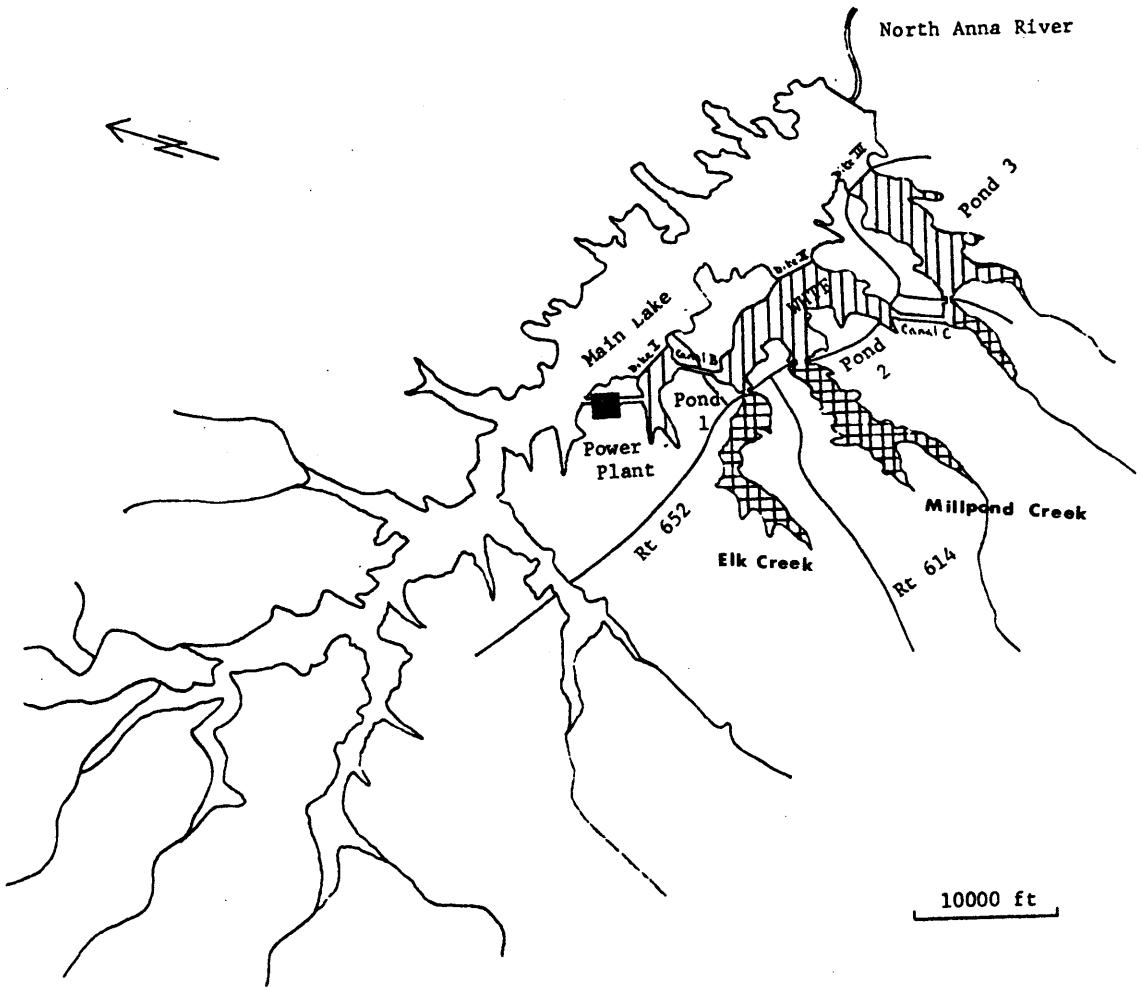

Figure 1.2 Map of the N. Anna Cooling System

The power station consists of two nuclear units, and plans call for a third unit as well. The nuclear units generate about 940 MWe per unit with an average efficiency of 32.7% and reject about 6.5×10^9 BTU/hr per unit of waste heat into the cooling system.

The condenser cooling water flow rate is about 2120 cfs per unit (4 pumps per unit at 530 cfs per pump), and the attendant temperature rise while passing through the condensers is about 14°F. Details of the cooling water flow system are shown in Figure 1.3.

1.2 North Anna Reservoir System for Waste Heat Dissipation

The North Anna Lake has been formed by impounding the North Anna River by construction of a dam (see Figure 1.2). Additional construction of dikes and dredging of channels formed a separate series of ponds, called the Waste Heat Treatment Facility (WHTF). Both the WHTF and the main lake participate in the dissipation to the atmosphere of the waste heat loading, but the WHTF dissipates the major portion.

At a design elevation of 250 ft. above mean sea level (MSL), the North Anna Lake has a surface area of 9600 acres, a volume of 10.6×10^9 ft^3, and an average depth of 25 ft. The maximum depth at the dam is 70 ft. The lake receives an average annual inflow of about 270 cfs. The lake elevation is maintained by three radial gates at the dam (the bottom of the gates is at an elevation of 219 ft. MSL) and by two near-surface skimmers. The outflow rate equals the inflow minus the rate of evaporation from the lake surface (annual rate of about 60 cfs for natural conditions).

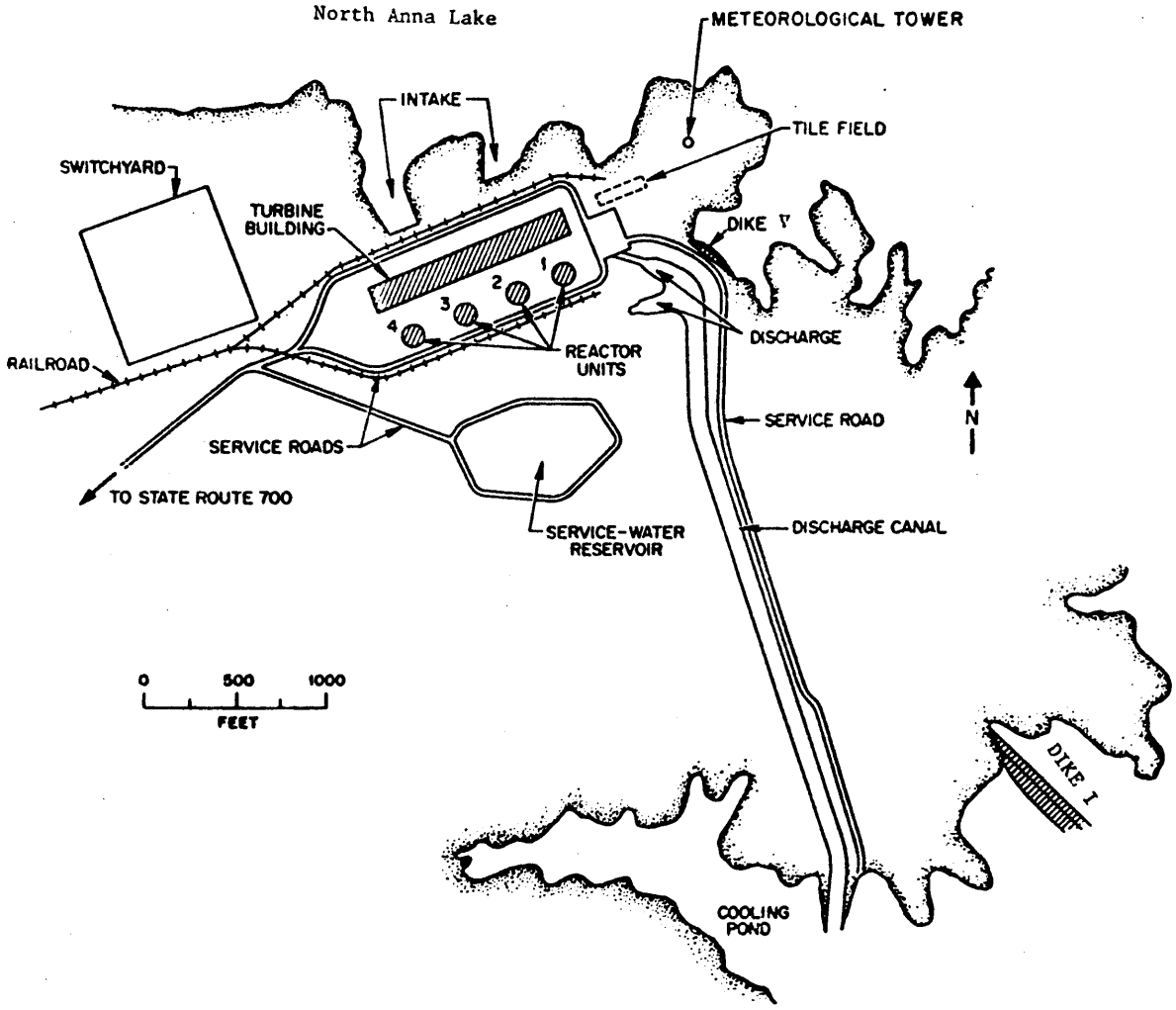

Figure 1-3: Plan View of the Cooling Water Flow System

The WHTF has a surface area of 3400 acres, a volume of 2.66×10^9 ft^3, and an average depth of 18 ft. The maximum depth is 50 ft. in the vicinity of the dikes. Referring to Figure 1.2, three dikes have been built to separate the WHTF from the main lake. Dike 1 forms Pond 1 of the WHTF. Pond 1 receives the cooling water via the discharge canal from the power plant. Connecting channels have been dredged between Pond 2 and Pond 3 (formed by Dike 3). These channels have a constant trapezoidal cross-section of 25 ft. depth and 160 ft. average width. After passing through Ponds 2 and 3, the cooling water is discharged into the main lake through a submerged discharge structure at Dike 3. After residence in the main lake, cooling water is withdrawn through near-surface intakes (the intake structure is over approximately the top 30 ft., from 250 ft. MSL to 221 ft. MSL) in the vicinity of the station.

In essence, a closed-cycle cooling system is formed, consisting of a series of ponds, which form the WHTF, and of the North Anna Lake. A major characteristic of the system is the existence of the long narrow side arms in the WHTF. These sidearms comprise about 1530 acres or 45% of the area of the WHTF.

1.3 Analysis Philosophy

Numerous steps were taken to develop a mathematical model to predict performance of the North Anna waste heat dissipation system. These steps included:

(i) development of a mathematical model incorporating the surface

heat transfer and fluid mechanics associated with the complex geometry of the system (This effect included basic research into general cooling pond behavior, the cooling effectiveness of dead-end side arms, and the specific formulation of mathematical models to represent the physics of the closed-loop system.);

(ii) an extensive data collection effort made throughout the Lake Anna system, including the acquisition of water temperatures, water current velocities and directions, and atmospheric meteorological variables over a period from 1974 to the present (pre- and post-operational data);

(iii) calibration of the model under existing conditions by means of the collected data;

(iv) verification of the performance of the cooling pond and lake model; and

(iv) the use of the mathematical model as a management tool with regard to compliance with thermal standards and evaluation of thermal mitigation strategies.

2. MODELING APPROACH

A description of the modeling approach can be found in Jirka et al (1977), but a summary of the basic structure, as originally developed, is included here. Subsequent modifications are described in Chapter 4. Other technical reports which have dealt with the basic research into sidearm circulation, general cooling pond behavior, and vertical heat transport mechanisms with reference to the N. Anna site are found in Watanabe et al (1975), Brocard et al (1977) and Octavio et al (1977).

2.1 Structure of the Mathematical Model

Because of the complex geometry of the heat dissipation system, a combination of several different mathematical approaches was used in the analysis. A schematization of the geometry utilized in the modeling approach is illustrated in Figure 2.1. Three distinct features are significant:

(i) the three cooling ponds of the WHTF,

(ii) the dead-end side arms of WHTF and main lake, and

(iii) the deeper main lake.

Different models were applied to the various sections.

2.1.1 Waste Heat Treatment System

Based on the typical dimensions of the WHTF reaches and the interconnecting channels (as presented in Chapter 1), two different vertical thermal structures were postulated for each segment based on that segment's densimetric Froude Number:

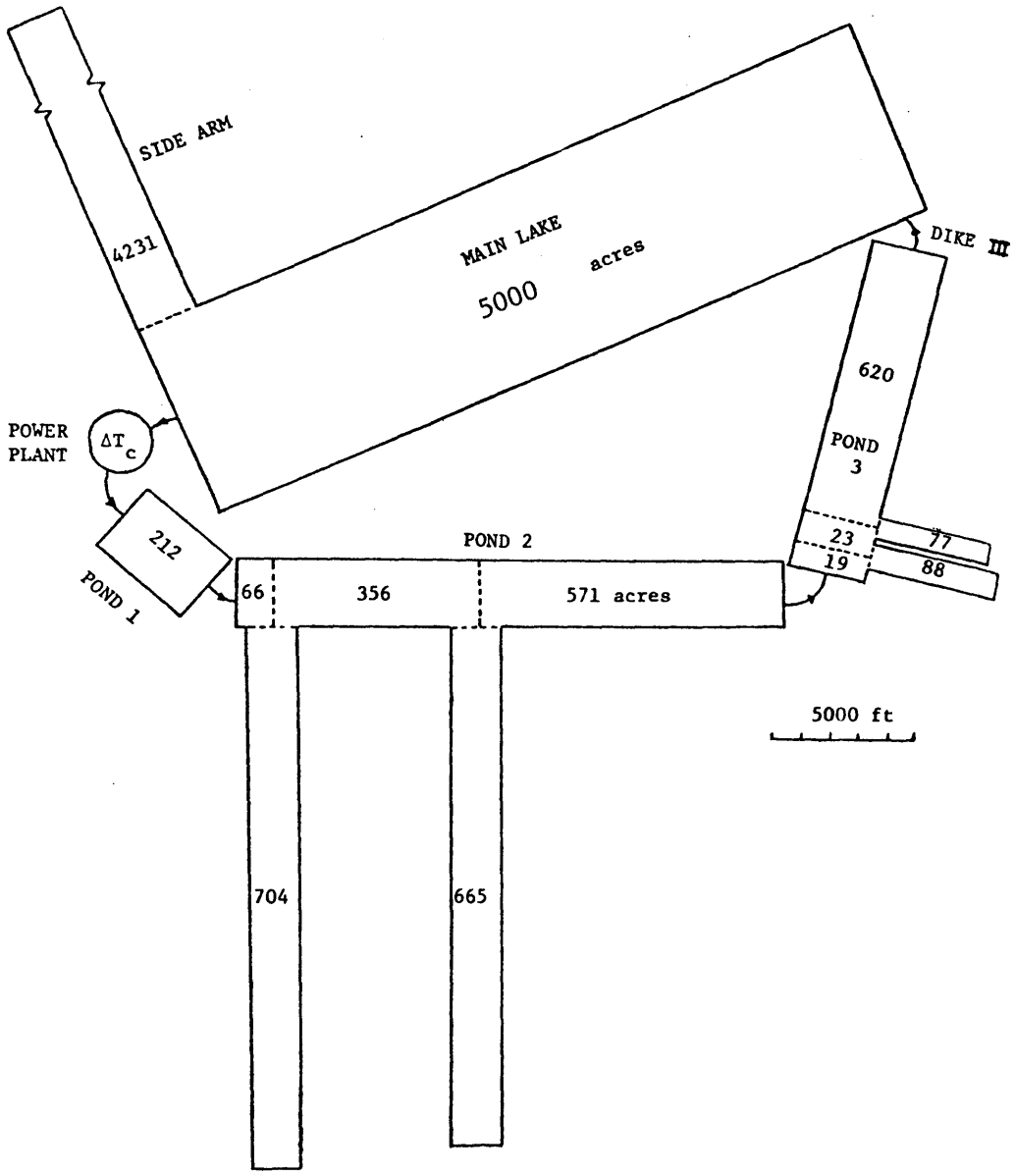

Figure 2.1: Schematization of the North Anna Cooling system used in the Segmented Model.

$$F = \frac{u_o}{\sqrt{\frac{\Delta\rho_o}{\rho} g h_o}} \qquad (2.1)$$

where u_o = characteristic velocity

g = acceleration due to gravity

h_o = characteristic water depth

$\Delta\rho_o$ = characteristic density difference between upper and lower layers

ρ = reference water density

Because of the relatively large dimensions of the three WHTF reaches, the average velocity was low, and thus $F << 1$. The WHTF reaches were then expected to stratify; a two-layer model, in which each layer was assumed to be vertically homogeneous, was utilized, with no heat or mass flux allowed through the interface between the layers, except at the ends.

Conversely, because of the small dimensions of the interconnecting channels, $F > 1$, and thus the channels were modeled as a fully mixed system.

A critical parameter in modeling the WHTF system is the quantity of mixing between an interconnecting channel and the downstream reach. Ideally, to promote maximum heat transfer, mixing should be minimized. The following empirical formula was utilized to calculate the dilution, D_s,

$$D_s = 1.4 \sqrt{1 + F^2 \left(\frac{h_o}{b_o}\right)^{1/2}} \left[\frac{0.75}{\left(\frac{h_{max}}{H}\right)}\right]^{0.75} \qquad (2.2)$$

where D_s = dilution ratio, $\frac{Q_o+Q_e}{Q_o}$

Q_o = discharge flow rate

Q_e = entrained flow rate

h_o = depth of discharge canal

b_o = half-width of discharge canal

h_{max} = maximum jet penetration of deep-water jet

H = water depth

F = densimetric Froude number within interconnecting channel

In order to obtain the dilution above, h_{max} was calculated from the buoyant surface jet model of Stolzenbach and Harleman (1971) as

$$\frac{h_{max}}{H} = 0.42 F \left(\frac{h_o}{b_o}\right)^{1/4} \sqrt{h_o b_o} \qquad (2.3)$$

(Data supporting Eqs. 2.2 and 2.3 can be found in Jirka et al (1981).)

2.1.1.1 Side Arm Dynamics

The convective circulation in a dead-end side arm (illustrated in Figure 2.2) is a phenomenon whereby warm surface water from the main pond or lake spreads into the side arm gradually losing its heat to the atmosphere. The gradual decrease in density difference causes the inflowing water to sink and to be replaced by new warm water. In the context of the N. Anna Model, the entrance temperature distribution and the surface heat flux were the independent variables,

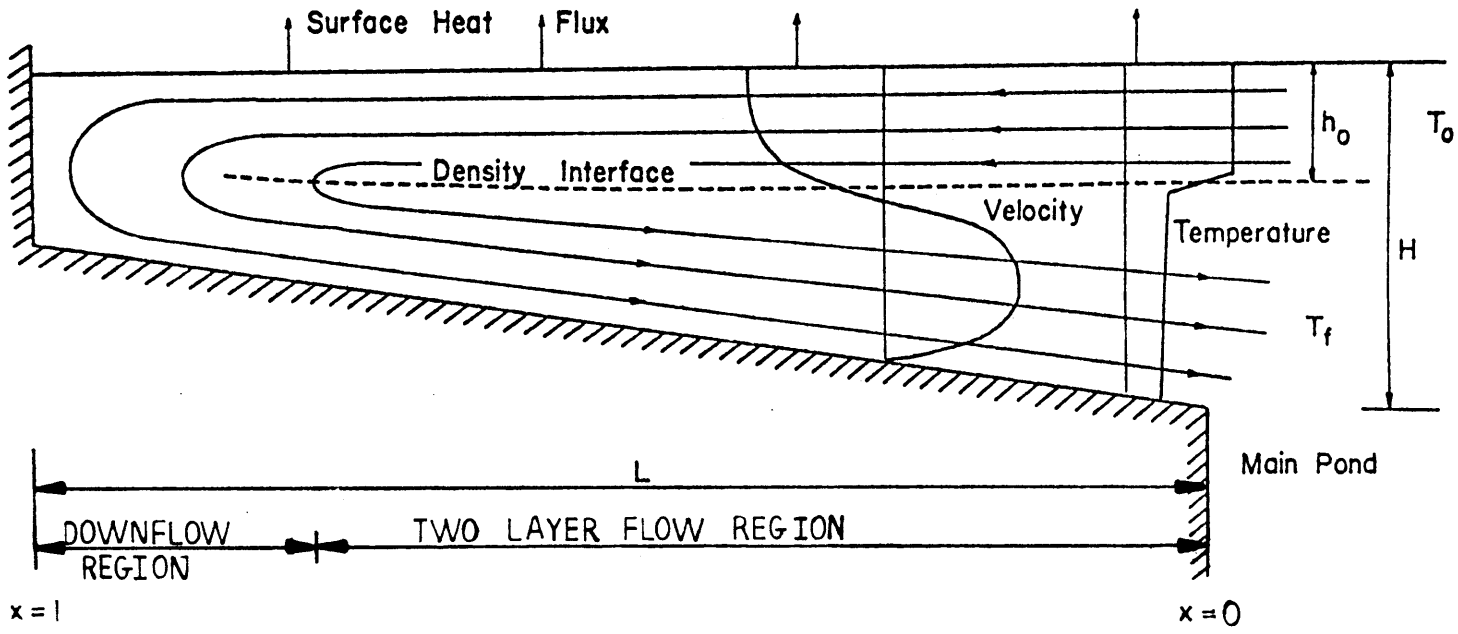

Figure 2.2: Schematic Drawing of the Side Arm Convective Circulation

while the flow rate and the temperature of the return flow were to be determined.

Brocard et al (1977) studied this phenomenon and presented a general framework for approaching and solving the problem. Several assumptions were made to simplify the analysis:

(i) horizontal bottom, i.e., $\frac{dH}{dx} = 0$

where H = depth of the side arm

x = longitudinal distance up the side arm;

(ii) downwelling occurs only at the end of the side arm;

(iii) small values of $\frac{KL}{\rho C_p q_o}$,

where L = length of side arm

q_o = side arm flow per unit width

ρ = density of water

C_p = specific heat of water

K = surface heat exchange coefficient (see Appendix A);

and (iv) negligible effect of the lateral bridge constriction on the side arm flow (see Figure 3.4).

The governing equation for determining side arm flow was

$$\frac{q_o}{kL} = \{B \frac{f_o L}{H} \frac{1}{4h_o}[\alpha(\frac{1}{h_o} - \frac{\Delta q-1}{1-h_o})^2(\frac{1}{h_o} + \frac{1}{1-h_o}) + \frac{(\Delta q-1)^2}{(1-h_o)^3}] \}^{-1/3} \quad (2.4)$$

where B = buoyancy term = $\frac{k^2 L^2}{\beta(T_o - T_E) g H^3}$

h_o = initial upper layer depth

β = coefficient of thermal expansion of water = $-\frac{1}{\rho}\frac{\partial \rho}{\partial T}$

$\Delta_q = q_1 - q_2 / q_o \simeq 0$

$\alpha = f_i / f_o \simeq 0.5$

T_o = initial temperature at side arm entrance

T_E = equilibrium temperature (see Appendix A)

f_o = friction factor

f_i = interfacial friction factor

q_1 = upper layer flow

q_2 = lower layer flow

k = kinematic surface heat exchange coefficient = $\frac{K}{\rho C_p}$

Equation 2.4 was tested against both laboratory and field data.

The temperature distribution along the side arm is determined once q_o is known. Neglecting flow across the interface, but considering longitudinal dispersion, the integrated conservation of thermal energy for upper and lower layers becomes:

$$\frac{dr_1}{d\bar{X}} = \frac{-kL}{q_o} r_1 + E_L^* \frac{d^2 r_1}{dX^2}$$

$$\frac{dr_2}{d\bar{X}} = 0 \qquad (2.5)$$

where r_1 = dimensionless temperature of the upper layer = $\frac{T_1-T_E}{T_o-T_E}$

r_2 = dimensionless temperature of the lower layer = $\frac{T_2-T_E}{T_o-T_E}$

T_o = initial temperature at the entrance to the side arm

$E_L^* = E_L \frac{H}{q_o L}$ = dimensionless dispersion parameter

($\sim$ 0.1 for WHTF side arm and $\sim$ 0.03 for main lake side arm)

E_L = dispersion coefficient

X = dimensionless distance up the side arm (see Figure 2.2)

The solution to Equation 2.5 with the appropriate boundary condition is

$$r_2 = r_1(X=1) = \frac{4a \exp(\frac{1}{2E_L^*})}{(1+a)^2 \exp(\frac{a}{2E_L^*}) - (1-a)^2 \exp(-\frac{a}{2E_L^*})} \qquad (2.6)$$

where $a = \sqrt{1 + 4 \frac{kL}{q_o} E_L^*}$

Alternatively, if one neglects longitudinal dispersion, the temperature distribution in the side arm as a function of X is

$$r_1(X) = \exp(-\frac{kL}{q_o} X). \qquad (2.7)$$

Equation 2.6 was found to be relatively insensitive to the choice of E_L^* (between 0 and 1). Furthermore, Equation 2.7 was found to be almost identical to Equation 2.6 in this range of E_L^* when X=0.8. Thus the

equation utilized in the N. Anna Model for the return temperature was

$$\frac{T_f - T_E}{T_o - T_E} = \exp(-0.8 \frac{kL}{q_o}) \qquad (2.8)$$

where T_f = final or return temperature.

The 0.8 factor in Equation 2.8 can be thought of as a dispersion effect, reducing the "effective" length of the side arm by 20%.

In order to solve for the side arm flow rate and the return temperature, the mixed layer depth and the temperature of the mixed layer in the WHTF pond were inputs to the side arm model (as well as the side arm geometry and the meteorological conditions).

2.1.1.2 WHTF Ponds

Basically, two situations existed with regard to the mathematical modeling of the temperature distribution in the WHTF ponds:

(i) one reach with no side arms (Figure 2.3a) and

(ii) two reaches with side arms (Figure 2.3b).

For the reach with no side arms, the temperature of the entrained water was equal to T_2, the temperature at the end of the reach, since no heat flux was allowed through the interface. By means of a heat balance, the temperature of the upper layer waters at the end of the mixing zone would be given by

$$T_1 = \frac{T_o + (D_s - 1)T_2}{D_s}$$

or

$$T_1 - T_E = \frac{(T_o - T_E) + (D_s - 1)(T_2 - T_E)}{D_s} \qquad (2.9)$$

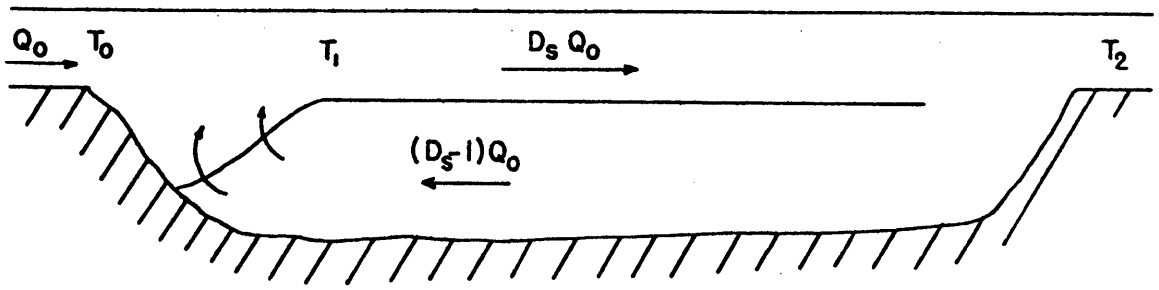

Figure 2.3 Schematization of a Reach without Side Arms

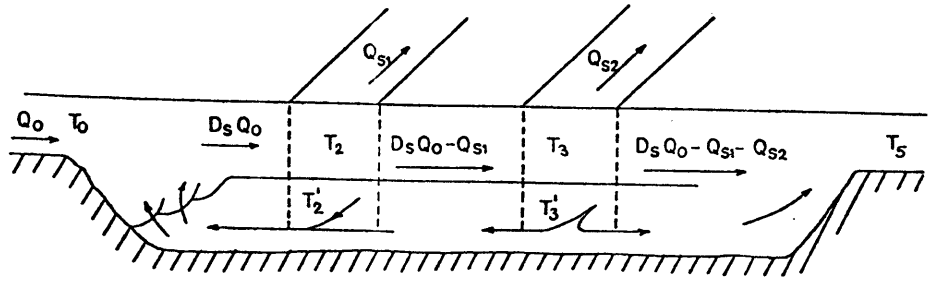

a) $Q_{s1} < (D_s - 1)\ Q_o < Q_{s1} + Q_{s2}$

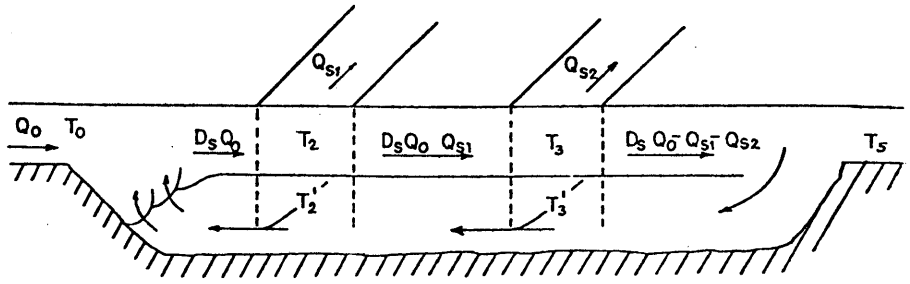

b) $(D_s - 1)\ Q_o > Q_{s1} + Q_{s2}$

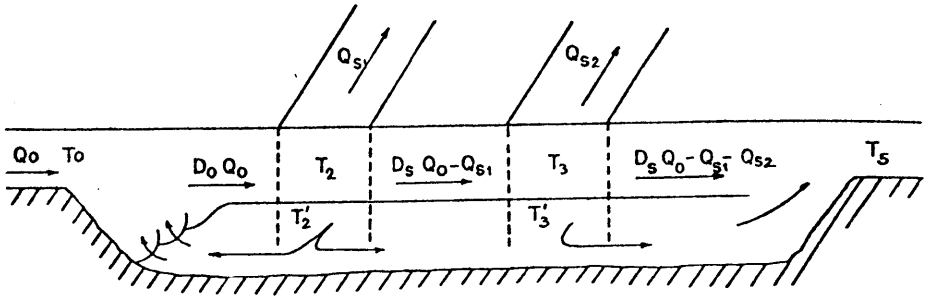

c) $(D_s - 1)\ Q_o < Q_{s1}$

Figure 2.3b: Various Flow Configurations in a Reach with Two Side Arms:

Treating the reach as a one-dimensional steady state system, the governing differential equation along the reach was

$$\frac{dT}{dA} = \frac{\phi_n}{\rho C_p Q} = \frac{-K(T-T_E)}{\rho C_p Q} \tag{2.10}$$

where A = incremental area

Q = flow rate in upper layer

ϕ_n = net heat influx (see Appendix A)

By integrating Equation 2.10 across the pond, the steady state equation for the temperature distribution in the first WHTF reach was

$$\frac{T_2-T_E}{T_1-T_E} = \exp\left[-\frac{KA}{\rho C_p D_s Q_o}\right] = e^{-r} \tag{2.11}$$

By eliminating T_1 from Equation 2.11 and 2.9, the governing equation in reach 1 was

$$\frac{T_2-T_E}{T_o-T_E} = \frac{e^{-r}}{D_s-(D_s-1)e^{-r}} \tag{2.12}$$

As shown in Figure 2.3b the flow in a reach with two side arms could take on three different forms:

(i) the jet entrainment flow is greater than the sum of the side arm flows,

$$(D_s-1)\ Q_o > Q_{s1} + Q_{s2},$$

(ii) the jet entrainment flow is greater than the first side arm flow but smaller than the sum of the sidearm flows,

$$Q_{s1} < (D_s-1)\ Q_o < Q_{s1} + Q_{s2},$$

(iii) the jet entrainment flow is smaller than the first side arm's flow,

$$(D_s-1)\ Q_o < Q_{s1}.$$

Similar to the analysis of temperature in the first reach without a side arm, the same governing equation (Equation 2.10) was integrated over sections of the reach between side arm locations and simplified by a heat balance relationship describing mixing of the flow within the reach and at the side arms' entrance/exit.

For case (i) above the equations for the temperature distribution were

$$\frac{T_5-T_E}{T_o-T_E} = \frac{e^{-r_1-r_2-r_3}}{\Delta} \tag{2.13}$$

$$\frac{T_2-T_E}{T_o-T_E} = \frac{e^{-r_1}}{\Delta} \tag{2.14}$$

$$\frac{T_3-T_E}{T_o-T_E} = \frac{e^{-r_1-r_2}}{\Delta} \tag{2.15}$$

$$\frac{T_1'-T_E}{T_o-T_E} = \frac{D_s-\Delta}{(D_s-1)\Delta} \tag{2.16}$$

where $r_1 = \dfrac{K_1 A_1}{\rho C_p D_s Q_o}$

$$r_2 = \frac{K_2 A_2}{\rho C_p (D_s Q_o - Q_{s1})}$$

$$r_3 = \frac{K_3 A_3}{\rho C_p (D_s Q_o - Q_{s1} - Q_{s2}}$$

$$\Delta = D_s - (D_s - 1 - \frac{Q_{s1}}{Q_o} - \frac{Q_{s2}}{Q_o})\, e^{-r_1-r_2-r_3}$$

$$- \frac{Q_{s1}}{Q_o} e^{-r_1-r_{s1}} - \frac{Q_{s2}}{Q_o} e^{-r_1-r_2-r_{s2}}$$

$$r_{s1} = \alpha \frac{K_{s1}A_{s1}}{\rho C_p Q_{s1}}$$

$$r_{s2} = \alpha \frac{K_{s2}A_{s2}}{\rho C_p Q_{s2}}$$

subscript 1' = pertaining to the water after entrance mixing

subscript 1 = pertaining to the area of pond before side arm 1

subscript 2 = pertaining to the area of pond between the two side arms

subscript 3 = pertaining to the area of the pond after side arm 2

subscript s1 = pertaining to side arm 1

subscript s2 = pertaining to side arm 2

α = 0.8, the side arm dispersive effect as shown in Equation 2.8

For case (ii) the same equations, 2.14, 2.15, 2.16, applied for $T_{1'}$, T_2, and T_3, except that

$$\Delta = D_s - \frac{Q_{s1}}{Q_o} e^{-r_1-r_{s1}} - (D_s - 1 - \frac{Q_{s1}}{Q_o}) e^{-r_1-r_2-r_{s2}}.$$

For the T_5 temperature, the approximate equation was

$$\frac{T_5-T_E}{T_o-T_E} = \{(D_s - \frac{Q_{s1}}{Q_o} - \frac{Q_{s2}}{Q_o}) e^{-r_1-r_2-r_3} +$$

$$(\frac{Q_{s1}}{Q_o} + \frac{Q_{s2}}{Q_o} - D_s + 1) e^{-r_1-r_2-r_{s2}}\} \Delta^{-1} \qquad (2.17)$$

For case (iii), Δ was again redefined as

$\Delta = D_s(D_s-1)e^{-r_1-r_{s1}}$, and Equations 2.13, 2.14, and 2.15 were still valid. The T_5 temperature was now:

$$\frac{T_5-T_E}{T_o-T_E} = \{(D_s - \frac{Q_{s1}}{Q_o} - \frac{Q_{s2}}{Q_o})\, e^{-r_1-r_2-r_3}$$

$$+(\frac{Q_{s1}}{Q_o} - D_s + 1)e^{-r_1-r_{s1}} + \frac{Q_{s2}}{Q_o}\, e^{-r_1-r_2-r_{s2}}\}\Delta^{-1} \qquad (2.18)$$

Since the solution for reach temperature involves several possible cases (i, ii, iii), an iterative solution was produced according to the flow chart in Figure 2.4.

2.1.2 Dike 3 Mixing

A schematic of the bathymetry of the jet, as taken from field surveys on June 26, 1978, is shown in Figure 2.5. In order to evaluate entrance mixing, the jet model of Stolzenbach and Harleman was again considered (see Equation 2.2). However, considering a critical condition at the triangular restriction (Figure 2.6) indicated that the computed entrainment flow often exceeded the flow which could be exchanged across the section. An analysis of critical flow provided an equation in dimensionless form to compute entrance dilution based on the geometry of the constriction:

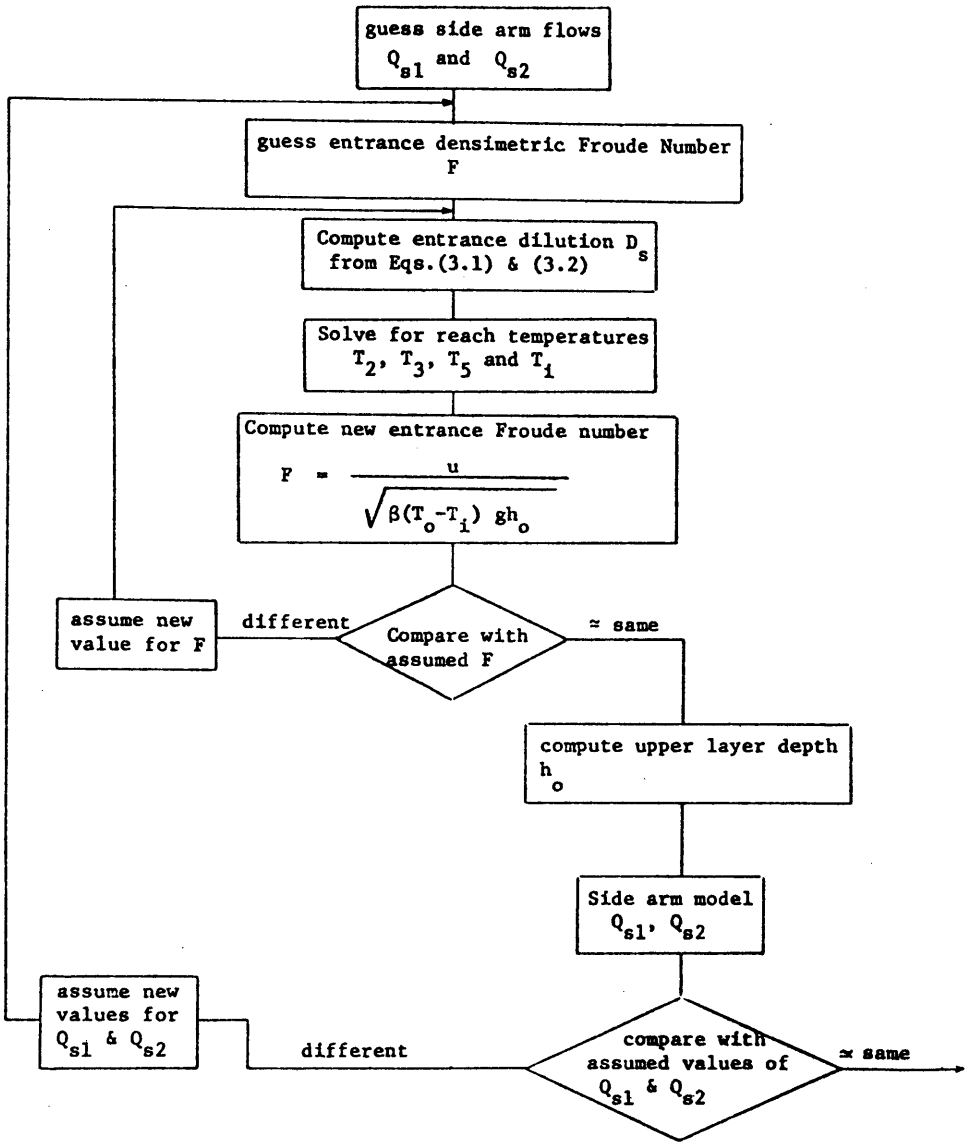

Figure 2.4: Flow Chart of Solution Procedure for Temperature Distribution in Reach with Two Side Arms

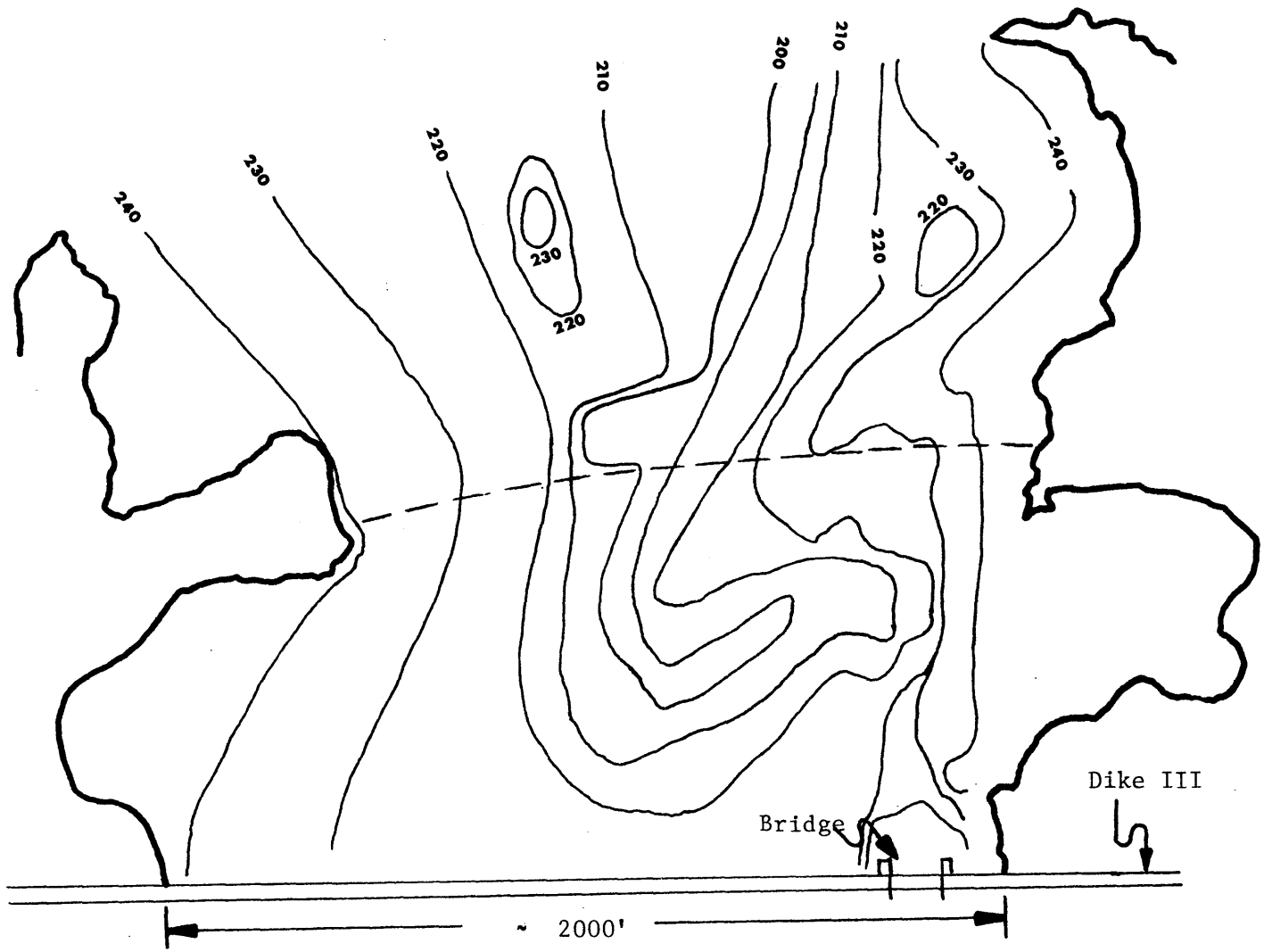

Figure 2.5: Sketch of Bottom Topography
on the Main Lake Side of the Dike III Jet

(Note: Elevations are in feet above MSL)

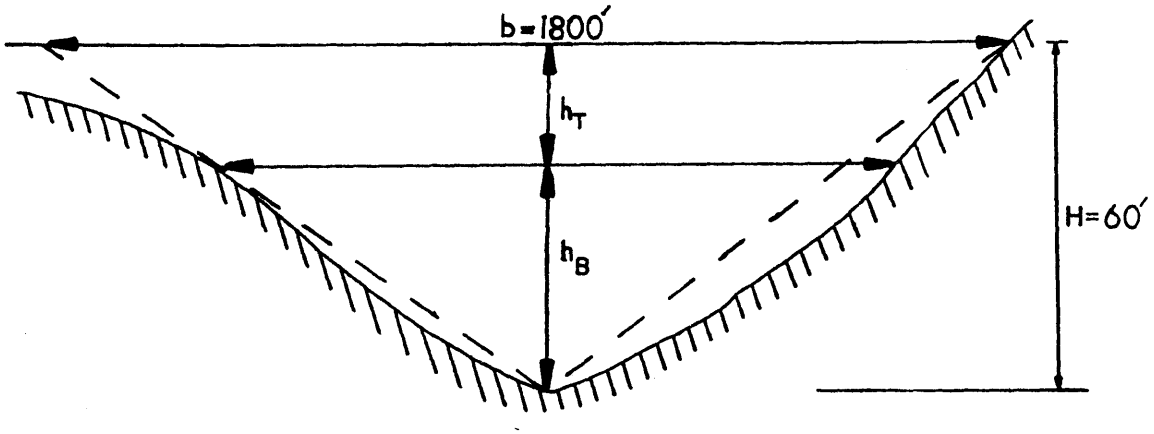

Figure 2.6: Cross Section of Dike III Restriction. (Depicting Idealized Triangular Restriction.)

$$\frac{(1 + \frac{Q_e}{Q_o})^3 (\frac{Q_e}{Q_o})^2 (1 + \frac{Q_e}{Q_o})}{(\frac{h_T}{H})^3 (2 - \frac{h_T}{H})^2 (1 - \frac{h_T}{H})^5} = \frac{b^2 H^2}{4Q_o^2} g (\frac{\Delta\rho}{\rho})_o , \qquad (2.19)$$

where h_T = depth of top section

H = total depth

b = top width

$(\frac{\Delta\rho}{\rho})_o$ = value of $\Delta\rho/\rho$ between the jet water and the entrainment cold water

Q_e = entrained flow

Q_o = jet discharge

This equation was solved by trial and error for the maximum value of Q_e/Q_o which obeyed the stipulation that $0 < \frac{h_T}{H} < 1$.

2.1.3 Main Lake Model

The main lake of N. Anna has been divided into three sections (Figure 2.7):

(i) a vertically well-mixed surface layer of constant thickness and horizontally-varying temperature distribution T(x,t)

(ii) a vertically stratified subsurface pool of uniform horizontal structure T(z,t), and

(iii) a side arm reach attached to the end of the main lake that has a return flow into the subsurface pool.

The combined surface and lower layer models were essentially modified from Ryan and Harleman (1973).

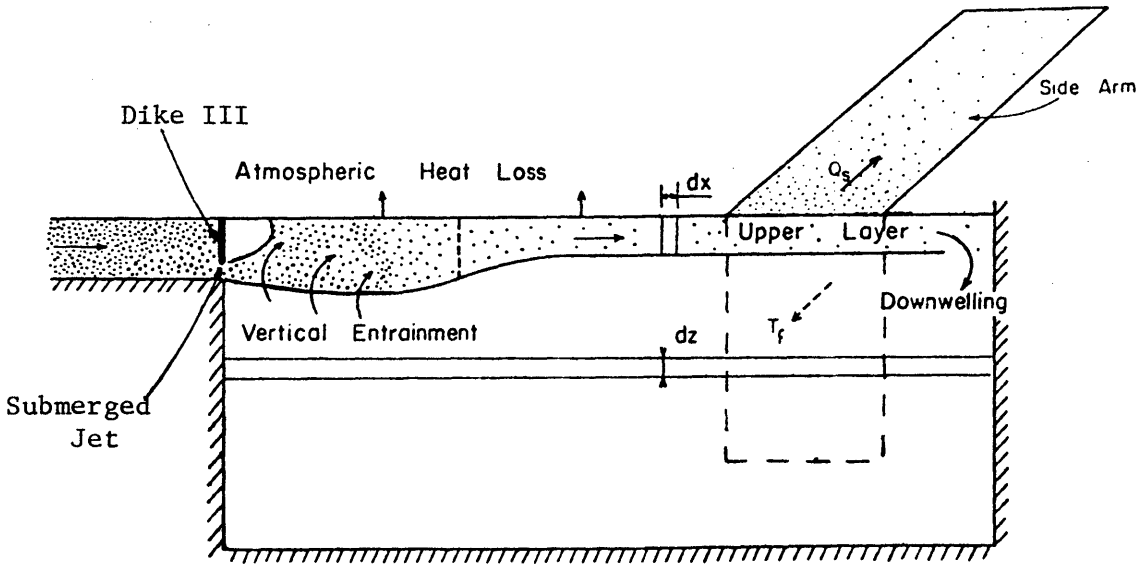

Figure 2.7: Schematic of Main Lake Model

2.1.3.1 Surface Layer Model

A one-dimensional, transient model was used based on the following governing equation:

$$\frac{\partial T}{\partial t} = -\frac{Q}{H_s}\frac{\partial T}{\partial A} - \frac{\phi_n}{\rho C_p H_s} \quad . \tag{2.20}$$

where H_s = depth of surface layer

ϕ_n = net surface heat flux (see Appendix A).

This equation was put into finite difference form, and the surface temperature along the lake, in areal increments, was predicted as a function of time.

In order to determine the mixed-layer depth, Watanabe, et al's (1975) equation for the layer thickness in a deep cooling lake was used:

$$H_s = \left[\frac{f_i}{4}\,\frac{Q_o^2\, D_{sv}^3\, L^3}{\beta\, \Delta T_L\, g\, A_p^2}\right]^{1/4} \tag{2.21}$$

where f_i ≡ interfacial friction factor

Q_o = discharge flow rate

D_{sv} = vertical entrance dilution

A_p = total pond area

L = longitudinal pond dimension

β = thermal expansion coefficient

ΔT_L = surface temperature difference between dam and intake

g = acceleration due to gravity

2.1.3.2 Stratified Subsurface Model

In the main lake of N. Anna, below the well-mixed surface layer, a series of horizontally uniform layers comprise the lake's vertical structure with thermal transport occurring by diffusion, advection, convective mixing and radiation absorbtion.

The governing mathematical equations for this one-dimensional vertical model are presented below:

HEAT TRANSPORT EQUATION:

$$\frac{\partial T}{\partial t} + \frac{1}{A}\frac{\partial}{\partial z}(Q_v T) = \frac{D_z}{A}\frac{\partial}{\partial z}\left(A\frac{\partial T}{\partial z}\right)$$

Advection — Diffusive Transport

$$+ \frac{Bu_i T_i}{A} - \frac{Bu_o T}{A} - \frac{1}{\rho C_p A}\frac{\partial(A\phi_z)}{\partial z} \qquad (2.22)$$

Inflow — Outflow — Internal Radiation Absorbtion

Surface Boundary Condition:

$$D_z\frac{\partial T}{\partial z} = \beta\phi_{sn} + \phi_{an} - \phi_{br} - \phi_e - \phi_c \quad \text{at } z=z_s$$

Bottom/Side Boundary Condition:

$$\frac{\partial T}{\partial z} = 0 \quad \text{at } z=0$$

CONTINUITY:

$$Q_v = B\int_o^z u_i(z,t)dz - B\int_o^z u_o(z,t)dz \qquad (2.23)$$

where:

$$\phi_z = \phi_o(1-\beta)e^{-\eta(z_s-z)}$$

ϕ_o = net incident solar radiation (see Appendix A)

ϕ_{sn} = net short wave solar heat flux

ϕ_{an} = net atmospheric heat flux

ϕ_{br} = back radiation heat flux

ϕ_e = evaporative heat flux

ϕ_c = conductive heat flux

β = fraction of short wave radiation absorbed at the surface (=0.5)

η = extinction coefficient ($=0.75m^{-1}$)

z_s = water surface elevation

B = width

u_i, u_o = velocity of inflow, outflow

Q_v = vertical flow (advection)

D_z = vertical diffusion coefficient

A = area

T_i = inflow temperature

These governing equations were expressed in finite difference form and solved along with the surface layer using an explicit time scheme. At the end of each time step the vertical stability of the water column was checked and, if necessary, convective overturning was performed.

2.1.3.3 Main Lake Side Arm

The analysis for this side arm parallels that presented in Section 2.1.1.1 on side arm dynamics. The return flow from this side arm entered the main lake within the lower subsurface layers at a level of equal density.

2.1.4 Intake Structure

The intake withdraws water over the top 30 feet of the main lake. In the model either a Guassian withdrawal distribution (centered at the intake location) or a uniform profile (over the upper 30 feet) could be specified.

2.1.5 Summary of the N. Anna Model

Linking together the diverse components of the model was an important aspect of the N. Anna analysis. The WHTF reaches and side arms were formulated as steady state models, while the main lake formulation was transient. In order to account for transience in the WHTF, a lagging criterion was used, based on the residence time of each reach.

The temperature prediction at day j, at the end of a reach with a residence time of n days was calculated from flow, and initial temperatures for day j - n. In this manner temperatures were lagged throughout the WHTF. The flow rate and temperature computed for the end of Reach 3 became the inflow rate and inflow temperature for the Dike III Jet Mixing Formulation of the Main Lake.

The diluted flow rate in the upper layer of the main lake exceeded

the condenser flow rate Q_c withdrawn at the intake by the amount of entrainment associated with Dike III mixing. This extra flow was downwelled to the sub-surface model. This downwelling took place from the last longitudinal segment in the finite difference representation of the surface layer model into the top segment of the finite difference representation of the sub-surface model. This assumption concerning downwelling was based on: (1) the low value of F computed for the surface layer (suggesting low interfacial mixing) and (2) the absence of much sensitivity to the assumption when analyzed by Watanabe (see Ch. 4 of Jirka et al, 1977).

To summarize, the inputs to and from the stratified sub-surface model were the Dike 3 entrainment, the main lake side arm return flow, the intake withdrawal and downwelled surface flow. Note that North Anna River inflow and outflow were neglected. The basis for this assumption was: (1) the generally small magnitude of these flows in comparison to the condenser flow rate, (2) the absence of sensitivity to their inclusion in prior sensitivity studies, and (3) the absence of data for inflow temperature during the historical period of 1957-66.

Once all these components were linked together, and an initial temperature was prescribed in the main lake, the model was able to run in a closed-cycle mode to provide multi-year simulation. A time step of 1 day along with daily average input data was used for all simulations.

2.2 Preliminary Analysis of the Model

Initial calibration of the N. Anna model (under pre-project operating conditions) and long-term simulation of the model (under conditions of project operation) were included in Jirka et al (1977), and its supplementary report by R.M. Parsons Laboratory (1977b). Additional work documented in R.M. Parsons Laboratory (1977a) explored modifications to improve heat transfer in the WHTF by means of physical changes in the geometry of the WHTF (by rerouting the flow to utilize the dead-end side arms and minimizing entrance dilution to each pond) and by means of increasing ΔT_c (by decreasing Q_c).

2.2.1 Calibration of the Model to Natural Conditions

The M.I.T. Lake and Reservoir Model (as described in Ryan and Harleman (1971) and Octavio et al (1977)) was utilized to predict natural temperatures as a base line against which predictions for the artificially heated calculations could be made.

The M.I.T. Lake and Reservoir Model is a time-dependent, one-dimensional (vertical), variable area, mathematical model. Processes which are modeled include the absorption and transmission of solar radiation, convection due to surface cooling, advection due to inflows and outflows and wind mixing. The model contained provisions for simultaneous or intermittent withdrawal from multi-level outlets and residence time calculations for inflows within the reservoir. Turbulent wind mixing in the epilimnion was treated by a mixed layer representation developed by Octavio et al (1977). Heat transport by turbulent diffusion in the hypolimnion subsurface was

neglected. Aside from the wind mixing formulation, the Lake and Reservoir model used for the natural temperatures is similar to the sub-surface portion of the main lake cooling pond model.

By obtaining reservoir water temperatures and meteorological data, the above model was calibrated on data taken between August 1974 and December 1976 (pre-operational). In the long-term simulations this model was utilized as the base line for natural conditions.

2.2.2 Long Term Simulation

The purpose of the long-term simulations was to calculate the response of the natural reservoir (both with and without heat loading) under a range of meteorological conditions characteristic of a significant portion of the life of the plant.

2.2.2.1 Meteorological Data

An eighteen year series (1956-1973) of synthetic daily average meteorological data was generated from available historical data at Richmond, Charlottesville and Quantico, using a regression analysis with a shorter record of site specific data as detailed in Appendix A of Jirka et al (1977). This procedure has been termed "regionalization." Since measurements of short wave solar radiation were unavailable, short wave solar radiation was computed using the following formula:

$$\phi_s = \phi_{sc} (1.0-0.65C^2) \qquad (2.24)$$

where ϕ_s = incoming short wave solar radiation

ϕ_{sc} = clear sky incoming short wave solar radiation (see Section 4.11)

C = cloudiness ratio (fraction of unity).

A summary of this meteorological data was presented in the Supplementary Data Report to Jirka et al (1977).

2.2.2.2 Historical Simulation

A ten year period (1957-1966) was chosen as a typical simulation decade - including average and extreme meteorological conditions - for which to run the natural model and the N. Anna cooling lake model. Typical results from this historical analysis for 1,2,3 and 4 nuclear units were presented in Jirka et al (1977), while a more comprehensive summary is available in the Supplementary Data Report. These results included statistics on temperature extremes, vertical profiles, and time-series plots of heated surface temperatures at the N. Anna Dam for natural conditions and conditions with 1,2,3, and 4 units.

2.2.3 Steady-State Modification Analysis

In a supplementary report to Jirka et al (1977), a steady-state analysis was performed of possible means to lower the temperature in the lake in order to comply with the existing temperature standards.

The possible contingencies explored were (i) minimizing entrance mixing within each of the WHTF reaches so that heat transfer could be increased due to higher temperatures in the initial reaches of the WHTF, (ii) rerouting of the flow in the WHTF through construction of an inter-connecting channel between the upper ends of the Elk Creek and Mill Pond Creek Side arms, and (iii) reducing the condenser flows Q_c resulting in a higher ΔT_c than the design value of 14°F.

These modifications were incorporated into the previously described "segmented model" which was then run until a steady-state was obtained utilizing constant weather data representative of summer and winter conditions.

2.2.4 Summary of Previous Investigation

The above work was completed and left for further analysis until the model could be calibrated and verified under actual plant operation. The process of calibration/verification involved two major components:

(i) a comprehensive data collection effort documenting water temperature, meteorological conditions and (side arm) current structure, and

(ii) a comprehensive analysis of the model's "correctness", including the model's basic assumptions and its bottom line ability to predict temperatures when compared with actual field data.

These two efforts are described in the following three chapters.

3. DATA COLLECTION EFFORT

An integral part of determining whether the conclusions documented in Jirka et al (1977) and the companion reports were accurate was to compare the model's performance against data during actual plant operation. Starting at the time the first nuclear unit came on-line in the summer of 1978, an intensive data collection network was established. This program has continued, with minor modifications, through the present time. (Note that North Anna Unit 2 came on-line in September of 1980 and was declared commercial December 14, 1980.)

Input to the mathematical model calls for daily average meteorological data (air temperature, wind speed measured at 2 meters above the water surface, relative humidity, cloud cover, and short wave solar radiation), plant flow rate (Q_c), plant temperature rise (ΔT_c), and an initial temperature structure in the main lake. These data were obtained along with information used for calibration / verification purposes, such as water temperature, current measurements, and data used to evaluate downstream thermal impact and compliance measurements, such as flow data from the N. Anna Dam.

3.1 Meteorological Data

Figure 1.3 shows the location of the main meteorological tower, which collected data from 150 feet and 35 feet above the land surface. Data were collected continuously and averaged over each hour of the day. Air temperature, wind speed and direction, dew point temperature, and

short wave solar radiation were measured at this station. An auxiliary 35 ft. tower was also located nearby that recorded wind speed and direction, redundant to the main tower.

In order to determine any differences in the meteorological variables at the meteorological tower and over the WHTF's water surface, hand-held meteorological data (relative humidity, wind speed and direction, and air temperature) were taken from a boat at five locations: Pond (Reach) 1, 2 and 3, Elk Creek Side Arm, and Millpond Creek Side Arm (see Figure 1.2). These measurements were collected twice during the sampling day at a frequency of about once a month. By checking the data collected in the WHTF against that collected simultaneously at the tower (which was utilized as input to the N. Anna model), any obvious biases were identified.

At times over the three-year period (1978-1981) data from the meteorological tower were absent. One of the nearest major weather stations was that of Richmond, Virginia (41 miles to the southeast). The reliability of Richmond weather data as correlated to meteorological conditions at N. Anna was explored.in Appendix A of Jirka et al (1977).

Data of interest from the National Oceanic and Atmospheric Administration (NOAA) from Richmond, Virginia included daily averaged values of air temperature, dew point temperature, wind speed, and sky cover. At any time when meteorological data were missing from the on-site towers, daily averaged Richmond data were utilized. Missing solar radiation data were back-calculated from the cloud cover values at Richmond by means of Equation 2.24.

3.2 Water Temperature Data

The extensive collection of water temperature data can be grouped into four types: continuous ENDECO recorders required by NRC, additional continuous ENDECO recorders supplied for the MIT verification study, weekly special temperature surveys, and monthly synoptic temperature surveys. The location of the sampling points is shown in Figures 3.1, 3.2 and 3.3. A substantial quantity of data was generated, with some stations exhibiting redundancy.

All of the continuous ENDECO, MIT and NRC recorders had surface probes (positioned about 1 meter below the surface), some (NRC 1,3,4,5, 6) had surface, middle and near bottom probes, and others (MIT INTAKE, ELK CREEK, MILL POND CREEK, AND DIKE 3) had just surface and bottom probes. The NRC data was digitized for hourly temperature measurements, while the MIT data was done in half hour segments.

The weekly special temperature surveys were performed at each station, with vertical measurements at every meter taken once during the sampling day. During the synoptic survey, vertical temperatures at 1 meter depths were analyzed almost every hour at each of the 17 stations over the sampling days' daylight hours.

3.3 Current Data

Since an important aspect of this research project was to assess the cooling effectiveness of the dead-end side arms. current measurements were taken at the mouths of the two major side arms - Elk Creek and Mill Pond - within the WHTF. Two types of current data were taken:

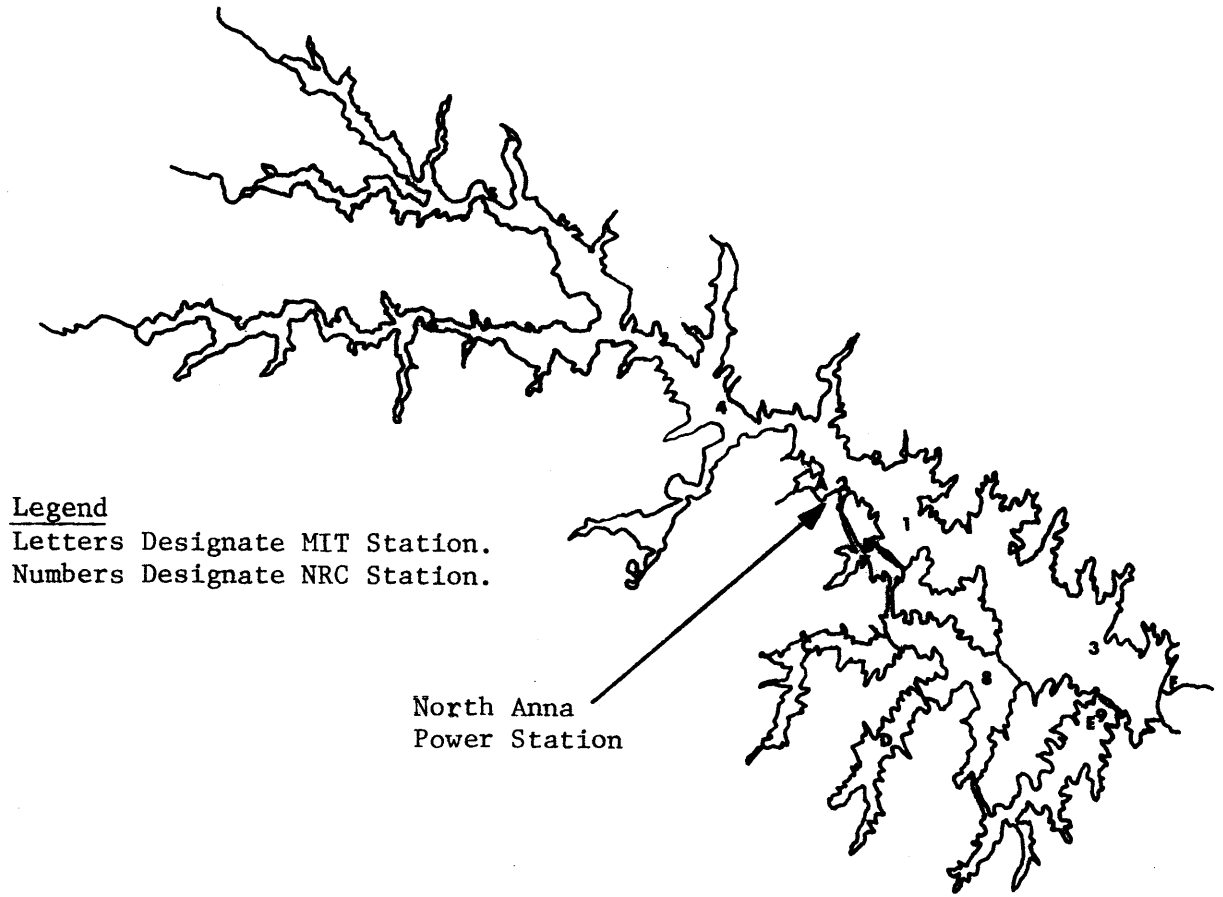

Figure 3.1 Continuous Monitoring Temperature Stations on Lake Anna

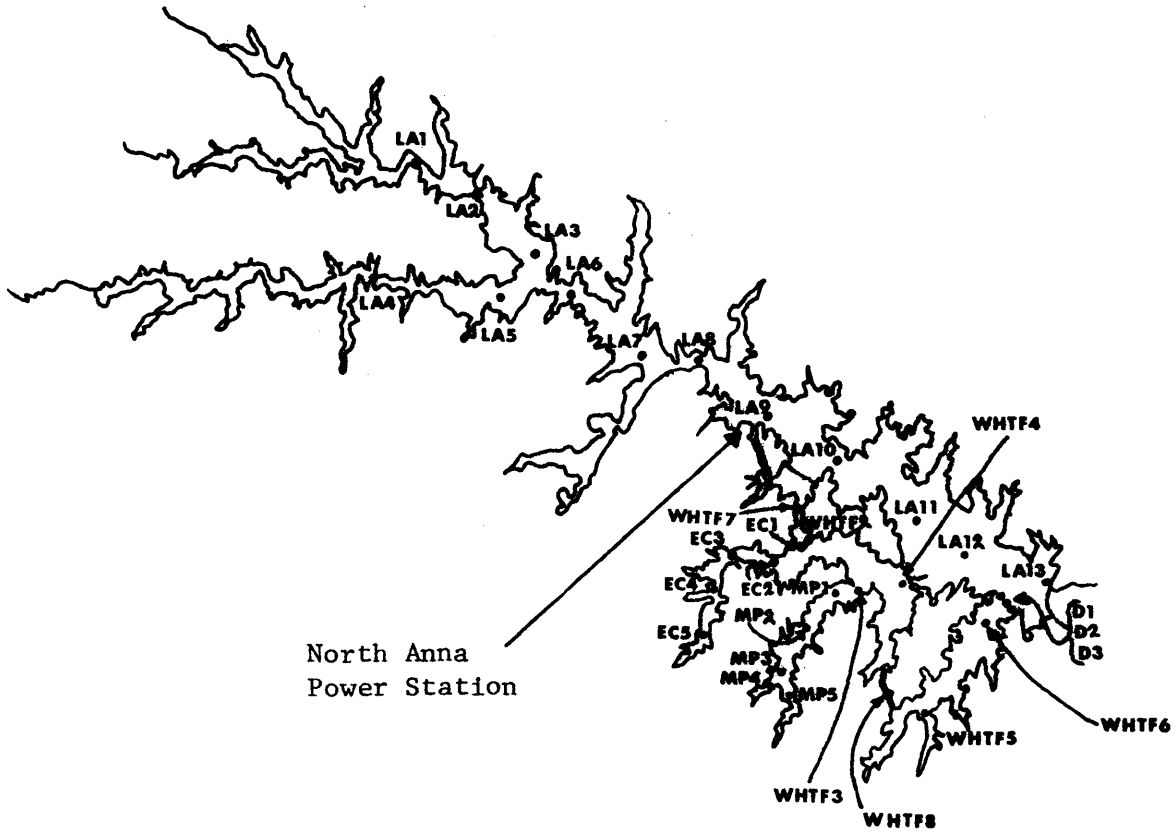

Figure 3.2 Special Temperature Survey Locations on Lake Anna

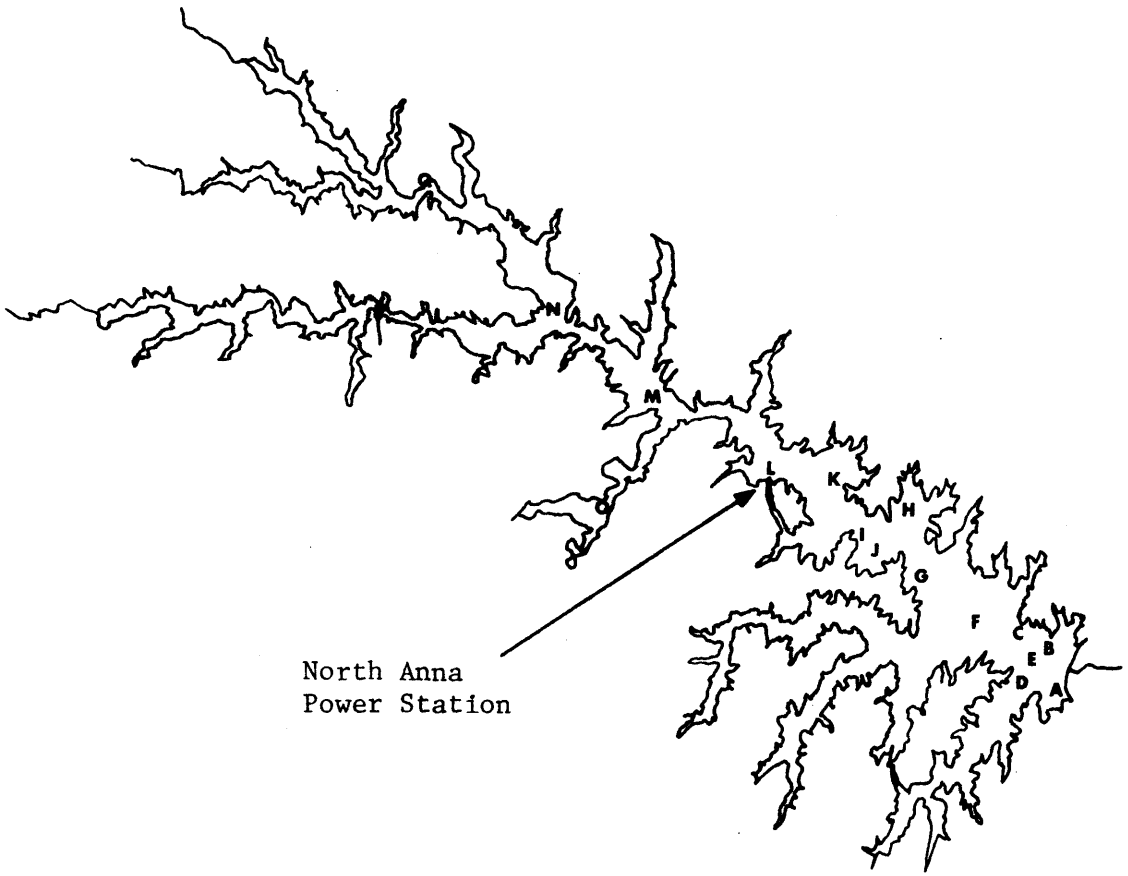

Figure 3.3 Approximate Location of Stations Occupied During Synoptic Temperature Surveys

continuous measurements from two Savonious Rotor current meters and approximately monthly current profiles taken from a portable electromagnetic current meter.

Two Aanderaa Model RCM 4 Savonious Rotor Meters were moored at the bridge crossing the Elk Creek side arm - one at an upper level (5.5 ft. below surface) and one at a lower level (20 ft. below surface). See Figure 3.4 for Elk Creek and Millpond Creek cross-sections. Continuous readings of current velocity, direction and temperature were discretized into two-hourly averages.

A Marsh-McBirney Model 201 electromagnetic current meter was utilized about once a month to obtain a velocity profile at one meter intervals. Measurements were made at the bridge constrictions leading to each side arm. Initially, measurements were also collected at the 208 Bridge which crosses the N. Anna River as it enters Lake Anna; however these were discontinued. Along with each current profile, a temperature profile was taken.

3.4 Plant Operational Data

Both the circulating plant flow (Q_c) and the temperature rise (ΔT_c) across the condenser were necessary inputs to the model. Operators at the Power Station logged the power level (0-100%) of each unit and the number of recirculating pumps which were operational. These statistics were compiled every hour of every day, and from this, daily average values were obtained.

In order to calculate daily average values of Q_c and ΔT_c from these plant statistics, the following relationships were utilized:

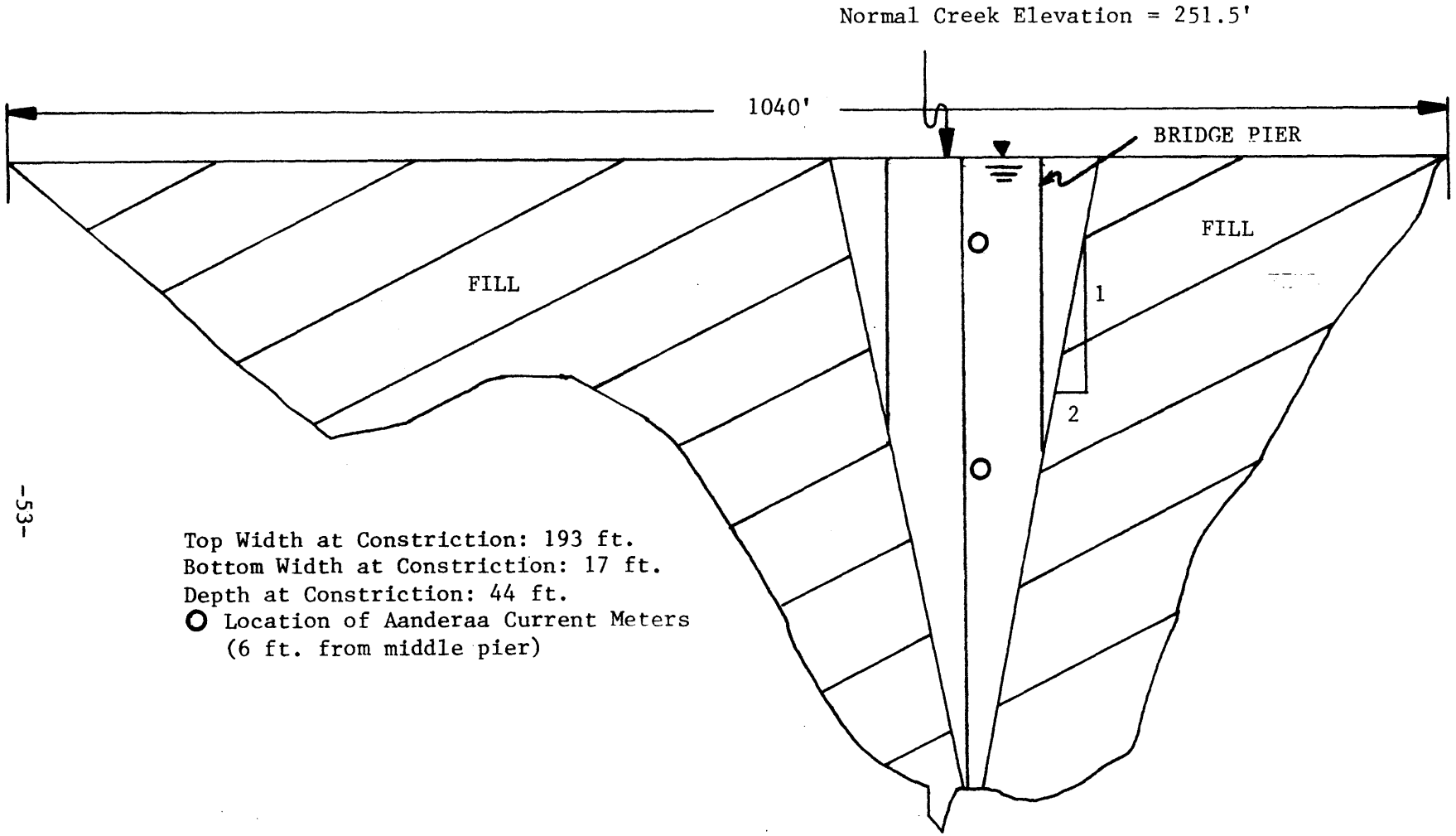

Figure 3.4a: Elk Creek Cross Section

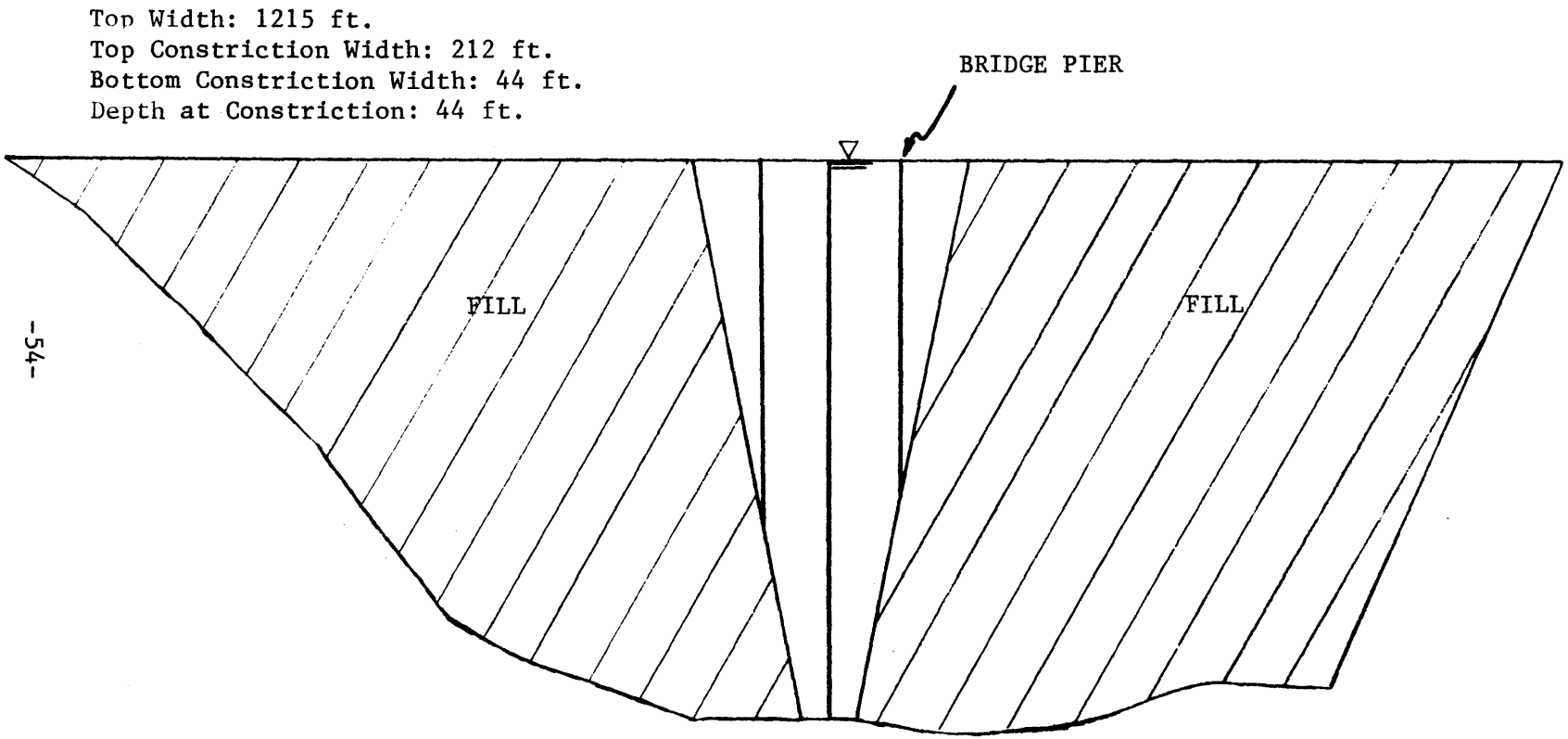

Figure 3.4b: Millpond Creek Cross Section

$$Q_c^{(cfs)} = 530 \frac{cfs}{pump} * N_p \quad (3.1)$$

$$\Delta T_c (°F) = \frac{56.8 * P}{N_p} \quad (3.2)$$

where N_p = number of pumps operating

P = power level (fraction of one unit full load; eg 1.5 for Unit 1 on full load and Unit 2 on 50% load)

Figure 3.5 shows the heat flux ($Q \times \Delta T_c$) from the power plant over the three years of calibration and verification. (Figure 4.15 illustrates the plant flow rate, Q_c, over the same period.)

3.5 North Anna Dam Flow Data

In order to gauge outflows from the lake, a flow recorder near the base of the N. Anna Dam (at the 601 Bridge) was installed in October of 1978. About 23 miles downstream of the N. Anna Dam, a gauging station for the N. Anna River at Doswell, Virginia had been established by the United States Geological Survey (USGS) providing a flow record for the last several decades.

The data from Doswell consisted of a daily average flow rate. Since actual N. Anna Dam release flows were not available before October 1978, a statistical correlation with Doswell's data was developed over the period 1978-1980. Considering the monthly average flow rates, in cfs, the statistical regression equation was

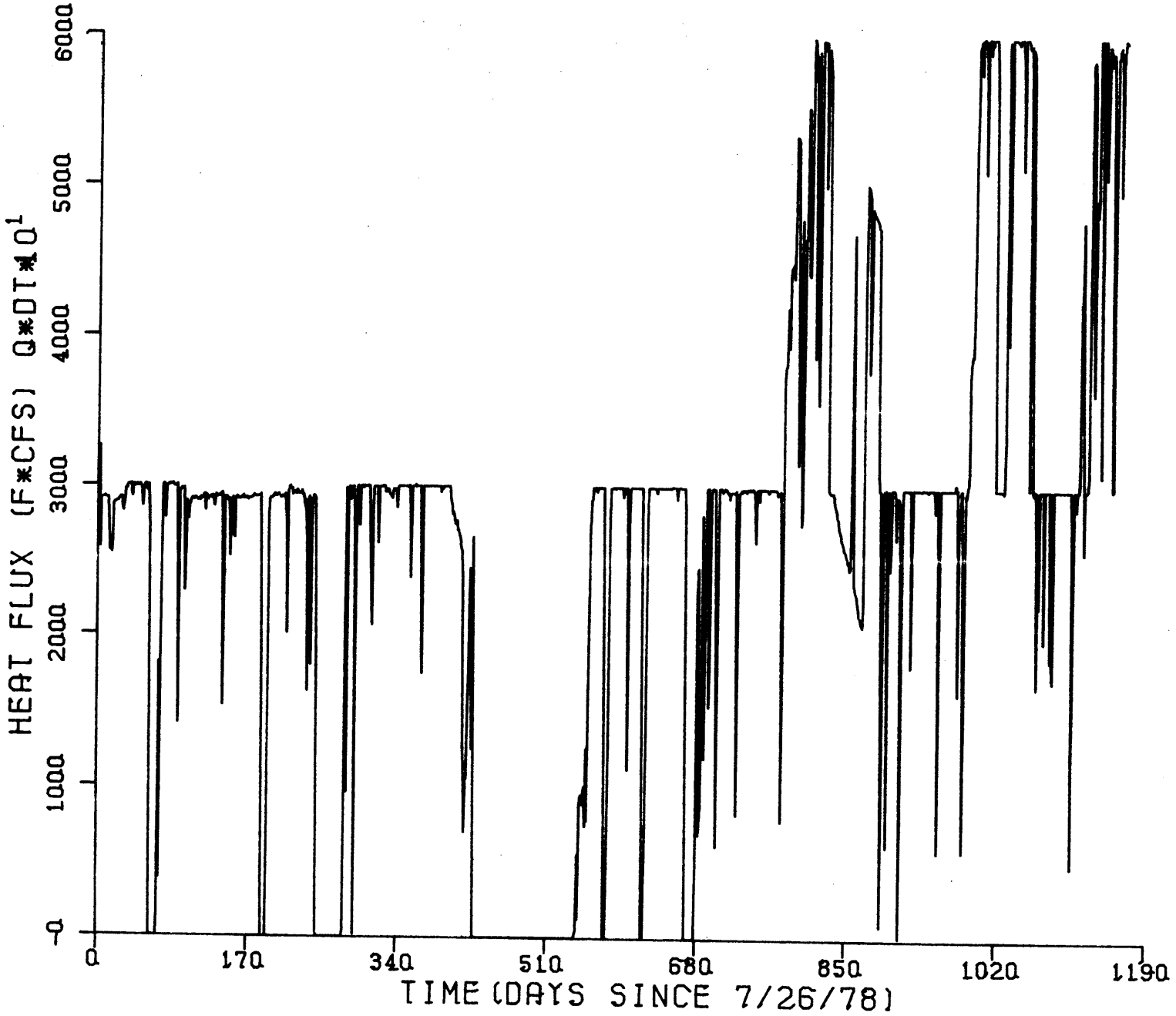

Figure 3.5: Heat Flux from the North Anna Power Station

$$Q_{601(\text{N.ANNA DAM})} = -2.657 + 0.7866\, Q_{\text{DOSWELL}} \qquad (3.3)$$

with an $R^2 = 0.994$. This relationship is shown in Figure 3.6. Thus, about 22% of the flow at Doswell is attributed to lateral inflows between the N. Anna Dam and Doswell, Virginia.

In order to back-calculate what flows at the N. Anna Dam would have been during 1957-1966 if the dam had existed, the computed flows from Eq. 3.3 were adjusted for evaporation from the lake surface. Thus:

$$Q_{\text{N.ANNA DAM}} = (-2.657 + 0.7866 Q_{\text{DOSWELL}}) - Q_{\text{EVAP}} \qquad (3.4)$$

where Q_{EVAP} = average summer time evaporation (cfs) with values set forth in Table 3.1

Table 3.1

Evaporation During the Summer for 1, 2 and 3 Units

Number of Nuclear Units	Average Summer Calculated Evaporation (cfs) (Based on 1959 Meteorological Conditions)
0	111
1	135
2	153
3	182

Note: These calculations were documented in a letter report to VEPCO dated March 27, 1979 by the R.M. Parsons Laboratory, MIT, entitled "Calculation of Water Consumption for North Anna Nuclear Power Station"

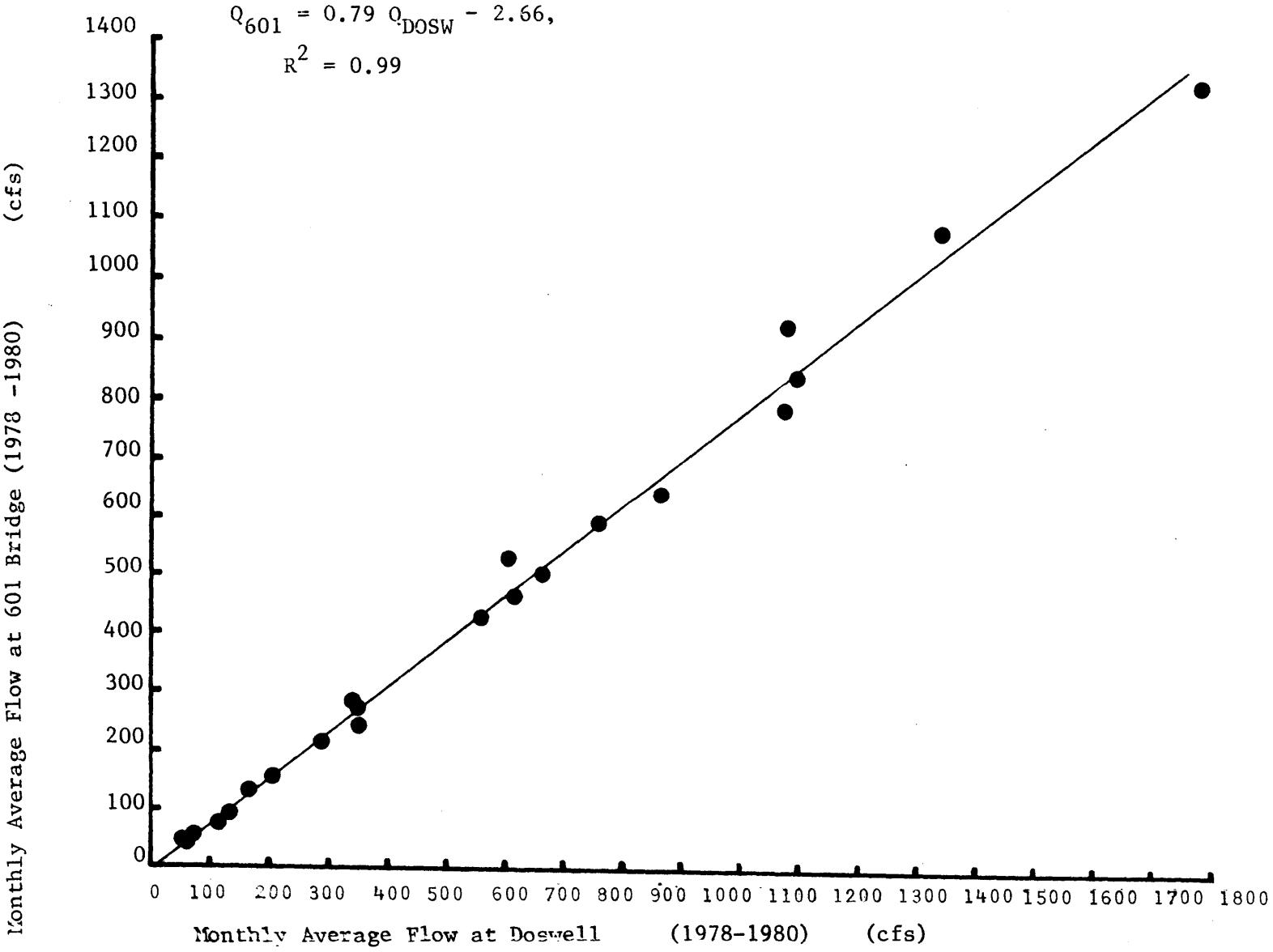

Figure 3.6: Relationship Between Flows at Doswell, Va. and at 601 Bridge for the North Anna River, Virginia

4. MODEL CALIBRATION

Comparison between model calculations and measurements indicated whether the various model assumptions were correct and allowed various model parameters to be fine-tuned. In this analysis the Lake Anna system was divided into four control points as illustrated in Fig. 4.1: the WHTF, Dike III mixing, the Main Lake, and the plant operation. At each point continuously recorded temperature data were available for comparison with model predictions.

Initially, the model was run in "open cycle mode", wherein measured temperatures were input to the model on a daily basis at each of the four control points identified on Figure 4.1. Comparison was then made between measured and predicted temperature at the downstream control point. Because measured temperatures were used upstream, any difference between downstream measurement and calculation could be attributed to error within the segment between control points.

Later, when more data were available, the model was run in "closed-cycle mode" wherein initial temperatures were input to the model and comparisons between model and data could be made over three years at each of the control points. Thus an error analysis could be performed at individual points or over the segments between the points. The former indicated how reliably the integrated model was able to predict temperatures at various points; in effect, this was the bottom line. The latter analysis told how well the

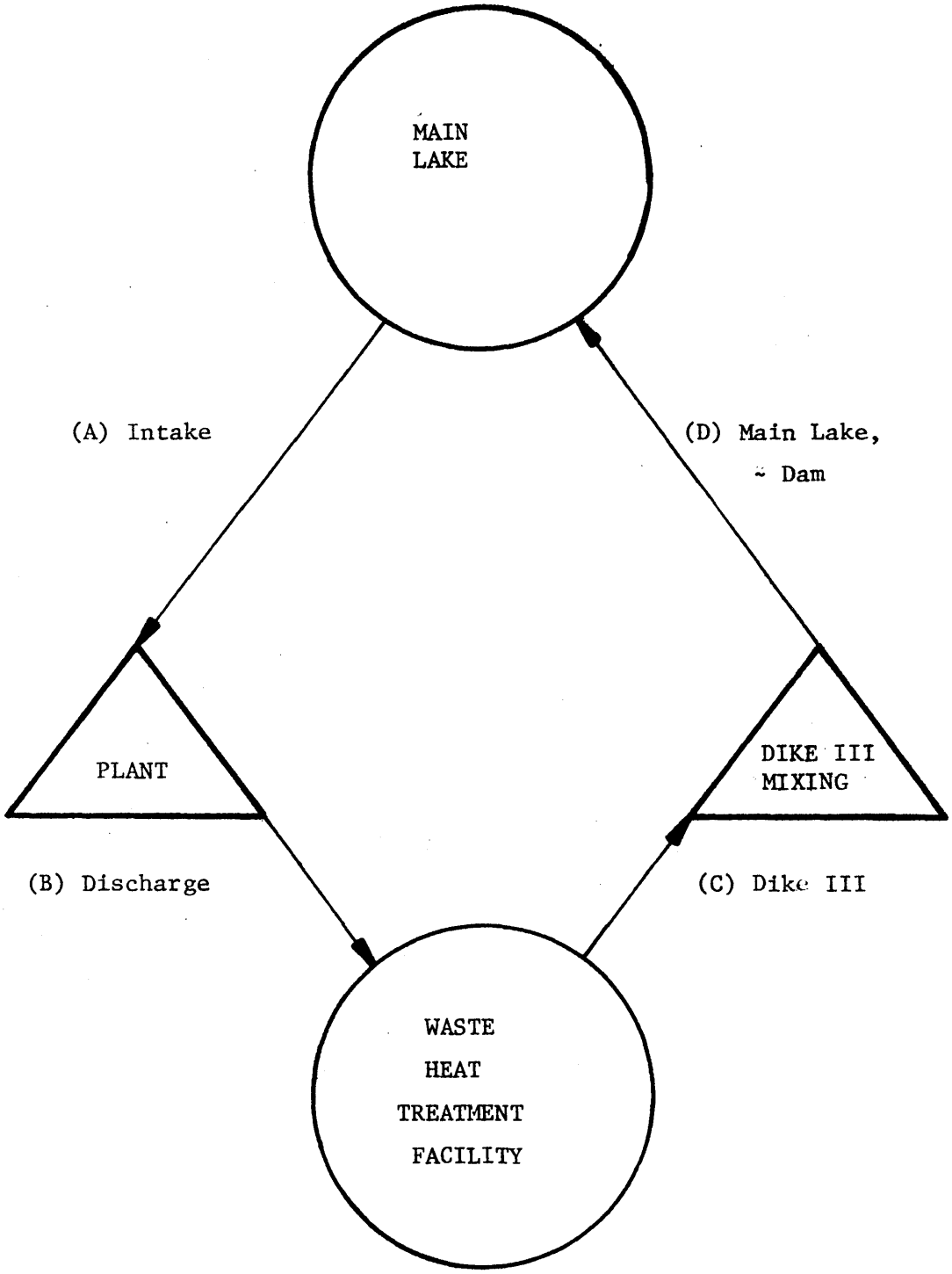

Figure 4.1: Error Analysis Control Points in the Closed Cycle Lake Anna Model

individual segments were being modeled; this information was useful for diagnosing individual model components. In the following, the "raw" error at a point was defined as model prediction minus measurement, while the "delta" error over a segment was defined as the predicted temperature change over the segment minus the measured change. If the upstream control point was designated i and the downstream point was designated f, then the delta error for the reach was

$$\begin{aligned} \Delta T_{error} &= (T_{i_{model}} - T_{f_{model}}) - (T_{i_{data}} - T_{f_{data}}) \\ &= (T_{i_{model}} - T_{i_{data}}) - (T_{f_{model}} - T_{f_{data}}) \\ &= \text{raw error at i - raw error at f} \end{aligned} \tag{4.1}$$

Time series plots and statistics of raw and delta error for the final calibrated runs are presented in Chapter 5, but they are also discussed in this chapter.

4.1 Surface Heat Transfer

Surface heat transfer was an essential component in the hydrothermal modeling of each model segment. The various components of the surface heat transfer (Figure 4.2) were determined from predicted water surface temperatures and measurements of the relative humidity, wind speed, air temperature, cloud cover, and the short wave solar radiation (see Appendix A). The accurate determination of

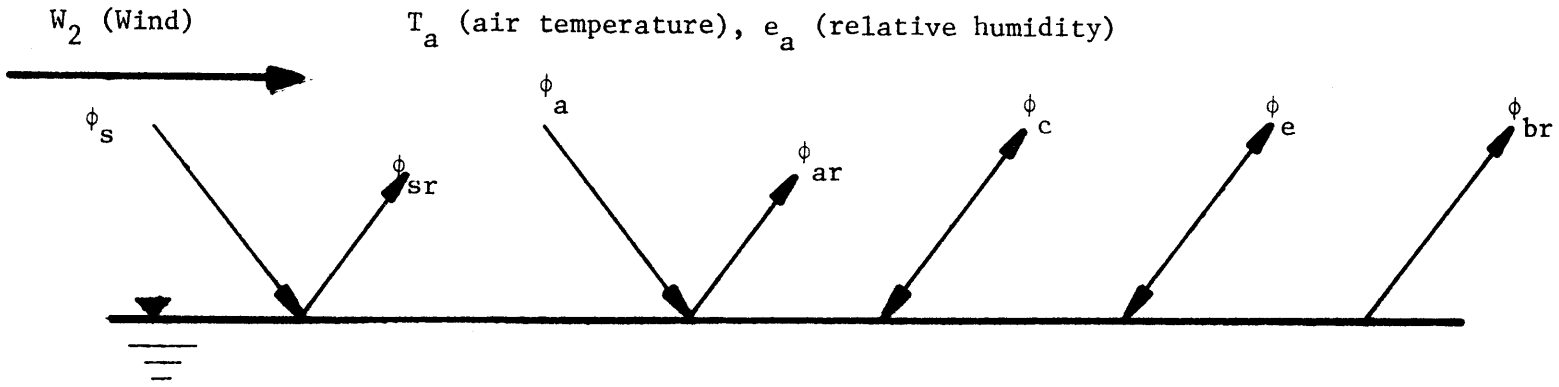

ϕ_s = incoming solar short wave

ϕ_{sr} = reflected solar short wave

ϕ_a = incoming atmospheric long wave

ϕ_{ar} = reflected atmospheric long wave

ϕ_c = conduction

ϕ_e = evaporation

ϕ_{br} = back radiation

Figure 4.2: Components of Surface Heat Transfer

these variables to a large degree dictated the success of the model during the calibration and verification stages.

4.1.1 Short-Wave Solar Radiation Measurements

Incoming solar radiation at the meteorological tower was measured by a pyrheliometer. If measurements were not available, solar radiation was calculated from a clear sky formula and corrected for cloud cover using Richmond data. This procedure is illustrated in Figure 4.3. A computer program for calculating the clear sky flux, ϕ_{SC}, was developed based on an equation presented in Thackston (1974). The equation, valid for latitudes between 26° and 46°, was

$$\phi_{SC} = 24.*(SRC1(LAT) - SRC2(LAT)*\sin(2\pi*DAY/366.0 + SRC3(LAT))) \quad (4.2)$$

where ϕ_{SC} = clear sky ϕ_S in Btu/Ft^2/day

SRC1(LAT), SRC2(LAT), SRC3(LAT) = constants dependent on the latitude (LAT) between 26 and 46 (for N. Anna at a latitude of 38, the constants were
SRC1(38) = 69.350
SRC2(38) = 40.188
SRC3(38) = 1.741)

DAY = Julian day of the year

One problem became apparent: over the three year period, the daily averaged, measured ϕ_S values were often either much higher or much lower than the empirical calculations (Equation 2.24), which have a range of about 250-2700 Btu/Ft^2/day.

After correcting seemingly erroneous values of ϕ_S which fell below 100 Btu/Ft^2/day (about 20 days over the 3 year period) to the calculated values based on Richmond cloud cover, many measurements were

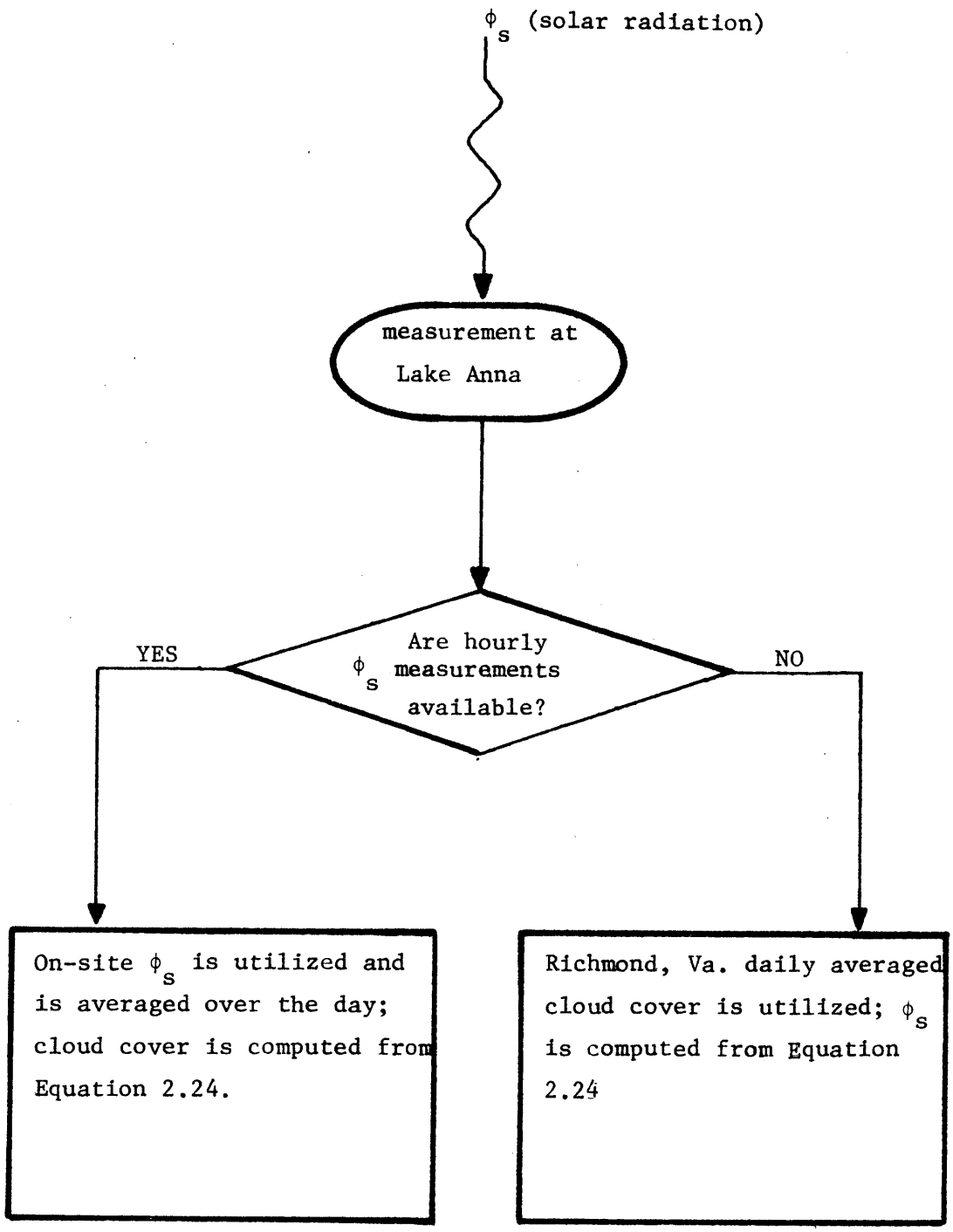

Figure 4.3: Procedure for Obtaining Short-Wave Solar Radiation at Lake Anna

still outside the theoretical "bands" (i.e., Equation 2.24 with C = 0.0 and C = 1.0), see Figure 4.4.

Since many of the ϕ_s measurements were outside the theoretical boundaries, which data should be used? A computer program was written that checked all the measured values of ϕ_s against calculated values of ϕ_s; if the measured ϕ_s came within a certain percentage of the calculated value (based on Richmond cloud cover), then the measured ϕ_s values were utilized; otherwise, the calculated values were used.

The percentage utilized as a criterion varied between 15% and 75%, and a "best" criterion was sought by analyzing the raw and delta error statistics (see Section 5.3). During the first two simulation years (1978-1980), a criterion of 40% reduced the model errors significantly; but over the entire three simulation years (1978-1981), no real improvement in the model statistics was realized by a general, consistent criterion of 40%. Finally, a criterion of 15% was used for analyzing the data when $\phi_{s_{measured}} < \phi_{s_{calculated}}$; otherwise the criterion was 75%. In effect, this assumes that relatively high readings of solar radiation were more likely to be correct than relatively low readings, resulting in generally higher input values of ϕ_s. (See Figure 4.5.) Unfortunately, using this criterion for ϕ_s did not appreciably alter the model statistics over the values of ϕ_s found in Figure 4.4. This means that measured values would have to be judged "individually" as to their relative merit.

In the error plots in Section 5 (Figures 5.6 - 5.9), large "raw"

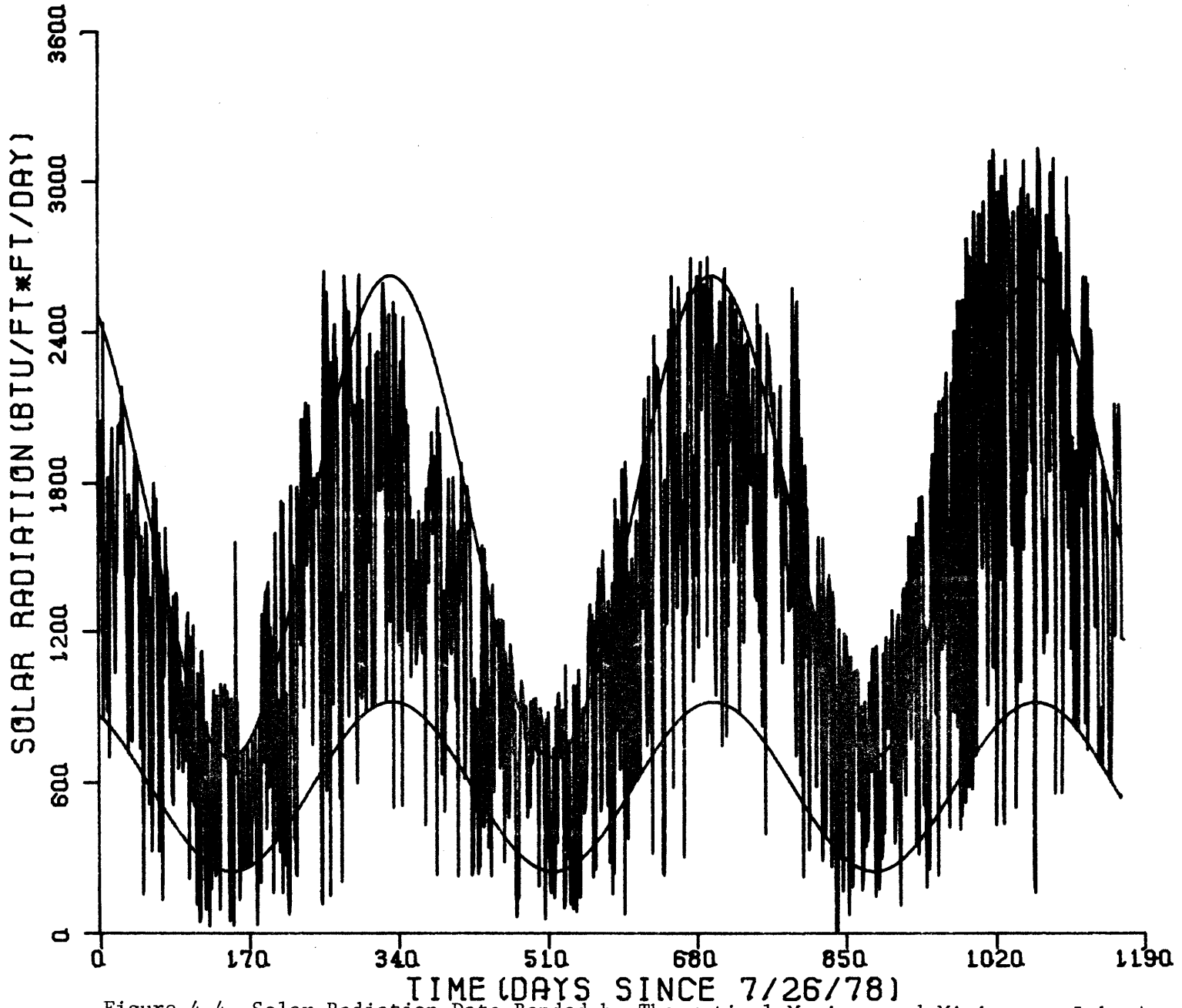

Figure 4.4 Solar Radiation Data Banded by Theoretical Maximum and Minimum at Lake Anna

errors in the cooling pond/lake system wereoften correlated with "extremes" (i.e., ϕ_s measurements falling outside the theoretical limits) on Figure 4.5. But while many of the "extremes" did give excellent agreement with the data, others did not. This is exemplified by the fact that the 1981 Spring/Summer ϕ_s measurements were so much different from the 1978-1980 measurements that no consistency in the error criterion seemed reasonable.

The preceding analysis presents some interesting conclusions about the validity of calculated ϕ_s often used in models where measurements are not taken. On the average, the trends of the calculated bands were followed by the measured data, but for the short term the calculations were inadequate. Specifically, several points seemed clear: (i) the upper limit on winter and spring ϕ_s calculations was often too low; (ii) fall values seemed somewhat consistent; and (iii) summer values exhibited little consistency.

4.1.2 Long-Wave Atmospheric Formulae

A large component in the meteorological forcing is the long-wave atmospheric radiation. This variable (averaging between 1500-3500 $Btu/Ft^2/day$) is usually about 50% larger than the short wave incident solar radiation on a daily average.

The long wave formula proposed by Swinbank (1963) was utilized in the model:

$$\phi_{an} = .97*1.2x10^{-13}(T_a+460)^6(1+0.17C^2) \qquad (4.3a)$$

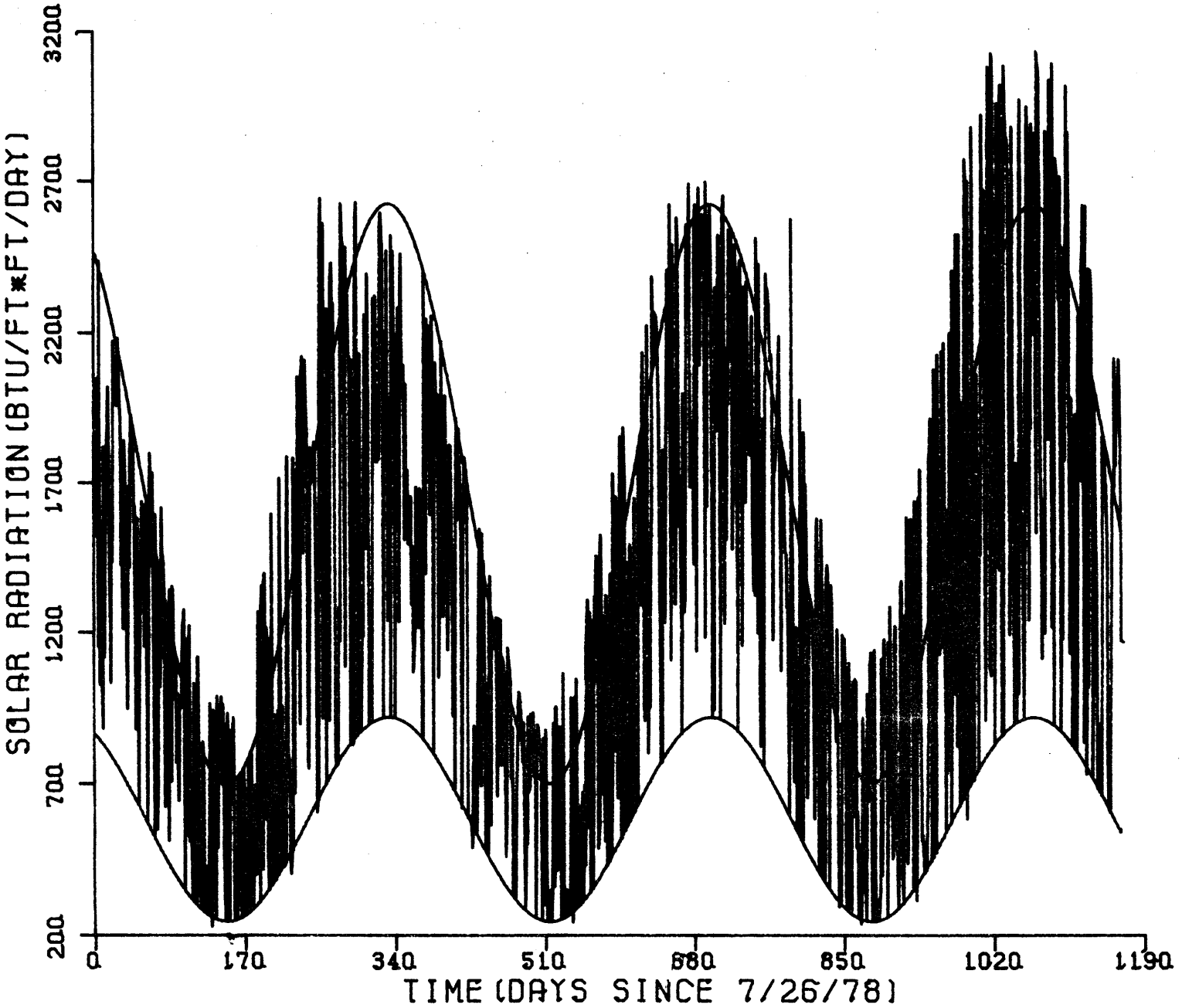

Figure 4.5 Modified Solar Radiation Date Banded by Theoretical Maximum and Minimum at Lake Anna

where ϕ_{an} = net atmospheric radiation (Btu/Ft^2/day)

T_a = air temperature (°F)

C = cloudiness ratio.

Ryan and Harleman (1973) suggest that this formula is valid only above 40°F (5°C); below 40°F (5°C), a formula by Idso and Jackson (1969) was recommended:

$$\phi_{an} = .97*4.15x10^{-8}(T_a+460)^4(1-0.261\ \exp(-2.4 \times 10^{-4}\ (T_a-32)^2))(1+0.17C^2). \qquad (4.3b)$$

Even though both formulas are almost identical above 50°F (10°C) (see Figure 4.6), Equation 4.3b gave higher winter time values.

Since in the diagnostic stages of running the model, the winter temperature predictions were usually too cool, utilizing Equation 4.3b improved the model's winter time performance.

4.1.3 Evaporative Transfer

Evaporation from an artificially heated water body consists of both forced and free convection from the water surface. An equation describing this evaporative flux was developed by Ryan and Harleman (1973):

$$\phi_e = \alpha[\underbrace{22.4(\Delta\theta_v)^{1/3}}_{\text{Free Convection}} + \underbrace{14W_2}_{\text{Forced Convection}}](e_s-e_a) \qquad (4.4)$$

where ϕ_e = evaporative flux in Btu/Ft^2/day

$\Delta\theta_v = T_{sv} = T_{av}$

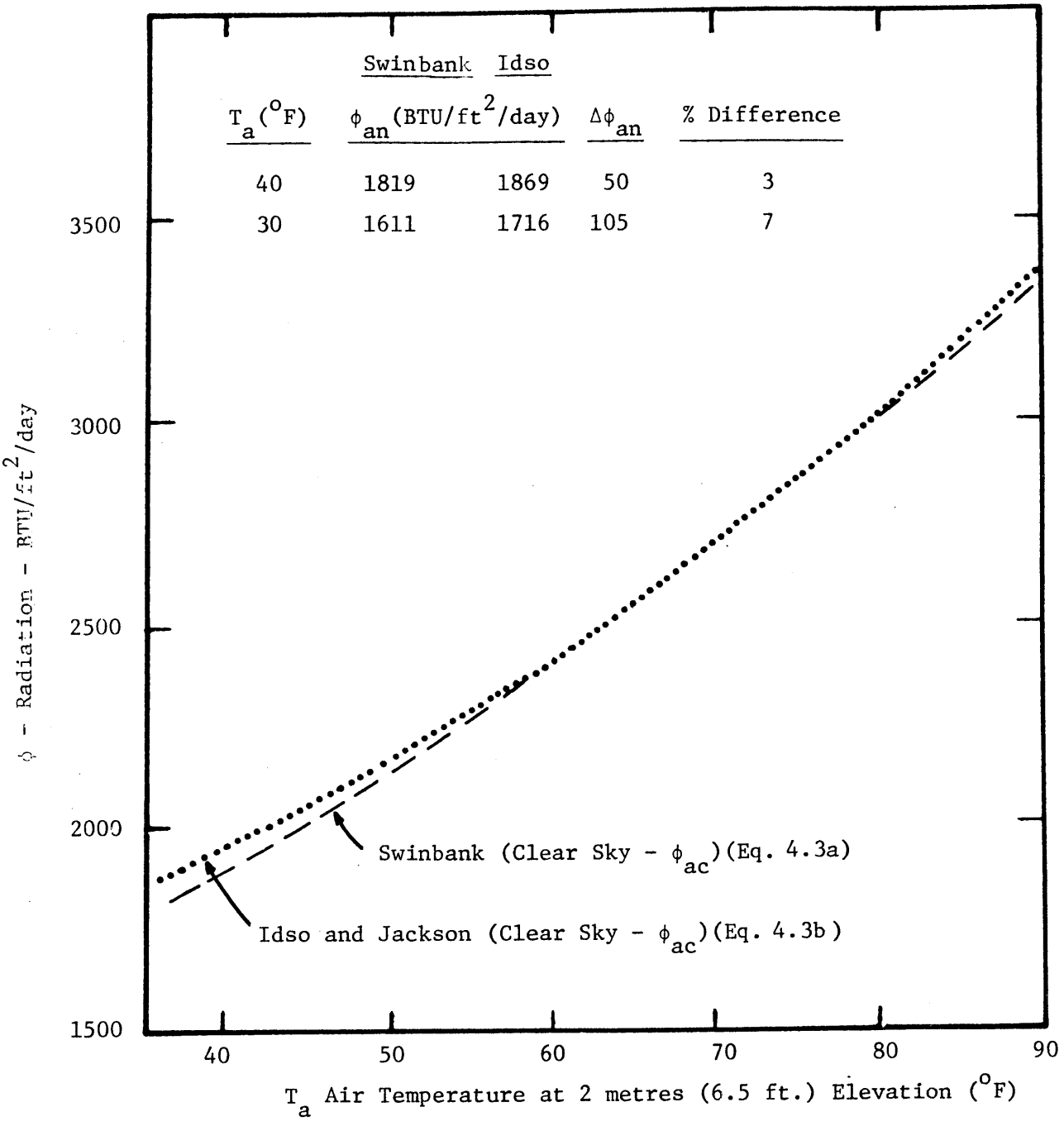

Figure 4.6: Longwave Radiation for Clear Sky

T_{sv} = $(T_s+460)/(1-.378\ e_s/p)-460$,

= virtual temperature of thin vapor layer in contact with water surface

T_{av} = $(T_a+460)/(1-.378\ e_a/p)-460$,

= virtual air temperature

e_s = saturated vapor pressure at surface temperature T_s

e_a = water vapor pressure at 2 meters above water surface

p = atmospheric pressure

W_2 = wind speed at 2 meters above water surface

$e_a = RH*25.4*\exp(17.62 - \frac{9500.8}{T_a+460})$

$e_s = 25.4*\exp(17.62 - \frac{9500.8}{T_a+460})$

RH = relative humidity (fraction)

α = calibration factor (Ryan, Harleman used $\alpha = 1.0$)

The variables required to compute the evaporative flux were T_a, T_s, RH, and W_2.

Daily average values of T_a, RH, and W_2 were compiled from data collected at the meteorological tower as discussed in Section 3.1. The wind speeds were assumed to follow a logarithmic velocity distribution in the atmospheric boundary layer and were "reduced" to a 2 meter (6.5 ft.) height by means of the following equation:

$$W_2 = W_z \frac{\ln \frac{2}{z_o}}{\ln \frac{z}{z_o}} \qquad (4.5)$$

where W_z = measured wind speed at height z (10.7 meters for N. Anna meteorological tower)

z_o = roughness height.

Using a value of z_o = 0.001m, the 2-meter wind speed was approximately 82% of the measured wind speed.

4.1.3.1 Comparison of Meteorological Data in the WHTF and from the Tower

Because of the sensitivity of ϕ_e to T_a, RH, and W_2, measurements of each of these variables were taken at five locations within the WHTF. Measurements were taken at approximately 2 meters above the water surface and were compared with corresponding measurements taken at the tower in Figure 4.7. Also plotted were measurements of wind direction from the tower.

Figure 4.7 showed that whenever the wind speeds in the WHTF were significantly lower than those in the tower, the wind direction was generally from the North. Conversely, when winds came from the South, the WHTF had similar or higher winds than the tower. These differences as a function of wind direction can be attributed in part to topographic and fetch effects. For example, the meteorological tower experiences its greatest exposure during northerly winds, while the WHTF receives its greatest exposure during southerly winds. Also note that the northerly winds (correlated with lower winds in the WHTF) generally occurred in winter, while the southerly winds generally occurred in summer. This is consistent with synoptic scale seasonal patterns (Linsley et al (1975)).

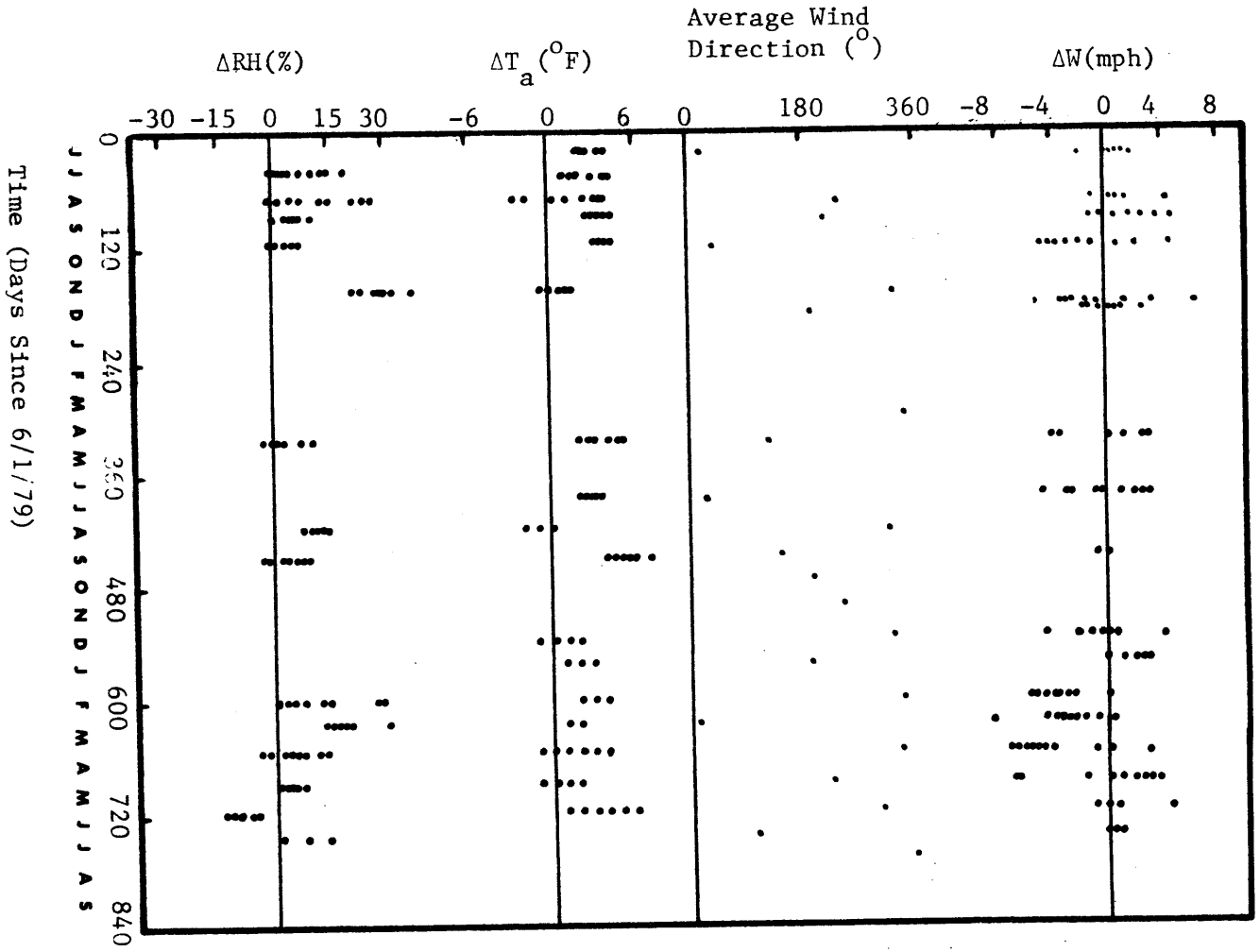

Notes: RH = relative humidity; T_a = air temperature; W = wind speed.

Figure 4.7: Meteorological Data Comparison (Lagoon Station - Meteorological Station)

Figure 4.7 also shows that both air temperature and relative humidity were generally higher over the WHTF than at the tower. The lower wind speed and higher air temperature and relative humidity all suggested that ϕ_e in the WHTF would be overestimated if computed from measurements at the meteorological tower.

4.1.3.2 Adjustment of Evaporation Formula in the Main Lake

Experience has indicated that the Ryan-Harleman evaporation equation (4.4) tends to overpredict evaporation for large scale cooling ponds (the size of the Main Lake). Based on work by Hicks and Wesley (1975), a factor of α=0.85 was used to multiply the evaporation computed by Equation 4.4 (which was based on measurements from the tower). Recent analysis by Helfrich (1981) corroborates this value of α.

4.1.3.3 Adjustment of Evaporation Formula in the WHTF

Because of the aforementioned differences between measurements in the WHTF and from the tower, a further reduction in evaporation was required in the WHTF. Because of the seasonal dependence on wind speed, a seasonal reduction to Equation 4.4 was implemented:

$$\alpha = [0.75 + 0.15 \cos(\frac{2\pi * DAY}{365.25} - \frac{151 * 2\pi}{365.25})] \qquad (4.6)$$

where DAY = Julian day of the year.

This periodic function was at its minimum (60%) on December 1 and its maximum (90%) on June 1 (as dictated by the wind's seasonality) and resulted in improved model error statistics (i.e., lower errors).

4.2 Main Lake Analysis

Several aspects of the main lake model were investigated: (i) jet mixing at Dike III, (ii) applicability of the one-dimensional (horizontal uniformity) assumptions for surface and sub-surface layers, and (iii) vertical transport below the upper mixed layer.

4.2.1 Dike III Mixing

Unlike the philosophy of preventing mixing for maximum heat transfer in the WHTF, the jet mixing at Dike III was designed to maximize dilution in order to meet thermal standards in the main lake and in the N. Anna River. The ability to predict the jet entrainment with the ambient lake water was important in predicting the surface layer temperatures throughout the Main Lake.

By analyzing temperature data in the vicinity of the Dike III mixing zone, an estimate was made of the actual dilution from

$$D_s = \frac{T(WHTF6) - T(D2)}{T(LA13) - T(D2)} \qquad (4.7)$$

where T(WHTF6), T(D2) and T(LA13) are recorded temperatures at locations indicated in Figure 3.2. (Surface values were utilized for T(WHTF6) and T(LA13), while the lower level (39.5 ft.) measurement was used for D2.),

D_s = dilution = $\frac{Q_e+Q_o}{Q_o}$,

Q_o = initial flow.

Comparisons between Equation 4.7 and 2.19 are shown in Table 4.1. (The model mixes the ambient water from 250 MSL to 218 MSL with

the discharged water from Dike III. This represents a mixing temperature determined by averaging temperatures from the surface to 32 ft. below the surface.)

It should be noted that it is difficult to define dilution based on temperature measurements when the ambient receiving water (the main lake) is stratified, because the formula assumes that the entrainment water has one unique temperature (measured by the lower level at station D2), whereas in reality, water is being entrained over a considerable depth with varying temperature.

The comparison of dilutions in Table 4.1 showed generally good agreement between model and data. The difficulty in computing observed dilutions may be largely responsible for the fact that summer time observed dilutions were somewhat lower than predicted. (Use of an intermediate level ambient temperature (between the upper and lower levels of D2) would lead to higher observed dilutions). The lower plume dilution could also be due to the plume's interaction with the right bank (see Figure 2.5).

The reasonable agreement between predicted and observed dilutions contributed to the generally excellent agreement between predicted surface layer temperatures near the dam and corresponding data (see Section 5.1).

Table 4.1 Comparison of Predicted and Actual Dilutions at Dike III

Date	Data	Dilution $(\frac{Q_e + Q}{Q})$ Model
8/16/78	1.4	2.4
9/18/78	1.2	2.5
11/9/78		2.3
3/21/79		2.4
4/30/79		2.0
5/16/79		2.3
6/20/79		2.3
7/26/79	1.2	2.3
8/23/79		2.3
9/19/79		2.5
3/12/80		2.5
4/17/80	3.2 (4/15)	2.2
5/21/80	1.3 (5/19)	2.5
6/18/80	1.7	2.5
7/28/80	1.1 (7/30)	2.5
8/13/80	1.2	2.5
9/26/80		2.5
10/16/80	∞ (Infinite Dilution)	2.5
12/17/80		2.6
2/18/81	5.0	2.5
3/12/81	8.0	2.3
4/13/81	2.1	2.4
5/13/81	1.6	2.3
6/12/81	1.4	2.4
7/15/81	1.3	2.6
8/17/81	2.6	2.5
9/17/81	2.3 (9/15)	2.4
Average over Comparison days: (excluding ∞)	2.3	2.4

4.2.2 Applicability of Model Dimensionality to the Main Lake

Schematization of the main lake as one-dimensional - both longitudinally (surface layer) and vertically (stratified lower layers) - invited comparison between model and data in regard to: (i) mixed layer depth prediction and (ii) the effect of the mixed layer depth and the one-dimensional assumption on the modeling of the intake withdrawal.

4.2.2.1 Mixed Layer Depth Prediction

Watanabe et al (1975) presented Equation 2.21 as a predictive model of the depth of the mixed layer. The use of this equation in the modeling runs of Jirka et al (1977) resulted in a more or less constant mixed layer depth between 14 and 18 feet regardless of the number of units operating.

A comparison of the actual mized layer depth in N. Anna revealed some apparent two-dimensional characteristics. (Note the vertical temperature profiles at the dam and at the intake in Figure 5.5 and Figure 4.8). Near the Dike III mixing zone, mixed layer depths on the order of 20 to 30 feet were observed, whereas near the plant intake, this depth was only between 15 and 20 feet. Thus, after the turbulent mixing zone of the jet, the surface layer depth gradually decreased until the intake was reached.

Trying to model this two-dimensional phenomenon with a one-dimensional model involved some compromise. The observed mixed layer depths near the intake were consistent with the predictions of Equation 2.21. However, in view of the importance of accurately predicting vertical temperature structure in the deeper areas near the dam, a larger depth of

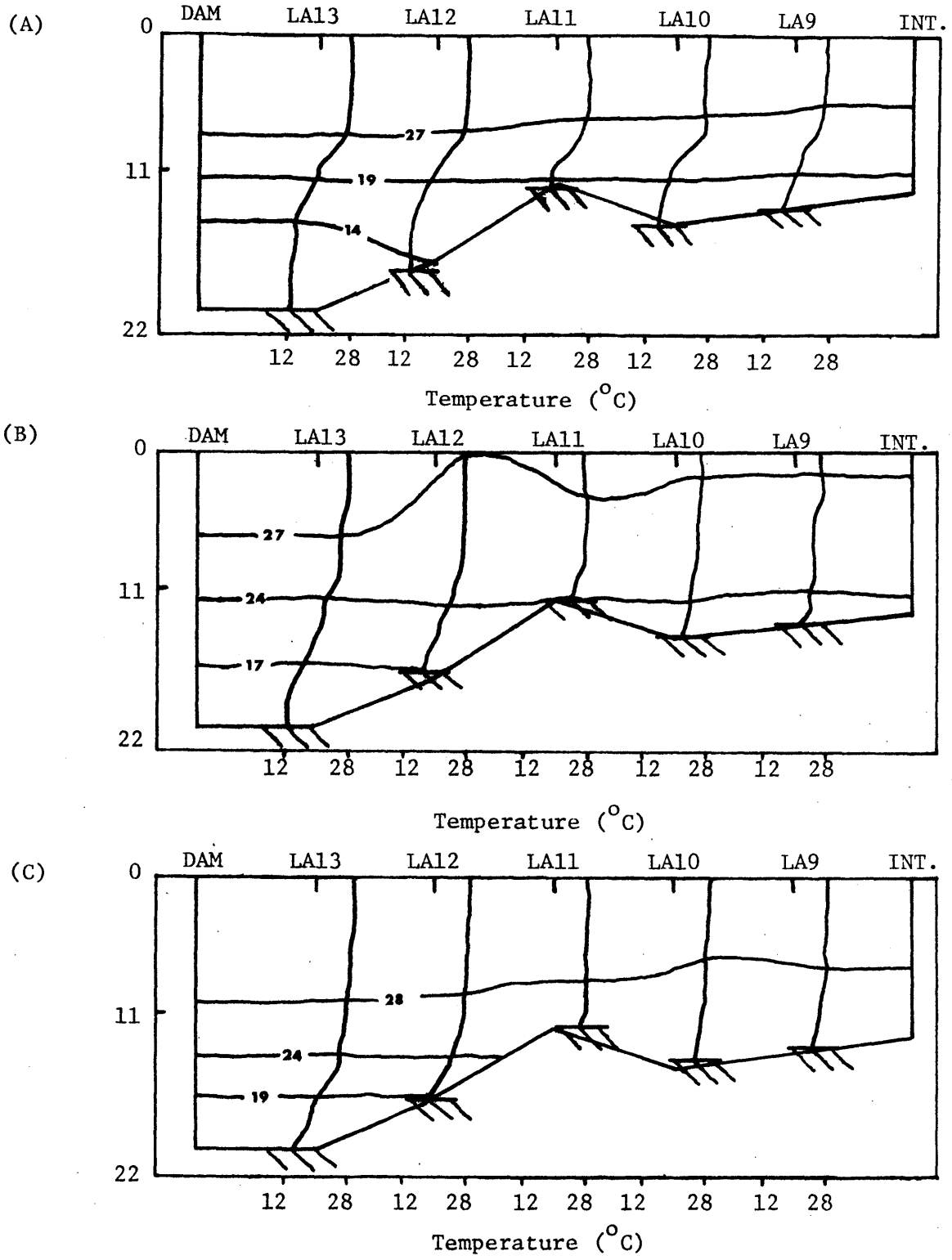

Figure 4.8: Typical Longitudinal Temperature Distributions in Lake Anna between the Dam and the Intake

a) 7/31/79
b) 7/15/80
c) 7/29/81

24' was used for the constant mixed layer depth. Based on the belief that mixing near Dike III is governed more by the constrictive topopgraphy than by the actual flow rates, this constant depth (24') was chosen independent of the number of units in operation.

4.2.2.2 Withdrawal Characteristics of the Intake

A consequence of the mixed-layer depth approximation just discussed was that conditions near the intake were not modeled exactly. The model withdrew water uniformly over the top 30 feet. (Figure 4.9 details the intake structure and a typical velocity profile showing that a depth average value over 30 feet was reasonable.) But the mixed layer depth at the intake was usually less than 24 feet, resulting in more stratification at the intake than was predicted by the model. (Figure 4.10 shows the actual degree of stratification at the intake by plotting the top (near surface) and bottom (∿30 feet below surface) temperatures at the MIT INTAKE ENDECO Meter.) This bias led to the withdrawal of warmer water through the plant than otherwise would have been predicted using an upper mixed layer depth of ∿14 feet (see Section 5.2).

4.2.3 Vertical Diffusion Analysis

The ability of the model to predict accurately the hypolimnetic temperature structure, especially during summer months, was extremely important if management strategies to mitigate temperatures in the

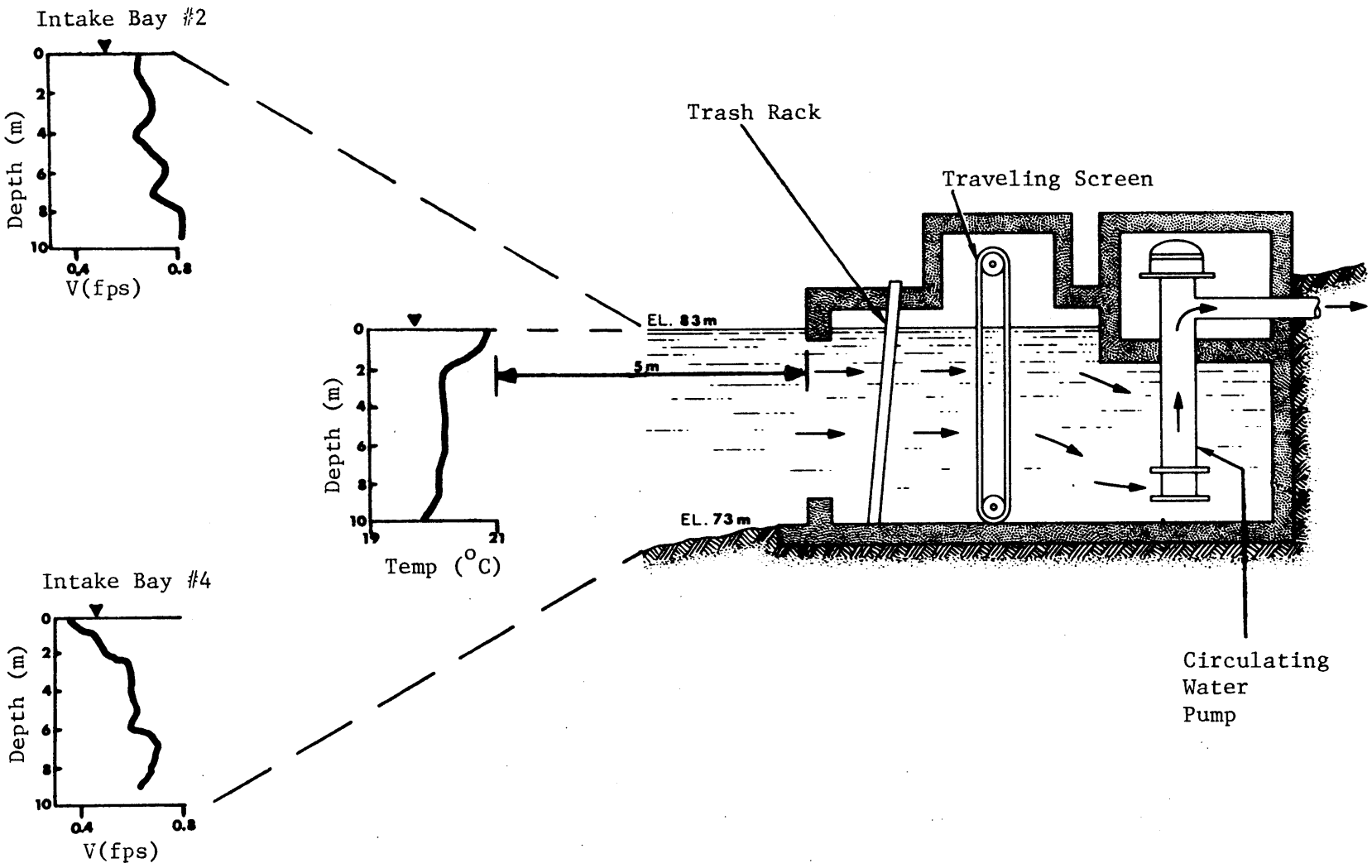

Figure 4.9 Typical Current Velocities at the Intake to the North Anna Power Station on 10/6/78

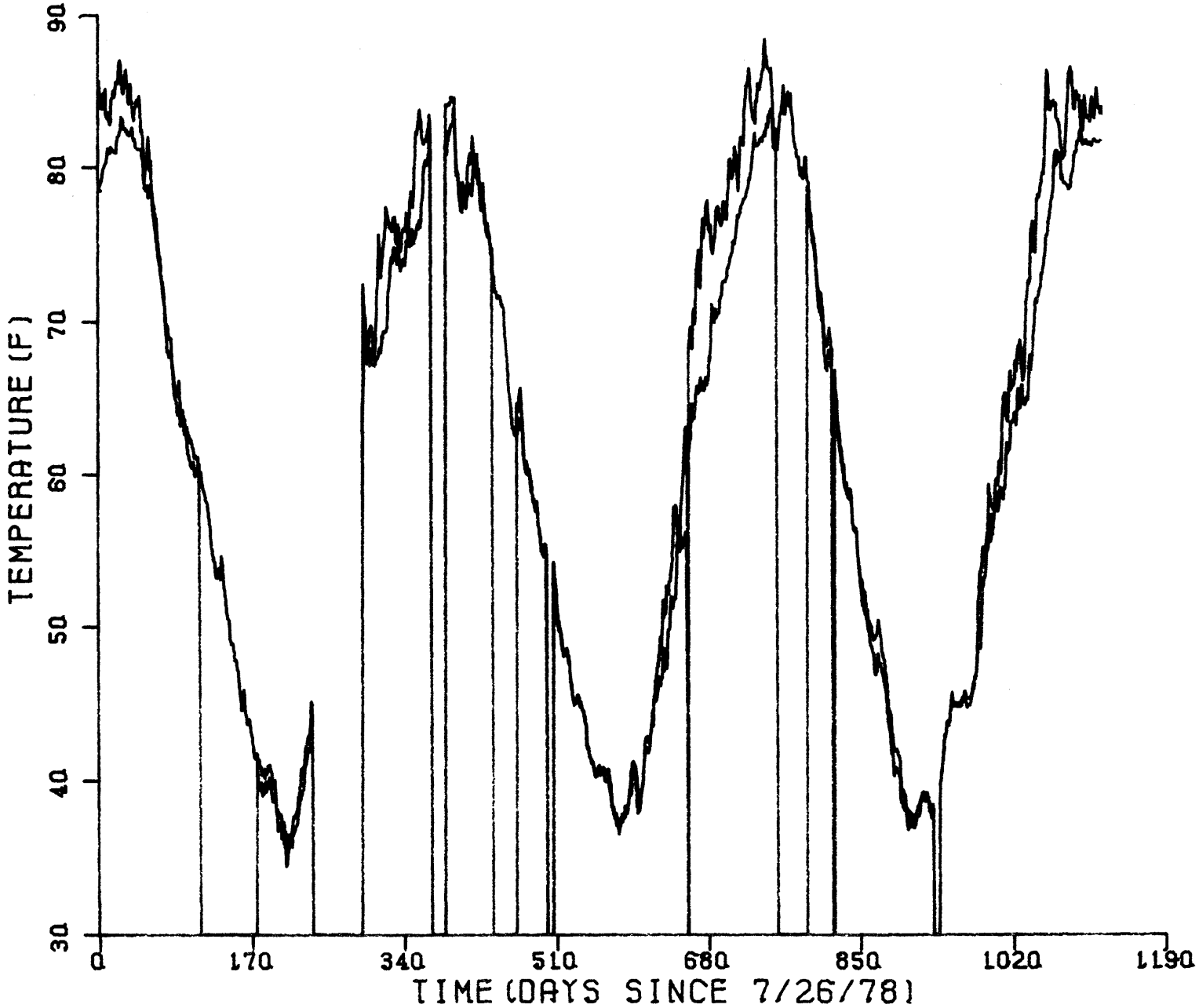

Figure 4.10 Top and Bottom Continuous Temperatures at MIT INTAKE

N. Anna River were to be utilized (e.g., mixing cooler hypolimnetic water with warm surface water by means of a siphon; see Chapter 7). Because of this need a predictive vertical diffusion formulation was developed.

In the earlier modeling effort (Jirka et al, 1977), either molecular diffusivity (.0125 m^2/day)or some constant multiple of molecular diffusivity was chosen. Because Lake Anna did not have a deep outlet (which would create vertical advection that might dominate diffusion), the hypolimnetic temperature structure was highly sensitive to the choice of D_z. Initial comparison between model and data suggested that a constant value of diffusivity was not adequate.

4.2.3.1 Investigation of Vertical Diffusion from Field Data

By analyzing the field data from Lake Anna, one can determine magnitudes of the diffusion coefficient, D_z, which, with a knowledge of the external forcing parameters, can help identify the basic functionality of the diffusion parameter.

In the hypolimnion, below the level of any significant light penetration or the influence of inflows or outflows, the one-dimensional heat transfer Equation (2.22) was simplified to

$$\frac{\partial T}{\partial t} = \frac{1}{A} \frac{\partial}{\partial z} (AD_z \frac{\partial T}{\partial z}) \qquad (4.8)$$

Bella (1970) put Equation 4.8 into finite difference form which allows one to evaluate the magnitude of D_z (at a depth h) from field measurements of temperature:

$$D_z = \frac{\left(\frac{H_h(t+TP) - H_h(t)}{TP}\right)}{\rho C_p A\left(\frac{\overline{T(h + \frac{\Delta z}{2})} - \overline{T(h - \frac{\Delta z}{2})}}{\Delta z}\right)} \qquad (4.9)$$

where H_h = total heat content (Btu)

TP = time period

t = time

Δz = depth interval to define temperature gradient

ρ = density (slugs/ft^3)

C_p = specific heat of water (Btu/lbm°F)

Using weekly and synoptic vertical temperature profiles, values of D_z were determined from Equation 4.9 and are plotted in Figure 4.11 for the summer months of 1979, 1980 and 1981. Values represent averages for the hypolmnion and were evaluated with h = 45 ft. and Δz = 30 ft. Note that D_z is significantly higher in 1980 and 1981 (average ≃ 80 times molecular diffusivity) than in 1979 (average ≃ 16 times molecular diffusivity) and that D_z tends to decrease as summer progresses.

Figure 4.12 presents a time series plot of top, middle, and bottom temperatures at NRC ENDECO No. 3 (see Figure 3.1). Note the rate of change of hypolimnetic temperatures in the three simulation years and the notable slope change in 1980 and 1981 as compared to 1979. To develop a cause-effect relationship between hypolimnetic temperature

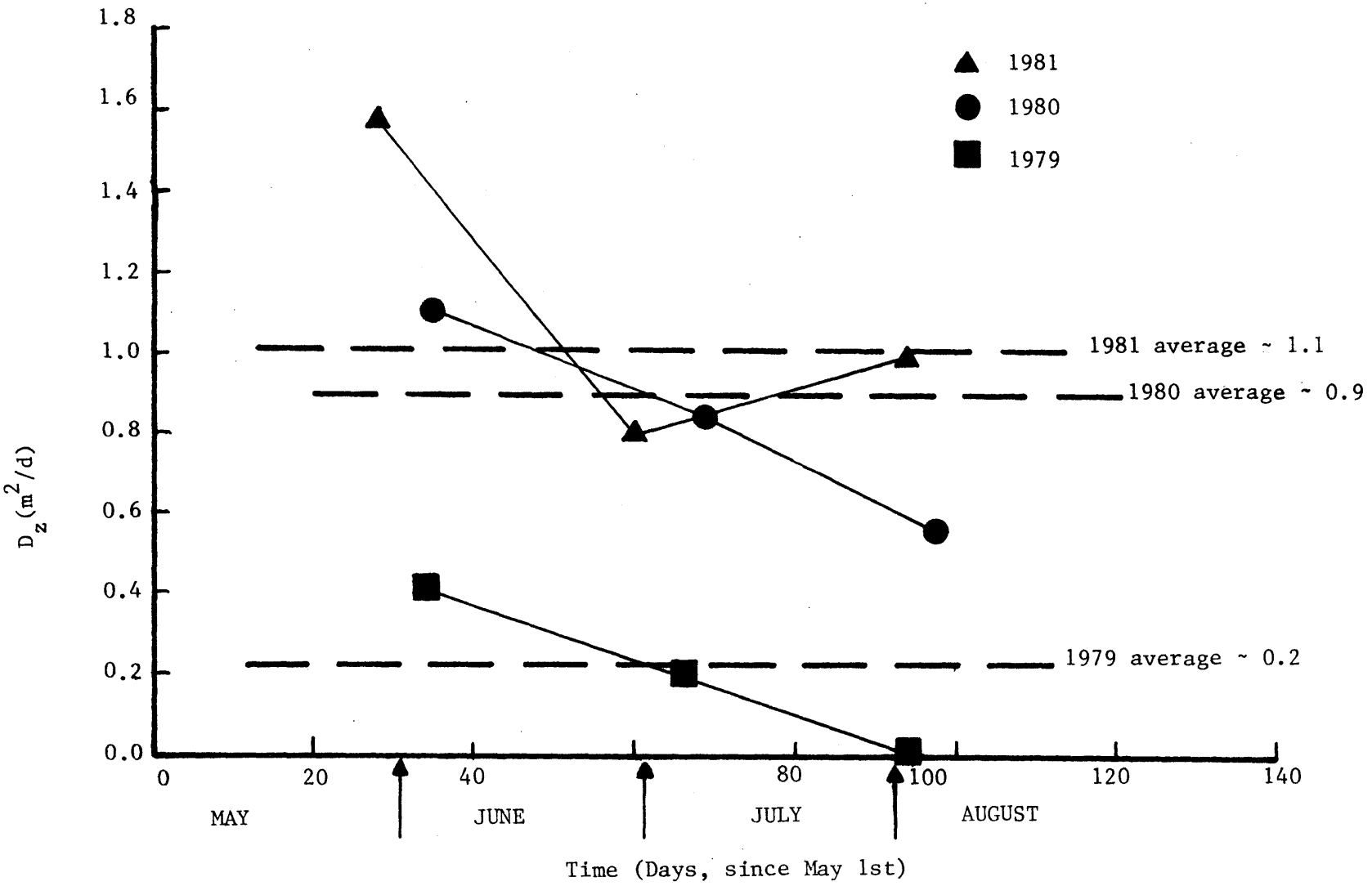

Figure 4.11: Diffusion Coefficients (m^2/d) Over Summer Periods of 1979, 1980 and 1981 at Lake Anna

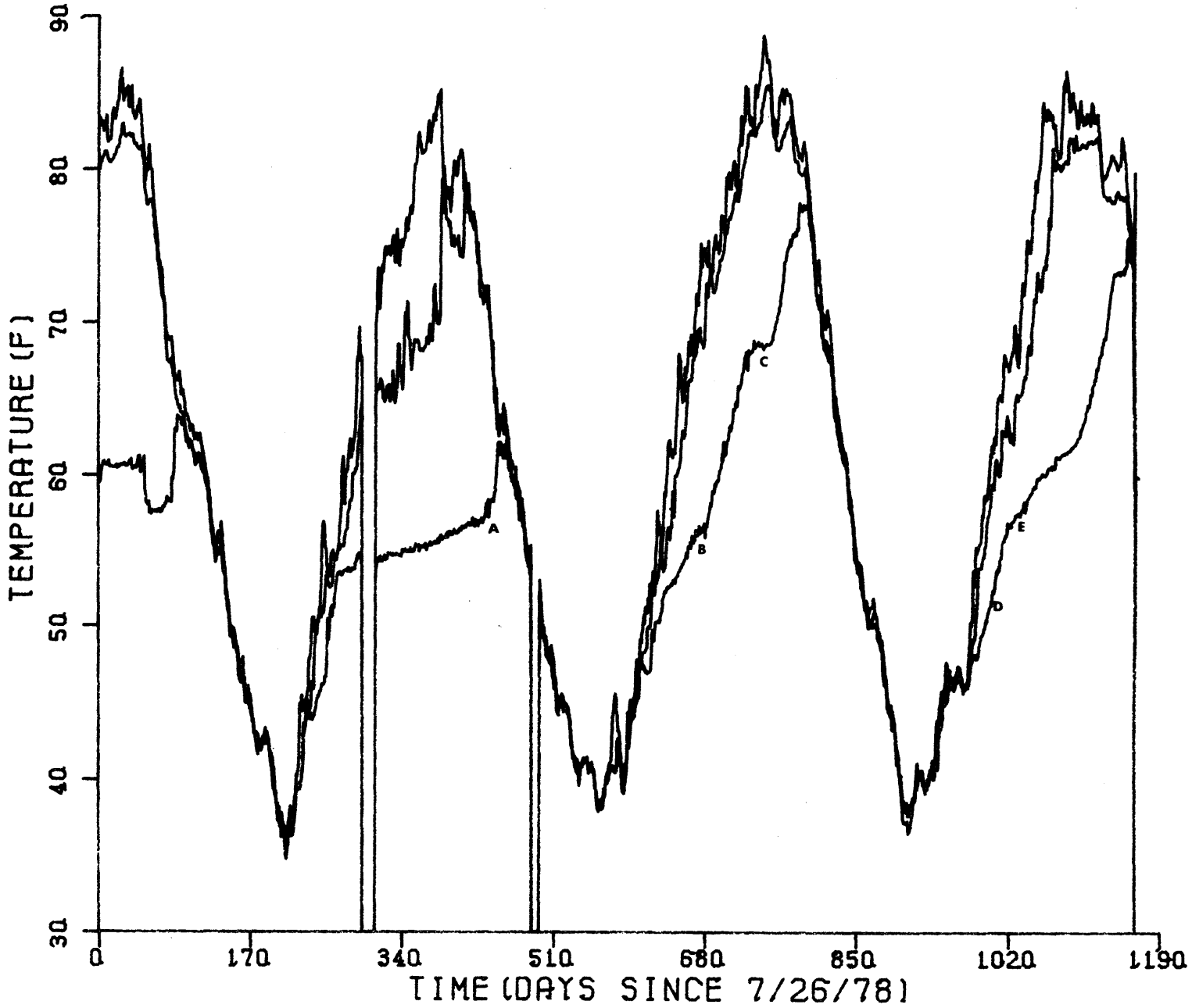

Figure 4.12 Top, Middle and Bottom Temperature in the Main Lake at NRC3

variability and outside forcing processes, several points in Figure 4.12 are marked, corresponding to abrupt changes in the hypolimnetic temperature structure. By referring to Figures 4.13, 4.14, 4.15 and 4.16, which show time series of wind speed, plant flow, and N. Anna River inflow (possible mechanisms for affecting D_z), one can note that each abrupt hypolimnetic temperature change is directly correlated with an external force. Also, the temperature slope change in Figure 4.12 is directly related to the plant flow rate (Q_c) increasing from basically one unit (1979) to two units (1980, 1981). Since no significant inflow occurred in the summer months (except late 1979), summer time hypolimnetic temperatures did not seem to be affected by the inflows (although such an affect would probably be seen during high inflows).

Causality has now been determined, and the functional relationship between D_z and these forcing processes is developed below.

4.2.3.2 Representation of Vertical Diffusion

Several researchers (Imberger et al (1978), Bachmann and Goldman (1965), Powell and Jassby (1974), Bedford and Babajimopoulos (1977), Henderson-Sellers (1976)) have represented D_z in stratified waters as nonstatic functions of geometry, density structure, and shear velocity. Usually the diffusivity function has the general form of

$$D_z = D_{z_o} F \qquad (4.10)$$

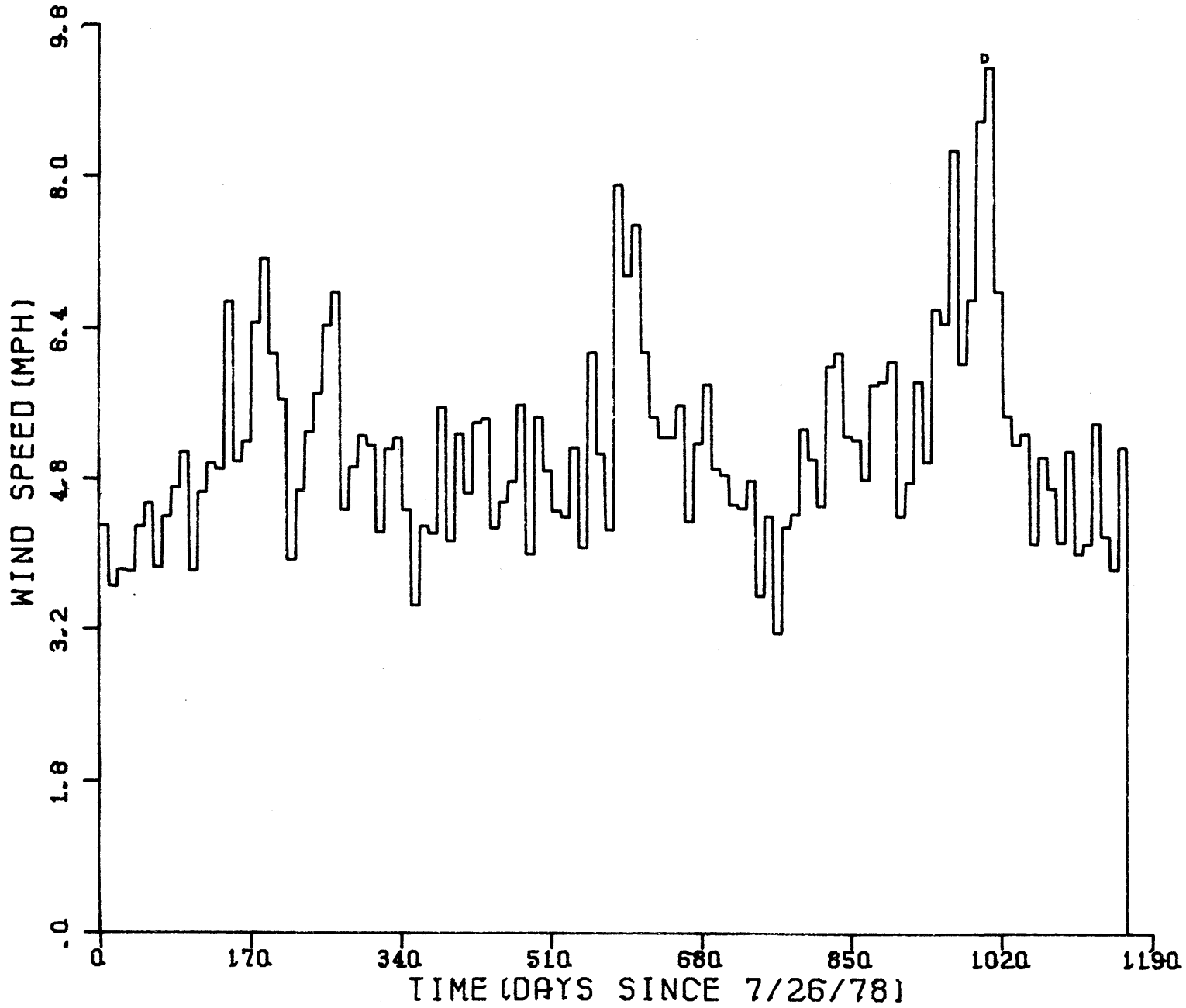

Figure 4.13 Ten-day Averages of Wind Speed at 2 Meters

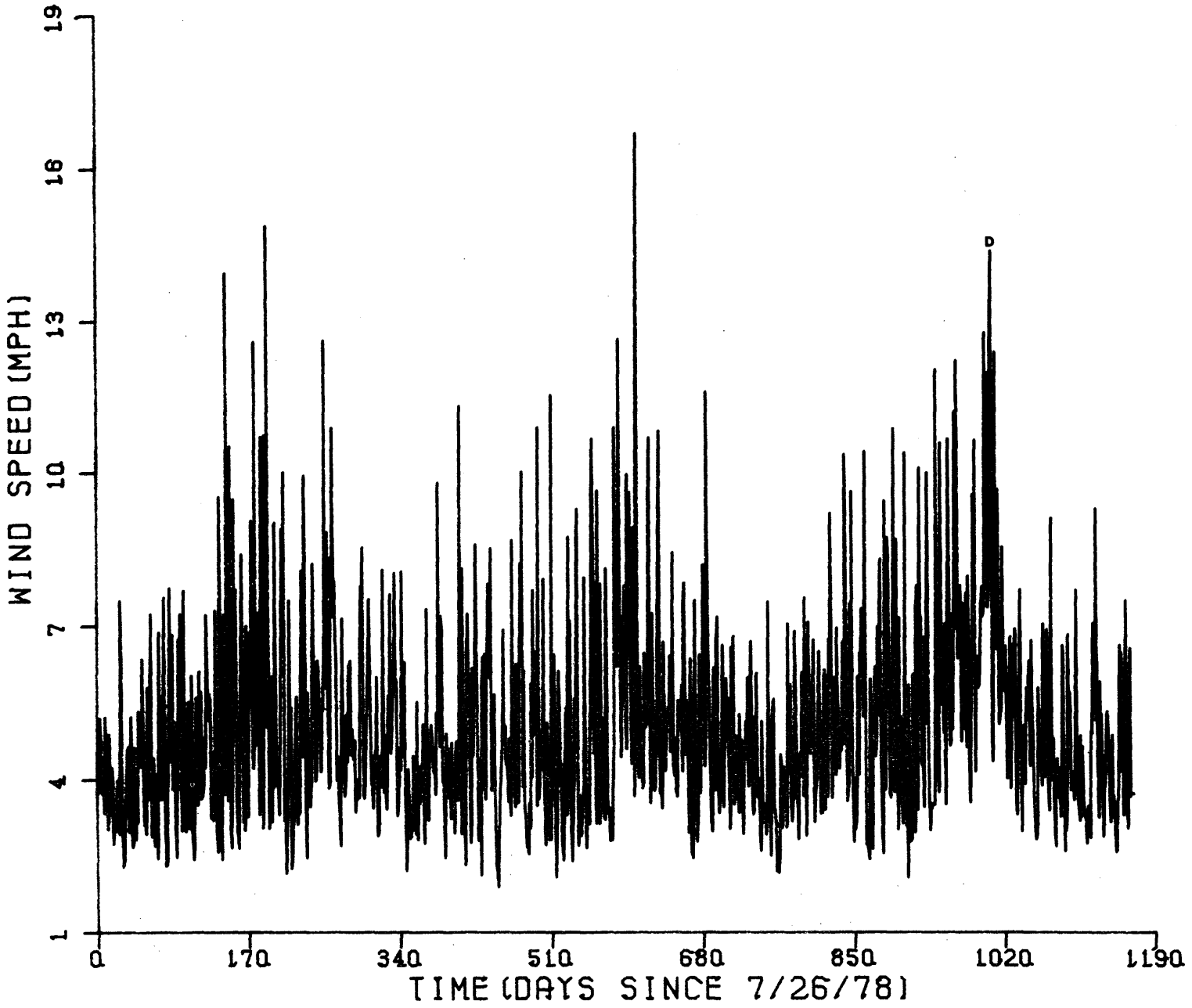

Figure 4.14 Daily Average Wind Speed at 2 Meters

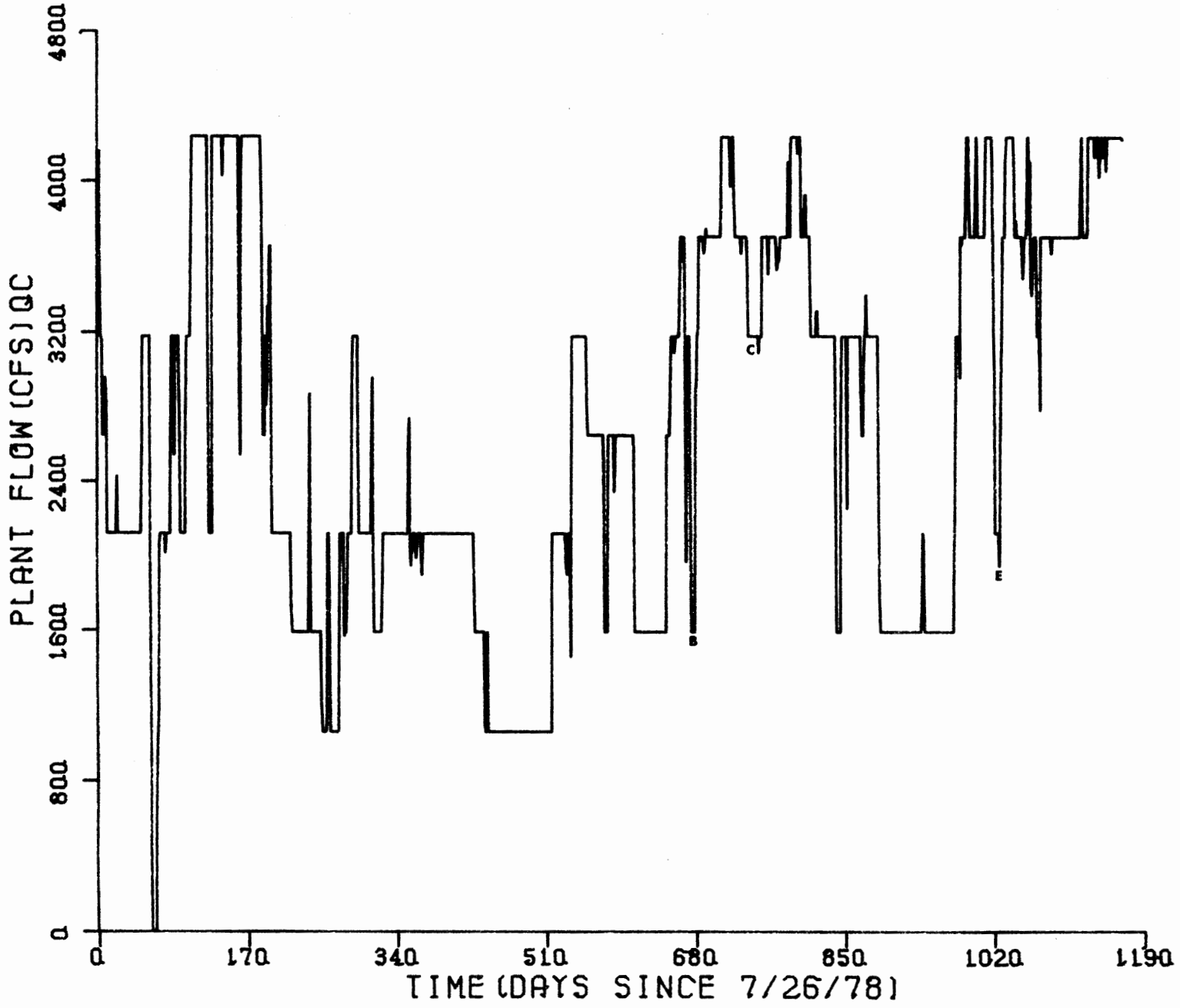

Figure 4.15 North Anna Condenser Plant Flowrate

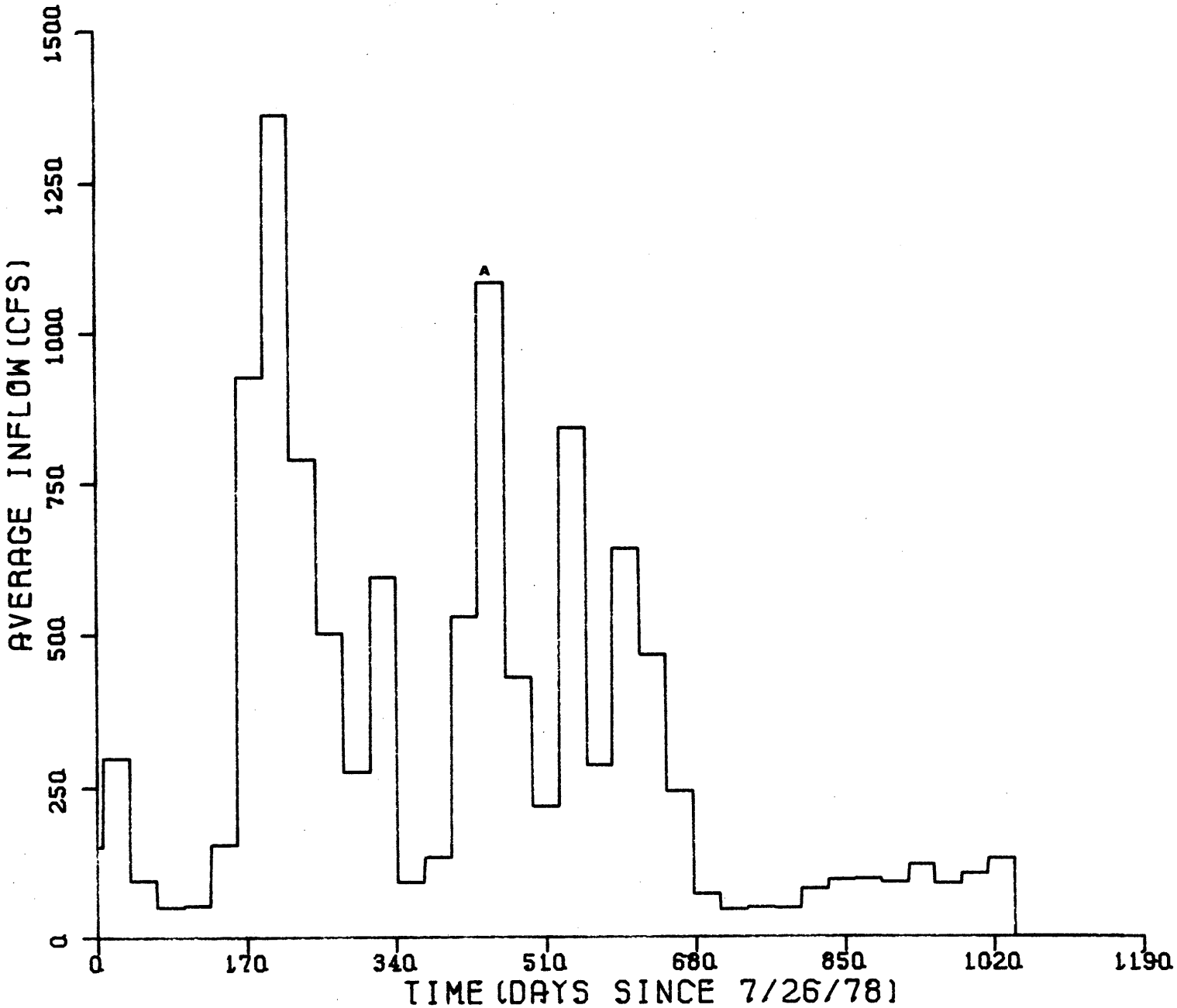

Figure 4.16 Monthly Average Outflows from the North Anna Dam

where F = non-dimensional decay function (variable with depth)

D_{z_o} = diffusion coefficient at the surface (presumably the maximum).

Many different functions have been used to describe the dependence of F on depth (Wells, 1980): linear, parabolic, exponential and dependent on Richardson number.

In the Richardson number formulation, the function F is approximated by

$$F = (1 + \beta \, Ri)^{-m} \tag{4.11}$$

where β, m = empirical constants

Ri = non-dimensional Richardson Number

$$= \frac{-\frac{g}{\rho}\frac{\partial \rho}{\partial z}}{(\frac{\partial u}{\partial z})^2}$$

$\partial\rho/\partial z$, $\partial u/\partial z$ = vertical density and velocity gradients respectively.

Two approximations can be utilized to derive a convenient form of D_z:

(i) $$D_{z_o} = c \, H \, u_* \tag{4.12}$$

where c = empirical constant

H = depth of mixed layer

u_* = shear velocity

(This is a typical formulation for D_z in a well-mixed system - Fischer (1967), Holley et al (1970), Pareek (1977) - as in a river, estuary, or in the epilimnion of a lake.) and

(ii) $$\frac{\partial u}{\partial z} = \frac{1}{\kappa}\frac{u_*}{z} \qquad (4.13)$$

where κ = von Karman constant

z = vertical length scale (average depth of hypolimnion).

Equation 4.10 now becomes:

$$D_z = \frac{c\, u_* H}{\left(1 + \beta\left(\frac{\frac{-g}{\rho}\frac{\partial \rho}{\partial z}}{\left(\frac{1}{\kappa}\frac{u_*}{z}\right)^2}\right)\right)^m} \qquad (4.14)$$

If a depth-averaged value is sought, Equation 4.14 may be reduced to

$$D_z = \frac{A\, u_*^{2m+1}}{(Bu_*^2 + \Delta\rho)^m} \qquad (4.15)$$

where $\Delta\rho$ = density gradient from the top of the hypolimnion to the bottom

A,B = dimensional constants specific to a particular site, with dimensions $M^m T^{2m} L^{-5m+1}$ and MT^2L^{-5} respectively, M = mass, T = time, and L = length.

Therefore, $D_z = D_z(u_*, \Delta\rho)$.

4.2.3.3 Determination of D_z for Lake Anna

Possible sources of u_* in Lake Anna included the plant flow (Q_c), wind (W), and inflows (Q_i), such that $D_z = D_z(Q_c, Q_i, W, \Delta\rho)$. The largest source of shear stress was probably the condenser flow rate. (This dependence was seen in Figure 4.12, as discussed in Section 4.2.3.1).

The hypolimnetic temperature change over time from 1 unit flow (1979) to 2 unit flow (1980, 1981) represented approximately an 8-fold increase, suggesting a cubic dependence on u_* (i.e., m=1). Note that several researchers - Okubo (1971), Koh and Chang (1973), and Lick (1976) - have suggested (on both theoretical and empirical grounds) that m is in the range of from 1 to 2. Also, Sundaram and Rehm (1971, 1973) have chosen m=1 in their studies of diffusion in temperate lakes. Allowing m=1 and B=0, Equation 4.15 becomes

$$D_z = \frac{A u_*^3}{\Delta\rho} \qquad (4.16)$$

The similarity of the D_z formulation developed, i.e., $D_z = D_z(\frac{u_*^3}{\Delta\rho})$, with surface mixed-layer models, such as Octavio et al (1977), Stefan and Ford (1976), and Bloss and Harleman (1979), is of interest in that the mixed layer models incorporate an energy balance between input kinetic energy ($\sim u_*^3$) by the wind and the stable potential energy ($\sim\Delta\rho$) preventing mixing. In a sense, the diluted condenser flow within the surface layer acts on the underlying hypolimnion in a manner similar to the wind acting on the free surface of a lake or reservoir without circulation.

Equation 4.16 produced reasonable agreement between measured and predicted summertime profiles when the proper value of A was selected and u_* was only a function of Q_c. However, better agreement was obtained by incorporating the wind speed as an additional independent parameter in the form,

$$D_z = \frac{\phi(Q_c/Q_o)^3 + \psi((W/W_o)^3 - 1)}{\frac{\Delta\rho}{\Delta\rho_o}} \qquad (4.17)$$

where D_z = vertical diffusion coefficient (m^2/d)

Q_c = daily average condenser flow rate (cfs)

Q_o = condenser flow rate for one unit (cfs)

W = daily average wind speed (mph)

W_o = 5 mph

$\Delta\rho$ = the density difference between the top and bottom of hypolimnion (Kg/m^3)

$\Delta\rho_o$ = 1000 Kg/m^3

ϕ = dimensional constant = 0.90 m^2/d

ψ = dimensional constant = 1.75 m^2/d.

In the approximation of Equation 4.17, if $W/W_o < 1$ and/or $\Delta\rho/\Delta\rho_o < 1$, they were set equal to one. The dependence on wind in Equation 4.17 suggests that it is sustained winds above a certain level - averaged over a 24-hour period - which contributed significantly to vertical mixing.

Equation 4.17 was applied during the critical summertime months. Another equation for D_z, dependent only on $\Delta\rho$, was calibrated to produce good spring, fall, and winter results:

$$D_z = \frac{A}{\Delta\rho^2} \qquad (4.18)$$

where A = dimensional constant = 1.4×10^6 Kg^2/m^4d

$D_z = m^2/d$

$\Delta\rho = Kg/m^3$.

The constant A accounted for similar effects each fall, winter, and spring - the plant flow, winds, and inflows. Due to the very strong functional and physical dependence on the density gradient, the constant A worked well each of the simulation years, even though W, Q_i, and Q_c varied. This means that the D_z formulation was insensitive to changes in Q_c, Q_i and W during those times but was dependent almost wholly on the stability of the lake, i.e., $\Delta\rho$.

In the winter, the value of D_z, computed from Equation 4.18, was constrained to a maximum of 60 m^2/d. This did not alter the results but saved considerable computational time. (The vertical model uses an explicit time scheme which required, for purposes of numerical stability, $D_z \frac{\Delta t}{(\Delta z)^2} \leq \frac{1}{2}$; if this criterion was not met, the time step was lowered, thus increasing computational time when D_z was very large.)

The decision as to when Equation 4.17 (summer) or 4.18 (winter, spring, fall) was to be used depended on which was larger. Figure 4.17 shows these two equations as a function of $\Delta\rho$ for 1, 2 and 3 unit flow and no wind.

4.3.3.4 Summary of Vertical Diffusion Analysis

According to Figure 4.18, the time series plot of D_z utilized in the model gives reasonable agreement with the calculated average D_z

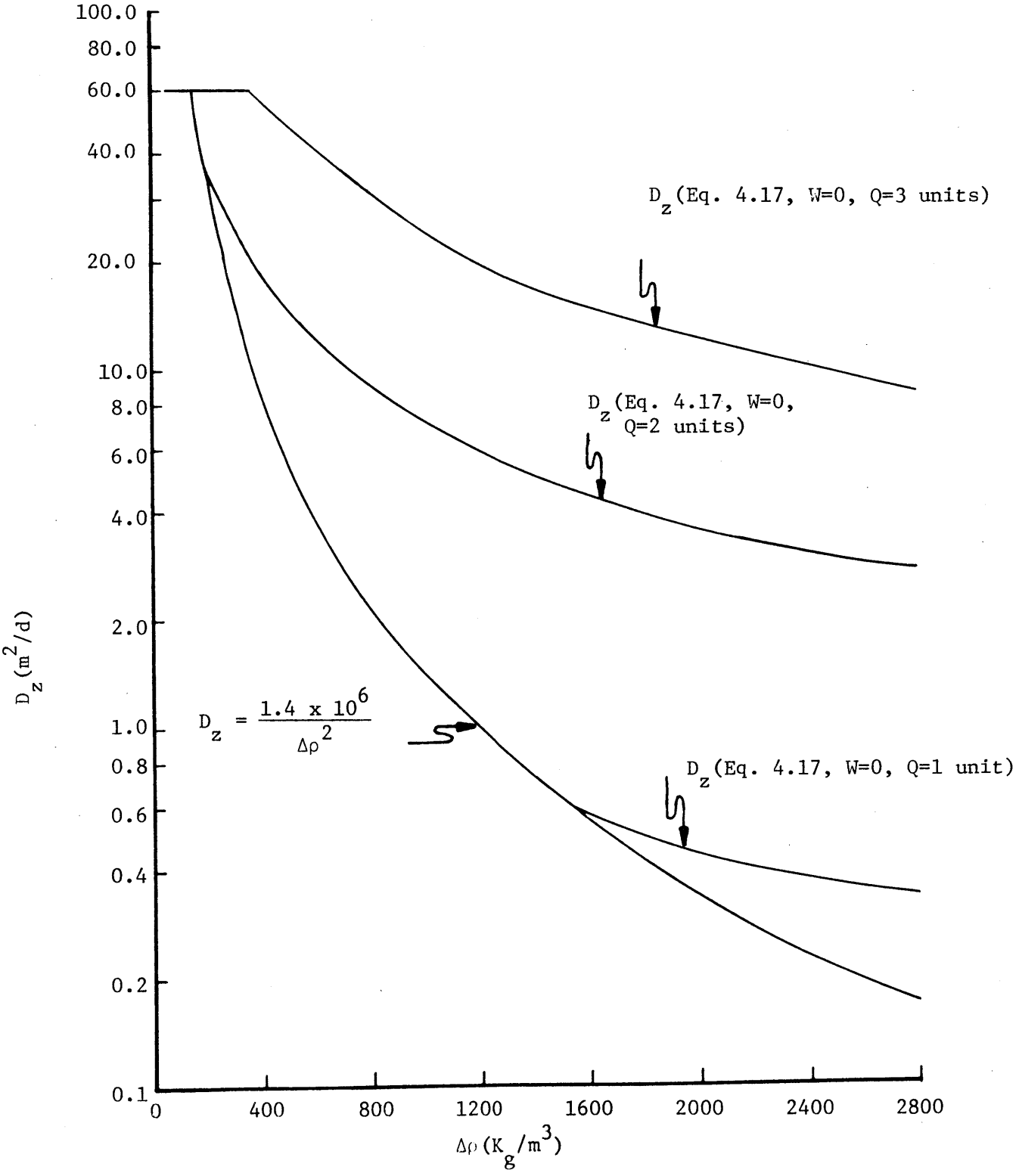

Fig. 4.17 Magnitude of Diffusion Coefficients Used in the N. Anna Model

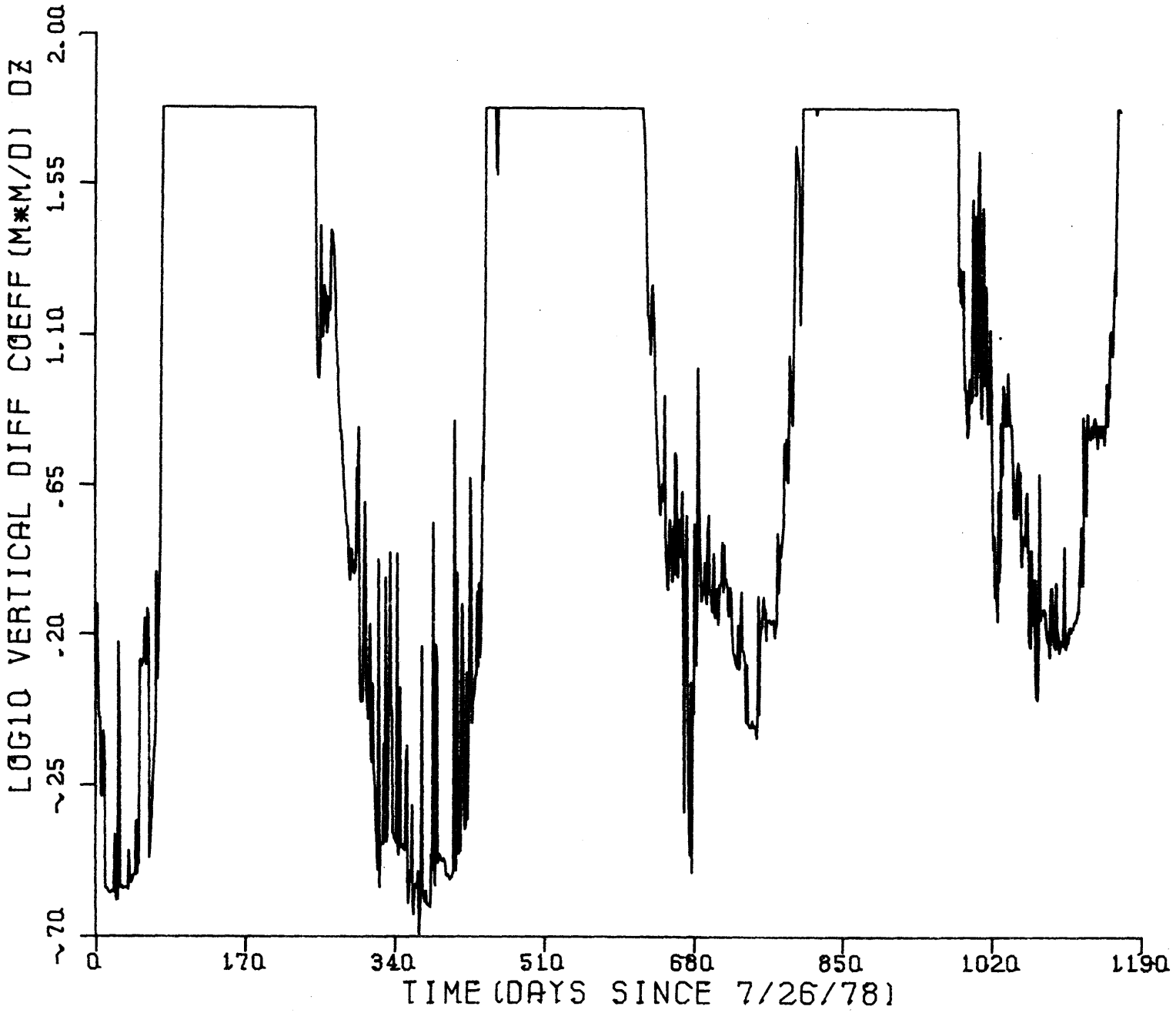

Figure 4.18: Calculated Vertical Diffusion Coefficient Used in the Main Lake Model

from the field data in Figure 4.11. Noteworthy is the dynamic nature of the wind in influencing vertical diffusion (large summer-time spikes in D_z), even though the average controlling forcing function was the plant flow. As shown in Chapter 5, the use of the aforementioned functional forms of D_z gave good agreement on a month-to-month basis for the vertical temperatures over a 3 year period.

4.3 WHTF Analysis

The following features of the WHTF were analyzed:

(i) lag time and filtering criteria

(ii) flow and mixing characterization of the reaches and canals

(iii) side arm flow dynamics.

4.3.1 Lag Time and Filtering Analysis

The WHTF was formulated in a steady-state framework because an adequate transient analysis was not available. However, this raised the fundamental question: how does one utilize a steady-state analysis to predict transient events?

Inherent in the development of the original steady state WHTF model was a residence time, lagging criterion. A residence time (t_r) was dynamically computed for each reach, and the temperature at the end of the reach was determined at time t using formulae provided in Chapter 3 based on lagged input values:

$$T(t) = f(Q(t-t_r), K(t), T_E(t), T_o(t-t_r)) \quad (4.19)$$

where T_o = upstream temperature in reach

K = surface heat exchange coefficient

T_E = equilibrium temperature

Q = plant flow rate

T = temperature at end of reach.

This lagging allowed for a measure of transience, but was inadequate since meteorological variability acted over the entire period of t_r days, rather than on one day t. Thus WHTF temperatures computed with Equation 4.19 showed too much variability (not enough damping).

Better transient representation was obtained by averaging, or filtering, the meteorological input variables over the residence time of the reach. The exponential filter, described by Adams and Koussis (1980), was implemented for filtering both T_E and K.

Whereas in arithmetic averaging an equal weighting was given to each day, in exponential filtering the filtered variable was a result of an exponentially decaying weighting over the residence time (see Figure 4.19). The equation used to describe the filter for T_E (and similarly for K by substituting K for T_E) was

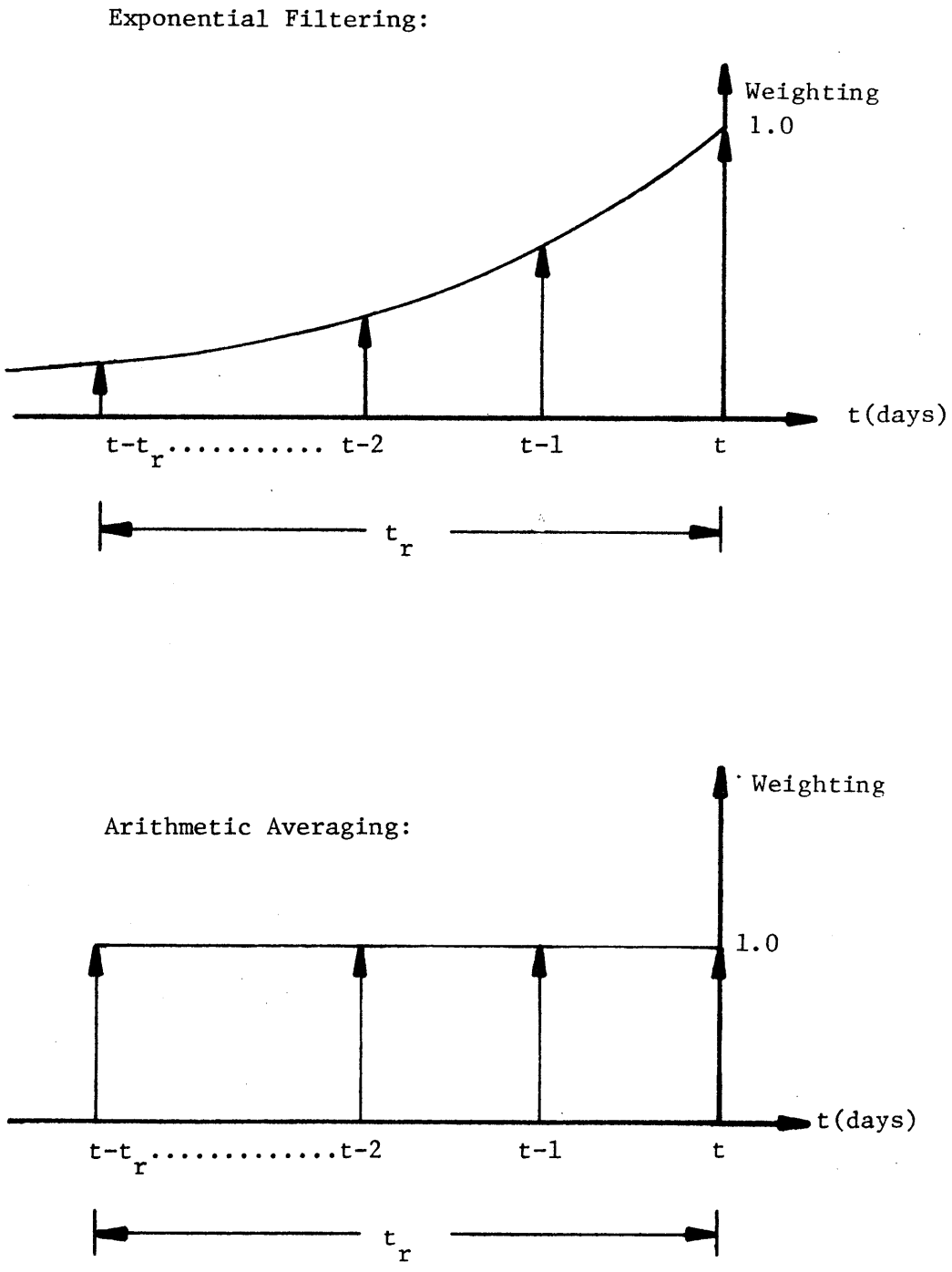

Figure 4.19: Comparison between Exponential Filtering and Arithmetic Averaging

$$\langle T_E(t)\rangle = \frac{\sum_{n=1}^{t_r/\Delta t} T_E(t-n\Delta t)\exp(-(n-1)k'\Delta t)}{\sum_{n=1}^{t_r/\Delta t} \exp(-(n-1)k'\Delta t)} \qquad (4.20)$$

where k' = kinematic surface exchange coefficient = $\frac{K'}{\rho c_p h}$

h = average depth of pond (18 ft. for each reach)

$\langle\ \rangle$ = filtered variable

Δt = time step (one day)

K' = filter surface heat exchange coefficient.

The filtered variable was weighted according to the residence time of the reach, i.e., the filter weighting went back t_r days, and the sum of the weights was then normalized to one. Slightly different procedures were used to compute residence times for $\langle T_E\rangle$ and $\langle K\rangle$. For $\langle K\rangle$ residence times for each reach and side arm were computed dynamically; i.e., once each day. For $\langle T_E\rangle$, an average residence time for the three reaches was determined based on one third of the volume of the WHTF (including side-arms) and based on weekly average flow rates. This residence time was 14, 7 and 3.5 days for 1, 2 and 3 units. Figure 4.20 summarizes the procedure for calculating $\langle T_E\rangle$ and $\langle K\rangle$.

Since calculation of $\langle T_E\rangle$ or $\langle K\rangle$ required a value of K', a problem arose as to how to determine this coefficient a priori Instead of iteration, an average K' was evaluated from curves in

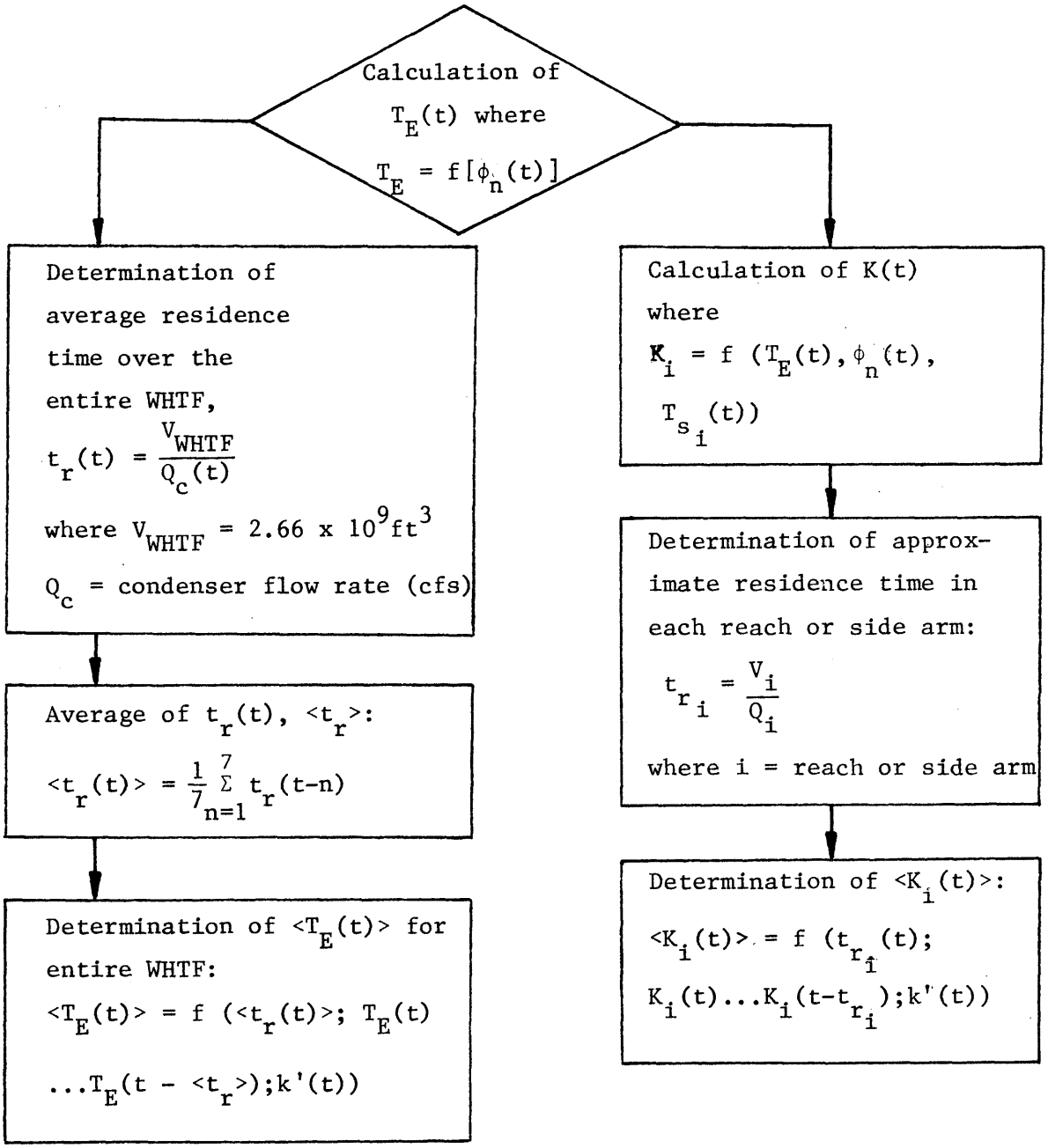

Figure 4.20: Calculation Technique for $<T_E>$ and $<K>$

Ryan and Harleman (1973) based on Lake Anna average wind speeds, Lake Anna average air temperatures, and average surface temperatures as a function of heat flux:

$$K' = A + B \cos\left[\frac{2\pi}{365.25} (DAY + 182)\right] \qquad (4.21)$$

where DAY = Julian Day

A,B = constants dependent on stated heat flux

$\frac{Q_c x \Delta T_c}{(cfs\ ^{o}F)}$	A	B
10,000-35,000	154	60
35,000-70,000	165	62
>70,000	179	64

For full load operation with 3 units, Equation 4.21 predicts K' ranging from 115 (winter) to 243 (summer) BUT/ft^2-°F-day.

In essence, the lag time filter procedure replaced the (steady) value of T_E in Equations 2.11 through 2.18 with $\langle T_E(t) \rangle$. Thus for a pond m with no side arm

$$T_m(t) = \langle T_E(t) \rangle + [T_{m-1}(t-t_{r_m}) - \langle T_E(t) \rangle]\, e^{-kt_{r_m}} \qquad (4.22)$$

The lagging and filtering combination resulted in a much smoother and accurate prediction of transient temperatures throughout the WHTF. To illustrate the extent of this filtering, Figures 4.21 and 4.22 show time series plots of T_E and $\langle T_E \rangle$ for the three simulation years 1978-1981.

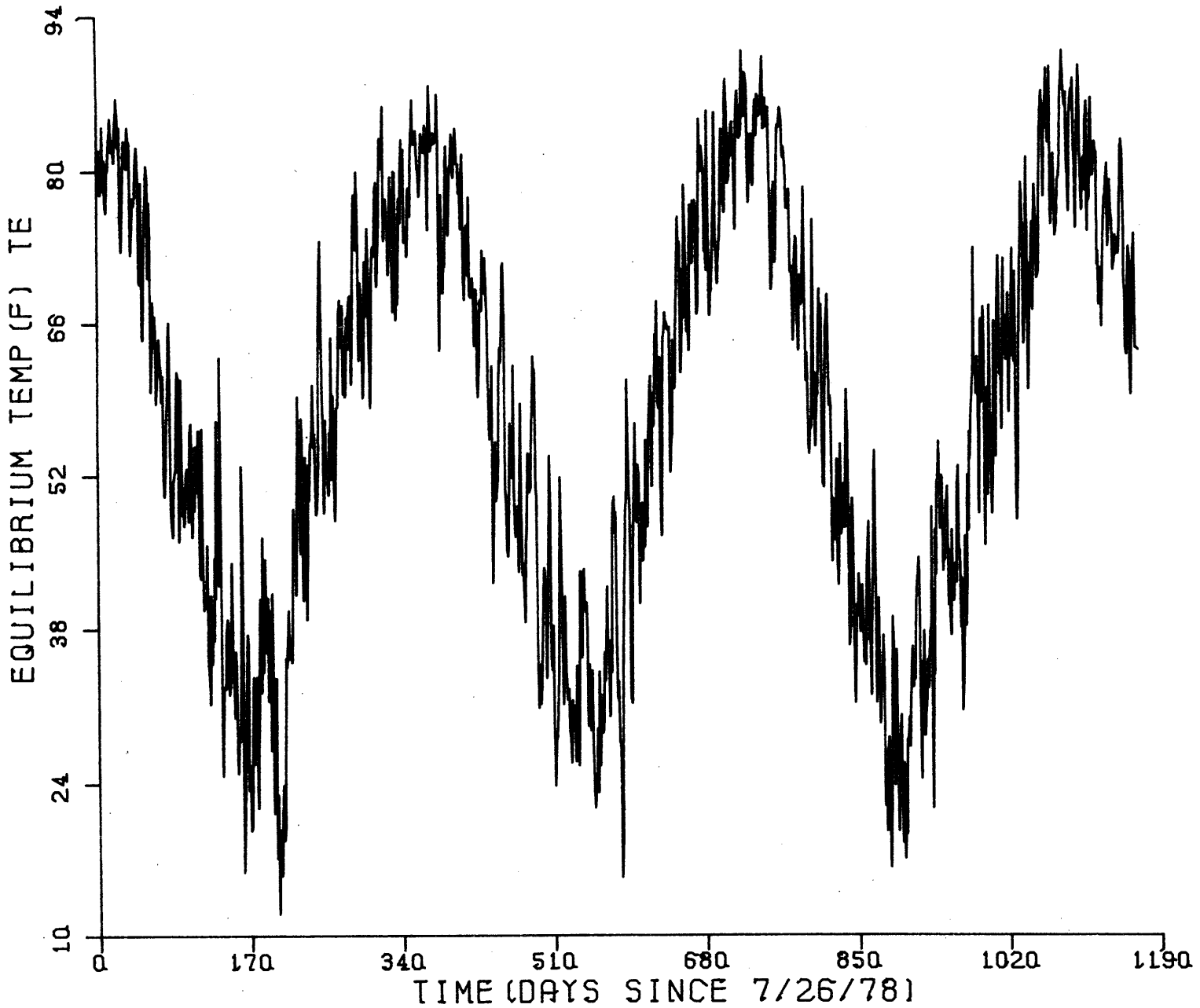

Figure 4.21: Unfiltered Equilibrium Temperatures at Lake Anna

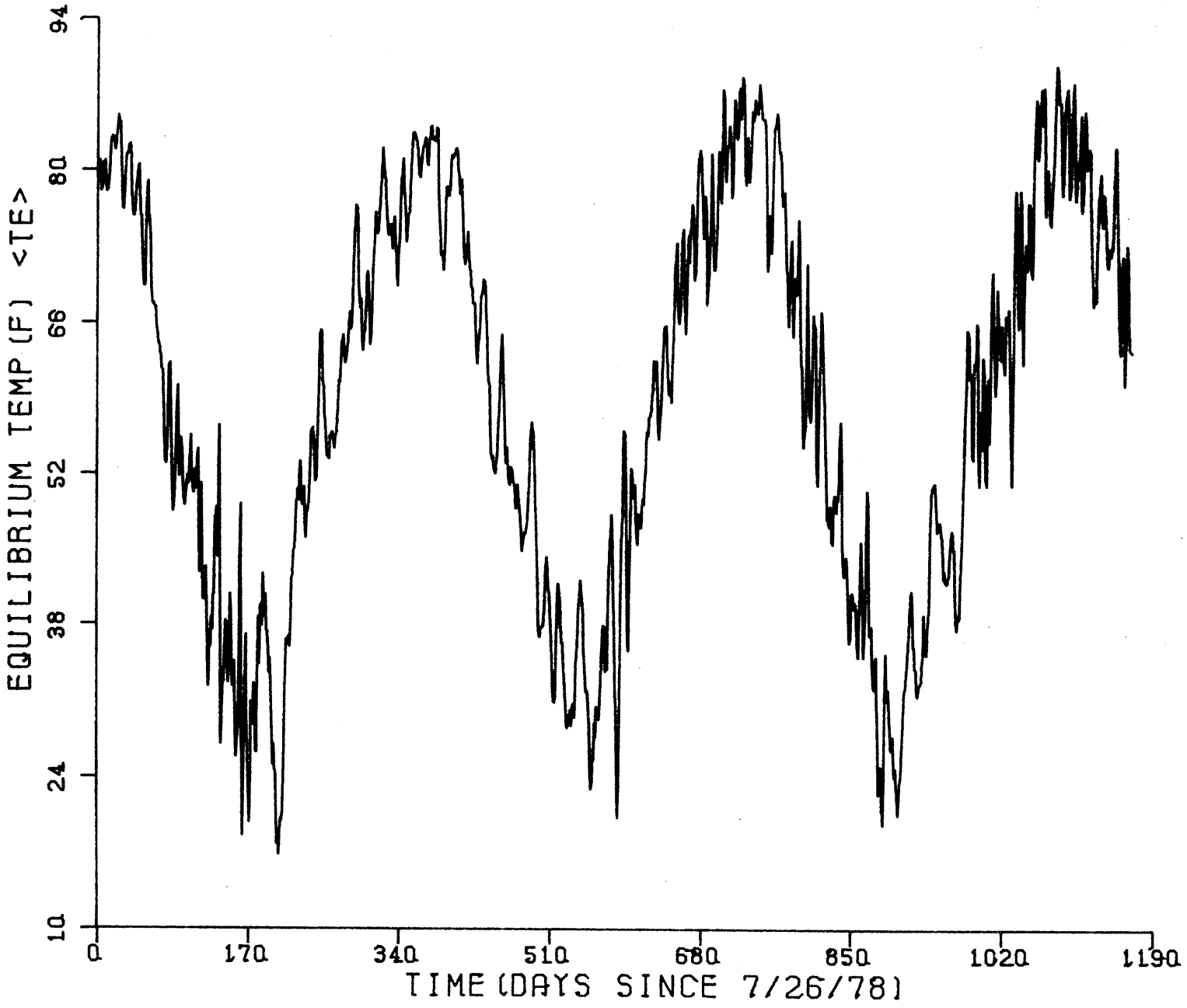

Figure 4.22: Filtered Equilibrium Temperatures for the WHTF at Lake Anna

4.3.2 Analysis of Flow and Mixing Characteristics of WHTF Reaches and Canals

Several assumptions were made regarding the WHTF reaches and the interconnecting side-arms:

(i) the canals were vertically fully-mixed and exhibited plug flow in the longitudinal direction;

(ii) the entrance mixing (dilution) from each canal into the following reach was characterized by Equation 2.2; and

(iii) two-layer flow was postulated for the reaches based on an upper layer depth calculation (Equation 2.21). The validity of these characterizations is examined below.

4.3.2.1 Temperature Structure in the WHTF Canals

Because of the expected value of the densimetric Froude number within the canals (see Section 2.1.1), these canals were modeled as vertically well-mixed. Data taken in these canals verified this assumption. Representative temperature profiles in canal 2 and canal 3 are shown in Figures 4.23 and 4.24 as station WHTF 7 and WHTF 8, respectively (see Figure 3.2).

4.3.2.2 Entrance Dilution within the WHTF

Similar to the Dike III mixing analysis presented in Section 4.2.1, the dilution predicted by the model at the entrance of each reach was compared to actual dilution calculations.

The equations used to compute dilution from the field data were

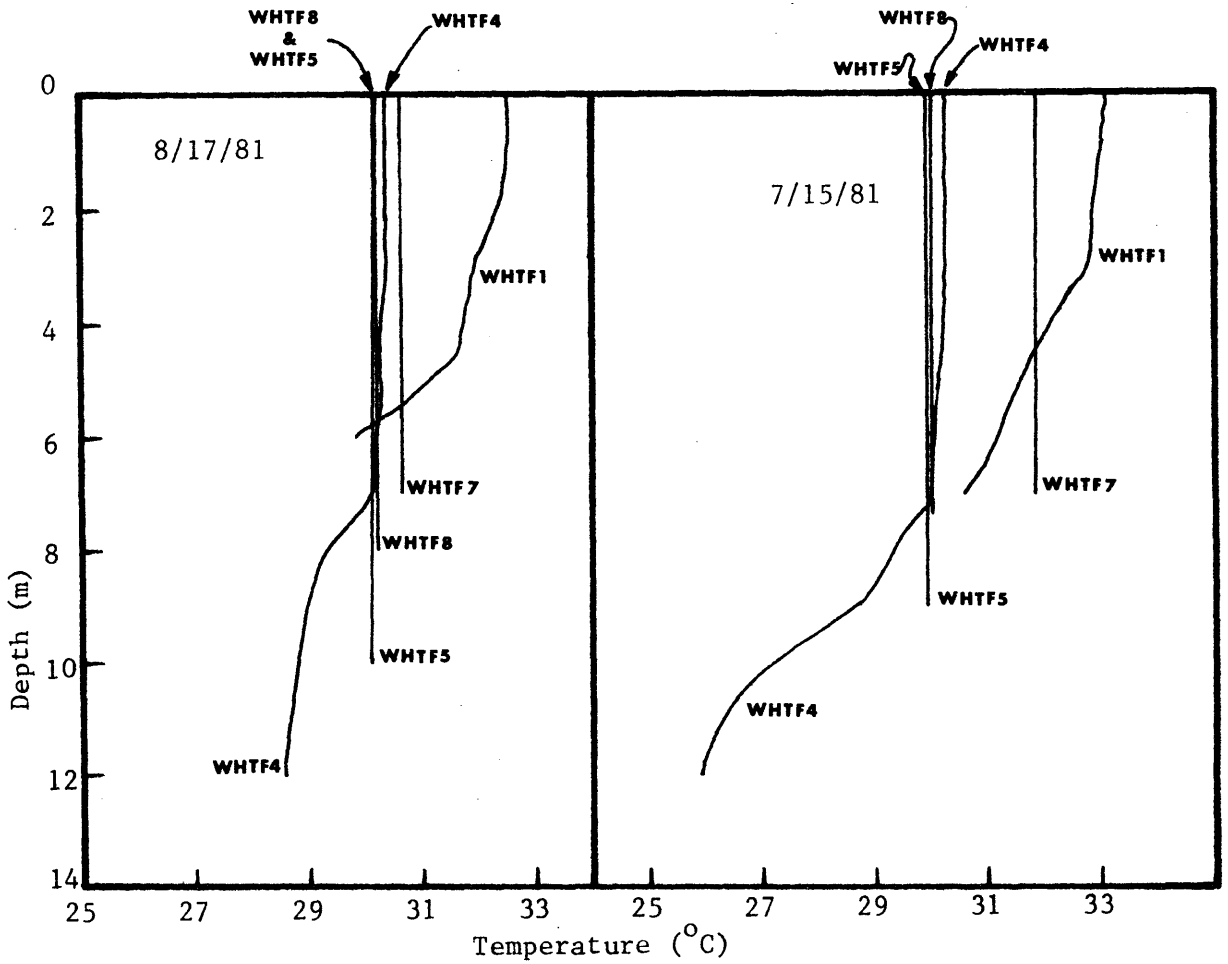

Figure 4.23: Temperature Profiles Throughout the WHTF for Typical Summer Conditions

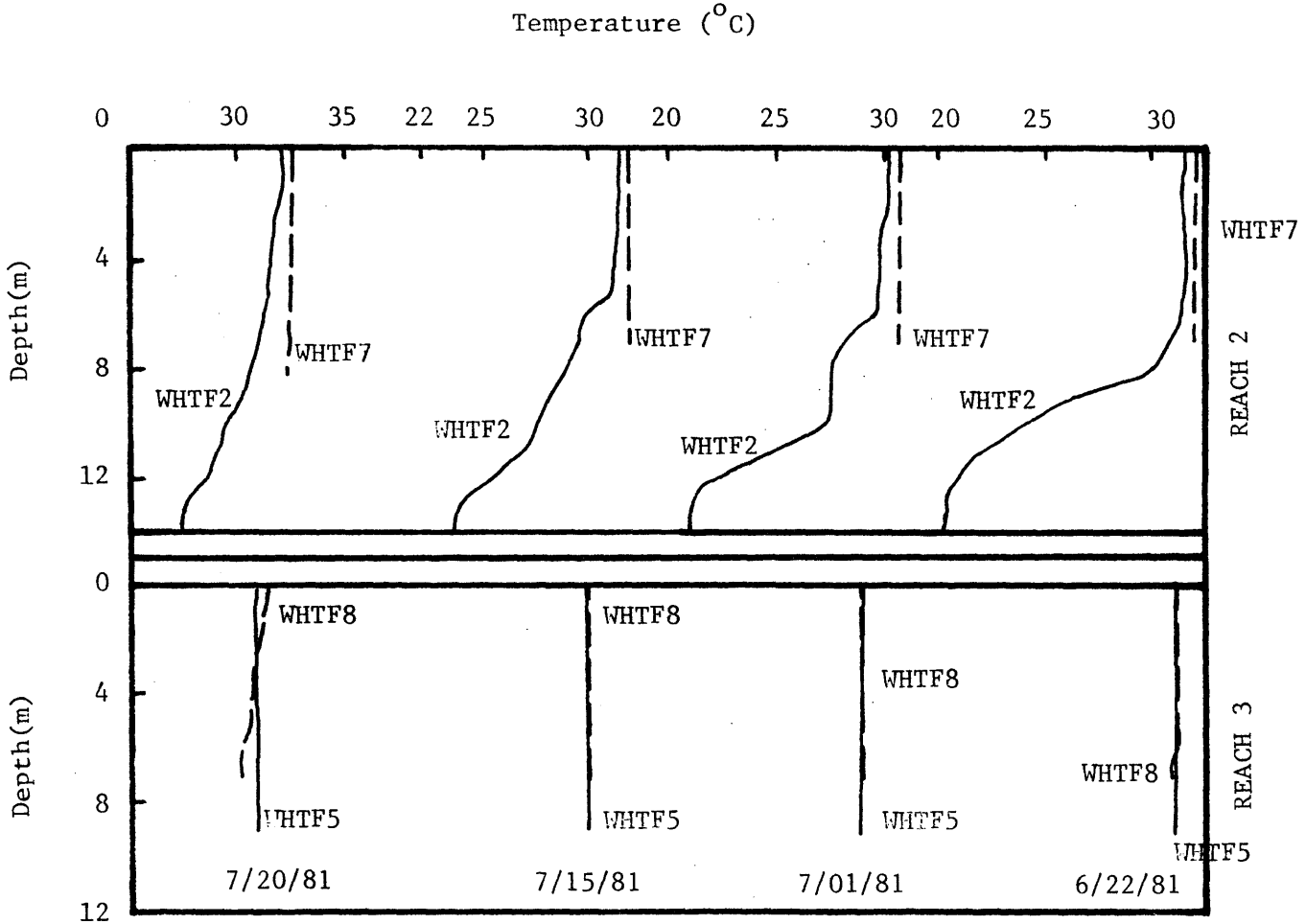

Figure 4.24: Entrance Dilution Temperature Profiles.

$$D_s(\text{Reach } 2) = \frac{T_{top}(\text{WHTF7}) - T_{bottom}(\text{WHTF2})}{T_{top}(\text{WHTF2}) - T_{bottom}(\text{WHTF2})} \qquad (4.23)$$

and

$$D_s(\text{Reach } 3) = \frac{T_{top}(\text{WHTF8}) - T_{bottom}(\text{WHTF5})}{T_{top}(\text{WHTF5}) - T_{bottom}(\text{WHTF5})} \qquad (4.24)$$

where WHTF2, WHTF7, WHTF8, WHTF5 are locations shown in Figure 3.2

top = average upper layer temperature

bottom = average bottom layer temperature

(Note that an accurate calculation for dilution into Reach 1 was not possible since temperature profiles were not taken in Reach 1 at distinct locations in the discharge canal and in the reach.)

Figure 4.23 shows typical temperature profiles for Reaches 2 and 3 that were utilized to compute the entrance dilution, and Table 4.2 compares calculated dilution with those predicted from Equation 2.2 for Reach 2. Since the water entering Reach 3 was typically well-mixed, the entrance dilution was not easily analyzed from the data; however, dilution was not a critical parameter for the model in Reach 3.

The dilutions calculated from the data and the model were very low, and any attempt to further reduce this dilution through physical modifications of the entrance canals seems unwarranted (see

Table 4.2 Predicted and Observed Entrance Dilution in Reach 2

Date	Observed Dilution	Predicted Dilution
5/29/81	1.2	1.9
6/02/81	1.4	1.6
6/12/81	1.5	1.6
6/15/81	1.4	1.9
6/22/81	1.2	1.9
7/01/81	1.2	1.7
7/15/81	1.1	1.7
7/20/81	1.3	1.9
7/29/81	1.4	1.8
8/05/81	1.5	1.9
8/10/81	1.2	1.9
8/17/81	1.3	1.7
Average	1.3	1.8

Note: The dilution calculated from the profiles in Figure 4.23 is from average top and bottom temperatures, i.e., these values are higher than would otherwise be determined if the actual top and bottom values were utilized.

Section 7.2.1). The good agreement between the model and the data for D_s was indicative that the entrance mixing was being modeled properly.

4.3.2.3 Temperature Structure in the WHTF Reaches

Typically, according to data, Reaches 1 and 2 usually showed some two layer flow, whereas Reach 3 was fully mixed. This is illustrated in Figure 4.23 where temperature profiles in each of the reaches and canals are shown during one day.

Table 4.3 details typical model predictions for the upper-layer depth on several representative summer days for each of the three reaches (compare 7/15/81 and 8/17/81 with Figure 4.24).

The model accurately predicted that Reach 3 was fully mixed and that Reach 2 showed some degree of stratification. With regard to Reach 1, usually the data showed that a stratified system predominates, but the model only predicts stratification intermittently. According to Figure 4.23 (note WHTF1 vs. WHTF7 profiles), there is somewhat more heat loss occurring in Reach 1 than is being predicted by the model. This would explain the fact that the model's downwelled temperature at the end of Reach 1 was a little high, thus leading to less predicted stratification than observed.

Basically, though, the fluid mechanics of the reaches and of the canals was modeled accurately.

Table 4.3 Model Predictions of the Upper Layer Depths in Each of the WHTF Reaches

	Upper Layer Depth Prediction (Ft)		
Date	Reach 1	Reach 2	Reach 3
5/13/81	22.8	15.7	25.0*
6/12/81	25.0*	19.2	25.0*
7/15/81	25.0*	22.2	25.0*
8/17/81	25.0*	22.0	25.0*
9/17/81	25.0*	21.0	25.0*

Note: the maximum depths in these reaches were schematized at 25 feet.

*fully mixed

4.3.3 Side Arm Analysis

Equations 2.4 and 2.8 were developed to determine the side arm flow and return temperature as a function of the upper layer depth, T_E, K, and the side arm geometry. During the calibration stages a number of assumptions in the development of these equations were re-examined and the flow predictions were compared with side arm flow field data.

4.3.3.1 Criteria for Side Arm Flow

Side arm flow should persist as long as there is a favorable longitudinal gradient of hydrostatic pressure in the side arm. This gradient exists because of the increase in water density as the flow cools from its temperature T_o at the side arm entrance towards the equilibrium temperature T_E. However if $T_o < T_E$ or if $T_o < 4^oC$ (39^oF) the motive force is removed and side arm flow should cease.

The equilibrium temperature often exceeded T_o when the plant was inoperative and when there were hot days. Actually, some type of reverse flow regime would probably be set up in the side arm during these conditions.

When the temperature of inflowing water into the side arm reaches its maximum density of 39^oF, it should sink and initiate a return flow at that point. Thus, if the initial temperature were 39^oF or less, no side arm flow was allowed. (This usually occurred during winter periods when the plant was inoperative.) Similarly, when T_o was greater than 39^oF, some side arm flow was allowed, but the downwelled temperature was not allowed to go below 39^oF even if T_E was much less

than $39^{o}F$. In this case, the area utilized to cool the side arm flow, the "effective" area, would be less than the given area, since downwelling would in effect take place, not at the end of the side arm, but at the point where the temperature became $39^{o}F$. In Equations 2.13 - 2.18, the r_{s1} and r_{s2} factors were then altered by the "effective" area, i.e. the area necessary to cool T_o down to $39^{o}F$ (found by inverting Equation 2.8).

A related aspect of the side arm flow which was analyzed was the calculation of the coefficient of thermal expansion, β. Ideally, β should be evaluated in Equation 2.4 at the average of T_o and T_F (the return temperature). The original model calculated β at T_o, which led to a slight overestimate of the side arm flow, q_o. Note that $q_o = \left[f(\beta)^{1/3}\right]$. Instead of an iteration scheme, a reasonable estimate of T_f was made a priori by means of

$$T_f^* = T_o - 0.6(T_o - T_E) \qquad (4.25)$$

where T_f^* is an estimate of the return temperature; β was then evaluated at $\frac{T_o + T_F^*}{2}$ rather than at T_o.

4.3.3.2 Analysis of Side Arm Flow Theory

Side arm flow takes place as the result of a hydrostatic pressure gradient set up by the elevated temperature at the side arm entrance. This hydrostatic motive force is resisted by the fluid inertia and by bottom and interfacial friction acting along the side arm. A steady-state balance among these forces yields, in essence, the predicted flow rate given by Equation 2.4.

Major features of both the Elk Creek and the Mill Pond Creek side arms (which are not accounted for by the theory) are the bridge constrictions. Not only may these constrictions contribute head loss (thus reducing the flow), but if they are sufficiently narrow, they may constrict the flow by creating a densimetrically critical control section. In this case

$$\mathbb{F}_1^2 + \mathbb{F}_2^2 = 1 \tag{4.26}$$

where $\mathbb{F}_1$ and $\mathbb{F}_2$ are the Froude numbers of upper and lower layers. Equation 4.26 can be re-written

$$\frac{Q_{1c}^2}{W_{b_1}^2 h_1^3 g \frac{\Delta\rho}{\rho}} + \frac{Q_{2c}^2}{W_{b_2}^2 h_2^3 g \frac{\Delta\rho}{\rho}} = 1 \tag{4.27}$$

where $Q_{1,2c}$ = critical side arm flow in layer 1 and 2

$W_{b_{1,2}}$ = width at the bridge in each layer

$h_{1,2}$ = depth of each layer.

If it is assumed that $W_{b_1} = W_{b_2} = W_b$ and $Q_1 = Q_2 = q_{oc}W$, then the governing equation for a critically controlled entrance is

$$\frac{q_{oc}}{kL} = \left[B\left[\frac{1}{h_o}^3 + \frac{1}{(1-h_o)}^3 \right] \left(\frac{W}{W_b} \right)^2 \right]^{-1/3} \tag{4.28}$$

Note in Equation 4.28 that q_{oc} is the flow rate per unit width in the full side arm (past the constriction) and W is the schematized side arm width.

If the head loss embodied in Equation 2.4 (that due to bottom and interfacial friction) plus the additional head loss due to the bridge constriction allow less side arm flow than the critical conditions predicted by Equation 4.28, then Equation 2.4, adjusted by the contraction's effect on h_o, would be the proper equation; otherwise Equation 4.28 should apply.

In order to make such a comparison, the head loss due to the constriction was evaluated. Refer to Figure 4.25 . Following Jirka et al (1977), the change in surface elevation $h_o - h_o'$ as the flow moves through the contraction is given by

$$\frac{\Delta\rho}{\rho}(h_o - h_o')\,H = \frac{q_o^2}{2gH^2}\left[\frac{1}{h_o^2} + \frac{1}{(1 - h_o)^2}\right]\left[\left(\frac{A}{A_b}\right)^2 - 1\right] \qquad (4.29)$$

where A_b = area of the contracted opening

A = area of the channel immediately past the contraction

Equation 4.29 was developed in analogy with the head loss expression for free surface flow and requires that the two-layer flow be sub-critical and that the interface elevation change be small.

In order to compare the sub-critical and critical flow equations, estimates were made for W_b/W and A_b/A. Based on the actual average W_b and the model schematized W, W_b/W was determined to be 0.12 for Elk Creek and 0.18 for Mill Pond Creek. Since W was representative of the entire side arm (over which heat loss takes place), but not of the region immediately past the contraction, the ratio of areas A_b/A differs from W_b/W; for Elk Creek $A_b/A \simeq 0.16$ while for Mill Pond Creek $A_b/A \simeq 0.13$ (see Figure 3.4a and 3.4b). Table 4.4 compares predicted

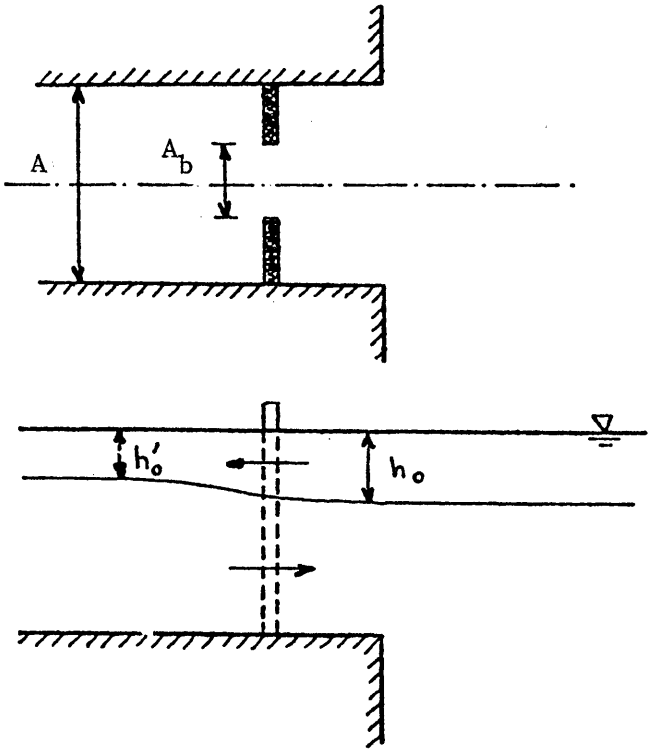

Figure 4.25: Lateral constriction near the entrance of a side arm.

Table 4.4 Comparison of Predicted Critical and Non-critical Flows in the WHTF Side Arms

Variables	q_o (ft^2/s) - Elk Creek[1]			q_o (ft^2/s) - Millpond Creek[2]		
	no constr. (Eq. 2.4)	head loss (Eqs. 2.4, 4.29)	crit flow (Eq. 4.28)	no constr. (Eq 2.4)	head loss (Eqs. 2.4, 4.29)	crit. flow (Eq. 4.28)
Summer met.[3], f_o = 0.02						
α = 0.5, h_o = 0.5	2.85	2.39	1.46	2.85	2.16	1.78
α = 0.5, h_o = 0.3	2.14	1.42	1.08	2.14	1.31	1.31
α = 1.0, h_o = 0.5	2.34	2.07	1.46	2.34	1.91	1.78
α = 1.0, h_o = 0.3	1.71	1.29	1.08	1.71	1.17	1.31
Winter met.[4], f_o = 0.02						
α = 0.5, h_o = 0.5	1.56	1.25	0.80	1.56	1.12	0.97
α = 0.5, h_o = 0.3	1.17	0.77	0.59	1.17	0.68	0.72
α = 1.0, h_o = 0.5	1.28	1.10	0.80	1.28	1.01	0.97
α = 1.0, h_o - 0.3	0.94	0.68	0.59	0.93	0.61	0.72

Notes:

(1) for Elk Creek, L = 15000', H = 40'

(2) for Mill Pond Creek, L = 12000', H = 40'

(3) Summer meteorological conditions: $T_e = 85^oF$, $T_o = 99^oF$, K = 225 BTU/ft^2-^oF-day

(4) Winter meteorological conditions: $T_e = 40^oF$, $T_o = 54^oF$, K = 150 BTU/ft^2-^oF-day

side arm flows for Elk Creek and Millpond Creek: (1) assuming no influence of the constriction (Equation 2.4), (2) assuming flow is subcritical, but that the contraction contributes headloss (based on Equation 4.29; flow computed with Equation 2.4 with h_o' substituted for h_o) and (3) assuming critical flow (Equation 4.28).

Considering both Millpond and Elk Creek sidearms, the expected reduction in q_o from Equation 2.4 if the head loss at the constriction is considered would be from 16-42% (for $\alpha = 0.5$ and $f_o = 0.02$), while for critical flow conditions this reduction would range from 38-50%.

Largely on this basis, the side arm flow predictions of Equation 2.4 for both side arms have been multiplied by 0.5 to account for anticipated critical flow at the constrictions. (Additional factors accounting for the reduction to 50% are discussed below.) Comparison with hand held velocity measurements at both side arm and with continuous measurements at Elk Creek indicate generally good agreement with a small tendency to underpredict flow in the winter and overpredict in the summer. (See Section 4.3.3.3.)

The continuous measurements at Elk Creek have also been used to compute the densimetric Froude numbers according to Equations 4.26 or 4.27. These measurements indicate that the flow is generally subcritical. This might indicate that the effective resistance to flow is greater than that represented by $f_o = 0.02$ and $\alpha = 0.5$, that the actual head loss is greater than predicted in Equation 4.29, or that the upper layer depth predicted by Reach 2 was too large. A more thorough analysis of the flow is warranted.

In addition to the anticipated occurrence of critical flow, another factor was responsible for reducing the estimate of flow predicted by Equation 2.4. This factor is concerned with the relationship between side arm flow rate and temperature loss. Obviously these are inter-related because it is the temperature loss which drives the flow and vice versa. The most precise calculations would employ iteration. To avoid iteration, however, an approximation was made to arrive at Equation 2.4. Without this approximation, Equation 2.4 would be written.

$$\frac{q_o}{kL} \; r_1^{-1/3} = B_f^{-1/3} \tag{4.31}$$

where $r_1 = \exp(-kLX/q_o) = \exp(-.8kL/q_o)$

$B_f^{-1/3}$ = RHS of Equation 2.4

For small values of kL/q_o ($kL/q_o < 0.3$) r_1 can be approximated as unity yielding Equation 2.4. However, using typical parameter values for Elk Creek ($L = 15{,}000$, $q_o = 0.625$ cfs/ft, $k = 3.7 \times 10^{-5}$ ft/s) yields $kL/q_o = .89$. In this case the approximation to the integral introduces an error of approximately 20% when Equation 2.4 rather than 4.31 is used.

Summarizing the analysis of side arm flow theory, a significant decrease in the side arm flow from Equation 2.4 would be expected based on theoretical grounds. In order to approximate this reduction equally in all the WHTF side arms, the side arm flow predicted from Equation 2.4 was reduced by 50%. This reduction factor is consistent with the orders of magnitude justified above on theoretical grounds and yields reasonable agreement between predicted and measured flows, particularly during summer. See the following section.

4.3.3.3 Analysis of Side Arm Flow Measurements

The extensive data collected in the WHTF side arms were used (i) to compare model predictions and data, (ii) to examine the assumption that downwelling occurs at the end of the side arm, (iii) to examine the adequacy of basing side arm flow calculations on daily - averaged data, and (iv) to investigate the criticality of flow at the Elk Creek bridge constriction.

As discussed in Chapter 3, two types of data were analyzed: (i) the portable velocity and temperature profiles taken weekly at Elk Creek and Mill Pond Creek and (ii) the continuous two-hour records of current velocity, direction, and temperature at Elk Creek. Figure 4.26 shows typical longitudinal-vertical cross-sections of temperature along Elk Creek as well as vertical velocity profiles at the Elk Creek bridge constriction. Flow rates were computed for the upper layer from these velocity profiles and are compared with predicted flow rates in each figure. In computing the flow rate, velocities were assumed to be horizontally uniform over the local channel width. Also shown on the figure are predicted entrance and exit temperatures which can be compared with the measured isotherms.

In general, the measured velocity structure fits the two layer assumption used in the model development and the measured and predicted flow rates show generally good agreement. The data can also be used to check the model assumption that downwelling occurs at the end of the side arm rather than as a continuous process along the side arm. The isotherms in Figures 4.26 suggest that this is the case on many of the dates, but that on others, downwelling occurs at intermediate points.

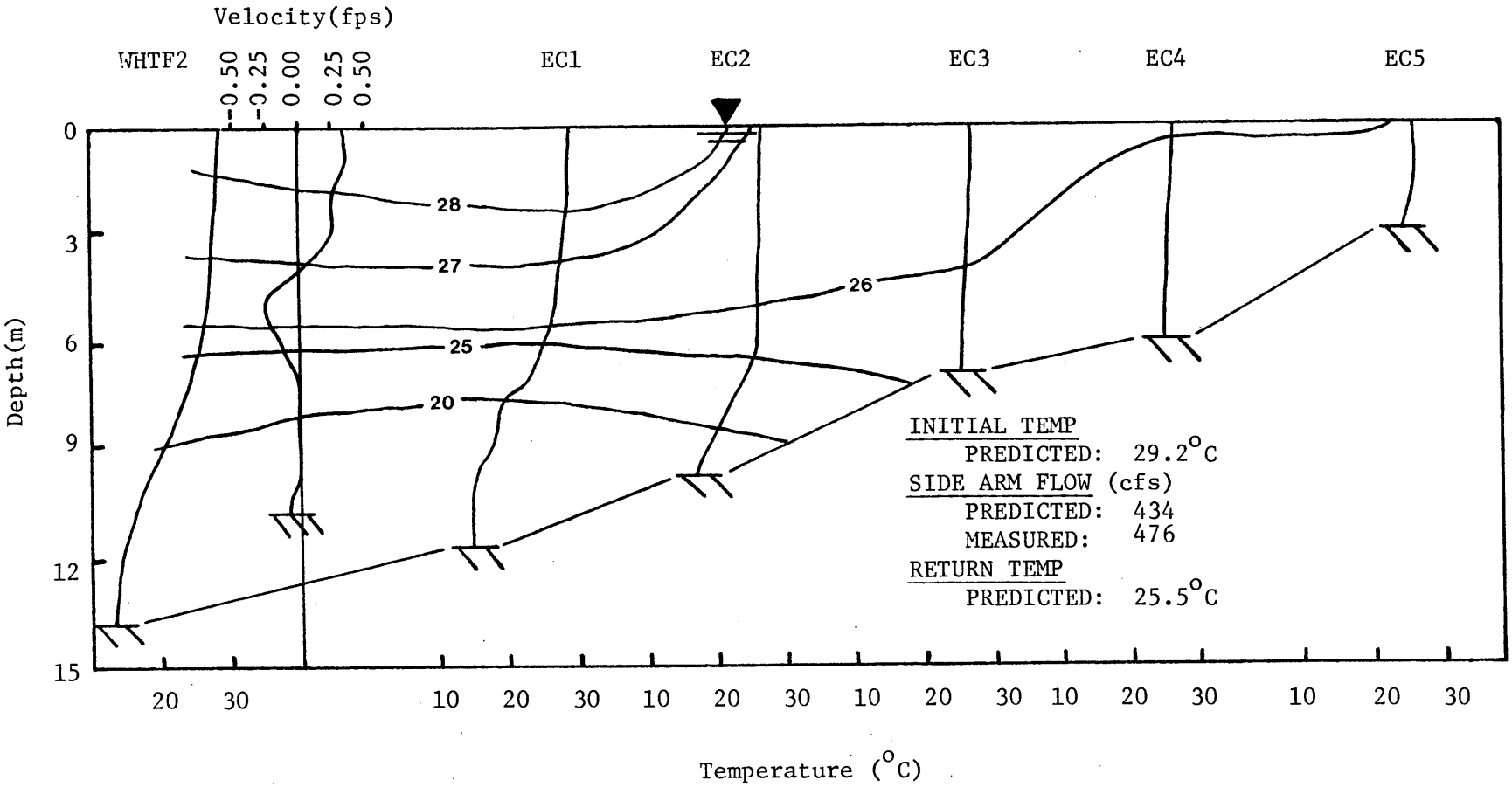

Figure 4.26a: North Anna Lake, Elk Creek Sidearm Analysis for 6/18/79

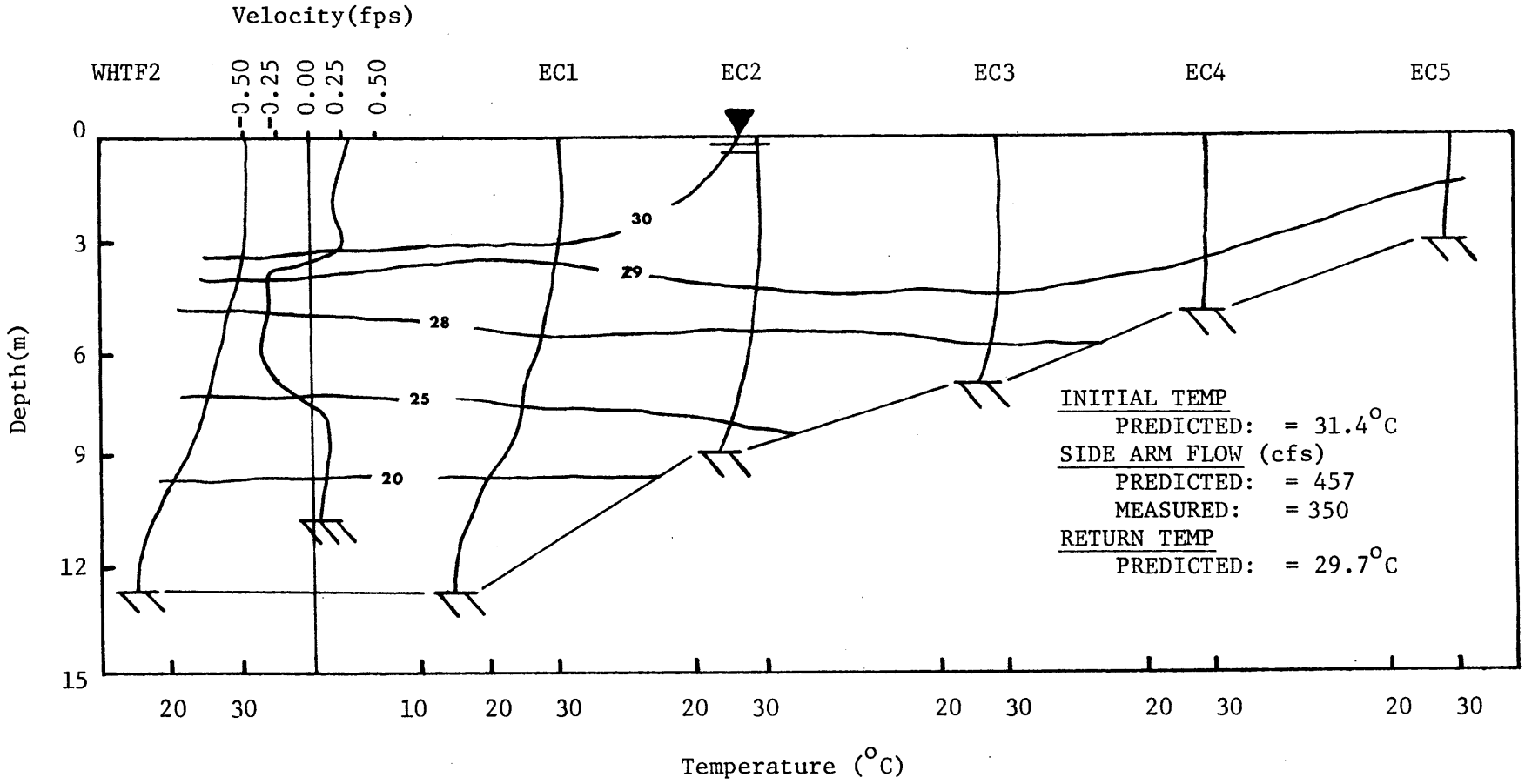

Figure 4.26b: North Anna Lake, Elk Creek Sidearm Analysis for 7/16/79

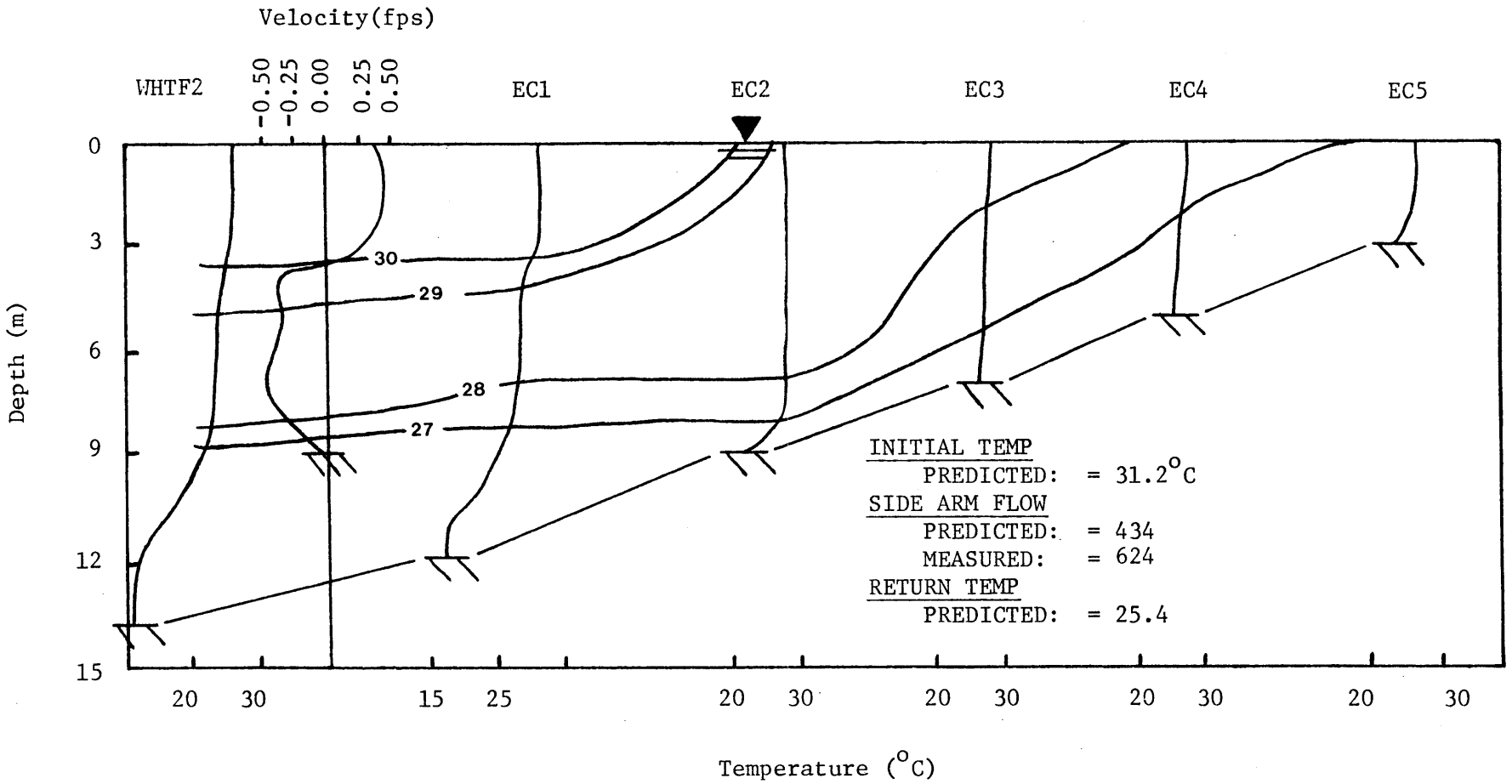

Figure 4.26c: North Anna Lake, Elk Creek Sidearm Analysis for 8/13/79

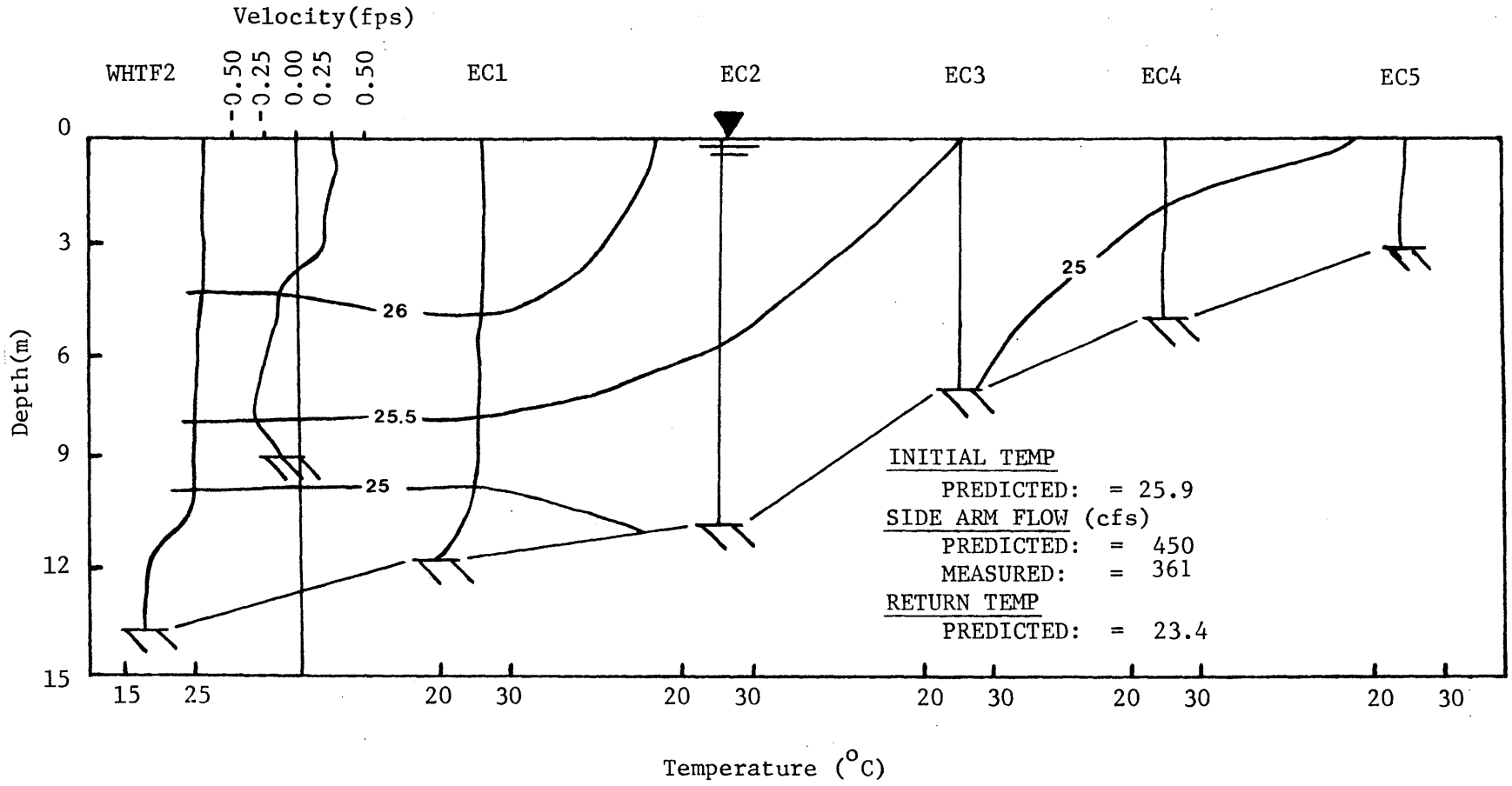

Figure 4.26d: North Anna Lake, Elk Creek Sidearm Analysis for 9/17/79

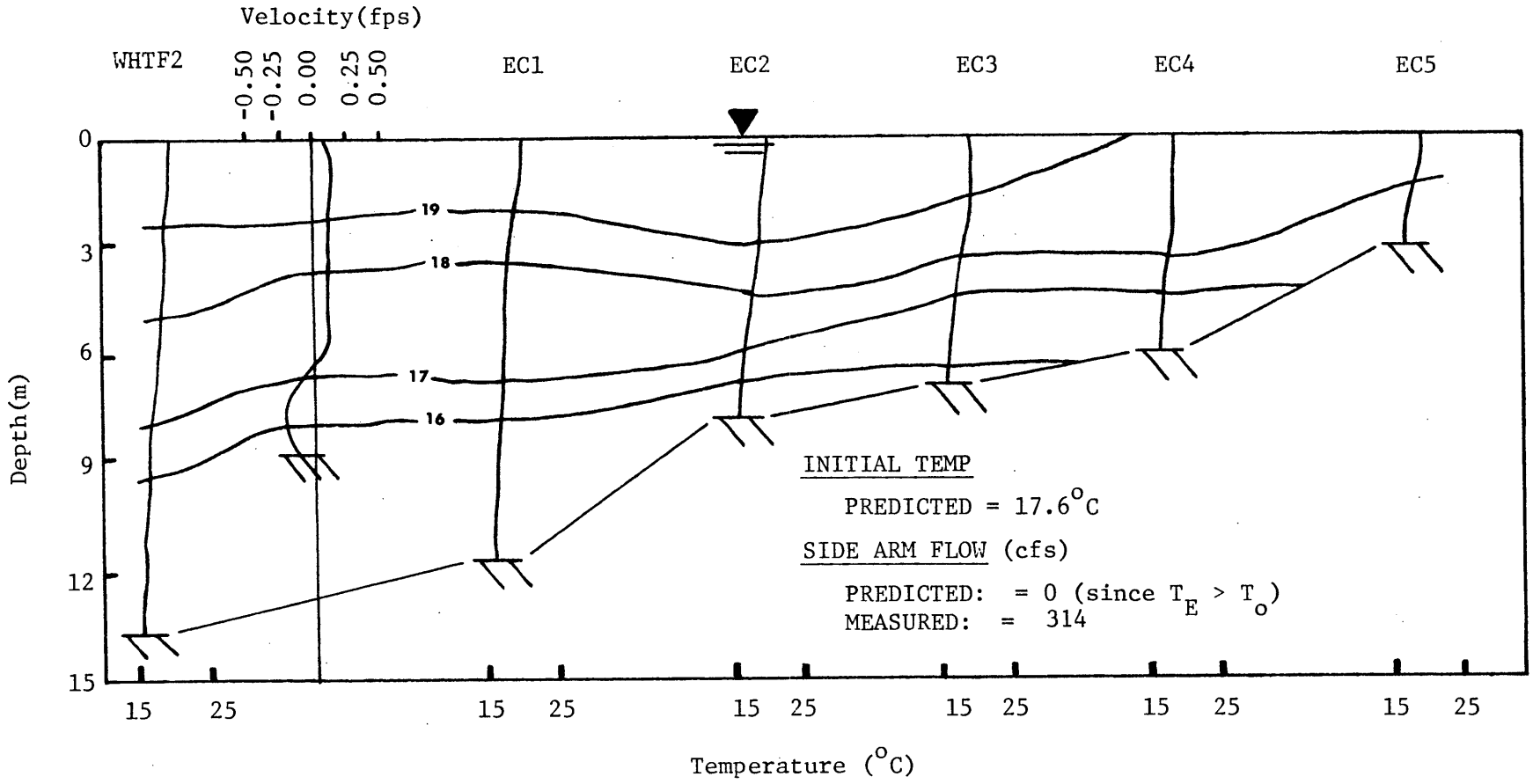

Figure 4.26e: North Anna Lake, Elk Creek Sidearm Analysis for 10/22/79

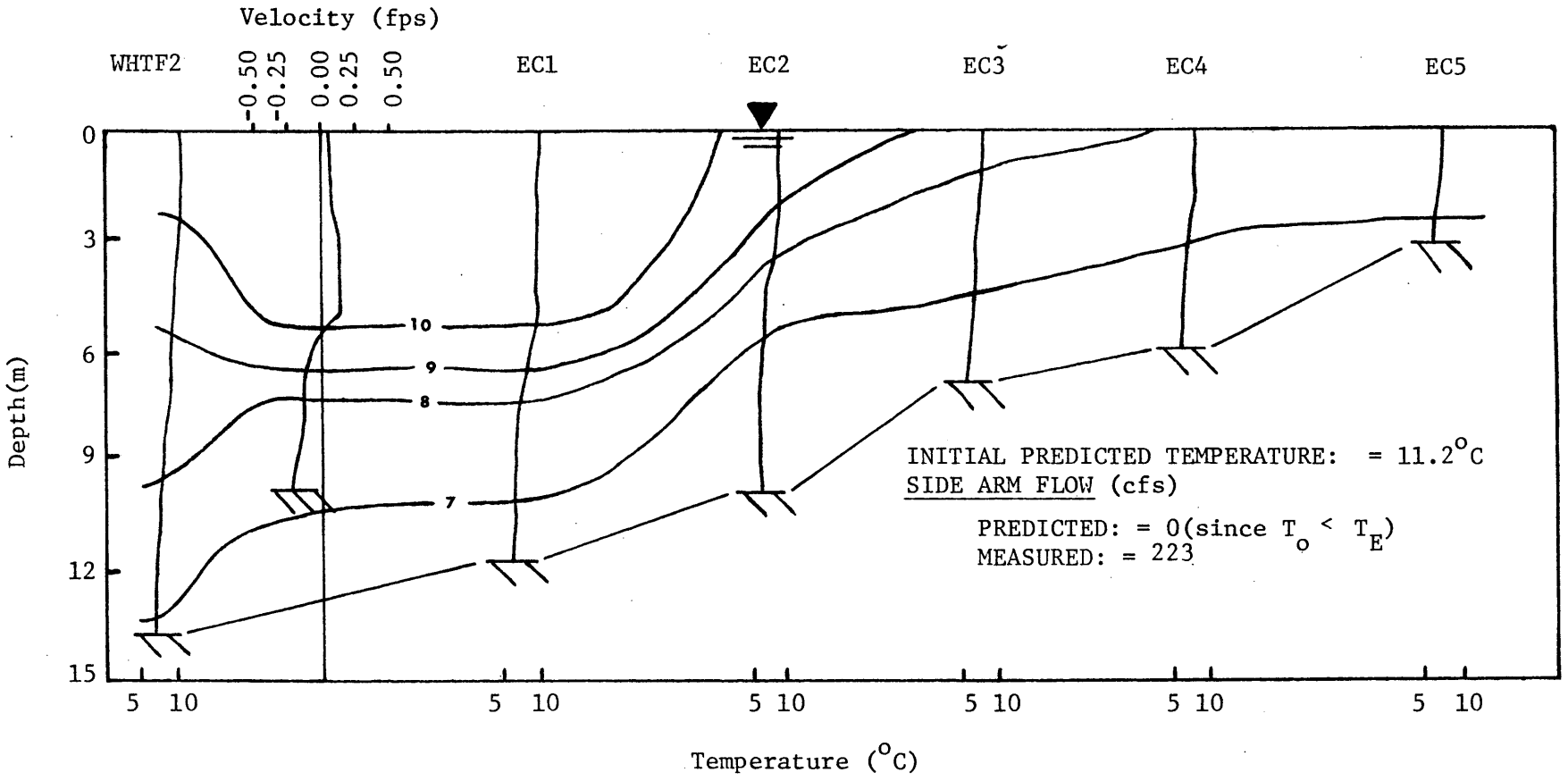

Figure 4.26f: North Anna Lake, Elk Creek Sidearm Analysis for 3/10/80

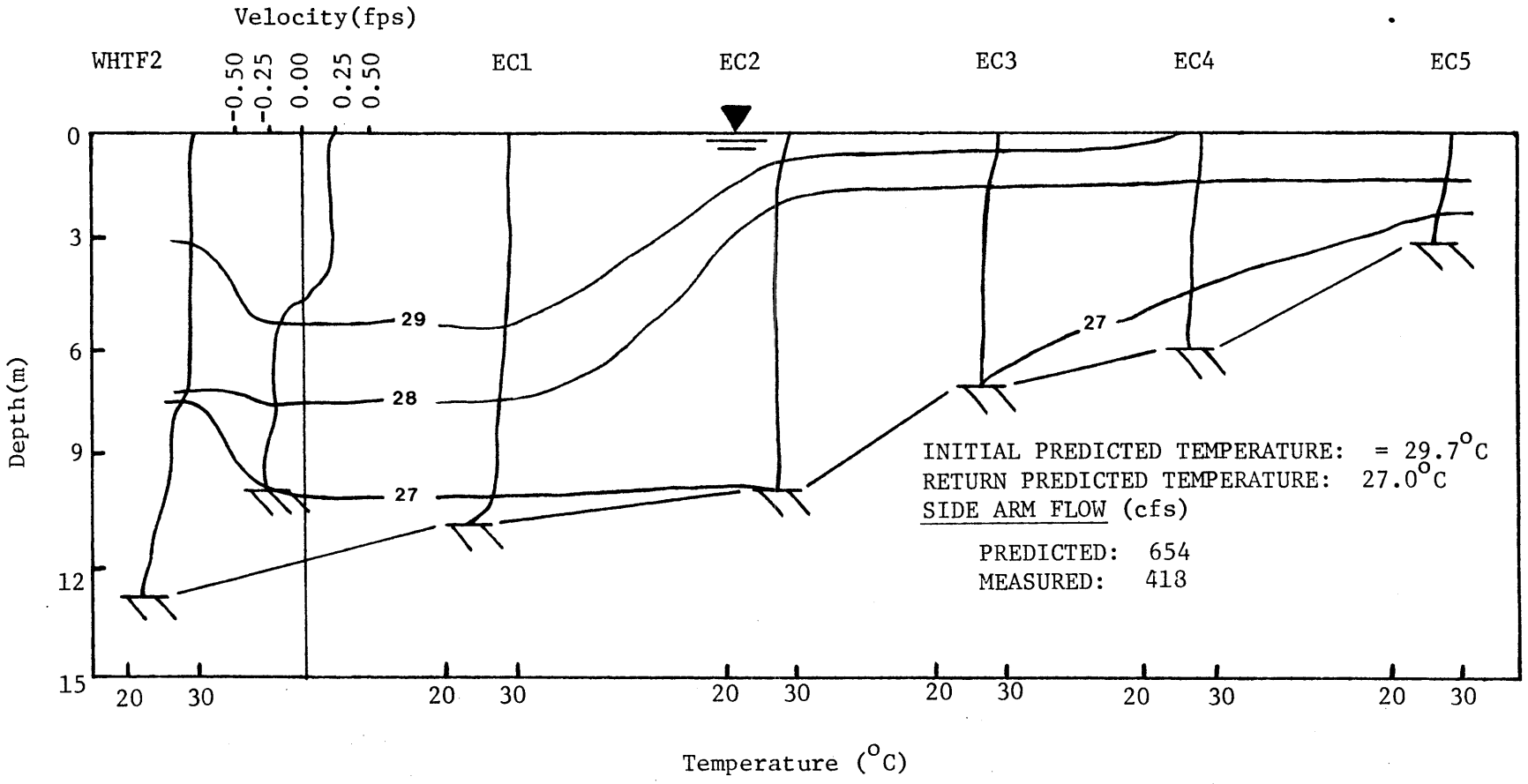

Figure 4.26g: North Anna Lake, Elk Creek Sidearm Analysis for 7/9/80

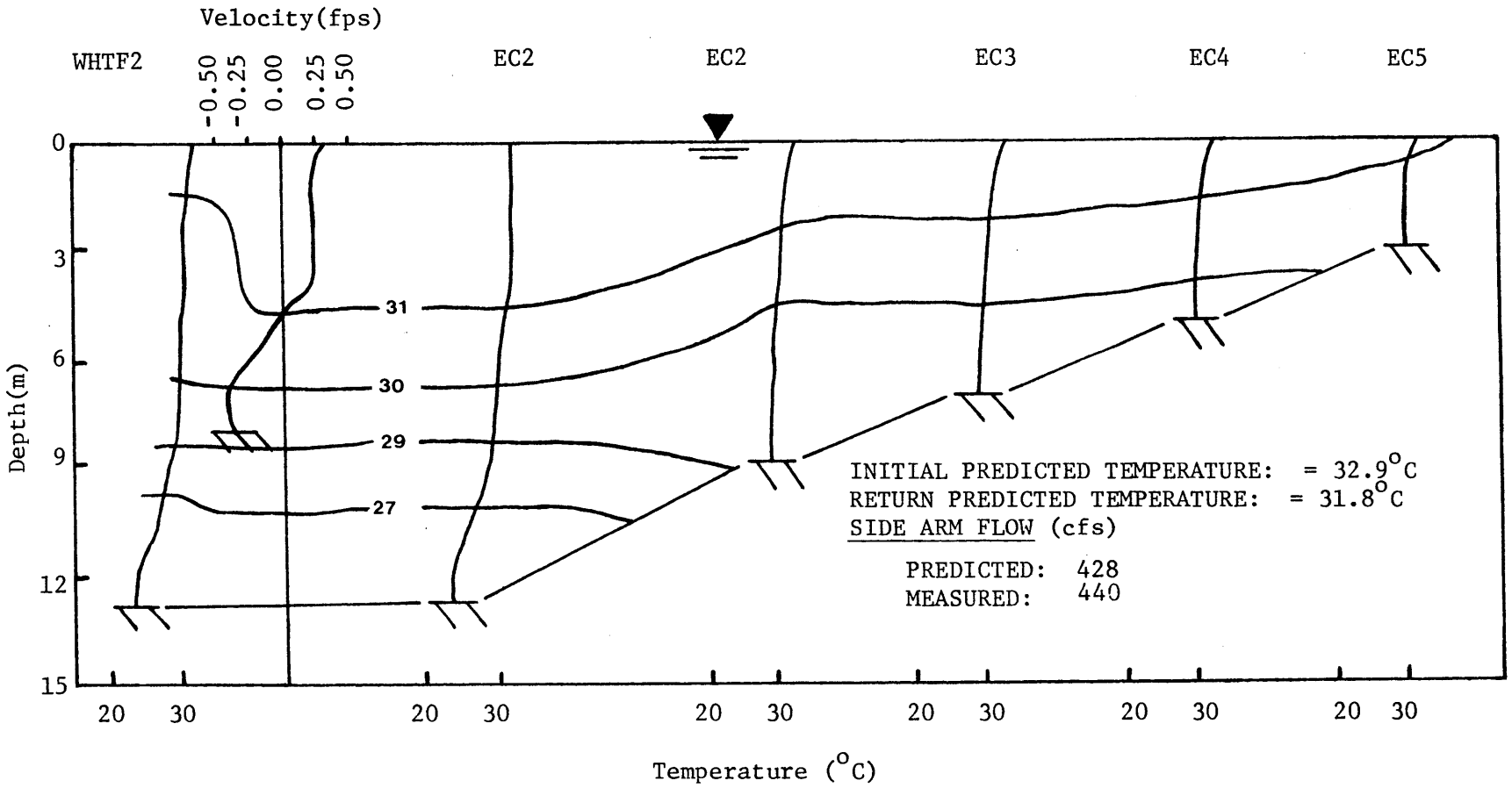

Figure 4.26h: North Anna Lake, Elk Creek Sidearm Analysis for 7/21/80

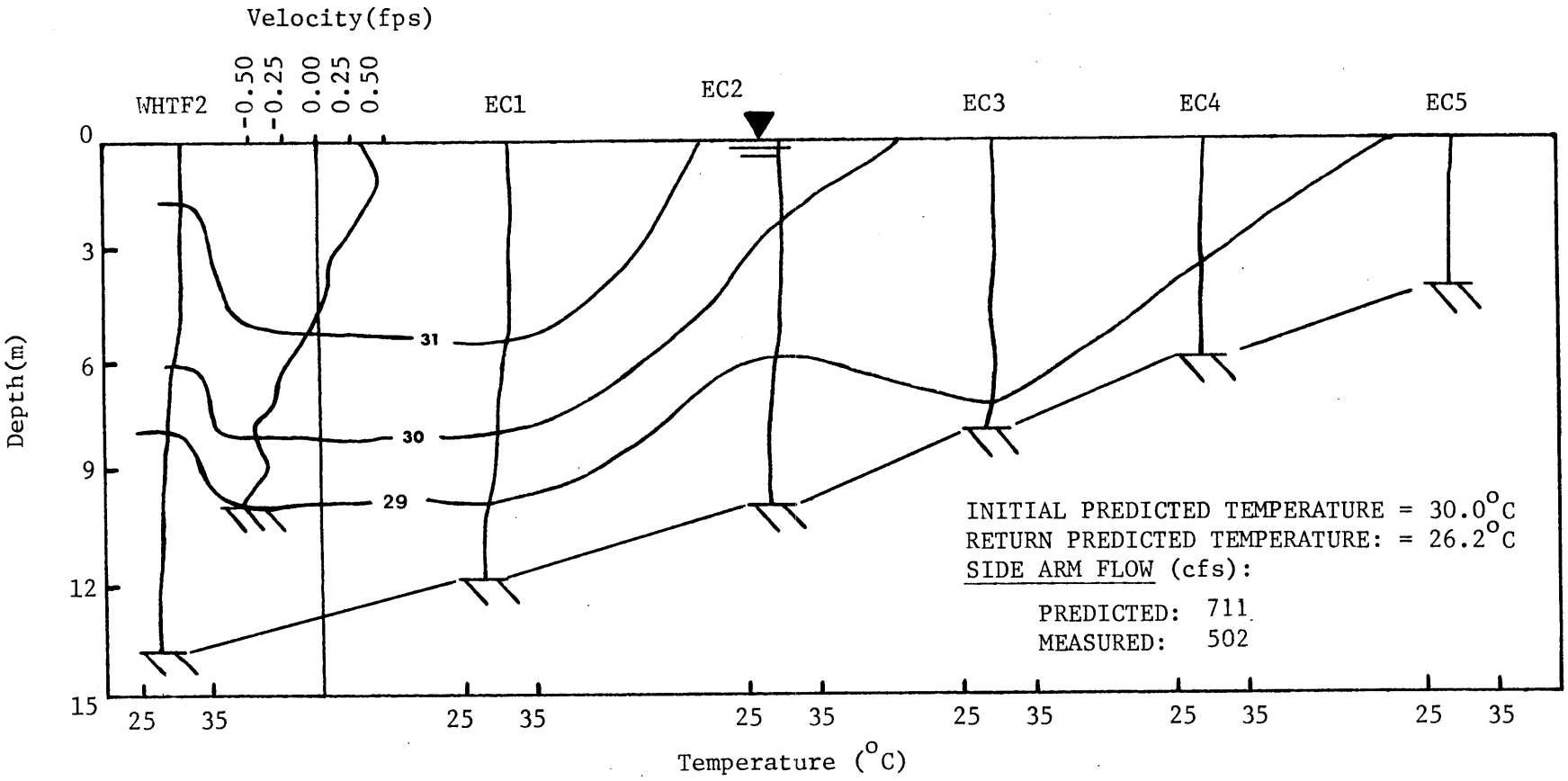

Figure 4.26i: North Anna Lake, Elk Creek Sidearm Analysis for 8/21/80

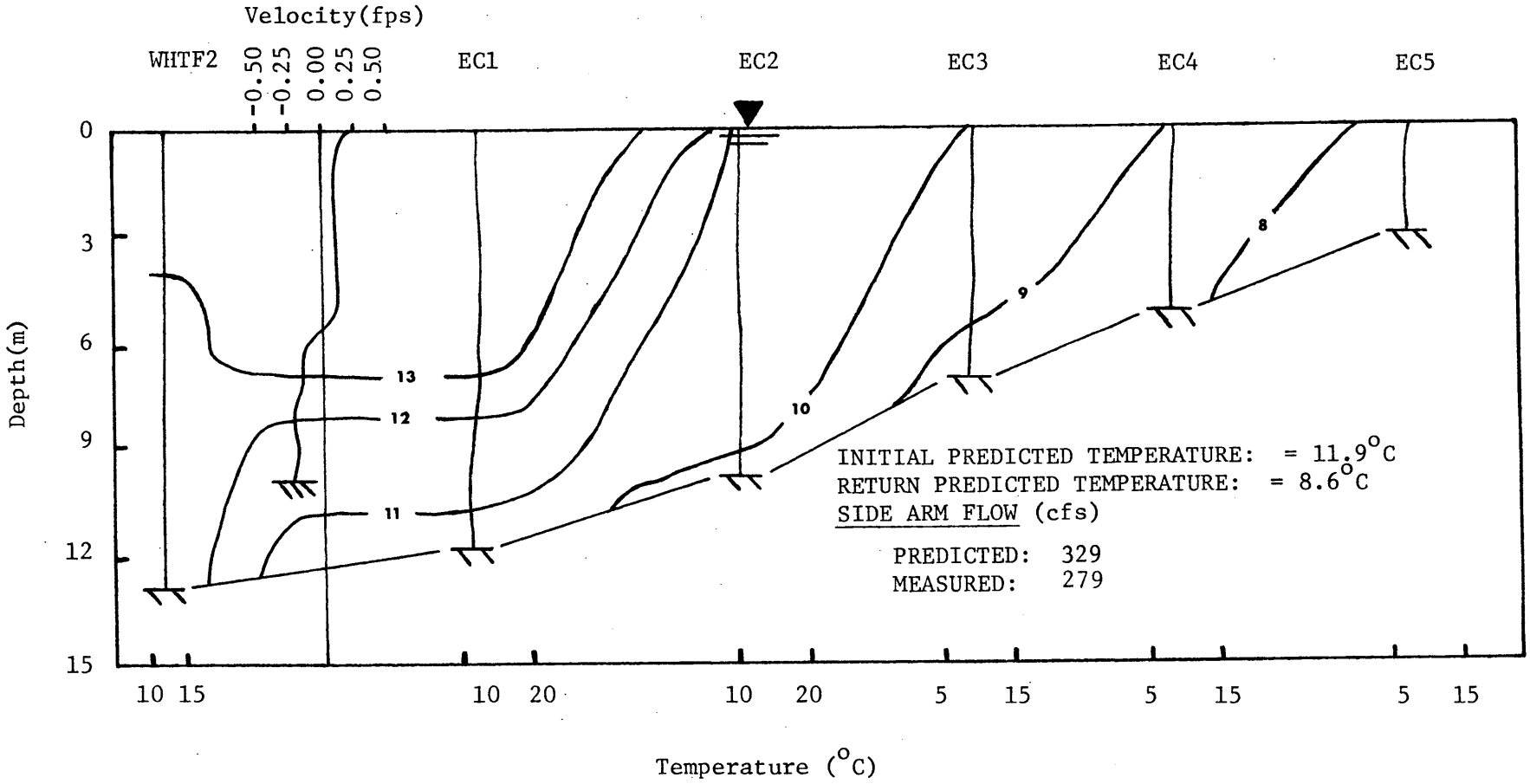

Figure 4.26j: North Anna Lake, Elk Creek Sidearm Analysis for 12/4/80

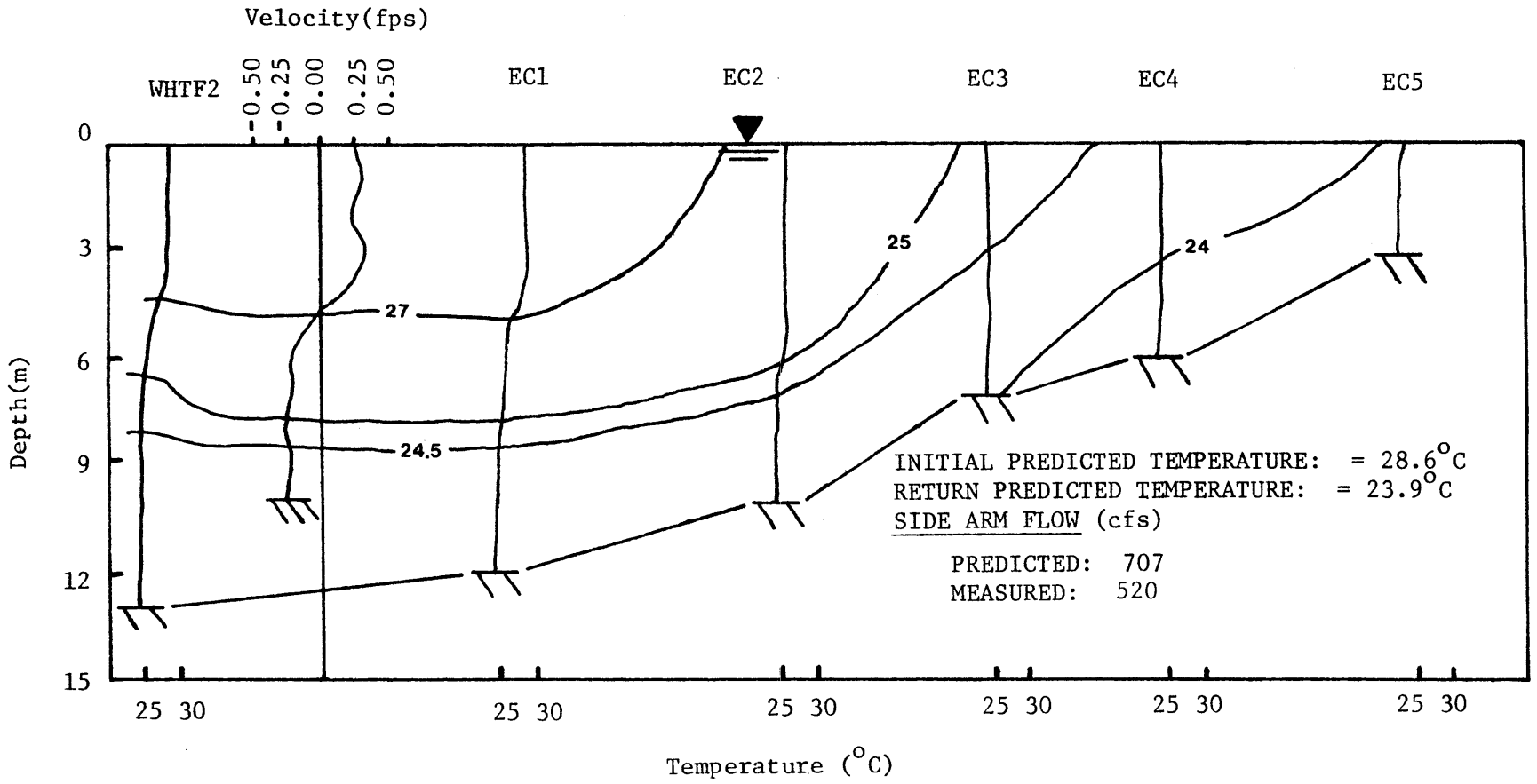

Figure 4.26k: North Anna Lake, Elk Creek Sidearm Analysis for 9/29/81

The Aanderaa current velocity data for upper and lower layers were broken into components normal and tangent to the bridge opening and averaged over each day. Flow rates in the upper and lower layers were obtained by assuming that the (velocity) interface between the layers was at a 4.4m depth and that the two measured velocities were representative of the entire respective layers. Flow rates for upper and lower layers were averaged and compared with model predictions in Figure 4.27. It should be noted that for the period September, 1980 - September, 1981, there were frequent intervals of missing data from the upper meter in which case only the bottom meter was used to determine flow rate.

Figure 4.27 clearly shows the ability of the model to predict the seasonal trends in the observed flow rates. Table 4.5 provides a more quantitative comparison between predicted and measured flow rates. Comparison is for the four summer months of June, July, August and September and the three winter months of December, January and February and has been broken down by the two measurement periods. Table 4.5 suggests a tendency to underpredict flow rates during the winter but overpredict flow rates during the summer

A question that might be raised is whether there was sufficient variability over the diurnal time scale to warrant the daily average analysis of the side arm flow. Spectral analysis techniques were utilized to compute the kinetic energy density of the side arm flow, and Figure 4.28 shows a power spectrum plot of $\omega S(\omega)$ vs $\log(\omega)$, where $s(\omega)$ is the kinetic energy density of the side arm flow ($cm^2/cph\text{-}s^2$) computed from the 2-hour Aanderaa data (i.e. before averaging) and ω is the frequency (cph). By plotting the spectrum in this manner,

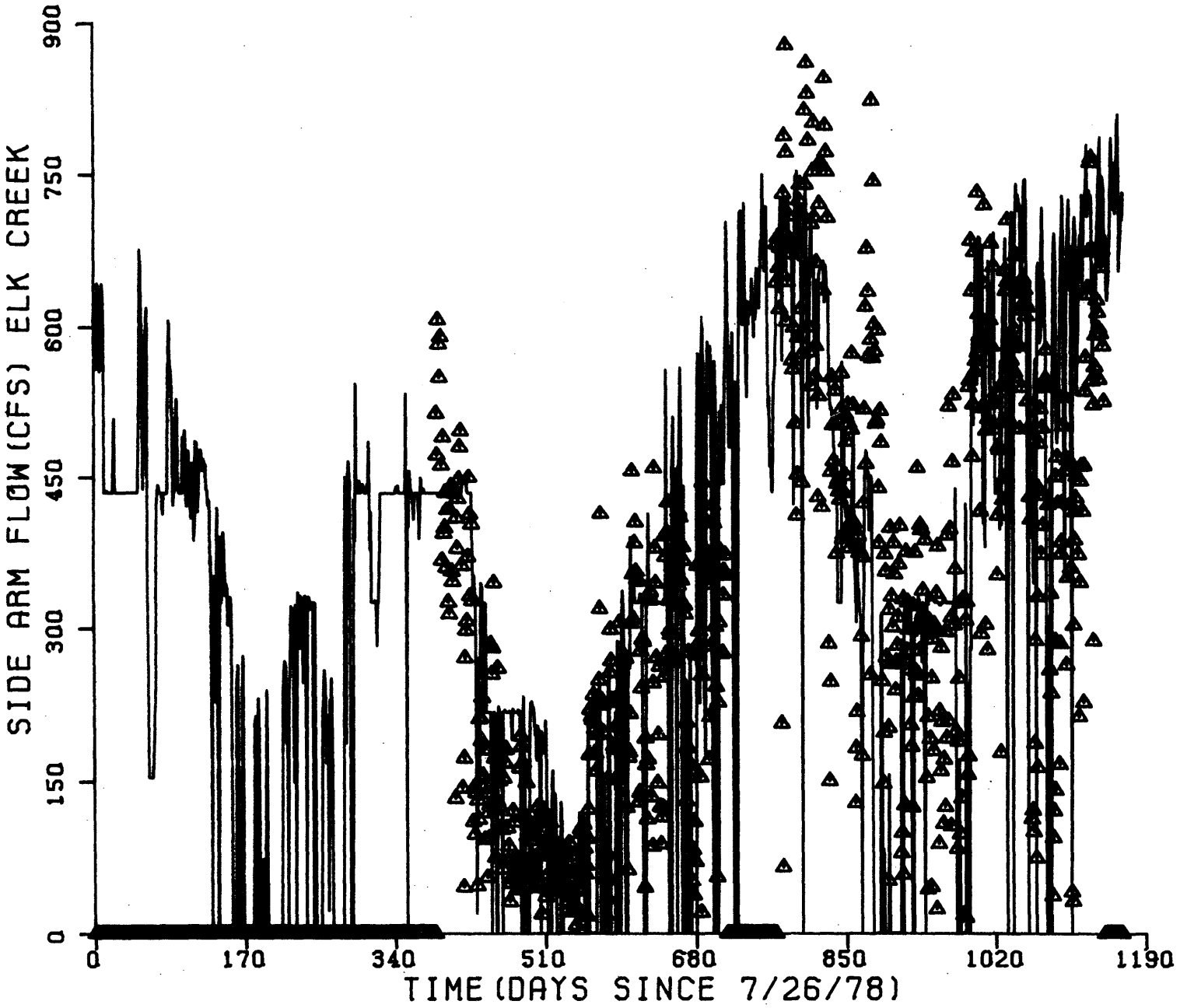

Figure 4.27 Elk Creek Side Arm Flow, Predicted (line) versus Aanderaa Data (triangles)

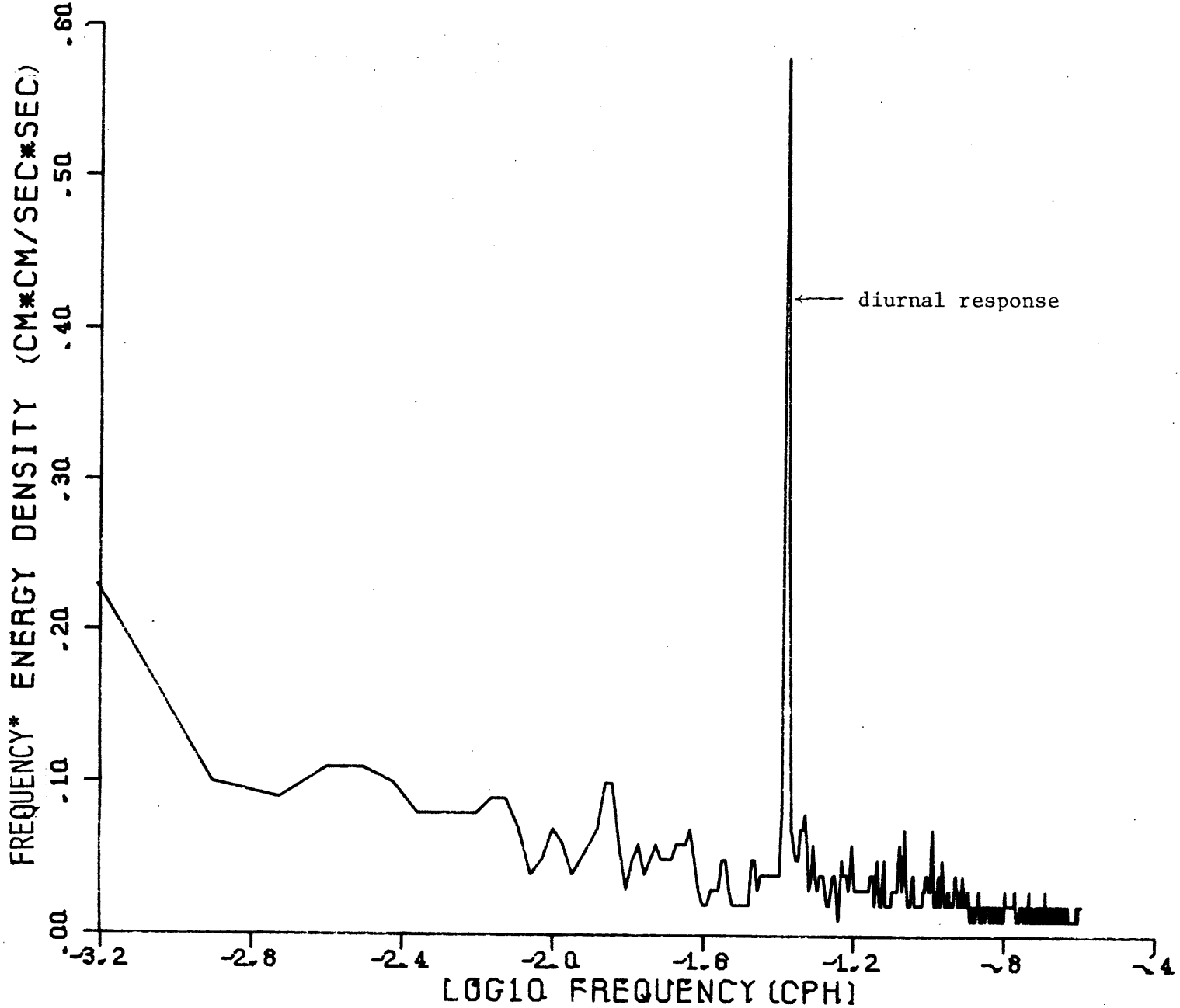

Figure 4.28 Power Spectrum of Upper Layer Elk Creek Side Arm Velocity (8/15/79 - 8/15/80)

Table 4.5 Comparison of Predicted Flow Rates with Measured Flow Rates (Aanderaa data) at Elk Creek.

	Model Flow Rate (cfs)	Measured Flow Rate (cfs)
a) Data for 8/15/79-8/15/80		
Summer months: June, July Aug., Sept.	399	328
Winter months: Dec., Jan., Feb.	77	104
b) Data for 9/3/80-9/10/81		
Summer months: June, July, Aug., Sept.	610	464
Winter months: Dec., Jan., Feb.	201	334

the energy contained within a given frequency band is directly proportional to the area under the curve between the two frequencies. Note that comparatively little energy is contained at periods of one day or shorter. Thus use of daily average data - which will filter information at these periods - is justified. There is a significant peak observed at the diurnal period. However the amplitude of velocity variation corresponding to this peak is only about 0.3 cm/sec which is small compared with the mean current velocity of about 6 cm/sec.

Analysis of the Aanderaa data allowed the Froude numbers for each layer to be calculated and thus the assumptions of criticality to be tested. Figure 4.29 shows time series plots of the sum of the squares of the upper and lower layer Froude numbers as used in Equations 4.26 or 4.27. Note that, for the period starting September, 1980 (Fig. 4.29b), upper layer velocity data was inaccurate but was computed from the lower layer velocity assuming a continuity balance. Also, whenever the temperature difference ΔT between upper and lower layer was less than or equal to zero, IF was set equal to a maximum value. Not including times when $\Delta T \leq 0$, for the period 8/15/79 to 8/15/80, critical conditions occurred only 11 days out of the 367 days, and during 9/3/80 to 9/10/81, critical conditions occurred only 28 days out of 376.

Since, for the most part, flow through the constriction was not critical, the entrance head loss and the internal frictional resistance to the flow, must contribute to more of a reduction than was previously expected with $f_o = 0.02$ and $\alpha = 0.5$. A more thorough analysis of these conditions is warranted.

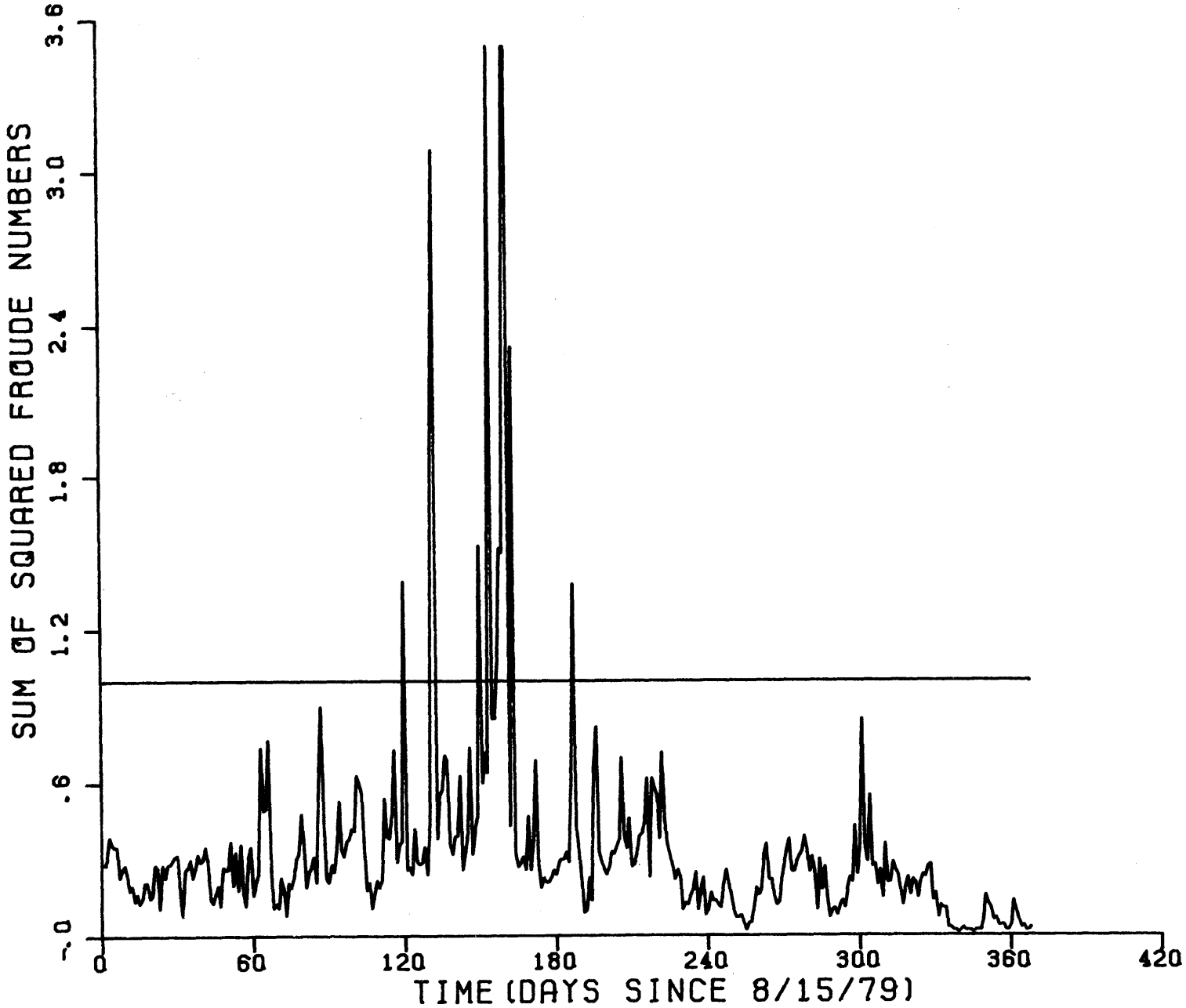

Figure 4.29a Sum IF^2 for Elk Creek Side Arm Aanderaa Data (8/15/79 - 8/15/80)
Note: When $\Delta T \leq 0$ sum of IF^2 set to 3.5

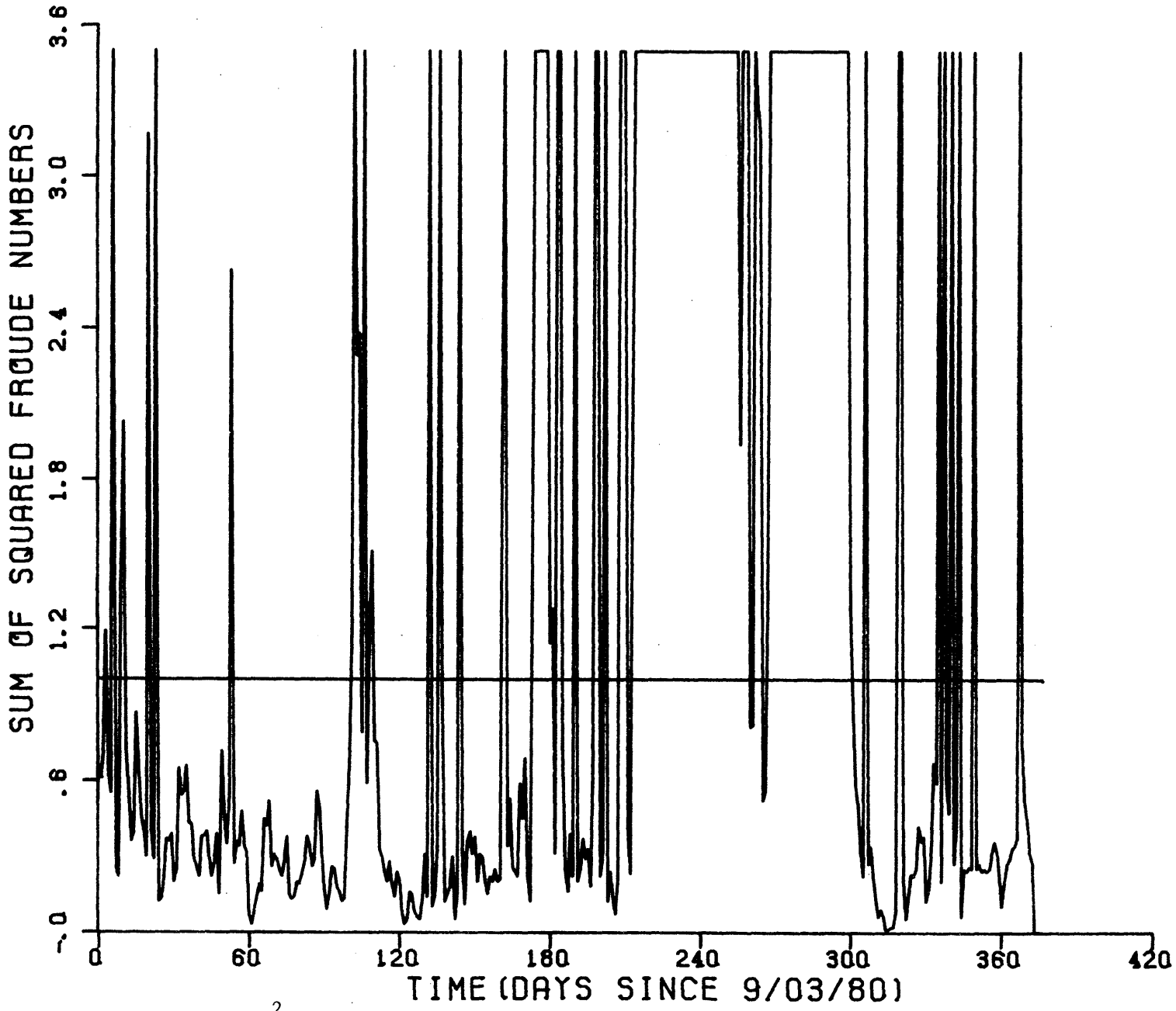

Figure 4.29b Sum of $\mathbb{F}^2$ for Elk Creek Side Arm Aanderaa Data (9/3/80 - 9/10/81)
Note: When $\Delta T \leq 0$, sum of $\mathbb{F}^2$ set to 3.5

4.4 Summary of Model Changes

Compared with the original model presented in Chapter 2 the following changes have been made: (i) adjustment of the long-wave atmospheric radiation formula used at low air temperatures ii) seasonal adjustment of the evaporation formula for the WHTF, iii) allowance for the condenser intake to withdraw equally over the upper 30 feet of the main lake , iv) inclusion of a time-varying vertical diffusion coefficient dependent on wind speed, condenser flow rate and vertical density gradient, v) use of a lag time and filtering procedure to account for transients in the WHTF, and vi) adjustment of side arm flow rates based on constriction due to the bridge piers.

5. MODEL VERIFICATION

Chapter 4 described model changes and calibrations which were guided in large part by comparing model predictions with appropriate segments of data. In this chapter continuous model predictions are compared with data over a three year simulation period. Because the three year simulation period includes the data segments used for calibration, this is not a completely independent verification. However, because of the wide range in meteorological and plant operational conditions which were experienced, it does allow a rigorous test of model performance. If data are available for future years, an independent verification can be performed as well.

5.1 Surface Temperature Verification

Figures 5.1-5.4 compare observed surface temperatures with corresponding predictions every day over three years 1) at the discharge point in reach 1 of the WHTF, 2) just upstream of Dike III in the WHTF, 3) in the main lake outside the Dike III jet mixing zone (at the dam) and 4) in the main lake near the plant intake. These plots verify that the calibrated mathematical model accurately simulates surface temperatures over a wide spectrum of meteorological and plant operating conditions.

5.2 Vertical Temperature Profiles in the Main Lake

Figure 5.5 details the measured and predicted profiles about every month for three years at two locations in Lake Anna: i) near the dam (measurement station A or LA13) and ii) near the intake (measurement station L or LA9). The dynamic nature of the data was

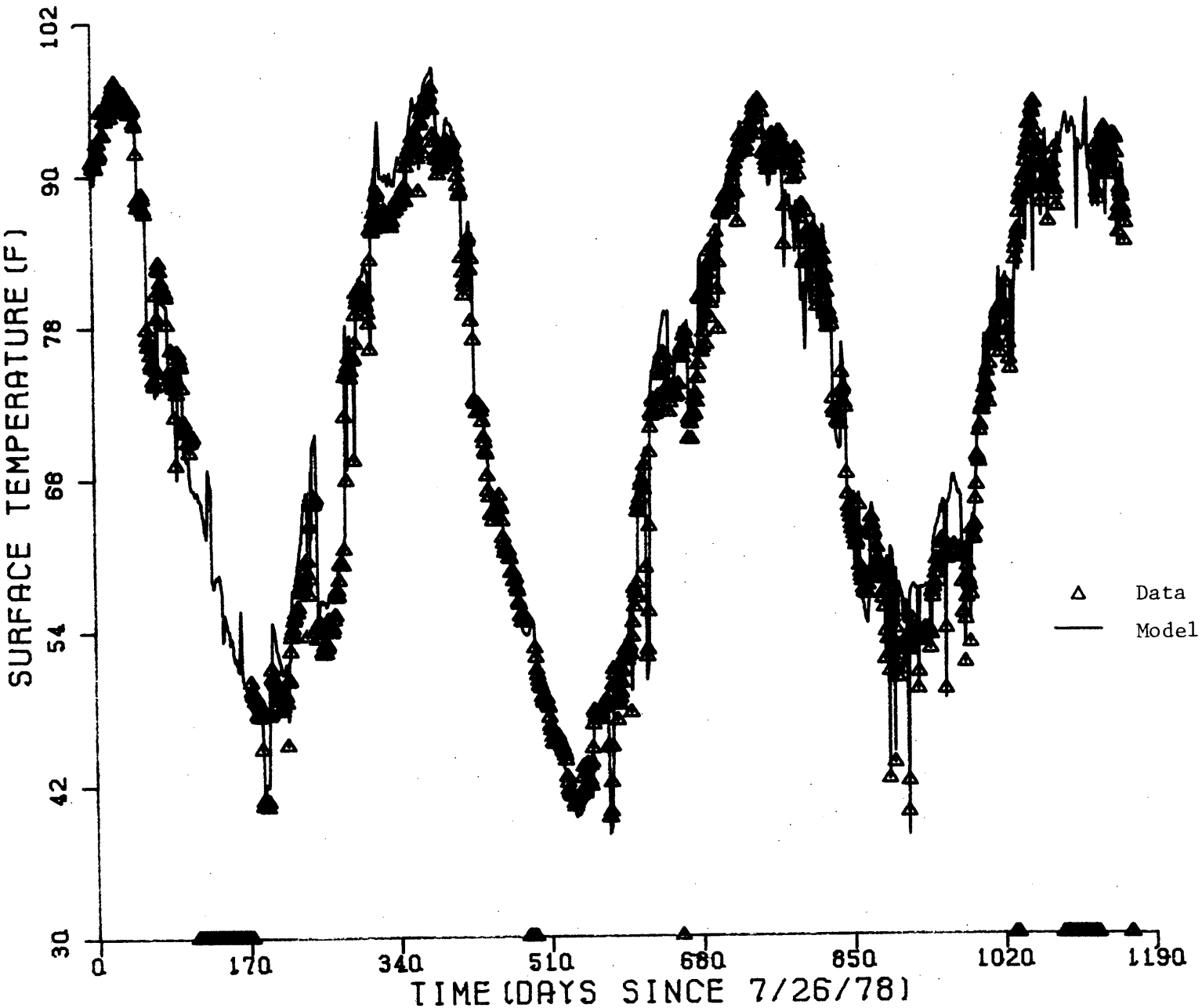

Figure 5.1 Model Predictions and Data Comparison at the Discharge into Reach 1

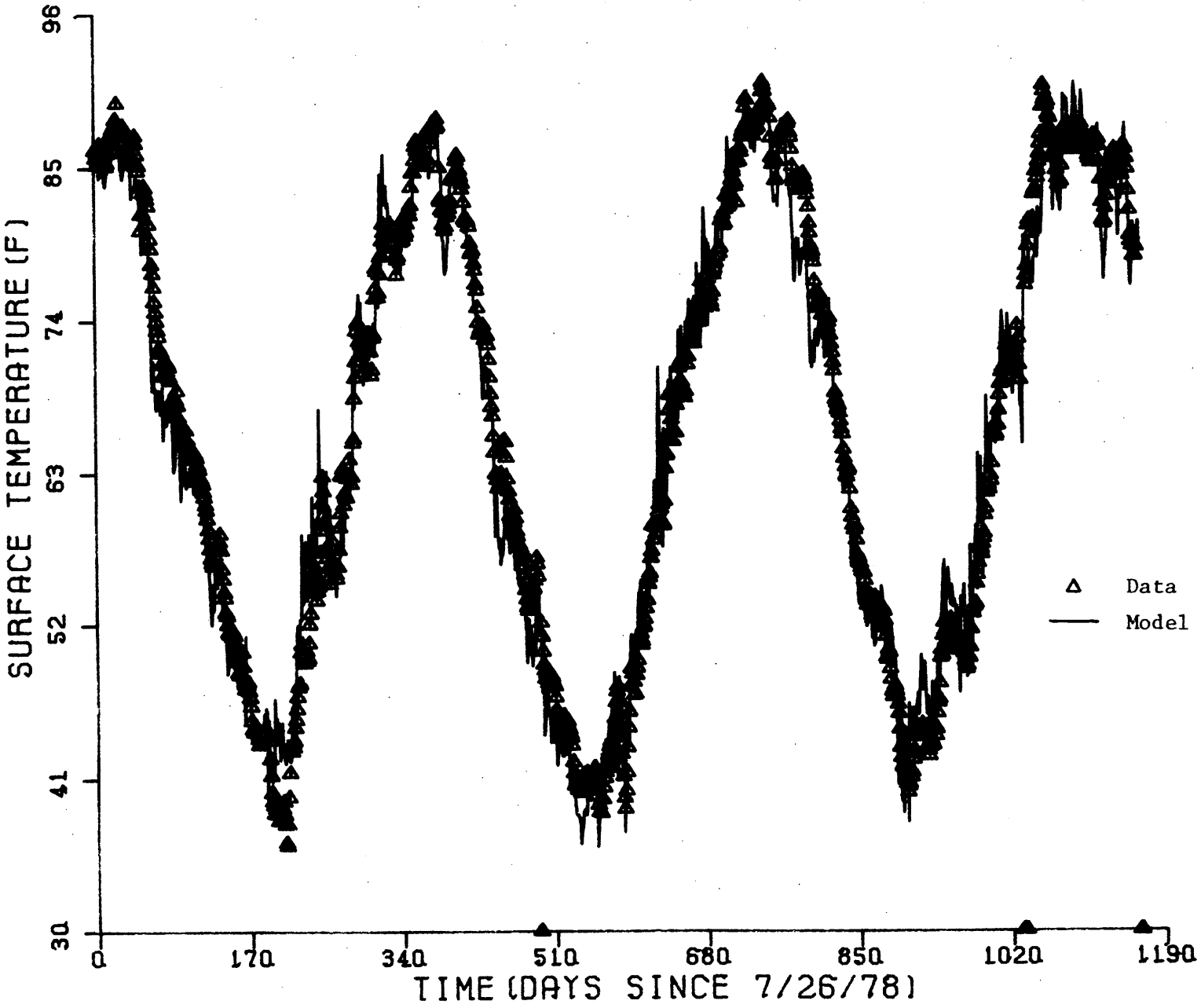

Figure 5.2 Model Predictions and Data Comparison at Dike 3 before the Main Lake

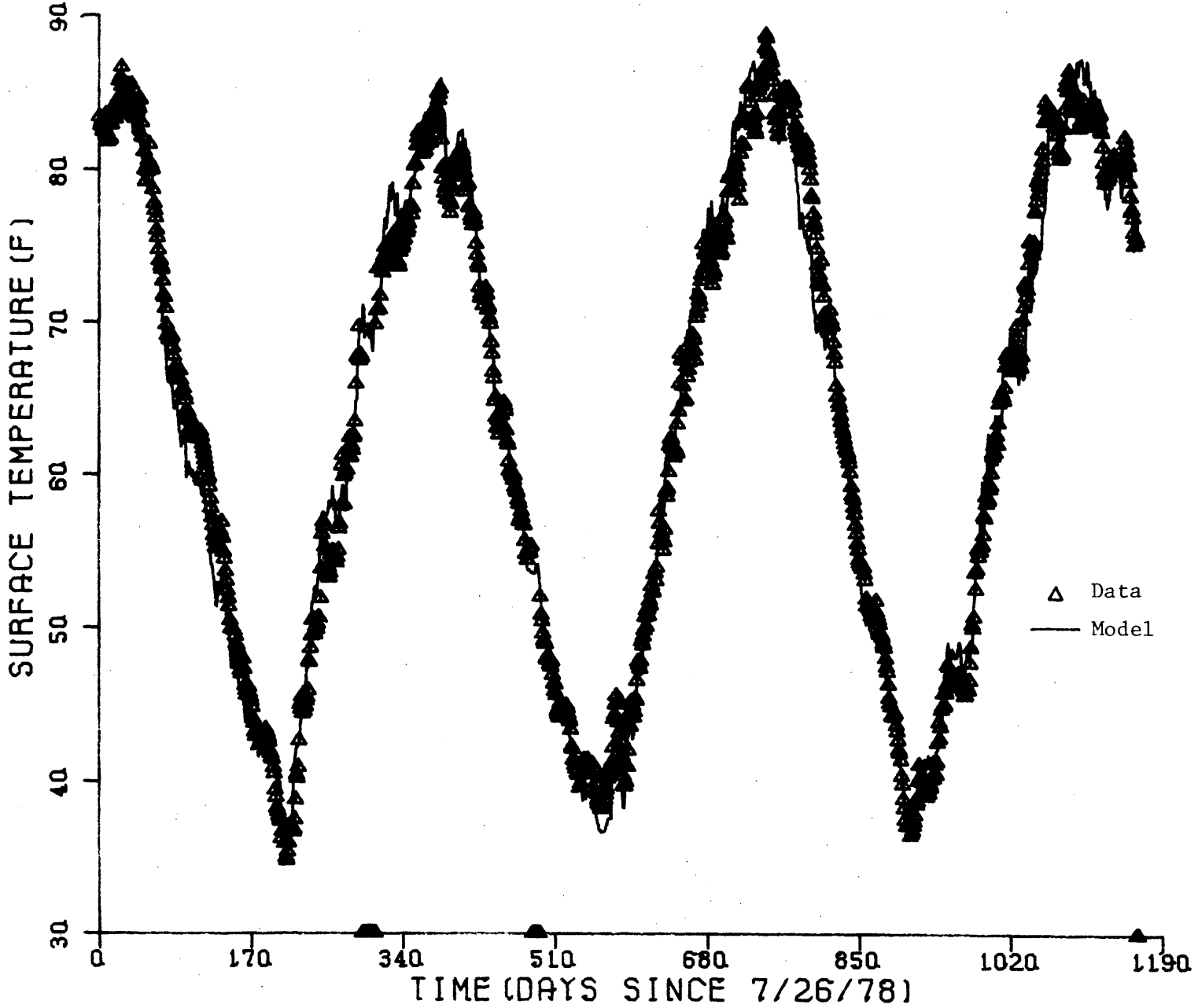

Figure 5.3 Model Predictions and Data Comparison at the Main Lake near the North Anna Dam

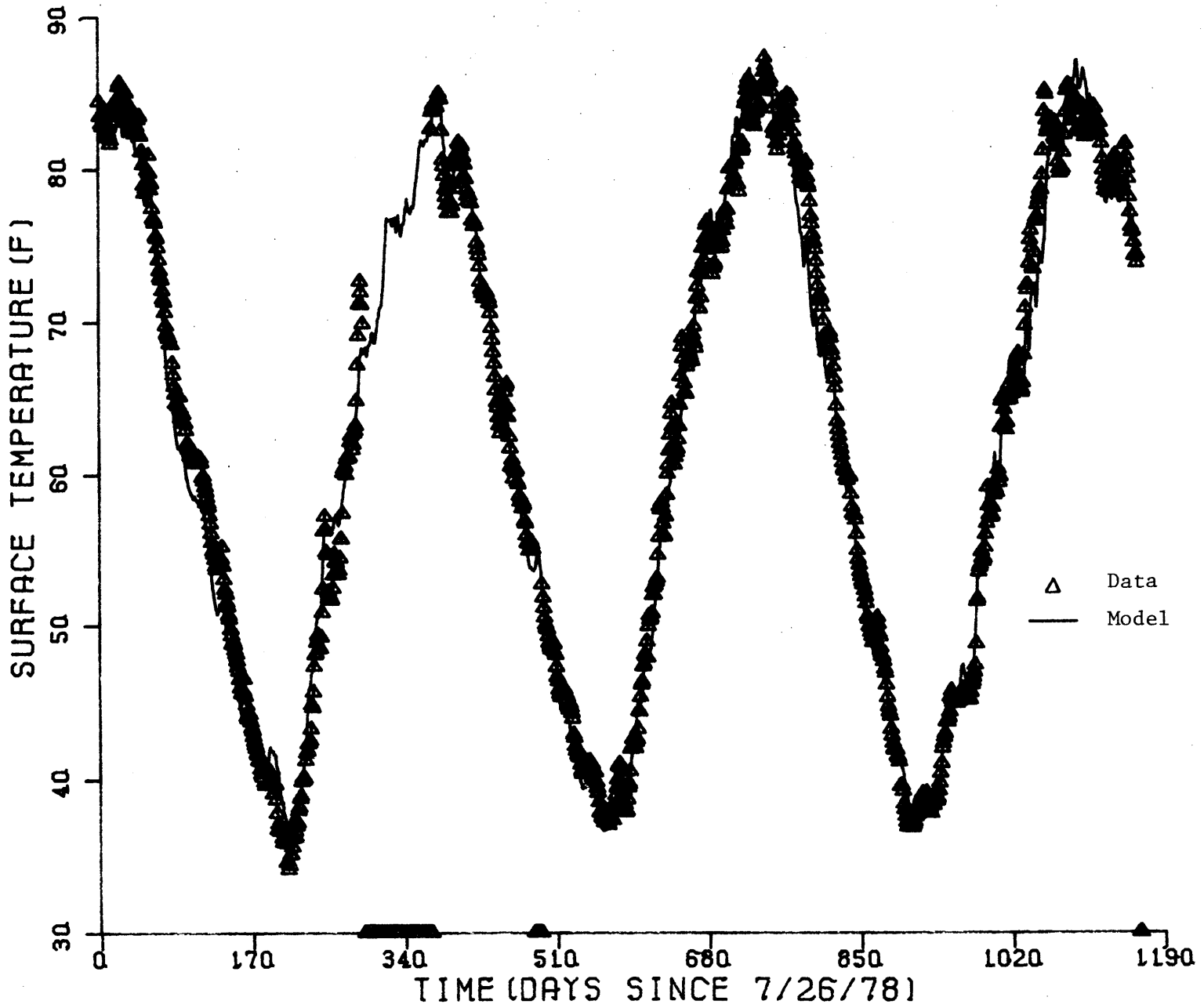

Figure 5.4 Model Predictions and Data Comparison at Main Lake near Intake

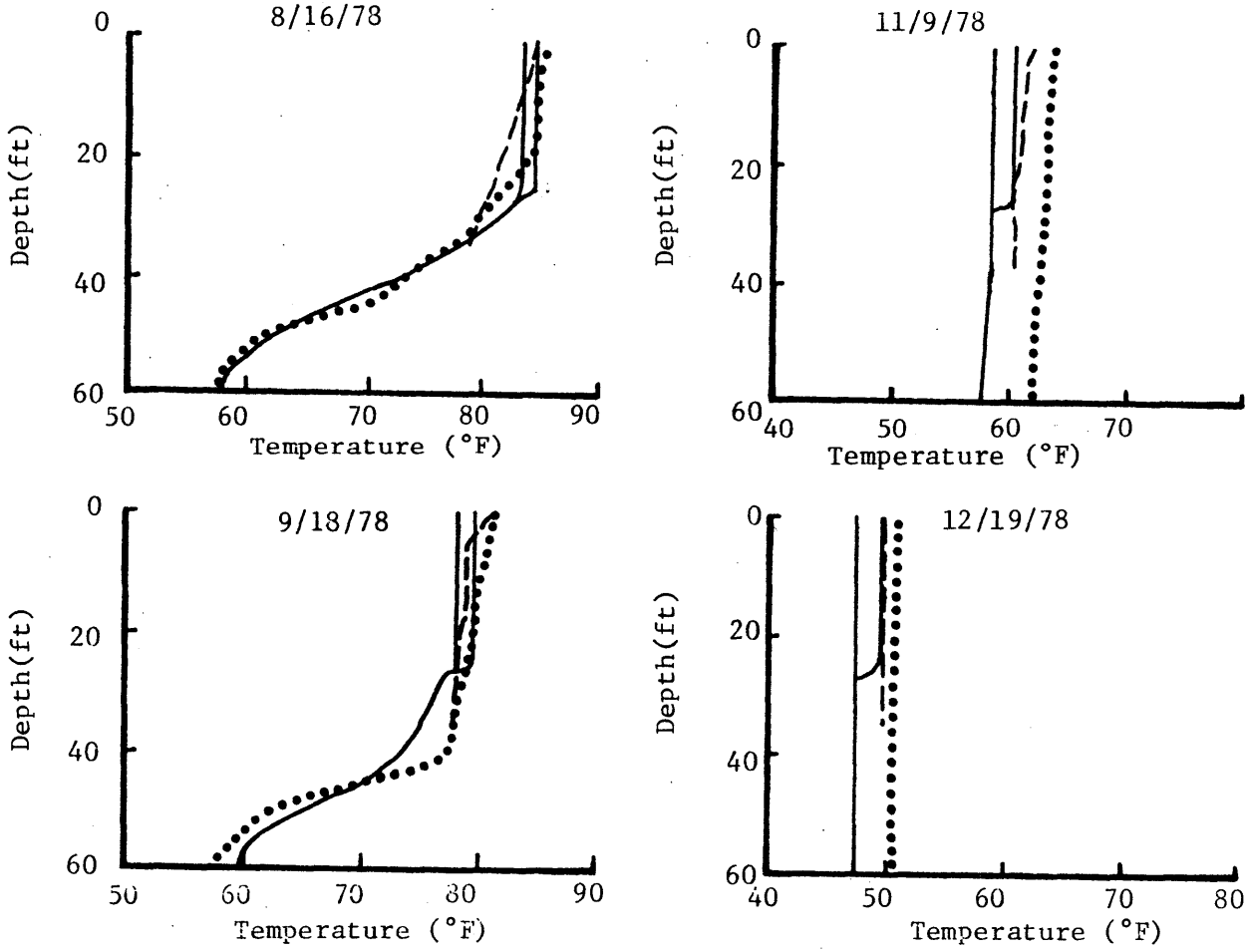

Legend: "——" = Predicted; "•••••" = Station A; "– – –" = Station L.

Figure 5.5a: Data and Predicted Vertical Temperature Profiles, 1978-1981

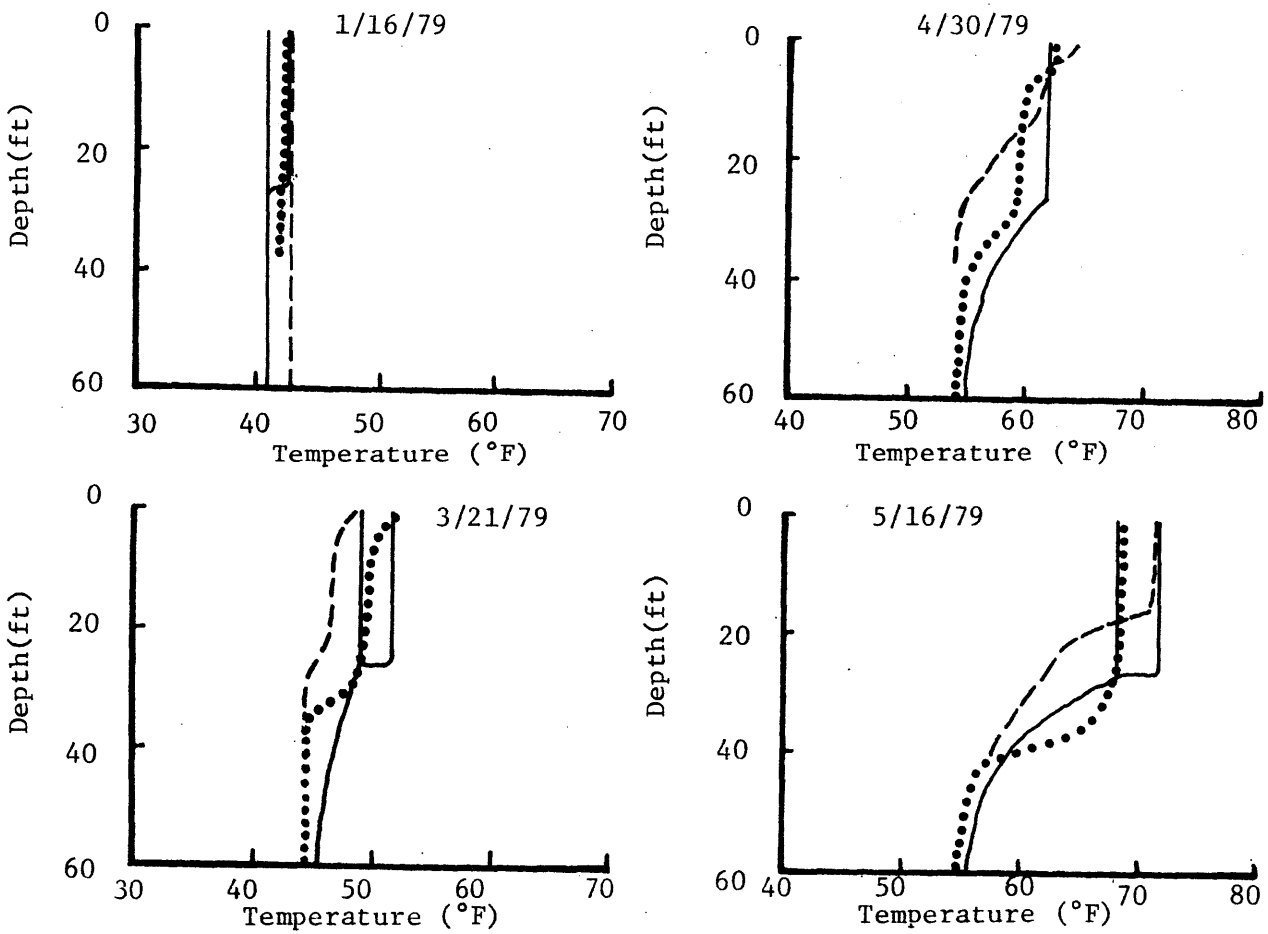

Legend: "———" = Predicted: "•••••" = Station A; "– – –" = Station L.

Figure 5.5b: Data and Predicted Vertical Temperature Profiles, 1978-1981

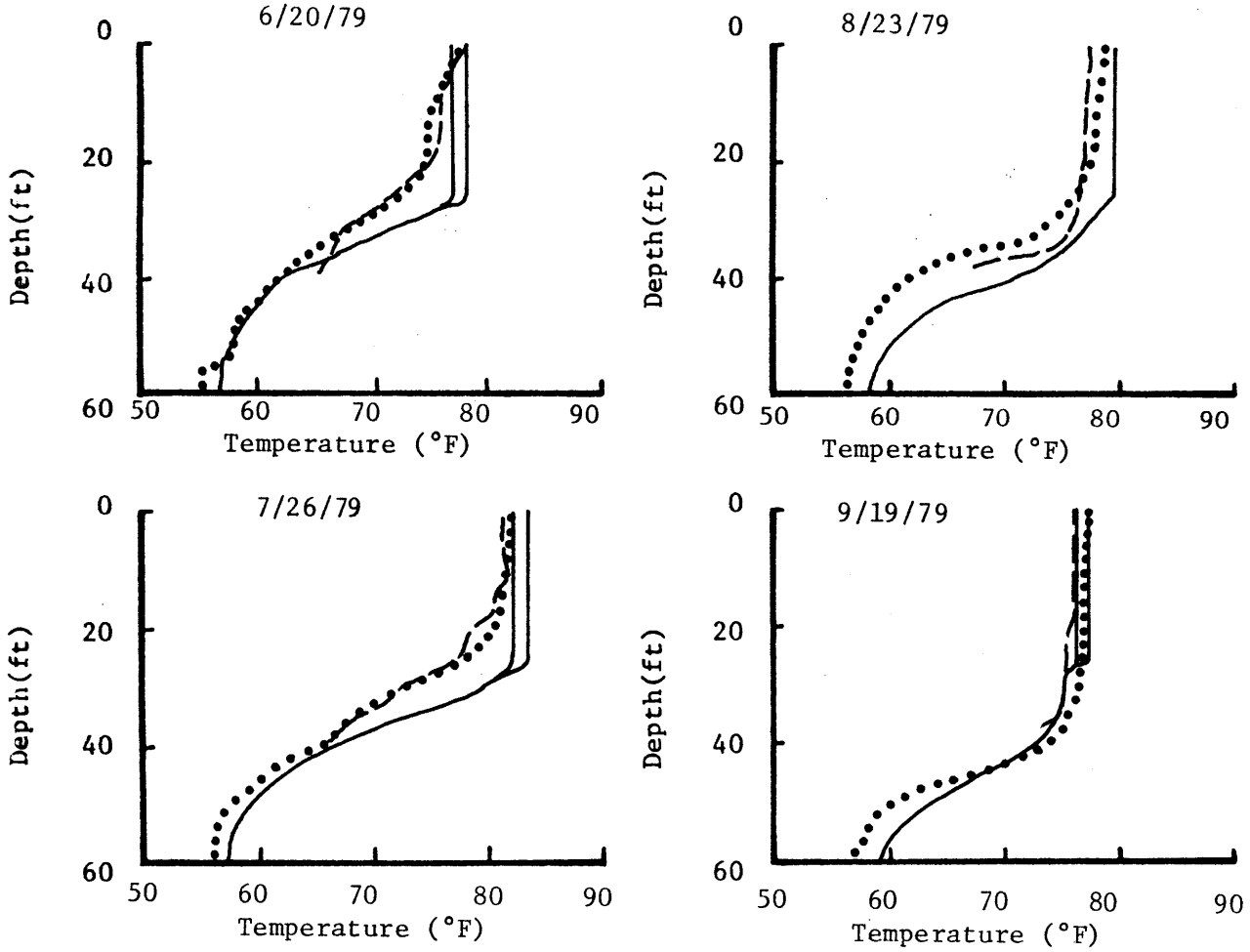

Legend: "——" = Predicted; "•••••" = Station A; "---" = Station L.

Figure 5.5c: Data and Predicted Vertical Temperature Profiles, 1978-1981

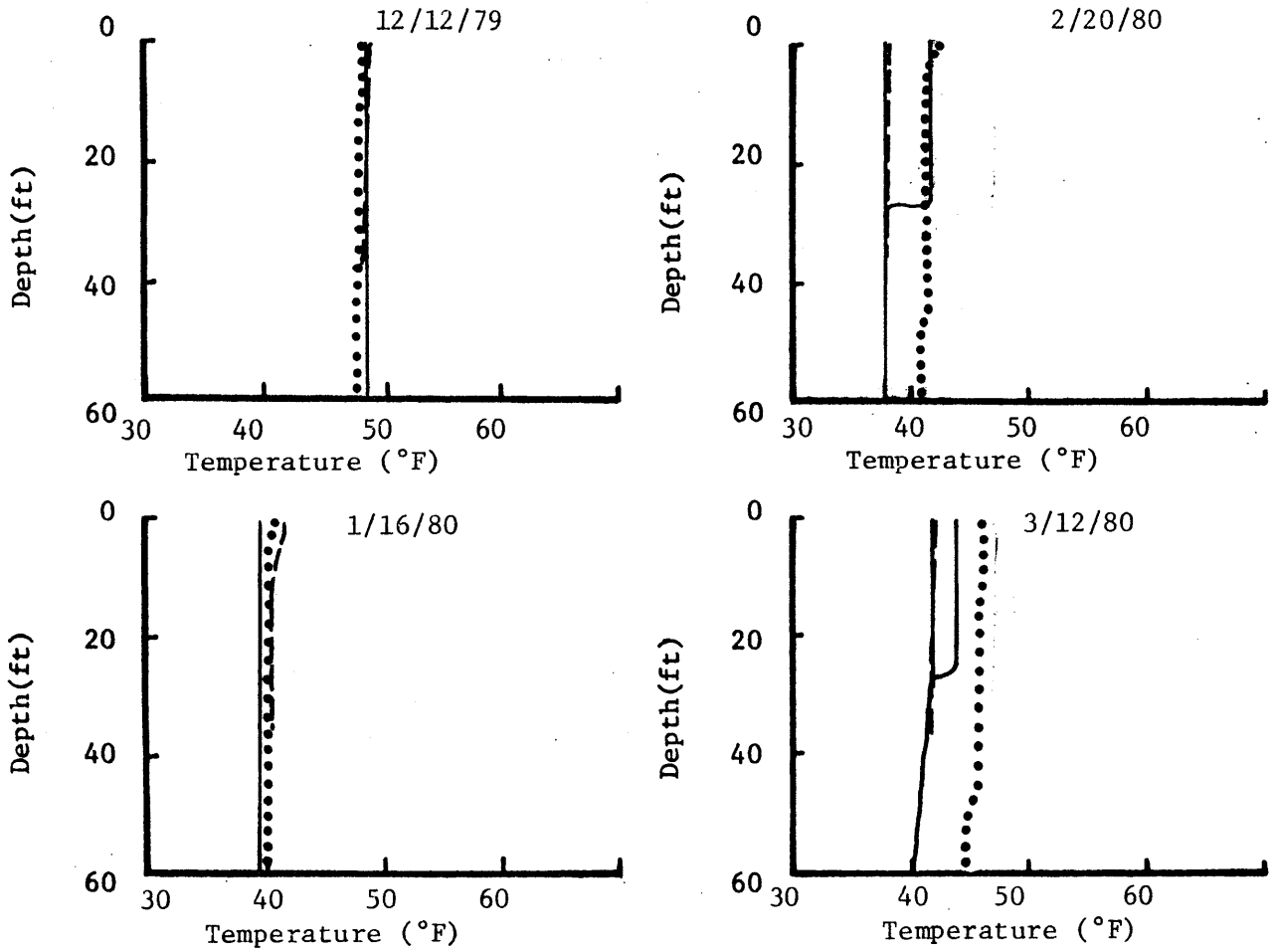

Legend: "——" = Predicted; "•••••" = Station A; "– – –" = Station L.

Figure 5.5d: Data and Predicted Vertical Temperature Profiles, 1978-1981

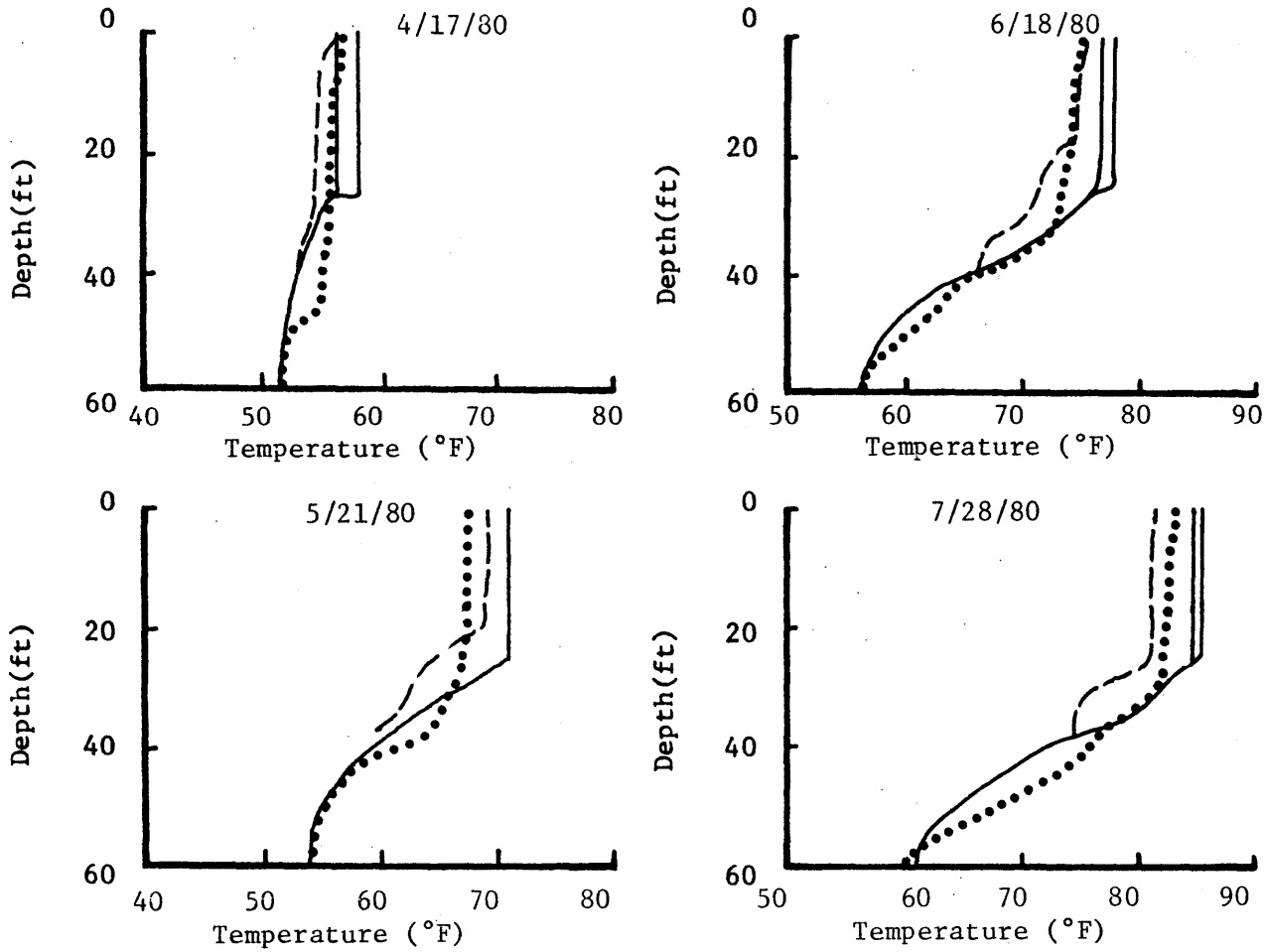

Legend: "——" = Predicted; "•••••" = Station A; "- - -" = Station L.

Figure 5.5e: Data and Predicted Vertical Temperature Profiles, 1978-1981

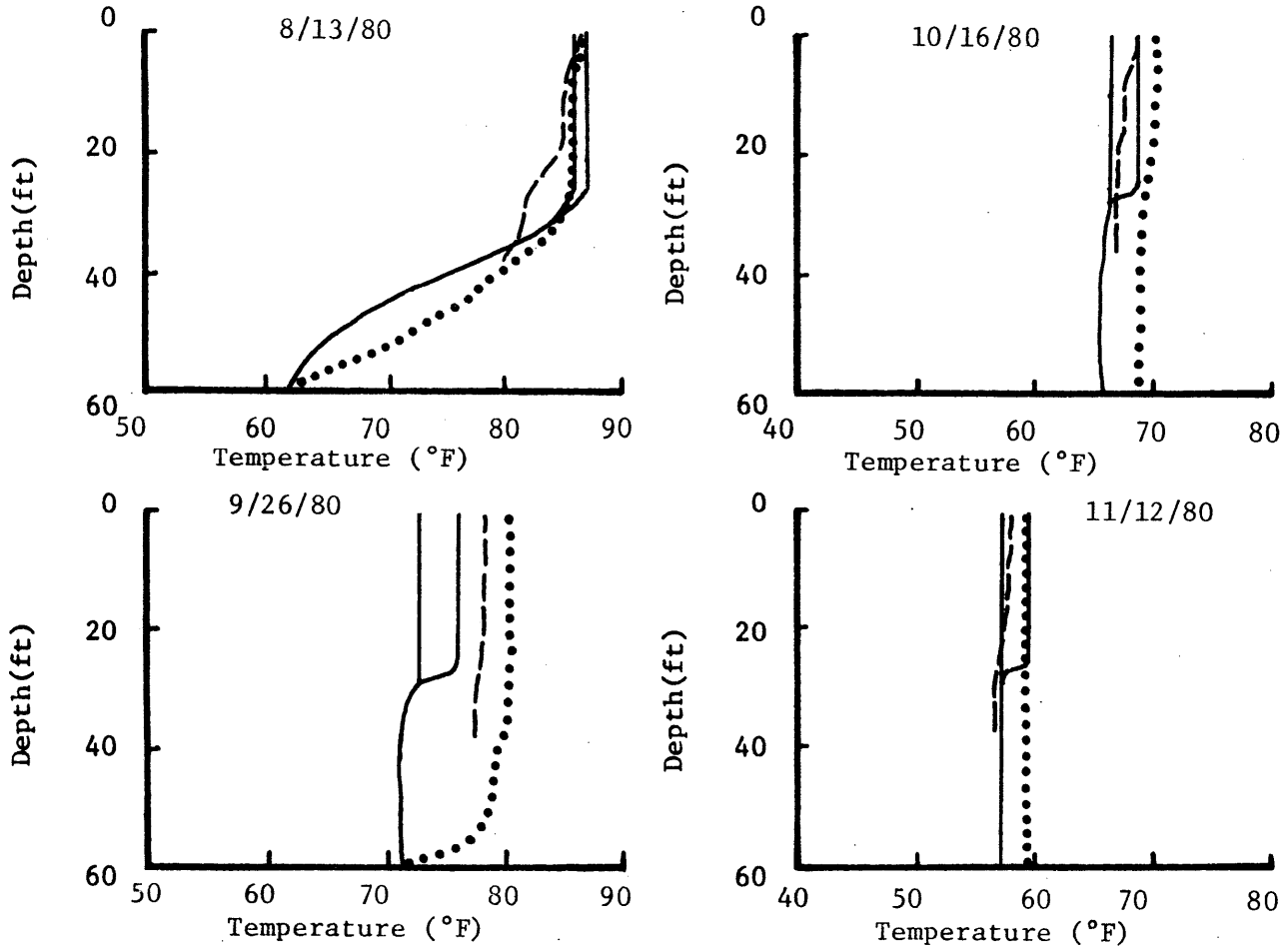

Legend: "——" = Predicted; "•••••" = Station A; "- - -" = Station L.

Figure 5.5f: Data and Predicted Vertical Temperature Profiles, 1978-1981

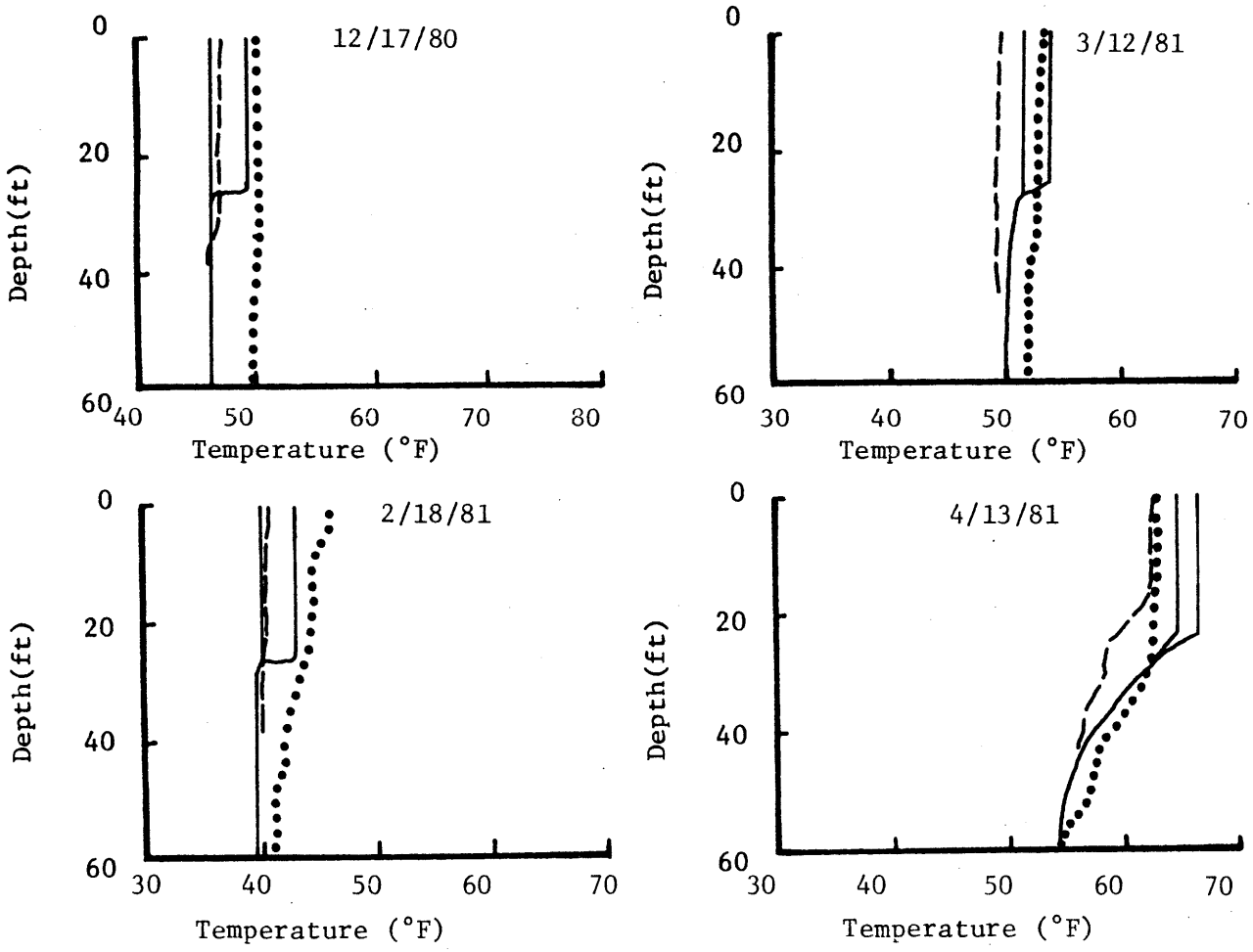

Legend: "——" = Predicted; "•••••" = Station A or LA13; "---" = Station L or LA9.

Figure 5.5g: Data and Predicted Vertical Temperature Profiles, 1978-1981

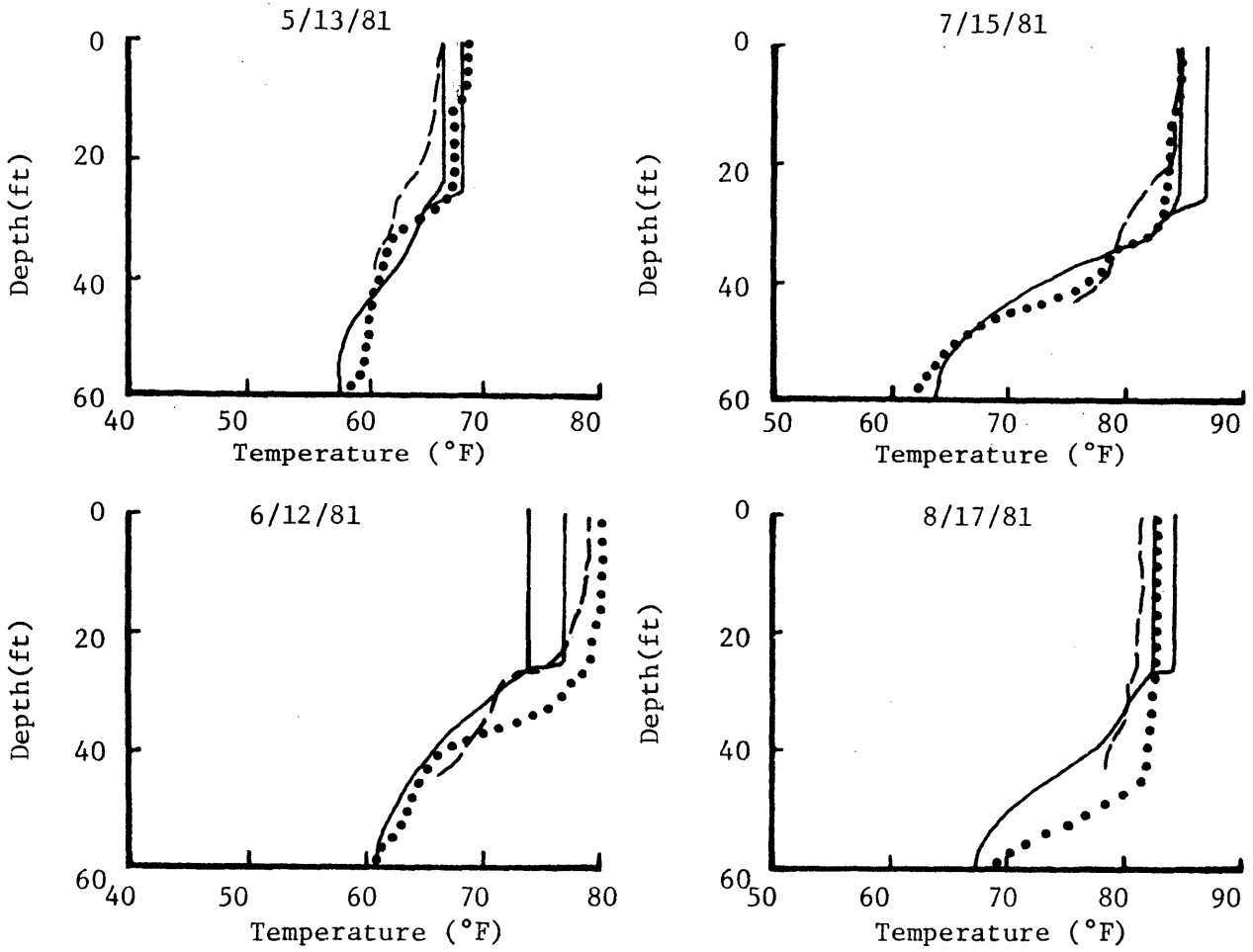

Legend: "——" = Predicted; "••••" = Station A or LA13: "---" = Station L or LA9.

Figure 5.5h: Data and Predicted Vertical Temperature Profiles, 1978-1981

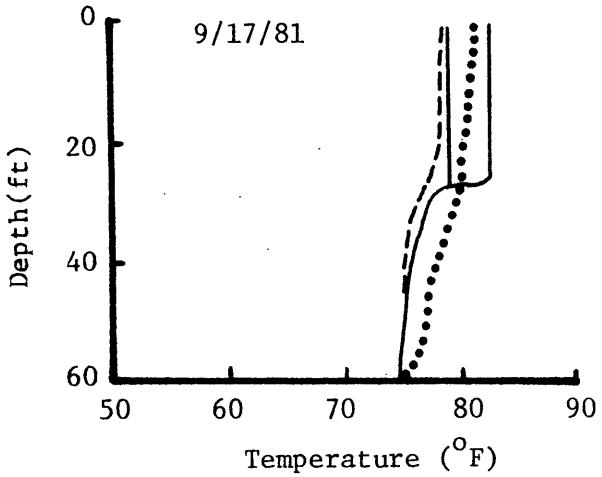

Legend: "———" = Predicted; "·····" = A; "-----" = L

Figure 5.5i: Data and Predicted Vertical Temperature Profiles, 1978-1981.

well represented by the model's characterization of the mixed layer and hypolimnetic diffusivity.

Realizing that a visual interpretation of Figures 5.1-5.5 might lead to subjective conclusions, a closer examination of model strengths and weaknesses is described below.

5.3 Surface Temperature Error Analysis

Figures 5.6-5.9 show the "raw" errors (model prediction-data) at the four control points listed in Section 5.1. (A positive error means that the model was predicting temperatures too high.)

Figures 5.10-5.13 show the "delta" errors (see Equation 4.1) associated with these segments: WHTF, Dike III mixing, the Main Lake, and the plant heat input. (Note that a positive error implies that, over that segment, the model is cooling too much.) These plots are useful in filtering out "carry-over" errors shown in the "raw" error plots. However, the carry-over errors are not completely eliminated. For example, if the model under-predicted heat loss in one reach, it would compensate in the next reach and tend to over-predict heat loss.

In Table 5.1 this same information is broken down by season. The table indicates a slight over-prediction of surface temperature of the dam in each summer and a slight underprediction of the same temperature in winter.

In order to summarize the error analysis, Table 5.2 includes a statistical analysis of the "raw" and "delta" errors, detailing the mean error, the standard deviation of the error, and the percentage of error which fell between $\pm$ 2°F.

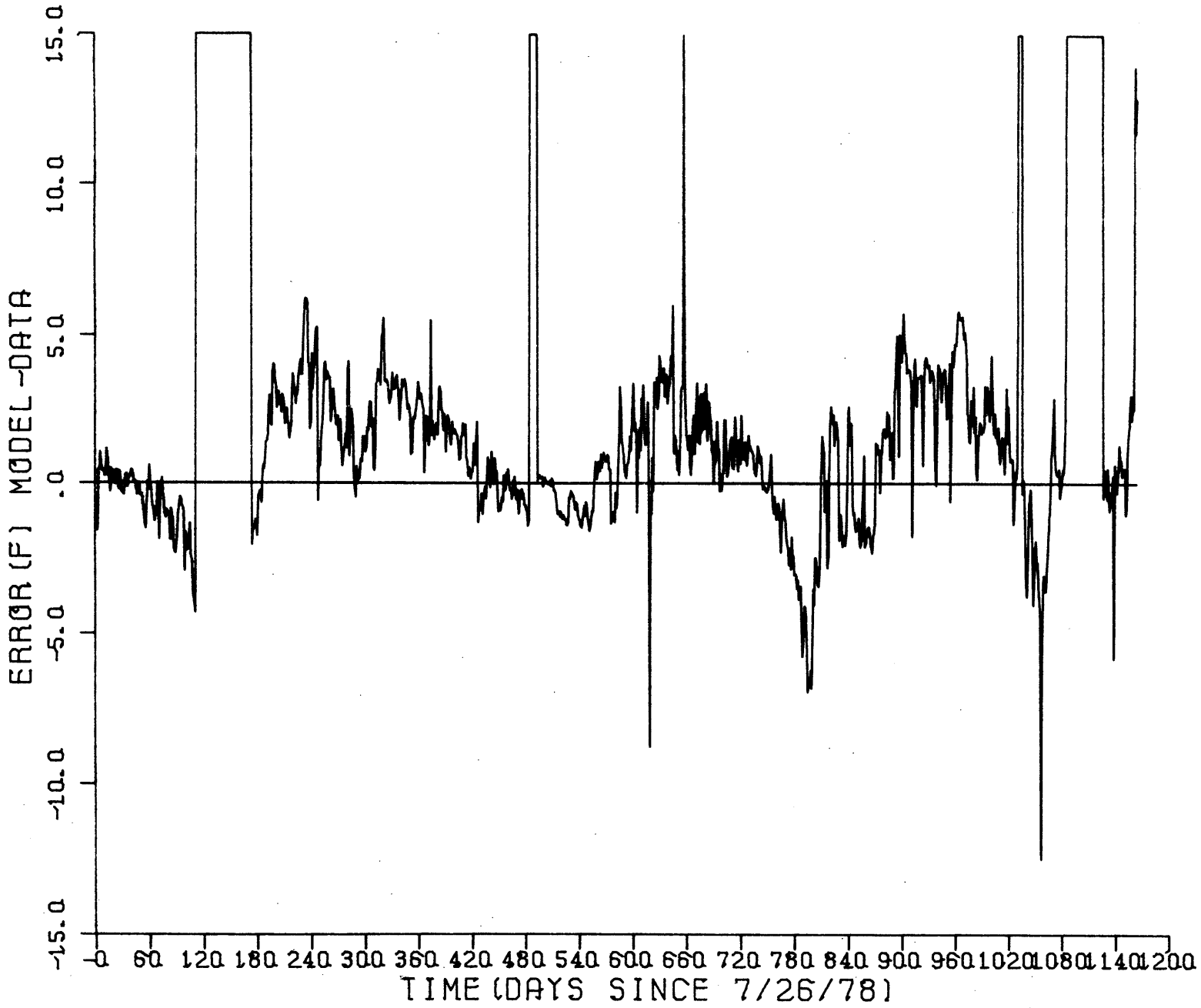

Figure 5.6: Raw Error at Discharge into Pond 1 (Note that 15°F indicates missing data)

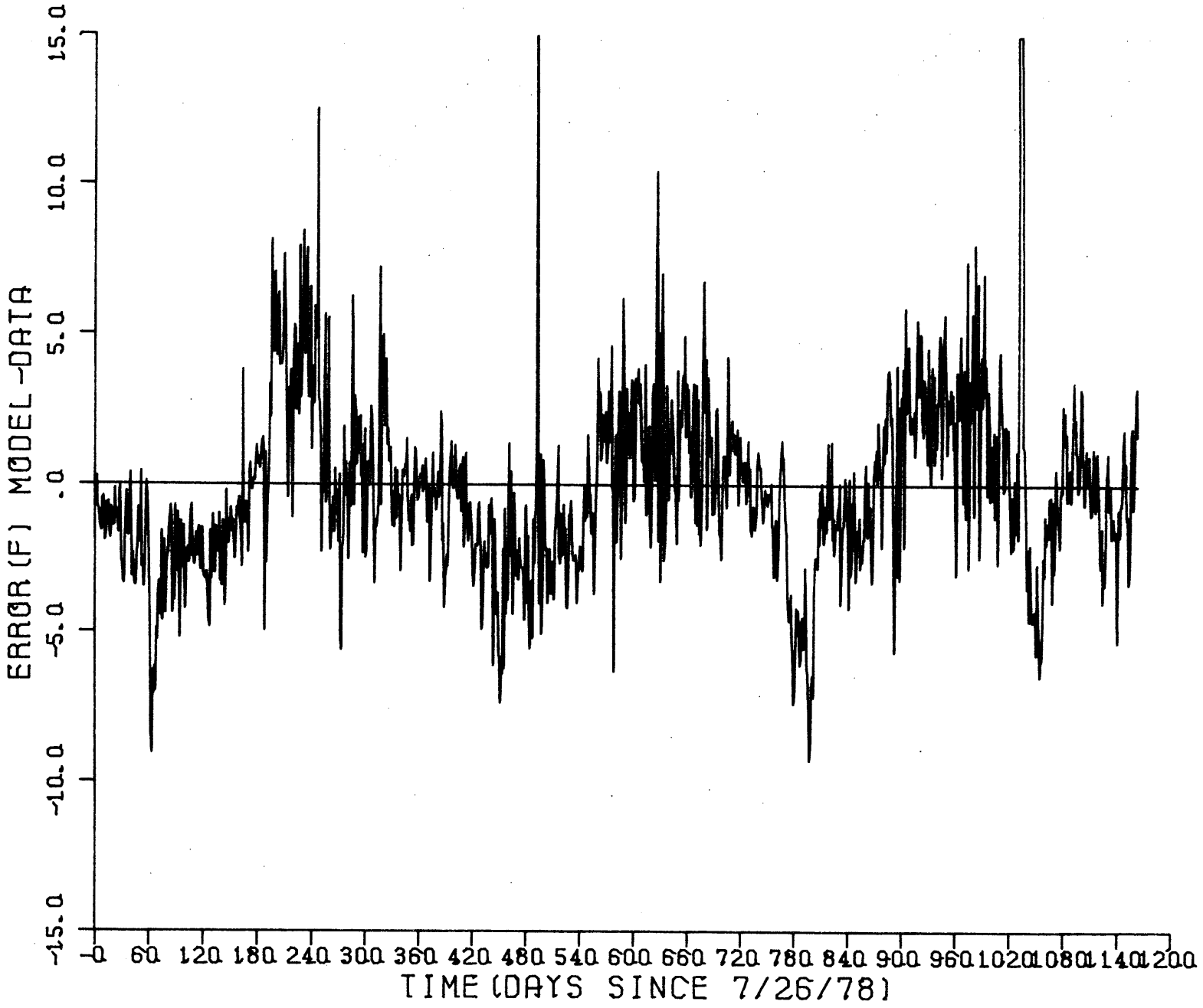

Figure 5.7: Raw Error at Dike 3 in the WHTF (Note that 15°F indicates missing data)

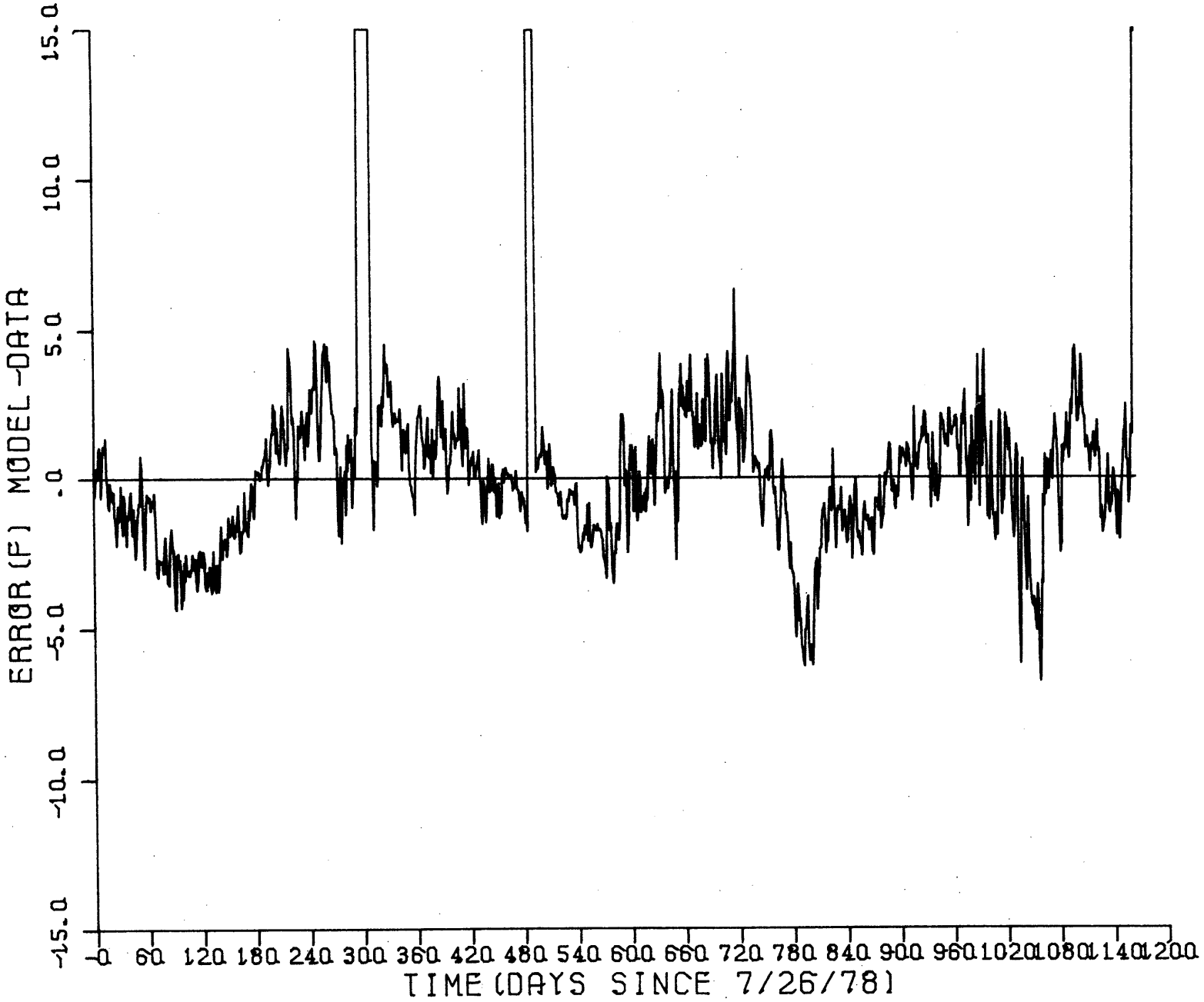

Figure 5.8: Raw Error in the Main Lake near the N. Anna Dam (Note that 15°F indicates missing data)

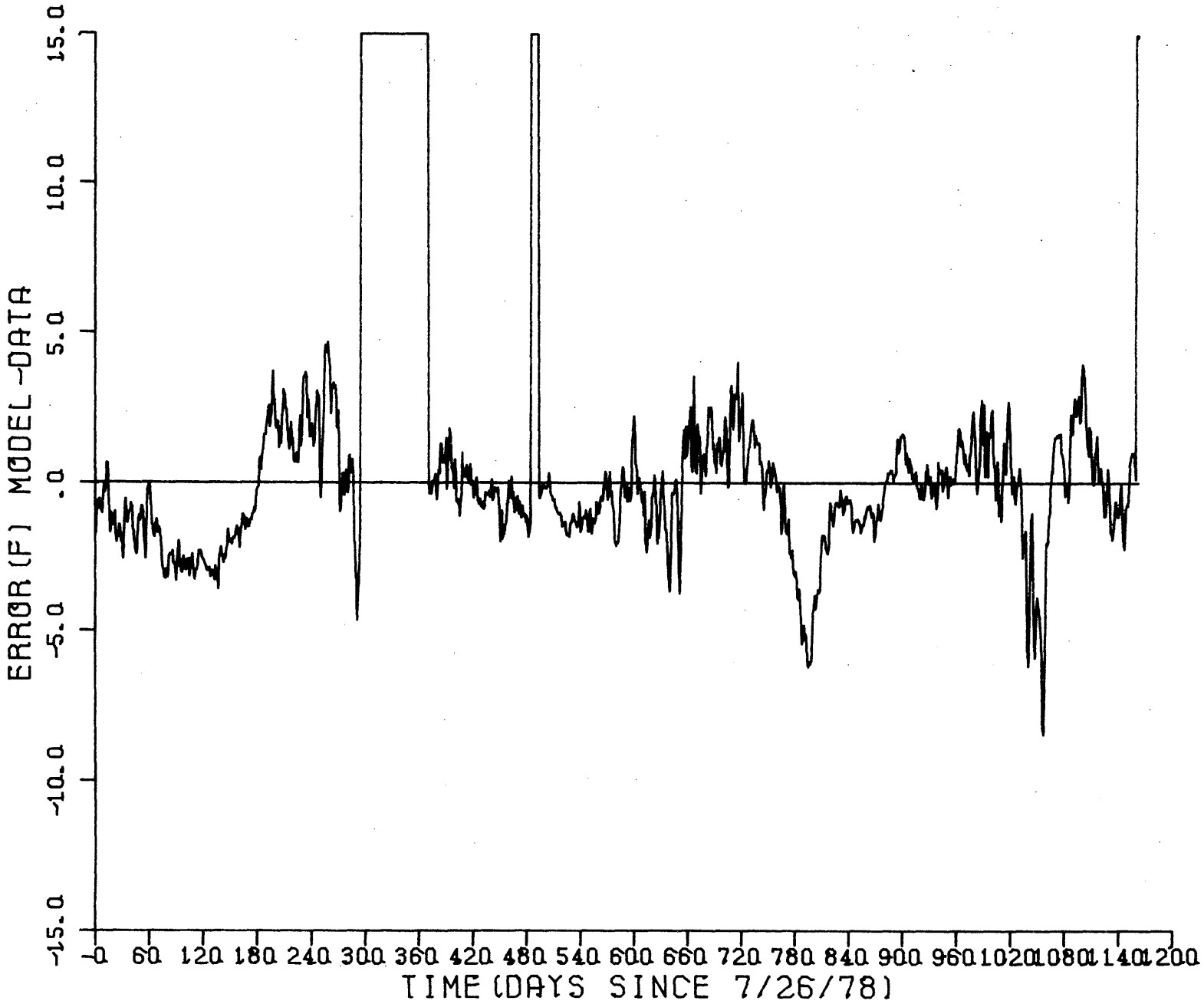

Figure 5.9: Raw Error in the Main Lake near the Intake (Note that 15°F indicates missing data)

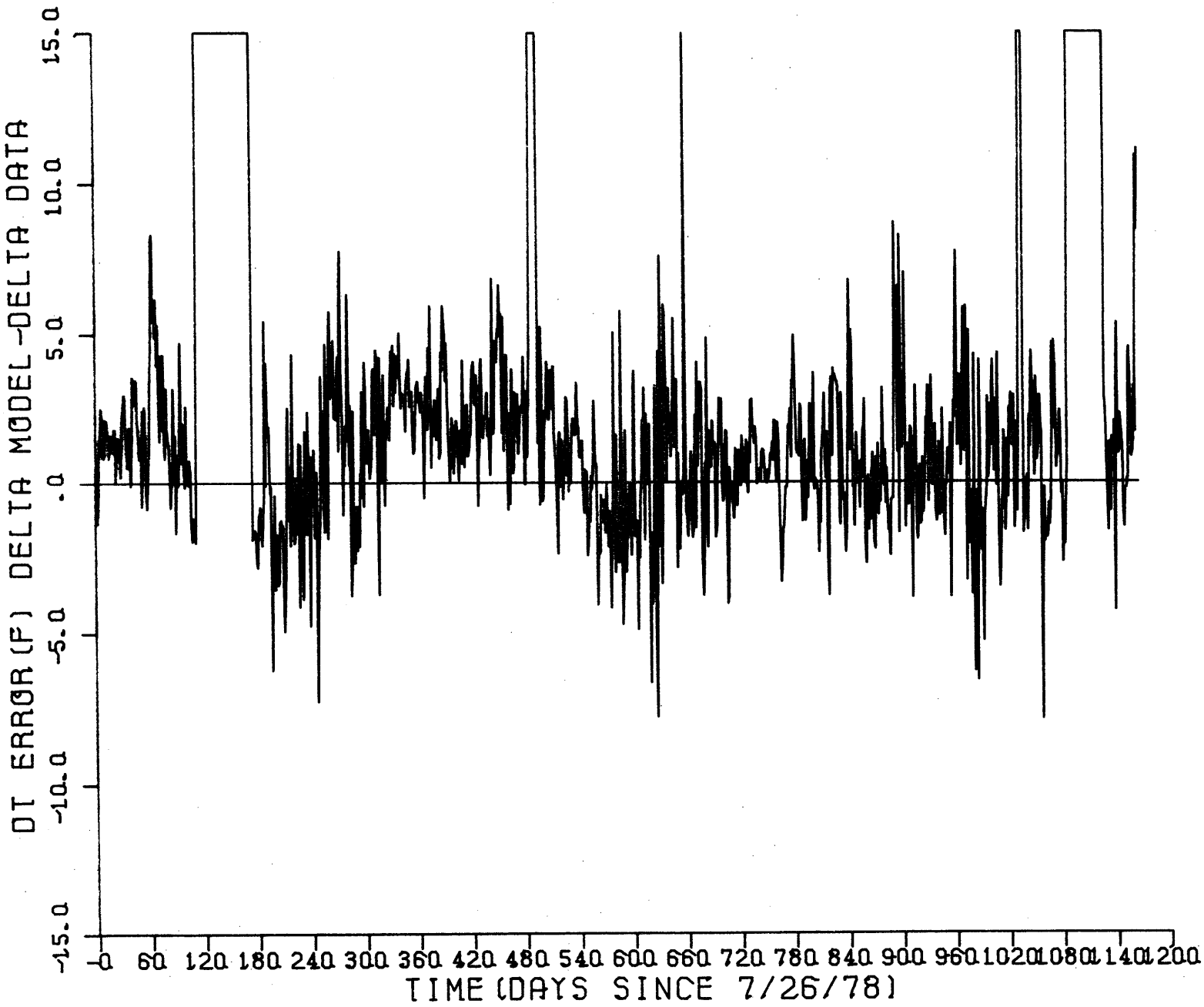

Figure 5.10: Delta Error over the WHTF (Note that 15°F indicates missing data)

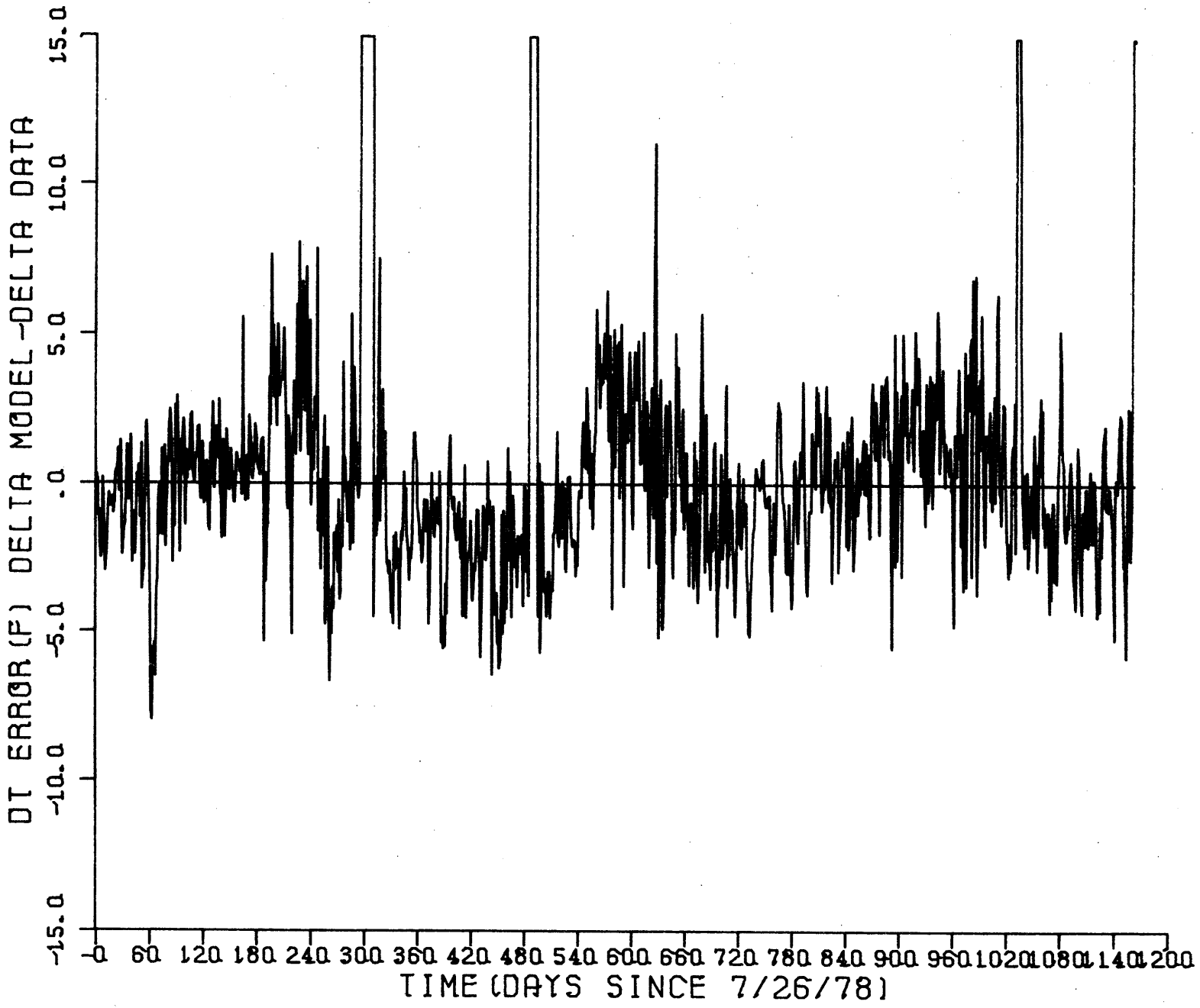

Figure 5.11: Delta Error for Dike 3 Mixing (Note that 15°F indicates missing data)

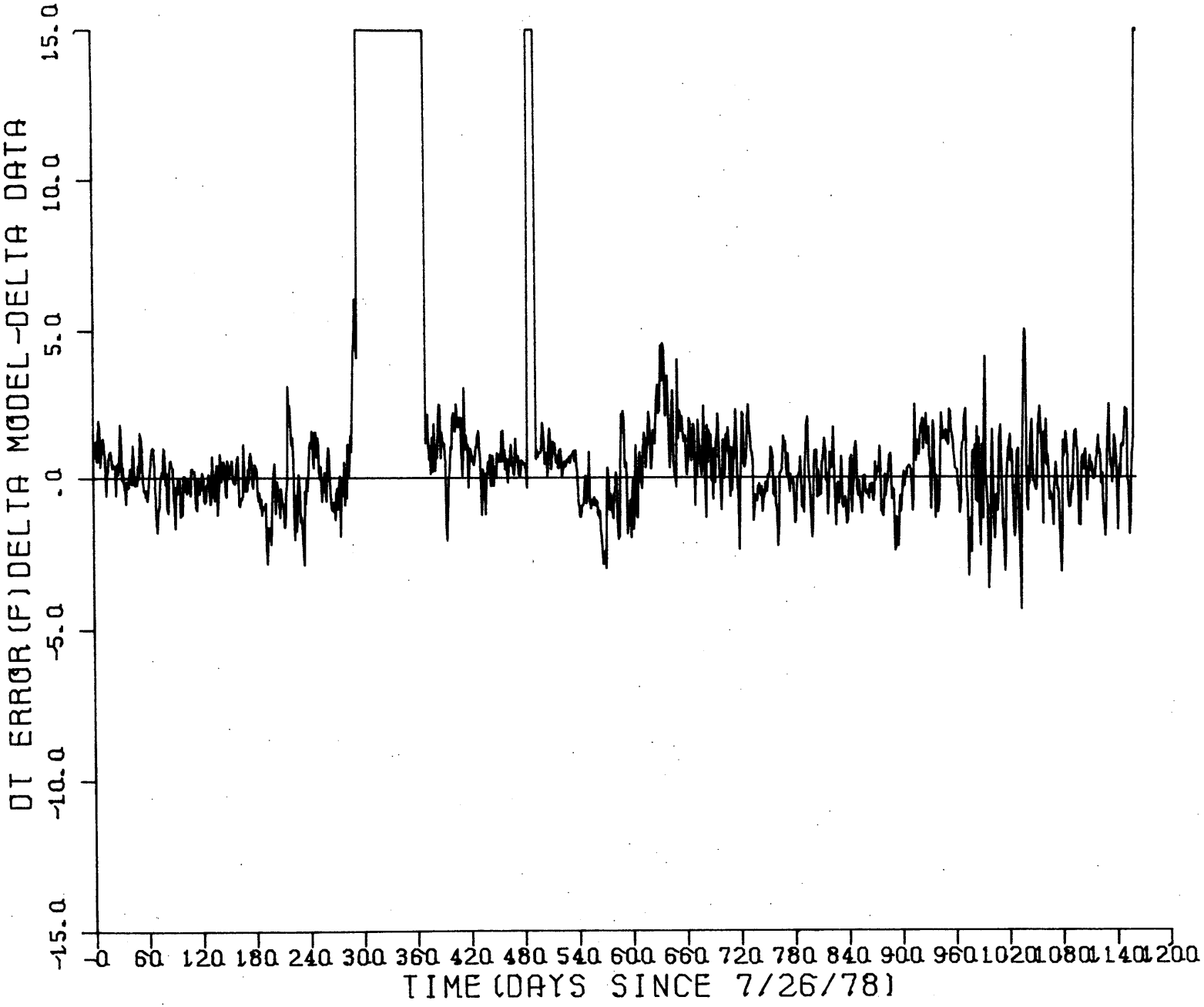

Figure 5.12: Delta Error over the Main Lake (Note that $15^{o}F$ indicates missing data)

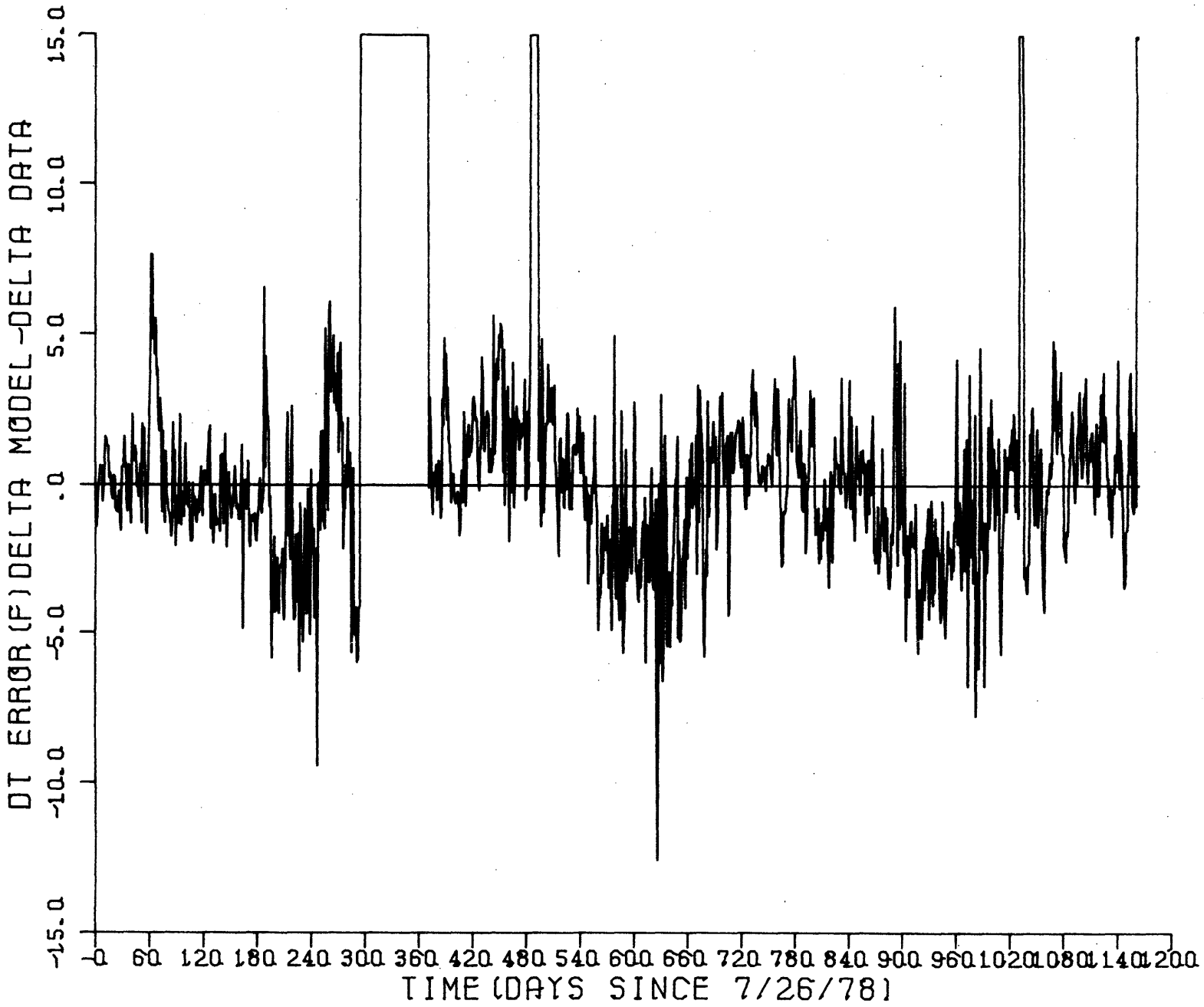

Figure 5.13: Delta Error for the Plant (Note that 15°F indicates missing data)

Table 5.1 Seasonal Bias in Surface Temperature Prediction at the Dam

"Raw" Error at the Dam

Season	% within ± 2°F	Mean(°F)	Std. Dev.(°F)
Summer (June, July, Aug., Sept. of 1978, 1979, 1980, 1981)	78.7	+0.29	2.16
Winter (Dec., Jan., Feb., 1978, 1979, 1980, 1981)	91.2	-0.51	1.49

Table 5.2 Statistical Summary of Errors in the N. Anna Predictions

Error	Percentage of Error within ± 2°F	Mean Error (°F)	Standard Deviation (°F)
"Raw" Errors	(Predicted-Measured)		
Discharge	71.4	+0.87	2.28
Dike III	65.2	-0.20	2.81
Dam	80.1	-0.07	2.03
Intake	83.2	-0.40	1.83
"Delta" Errors	(Predicted ΔT-Measured ΔT)		
WHTF	69.8	+0.98	2.38
Dike III Mixing	68.8	-0.14	2.54
Main Lake	96.3	+0.25	1.21
Plant	73.9	-0.17	2.39

Examination of Figures 5.6-5.13 shows the model's accuracy to be well verified with only modest seasonal biases (see Table 5.1 above). Interestingly, many of the larger errors shown in Figures 5.6-5.9 are correlated with unusual (possibly inaccurate) meteorological data, especially short-wave solar radiation (see Figure 4.5), and with periods of intermittent plant operation (see Figure 4.15).

6. HISTORICAL SIMULATION OF ONE, TWO AND THREE UNIT OPERATION

Since the model's validity was established, the model's ability to predict temperature conditions over a wide range of meteorological conditions was used to evaluate the plant's thermal effects on Lake Anna. The model was used to perform temperature simulations for the period April 1, 1957 through March 31, 1967. Meteorological data for these years was complied (see Section 2.2.2.1) and used with constant plant operating conditions for one, two and three nuclear units. The computer "runs" were performed in five year segments with initial conditions for the last 5 years (beginning April 1, 1962) taken from the last day of simulation of the first 5 year segment. Initial temperatures for the first five years were isothermal at 50.0°F, 54.0°F, and 58.0°F for one, two and three units, respectively, on April 1, 1957. The results from these simulations are grouped in the following manner: (i) summer surface and hypolimnetic temperatures at the North Anna Dam for each simulation year, (ii) representative vertical temperature profiles in the main lake, and (iii) average summer surface temperature decay in the main lake.

6.1 Temperature Conditions at the Lake Anna Dam

Figures 6.1, 6.2 and 6.3 show plots of temperature versus time for 1, 2 and 3-unit operation, respectively, at three vertical locations: (1) lake surface at the dam, (2) a depth of 44 feet below

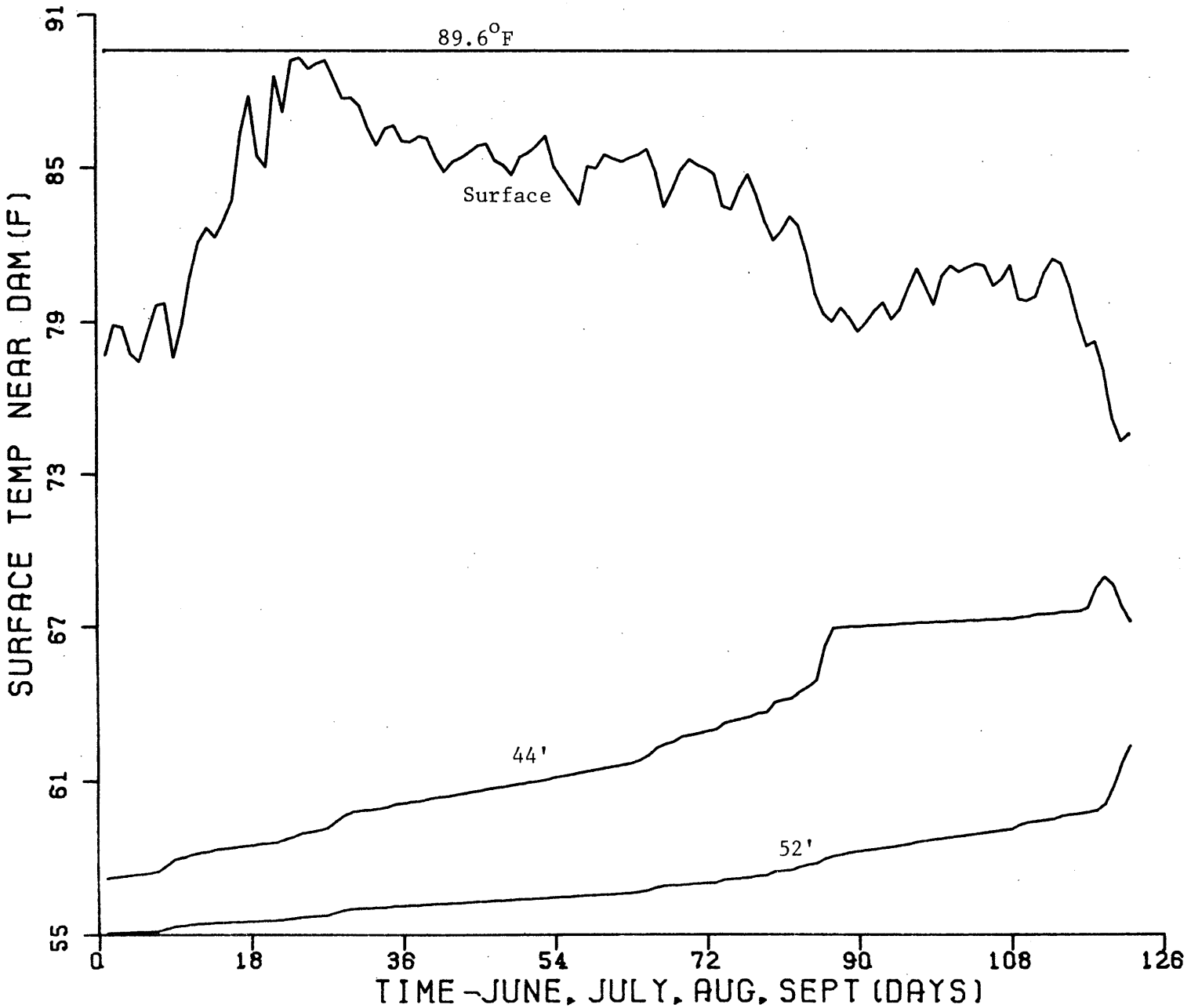

Figure 6.1a: Summer Temperatures at the North Anna Dam for One Nuclear Unit, 1957

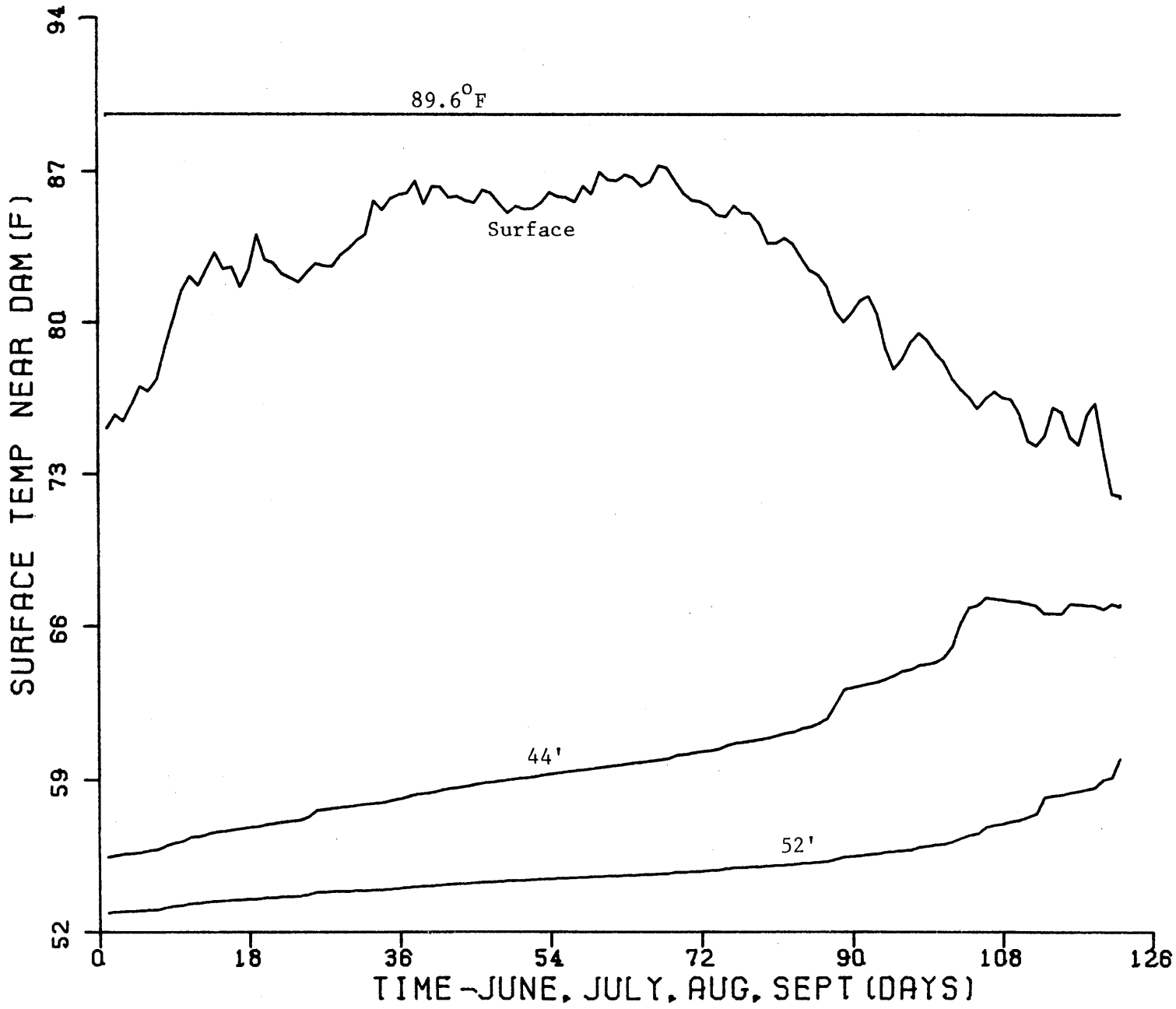

Figure 6.1b: 1958

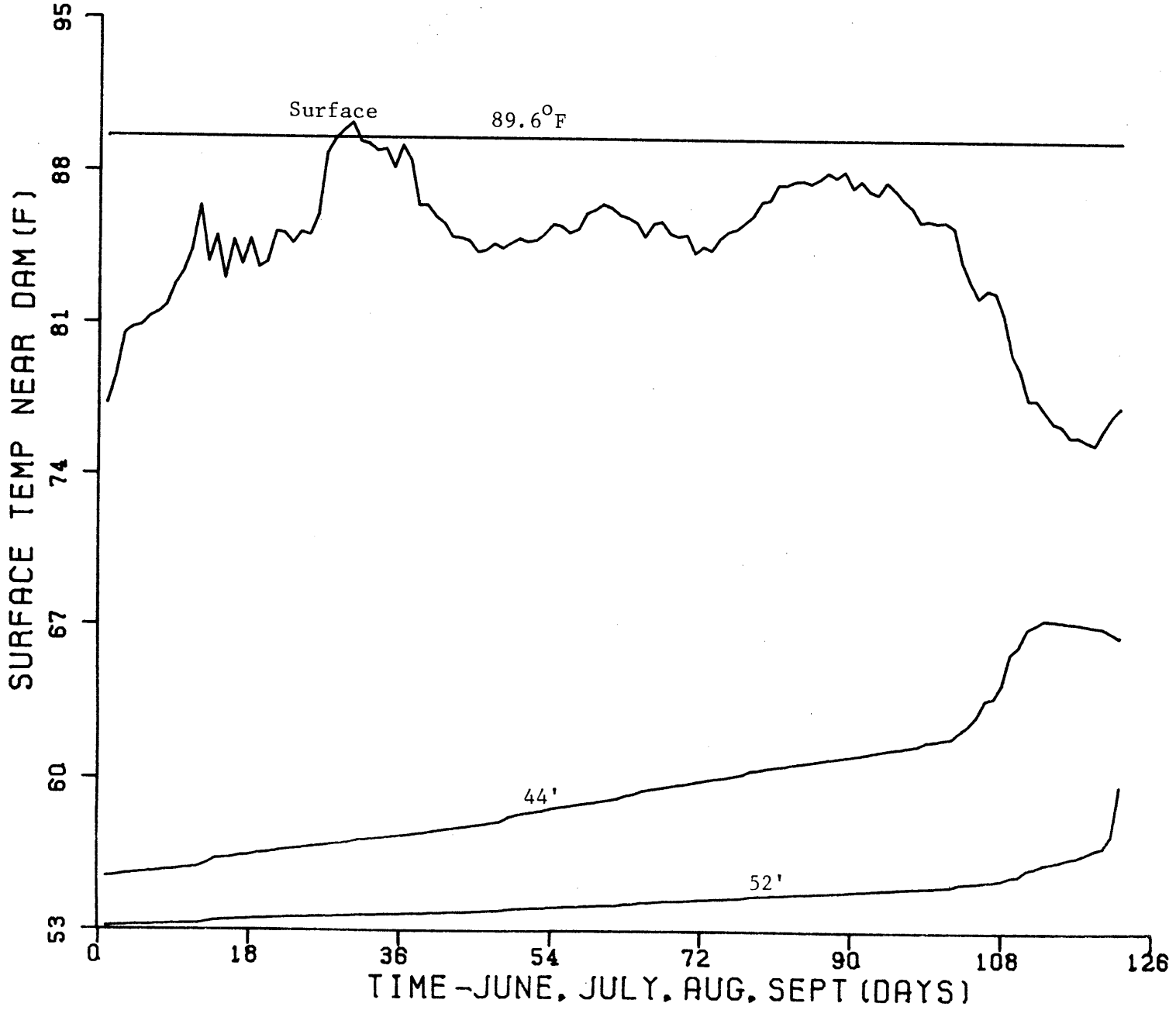

Figure 6.1c: 1959

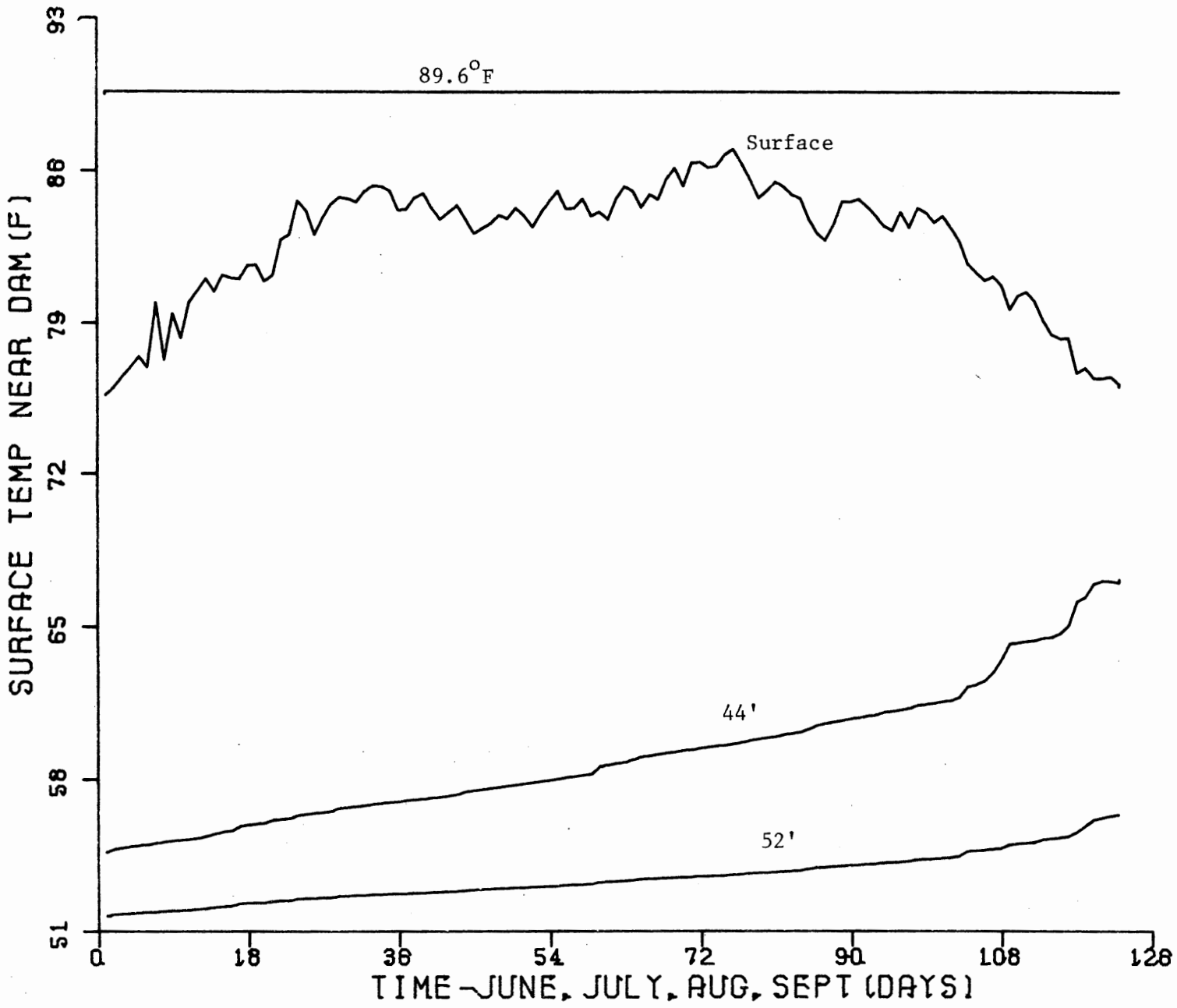

Figure 6.1d: 1960

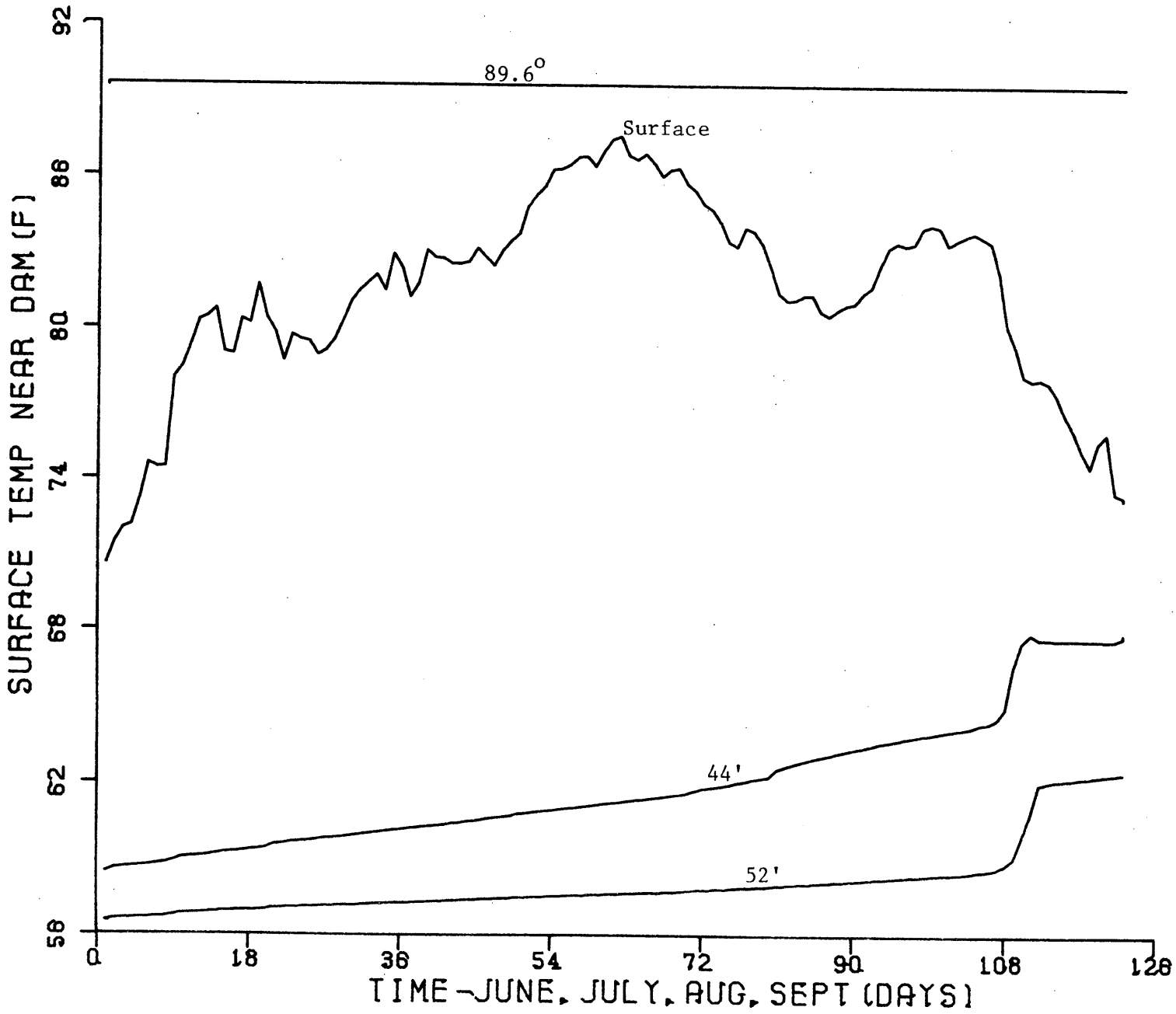

Figure 6.1e: 1961

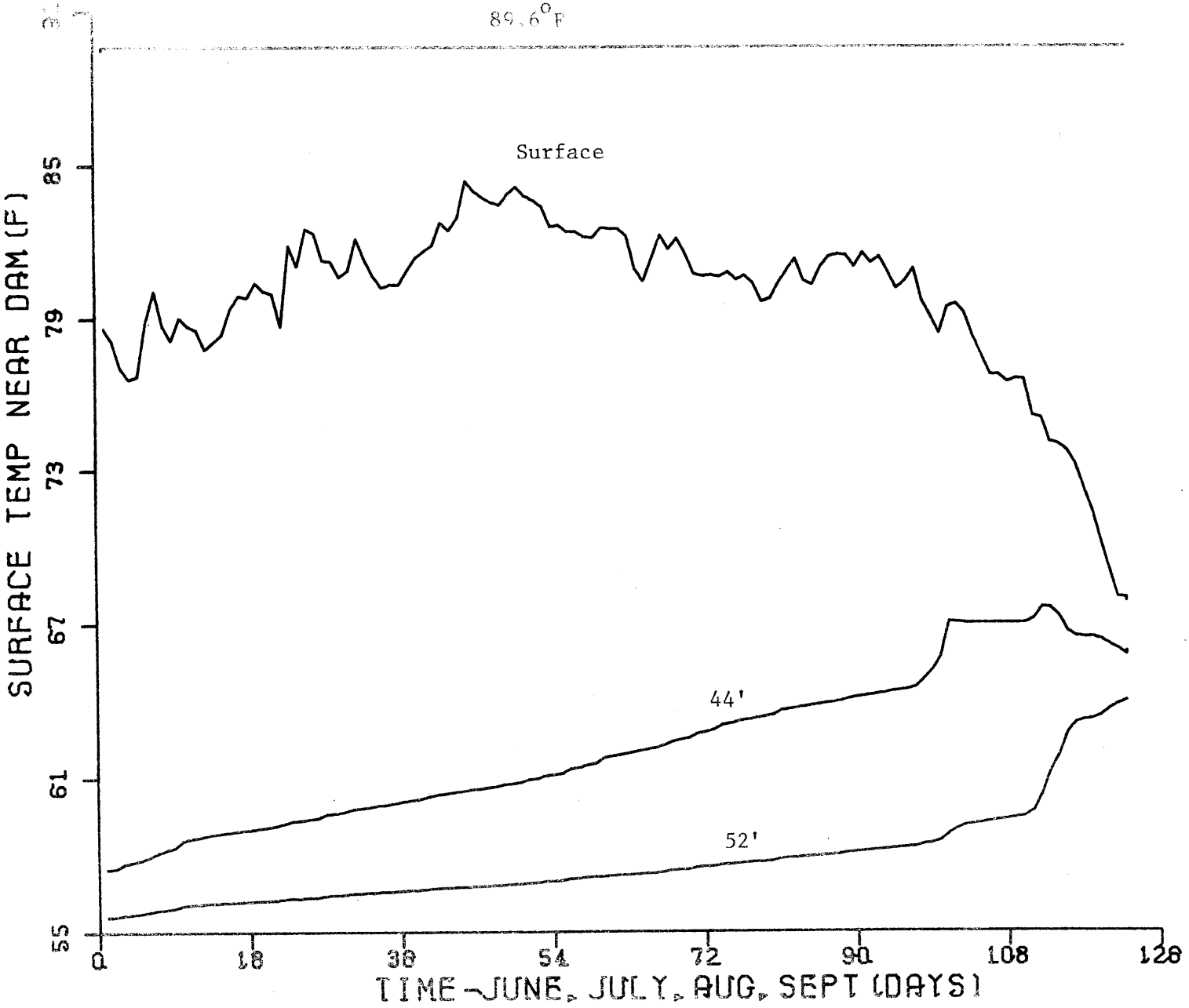

Figure 6.1f: 1962

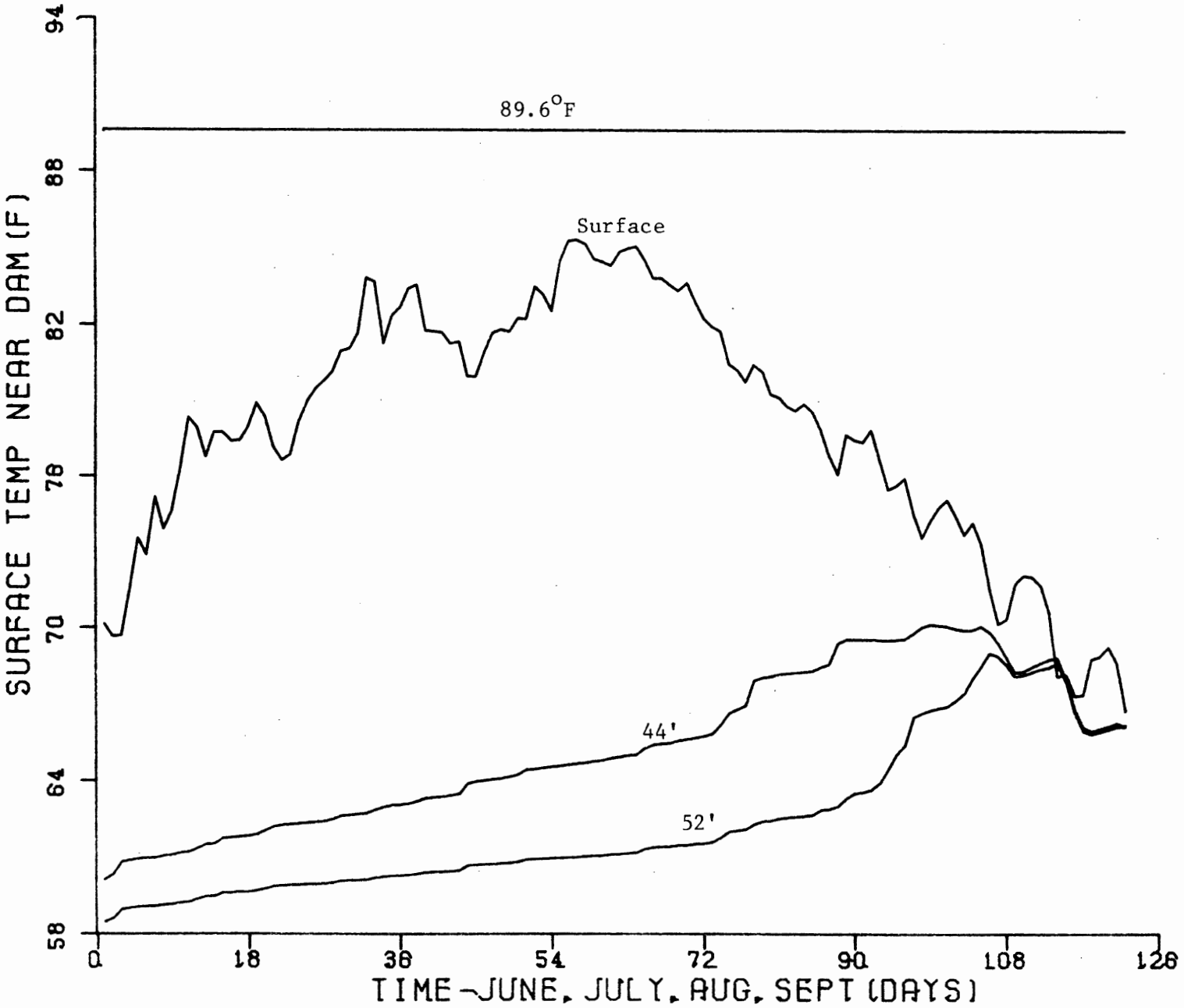

Figure 6.1g: 1963

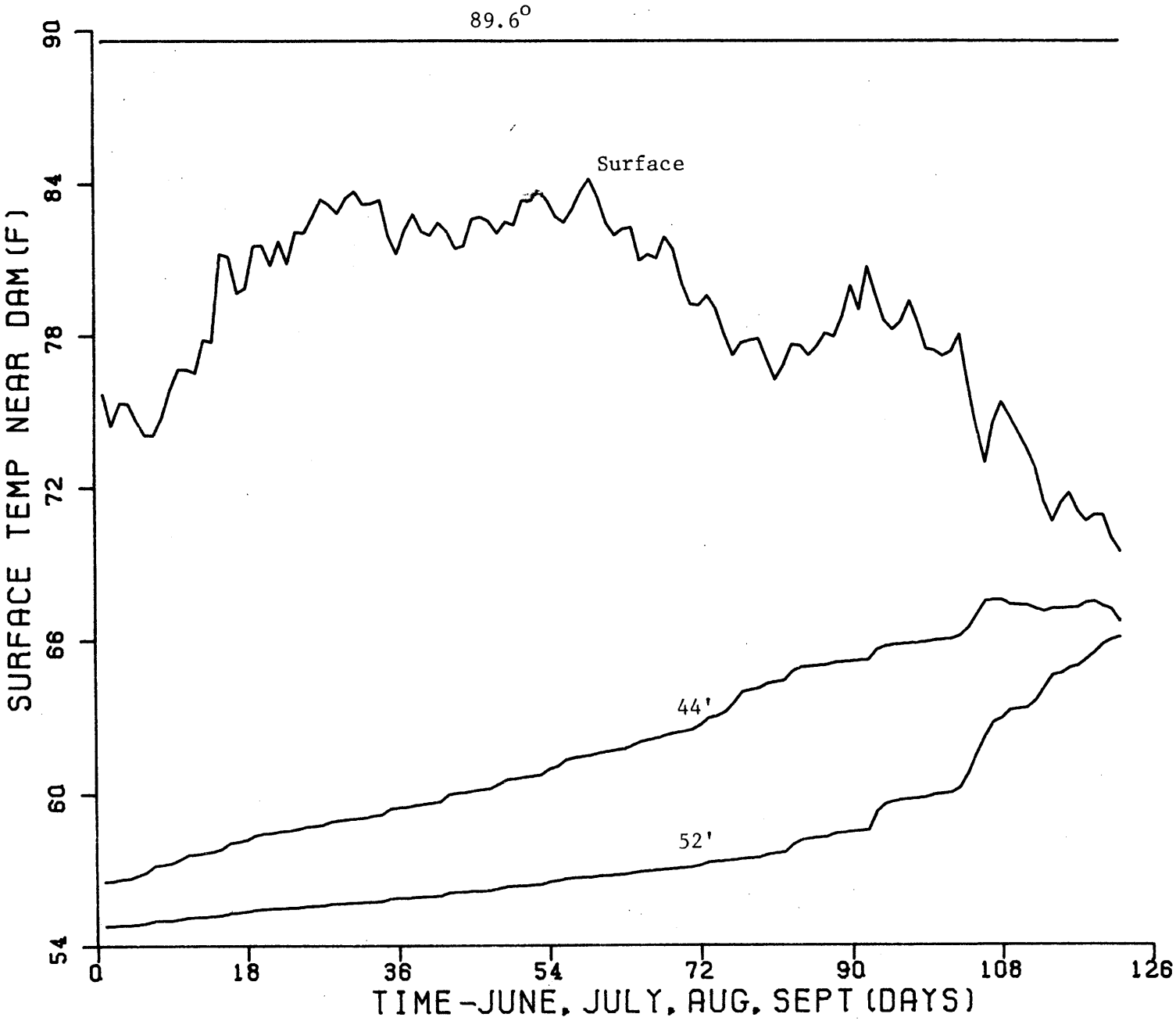

Figure 6.1h: 1964

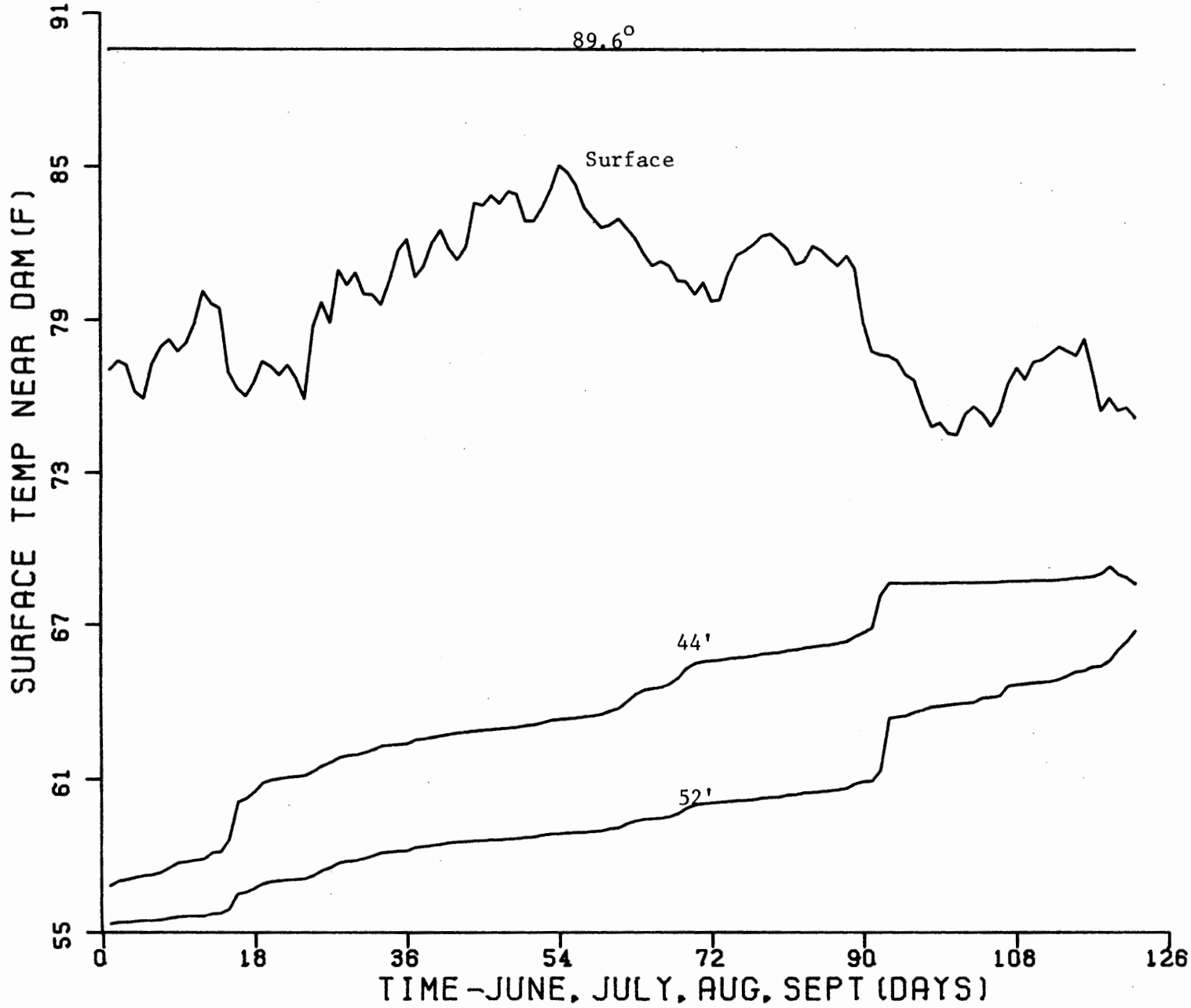

Figure 6.1i: 1965

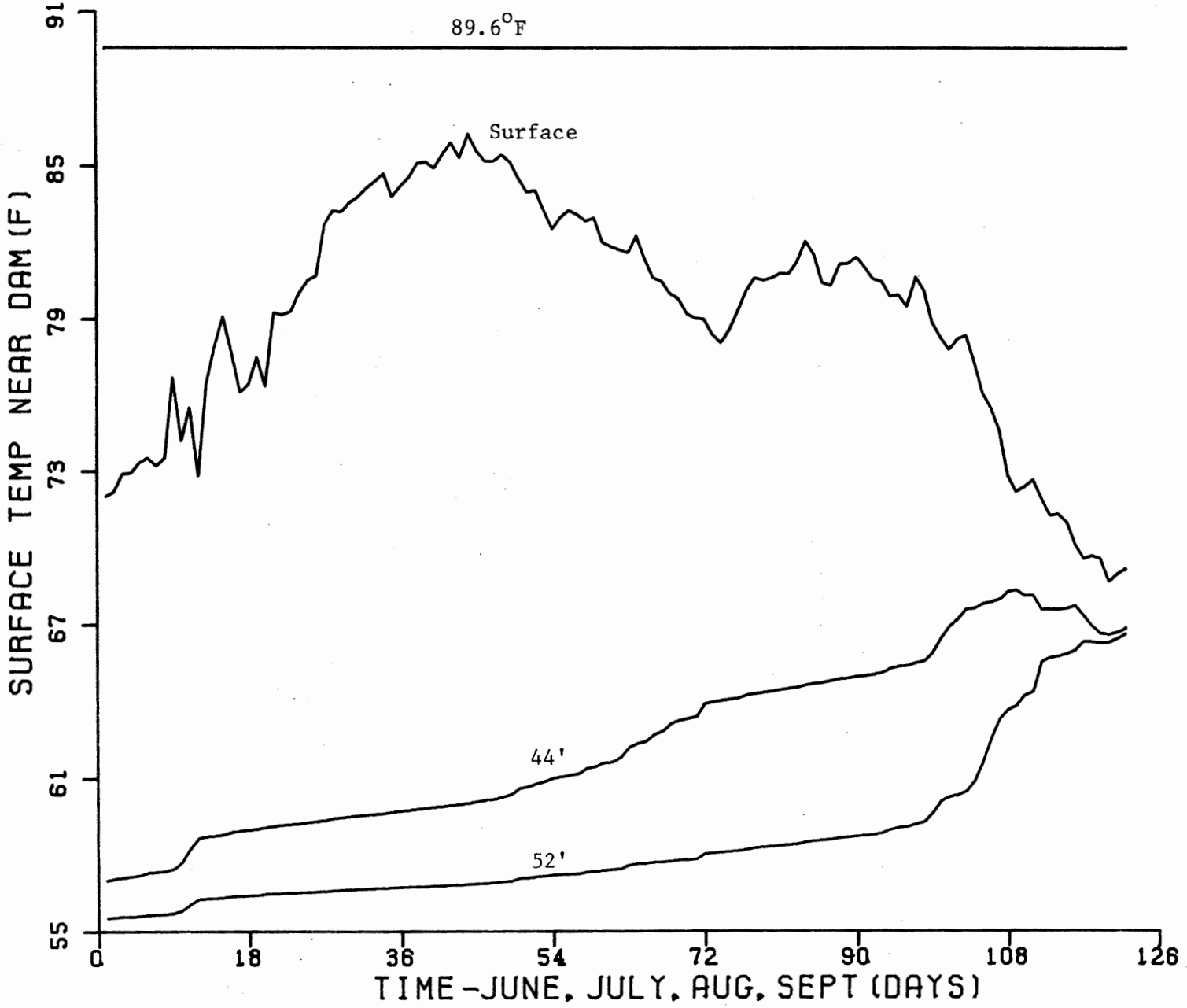

Figure 6.1j: 1966

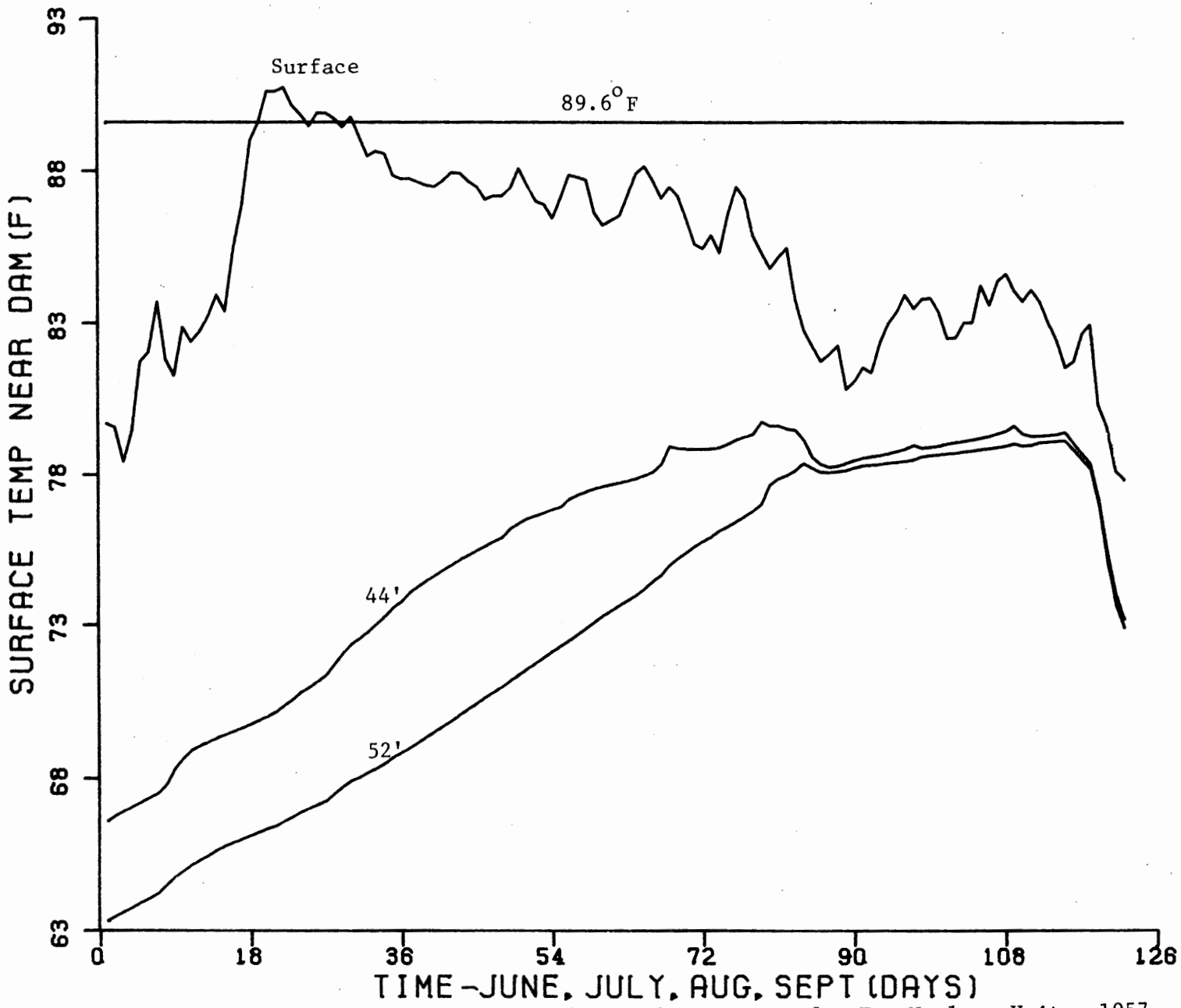

Figure 6.2a Summer Temperatures at the North Anna Dam for Two Nuclear Units, 1957

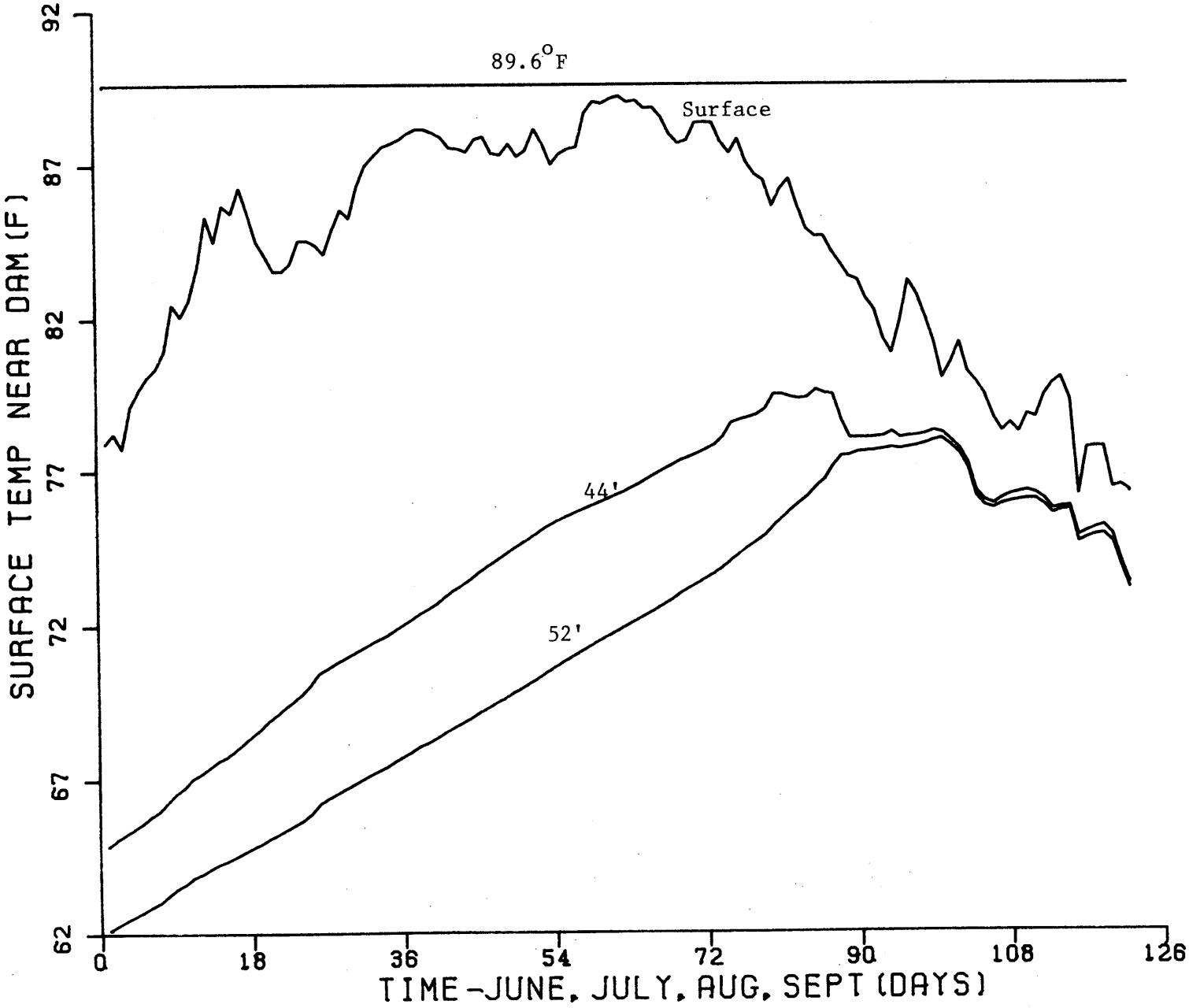

Figure 6.2b 1958

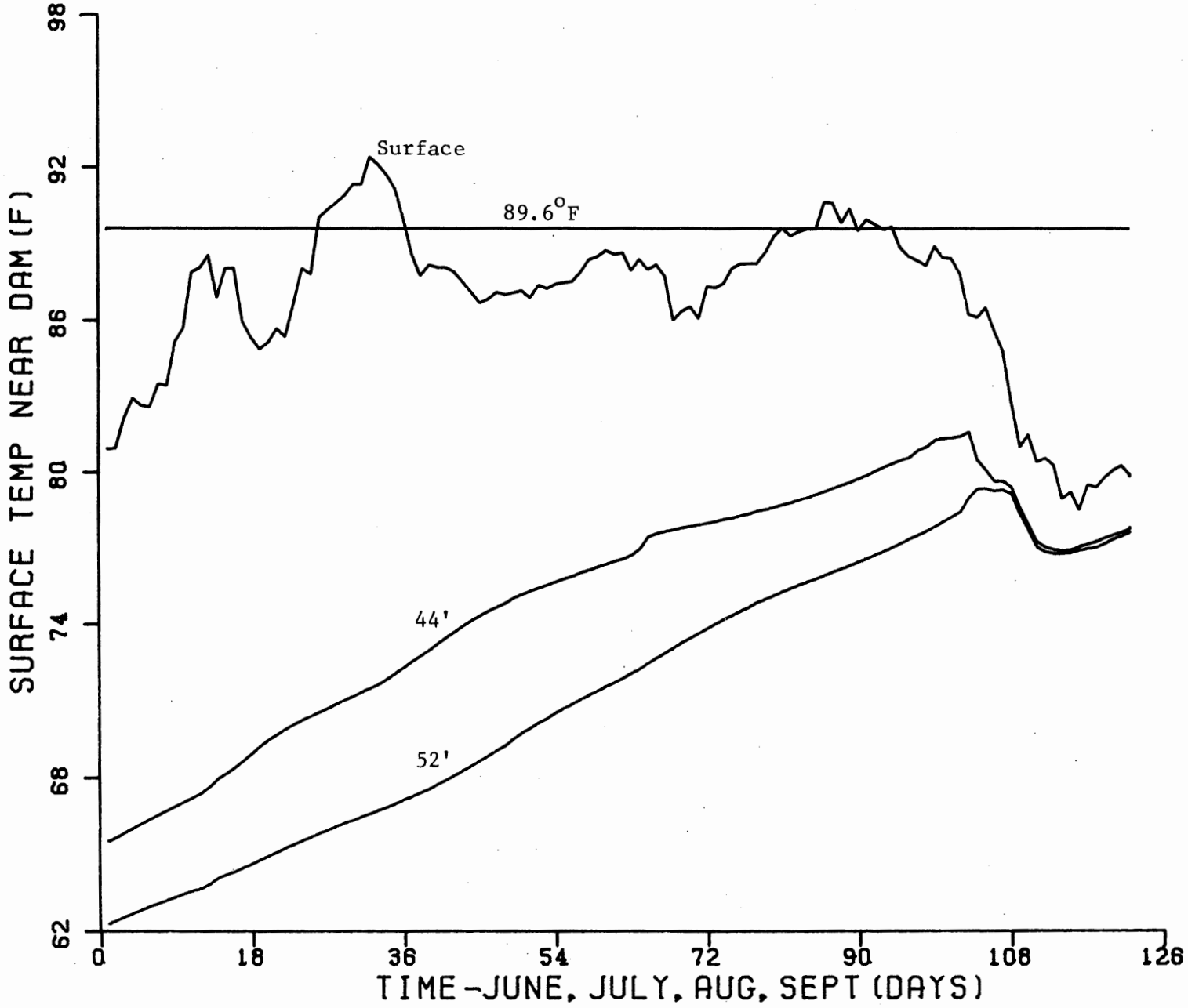

Figure 6.2c 1959

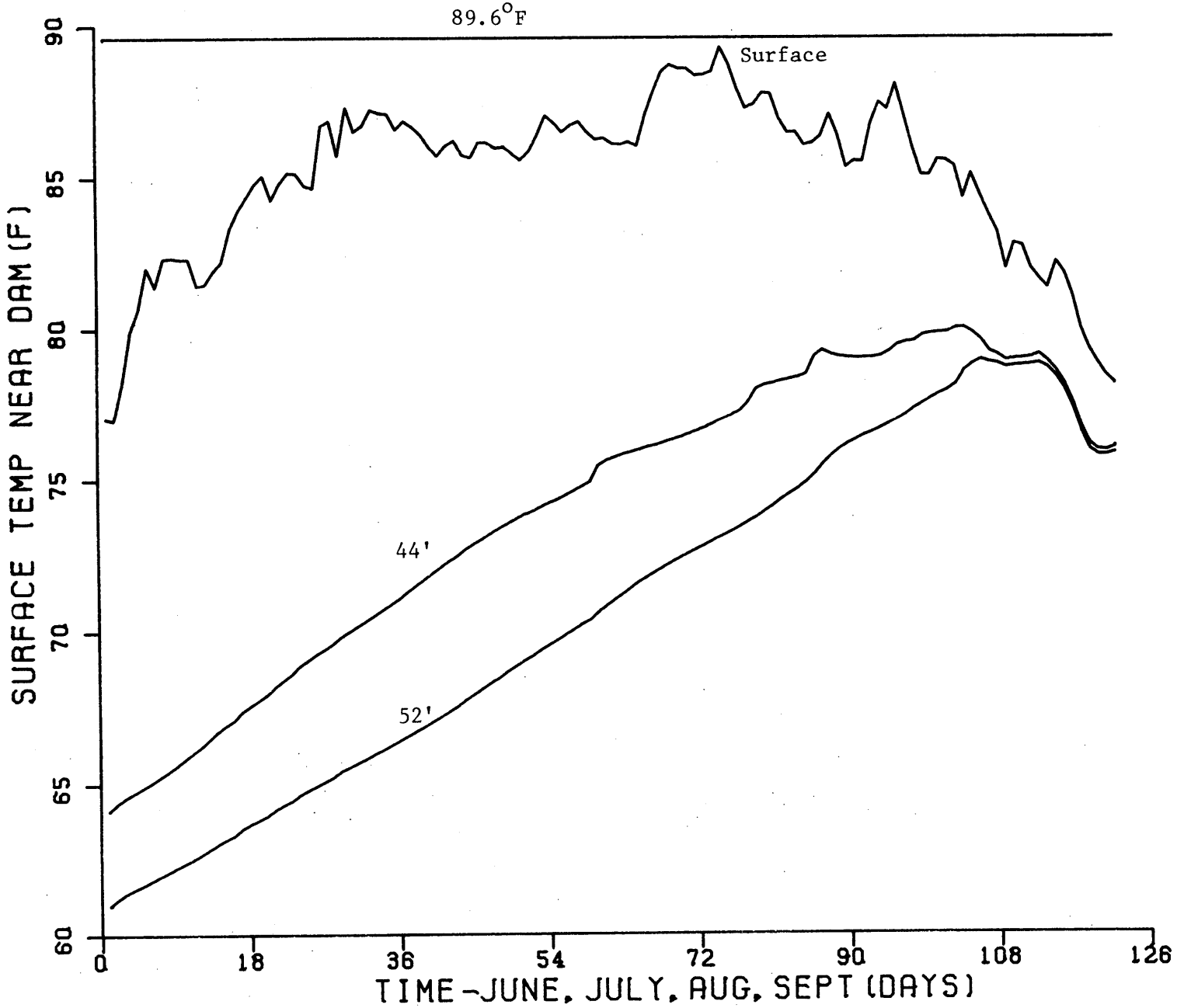

Figure 6.2d 1960

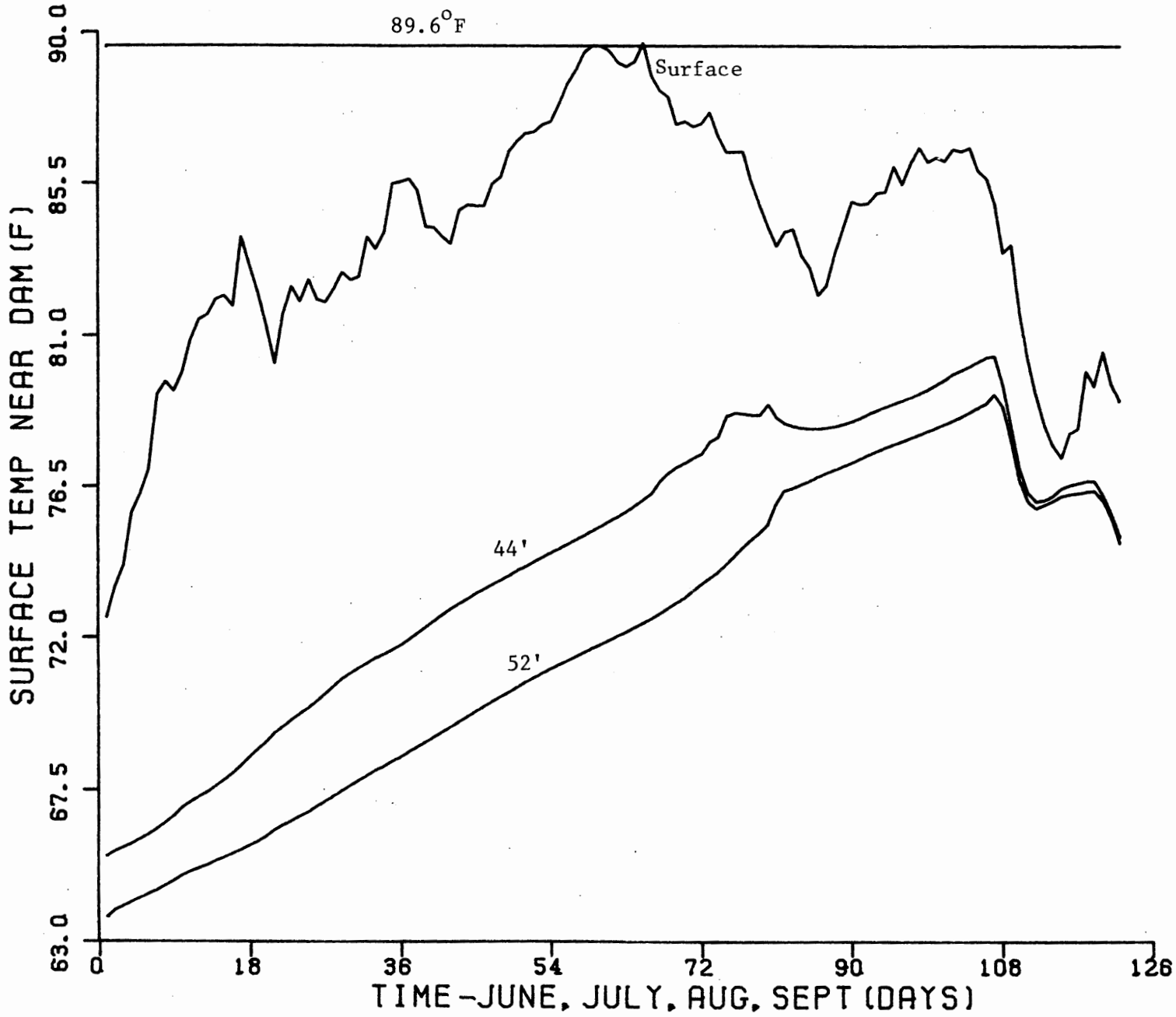

Figure 6.2e 1961

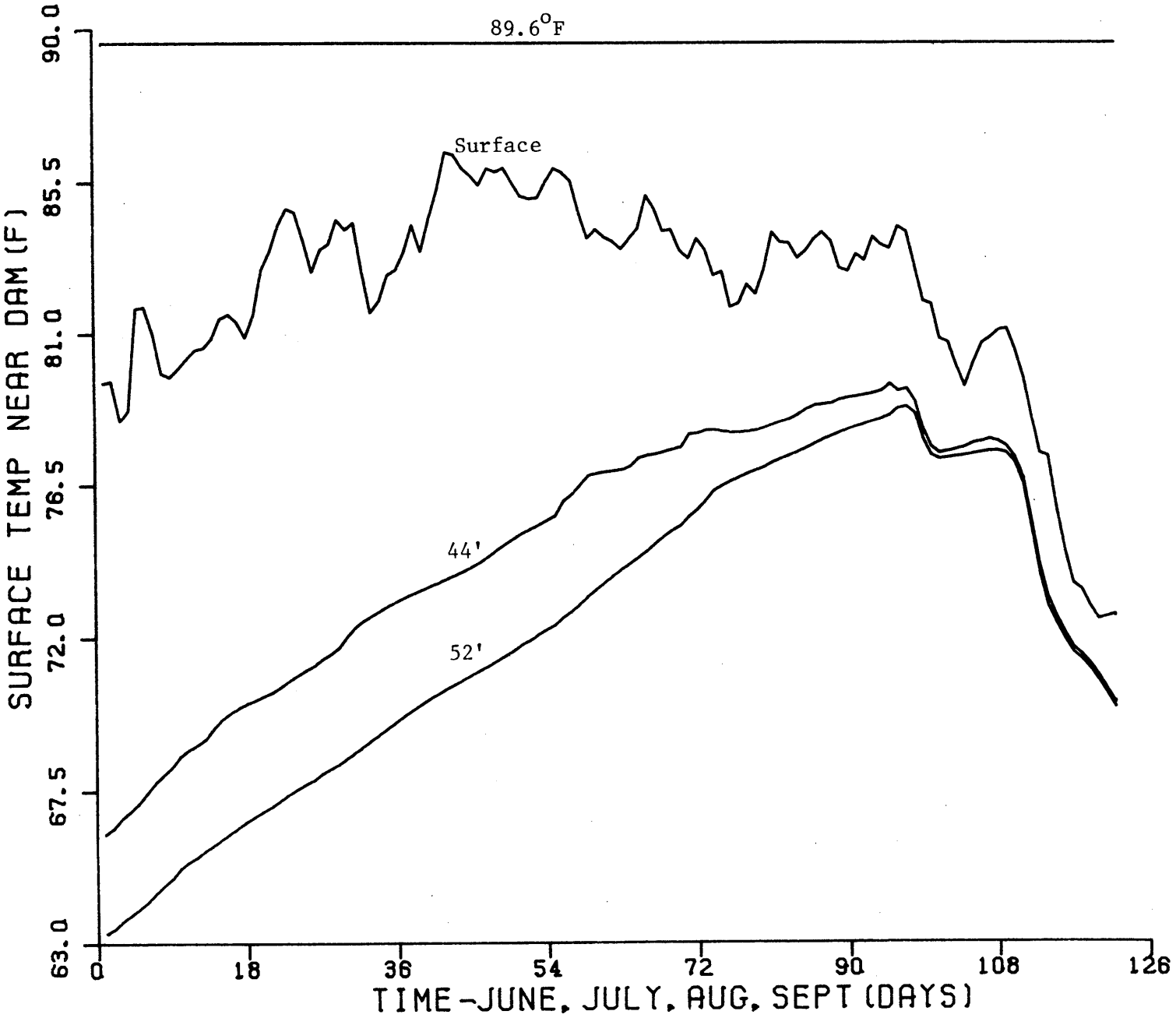

Figure 6.2f 1962

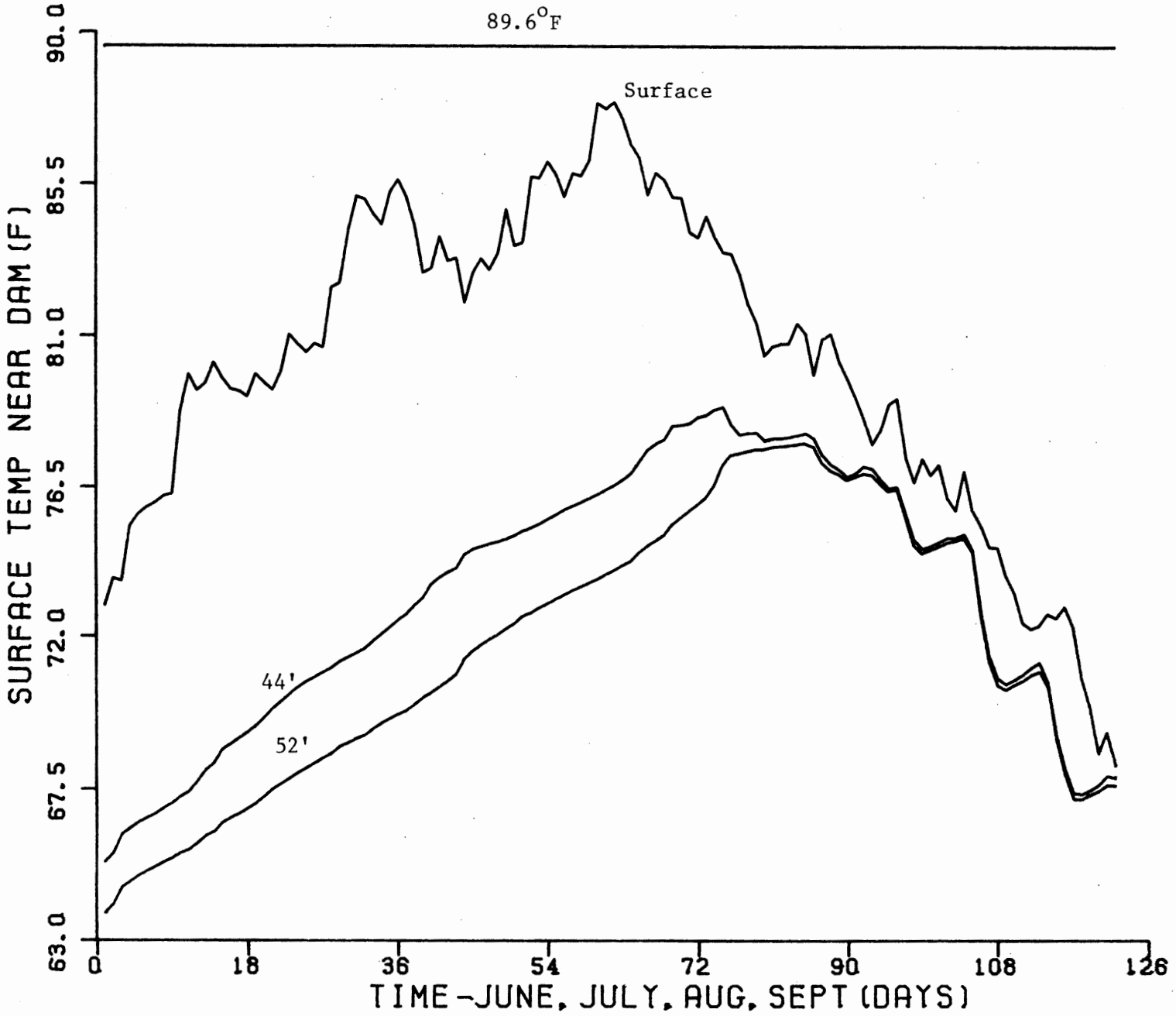

Figure 6.2g 1963

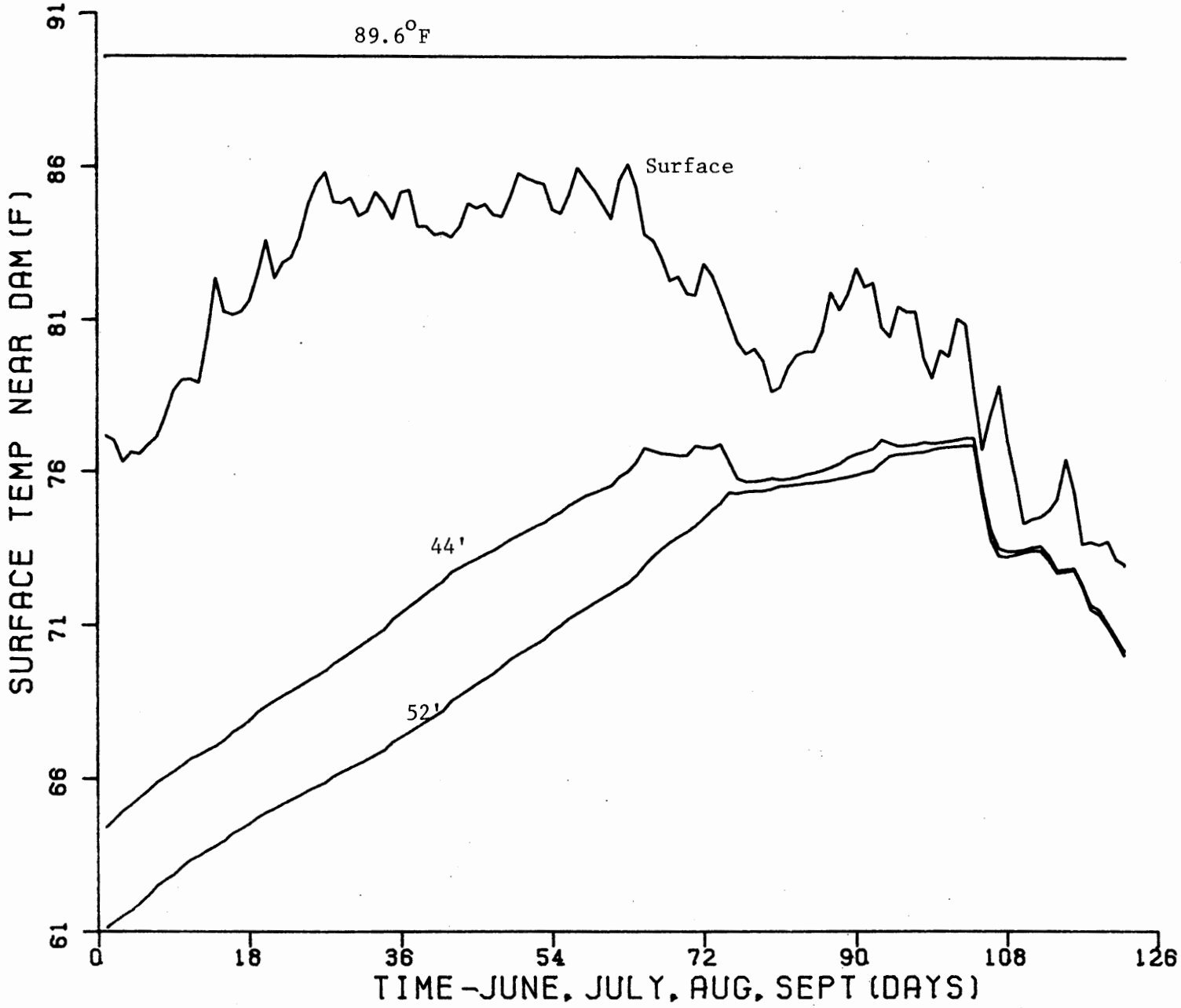

Figure 6.2h 1964

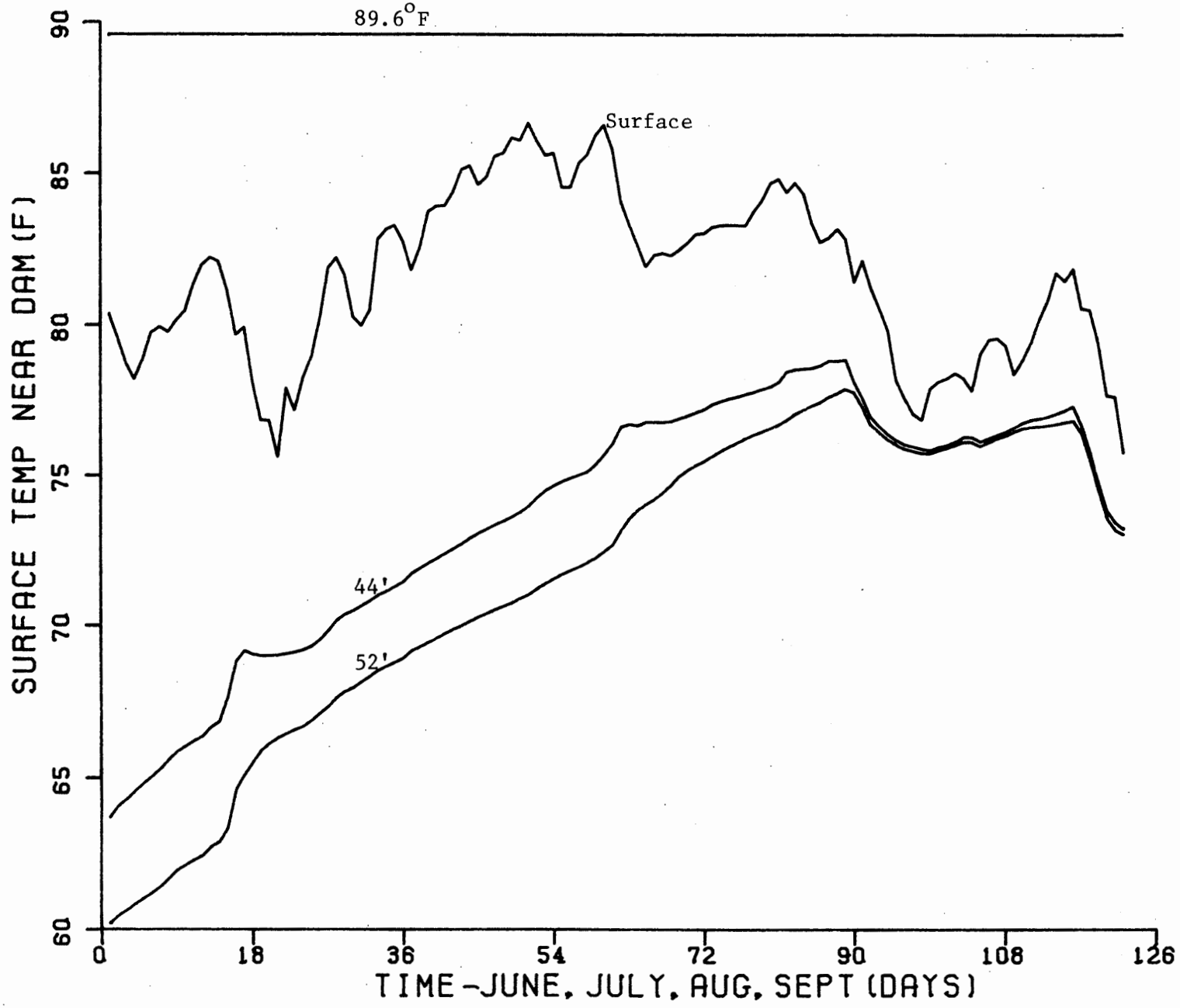

Figure 6.2i 1965

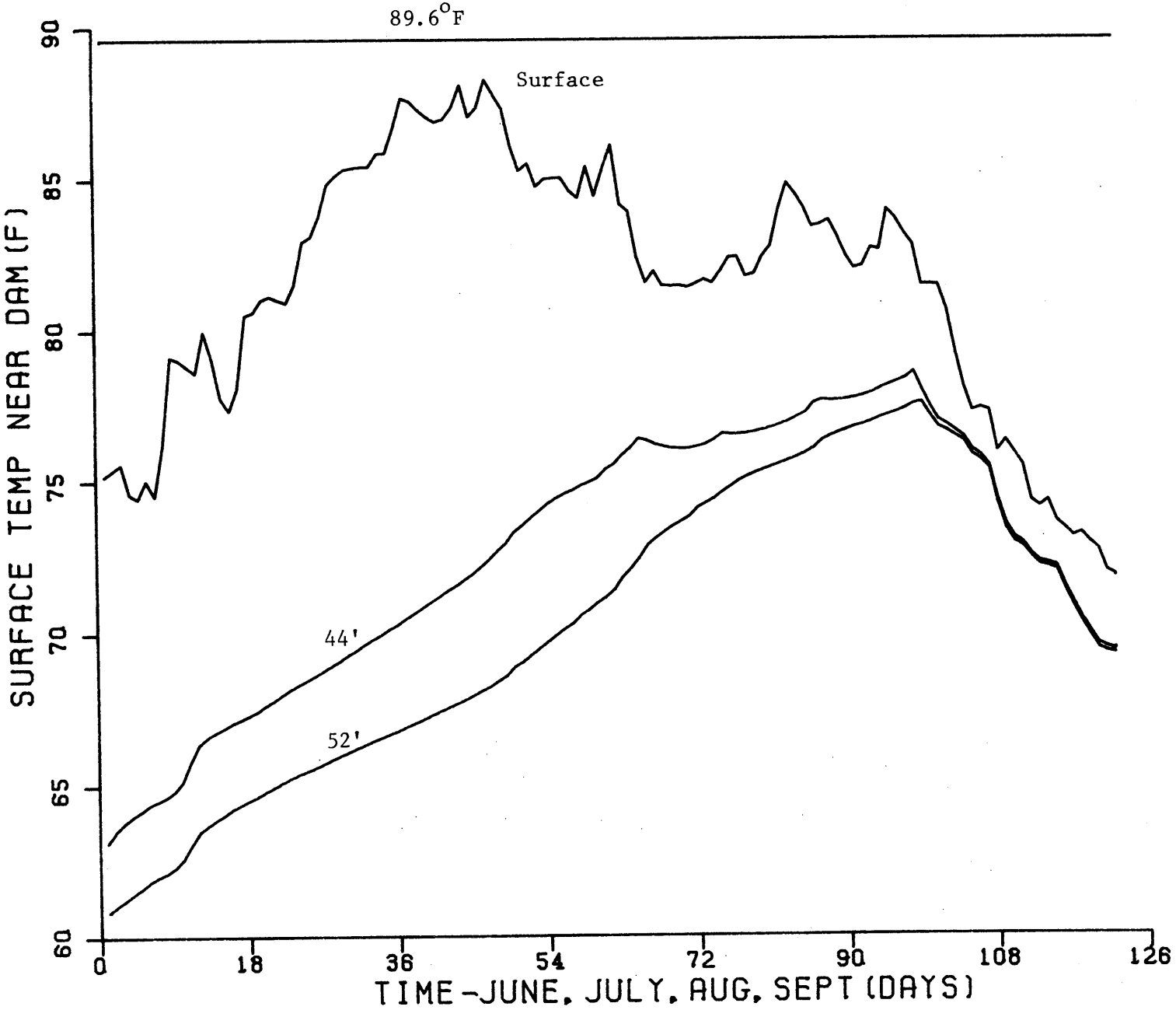

Figure 6.2j 1966

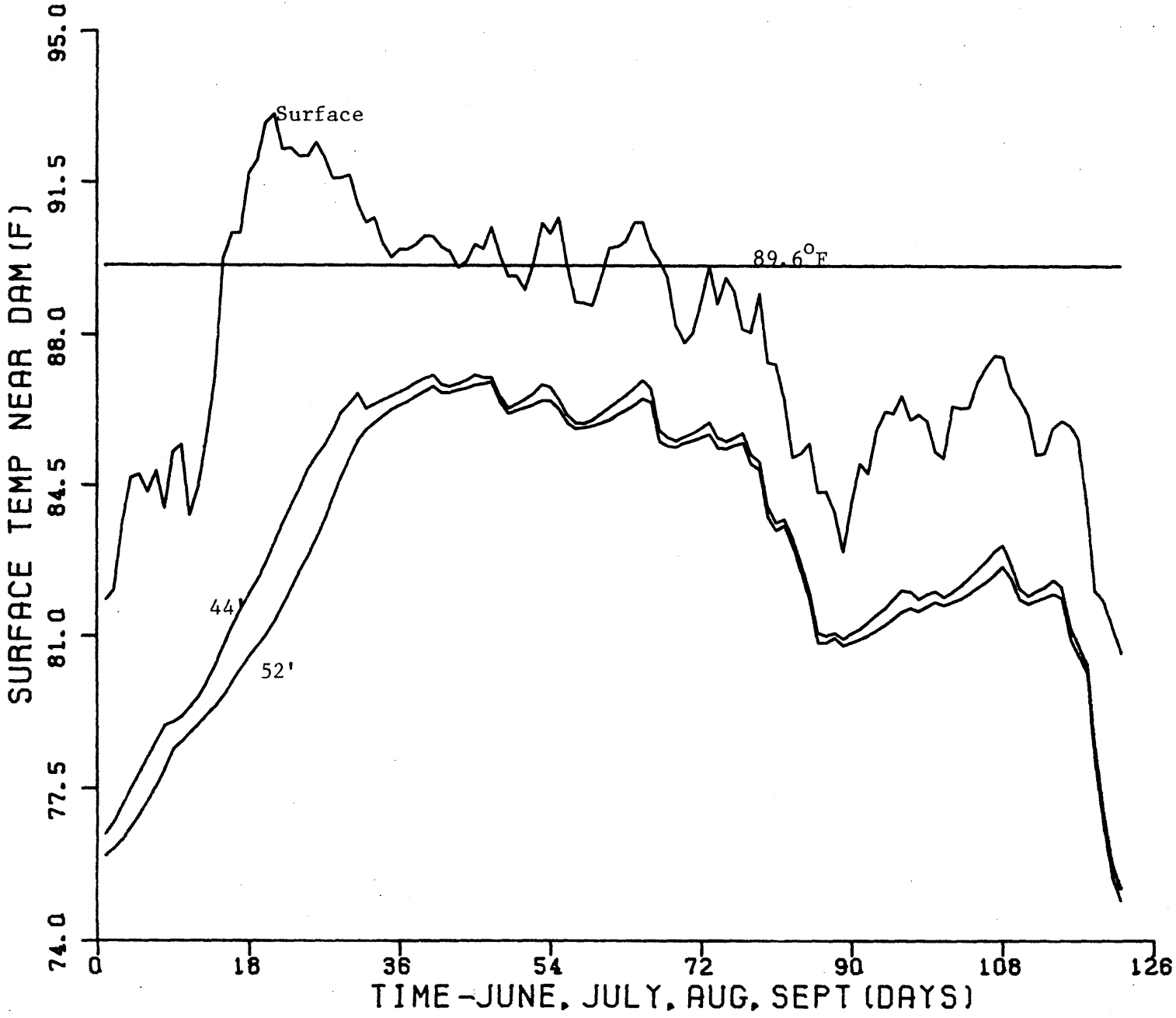

Figure 6.3a: Summer Temperatures at the North Anna Dam for Three Nuclear Units, 1957

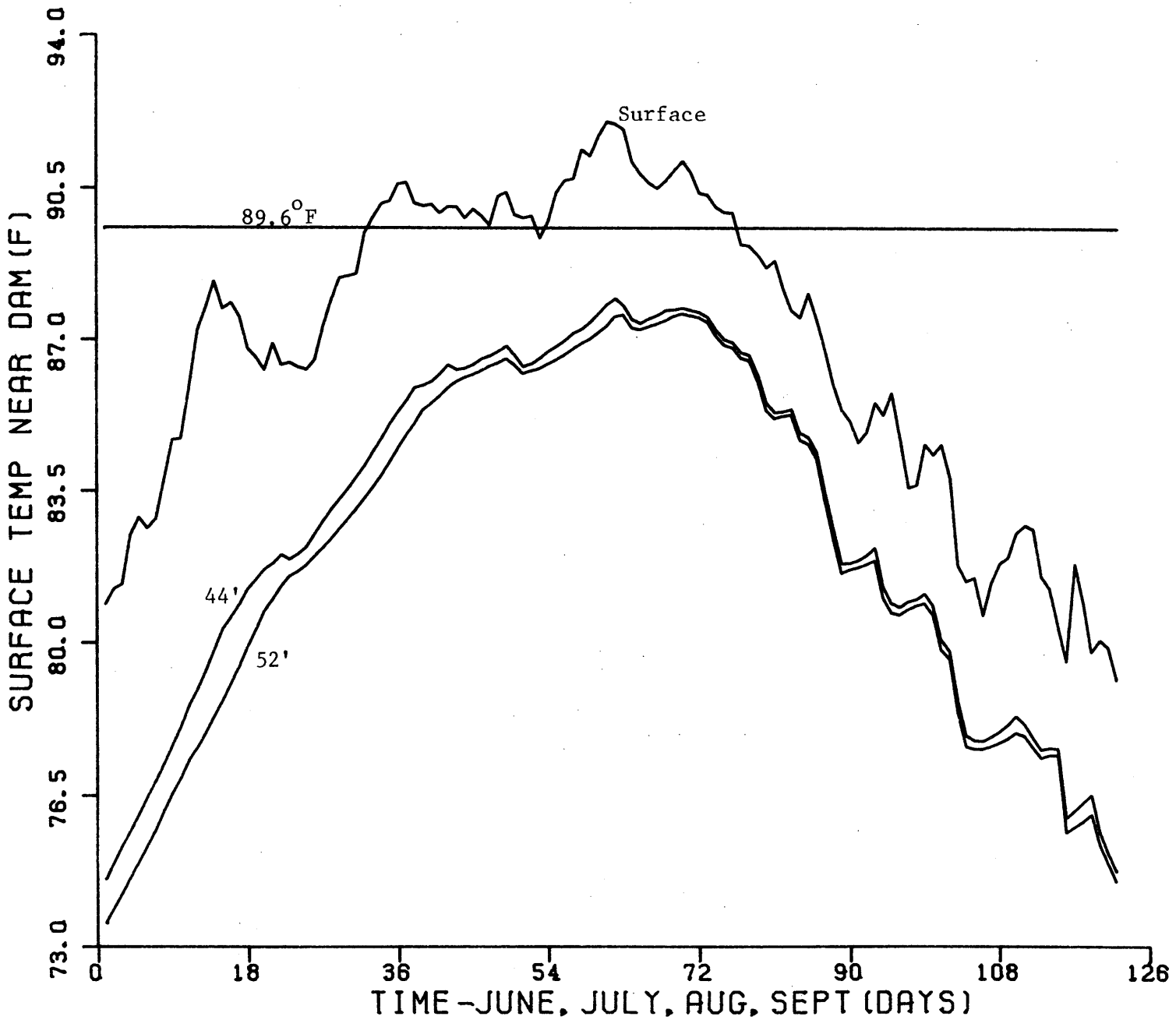

Figure 6.3b: 1958

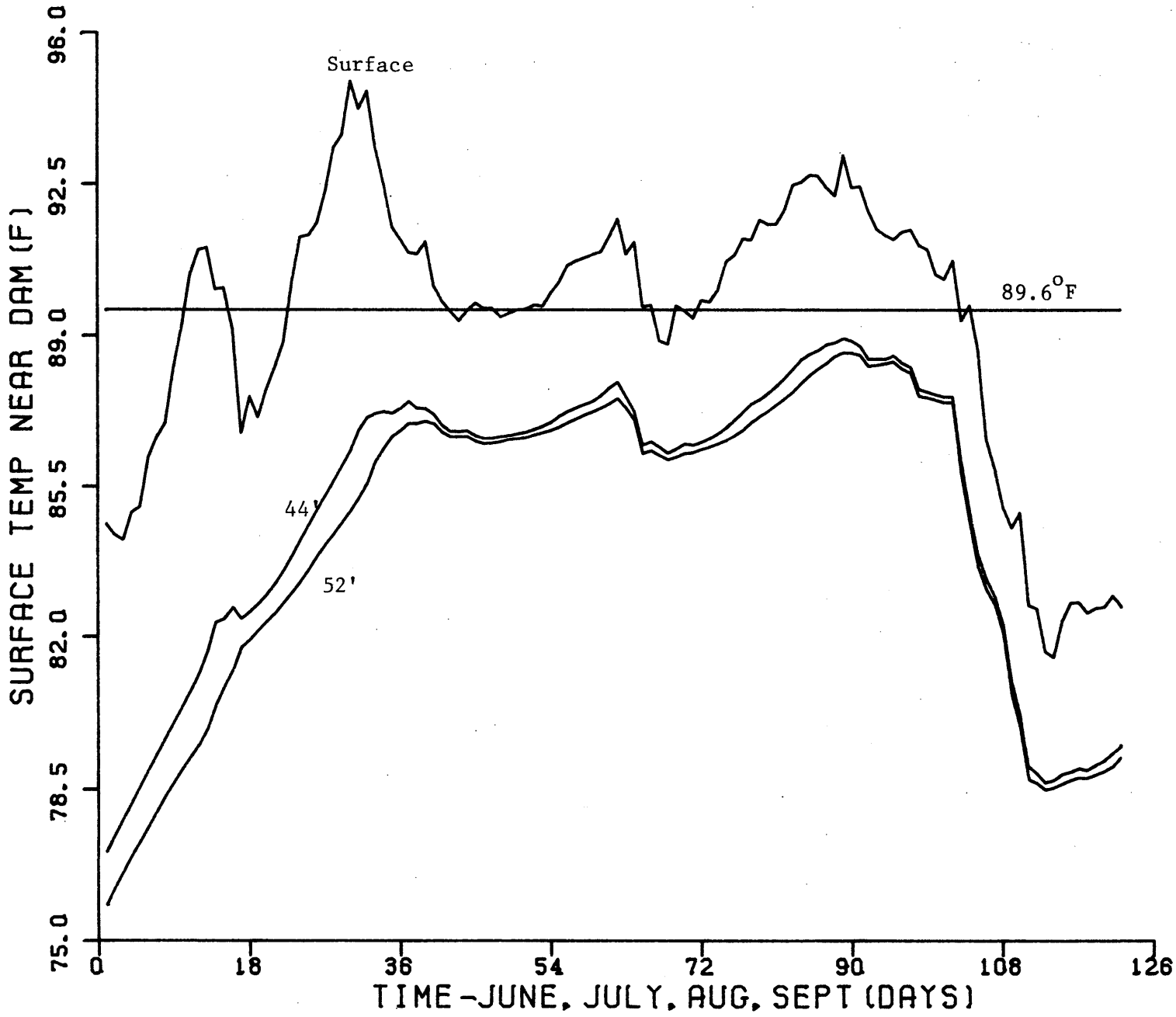

Figure 6.3c: 1959

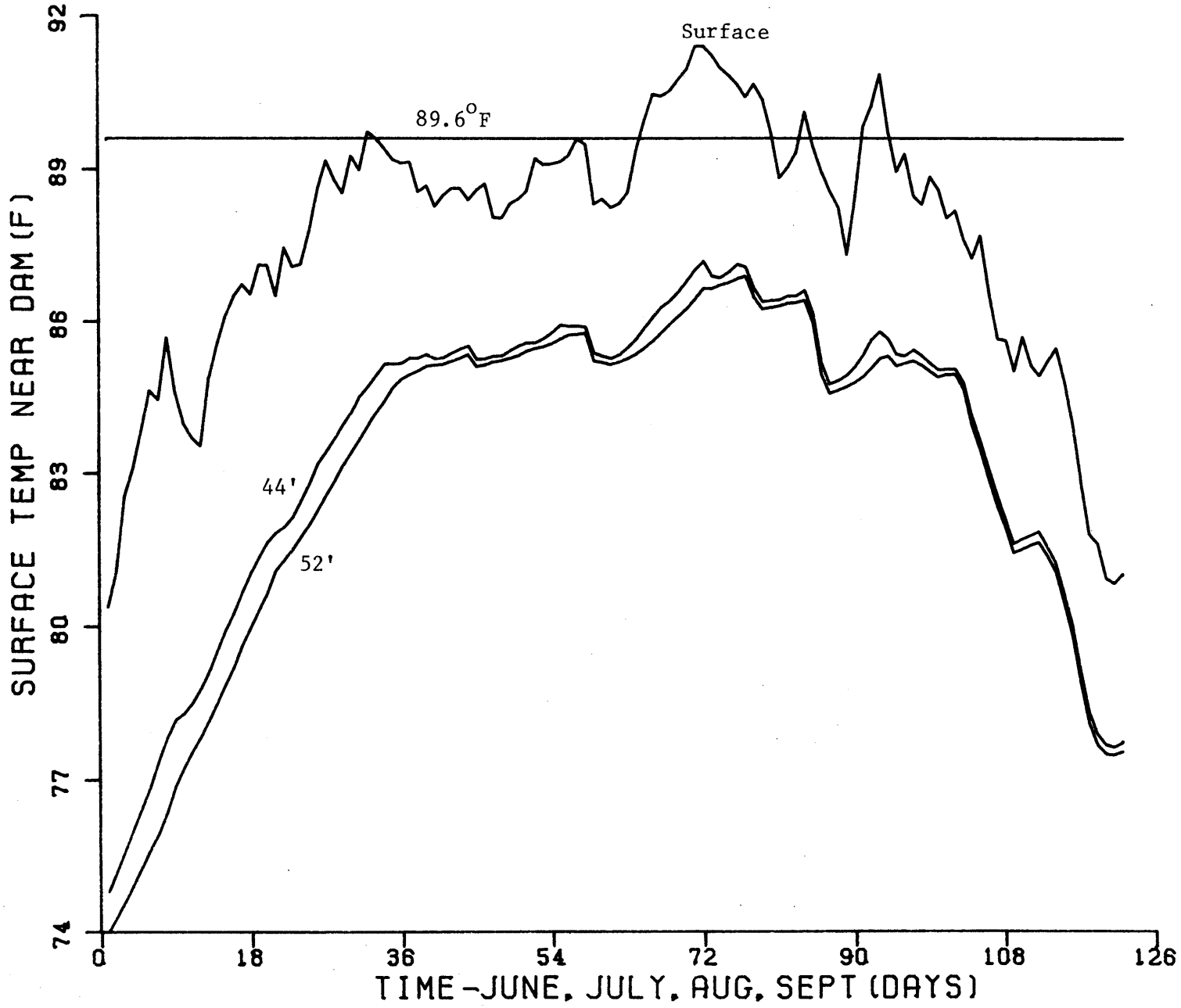

Figure 6.3d: 1960

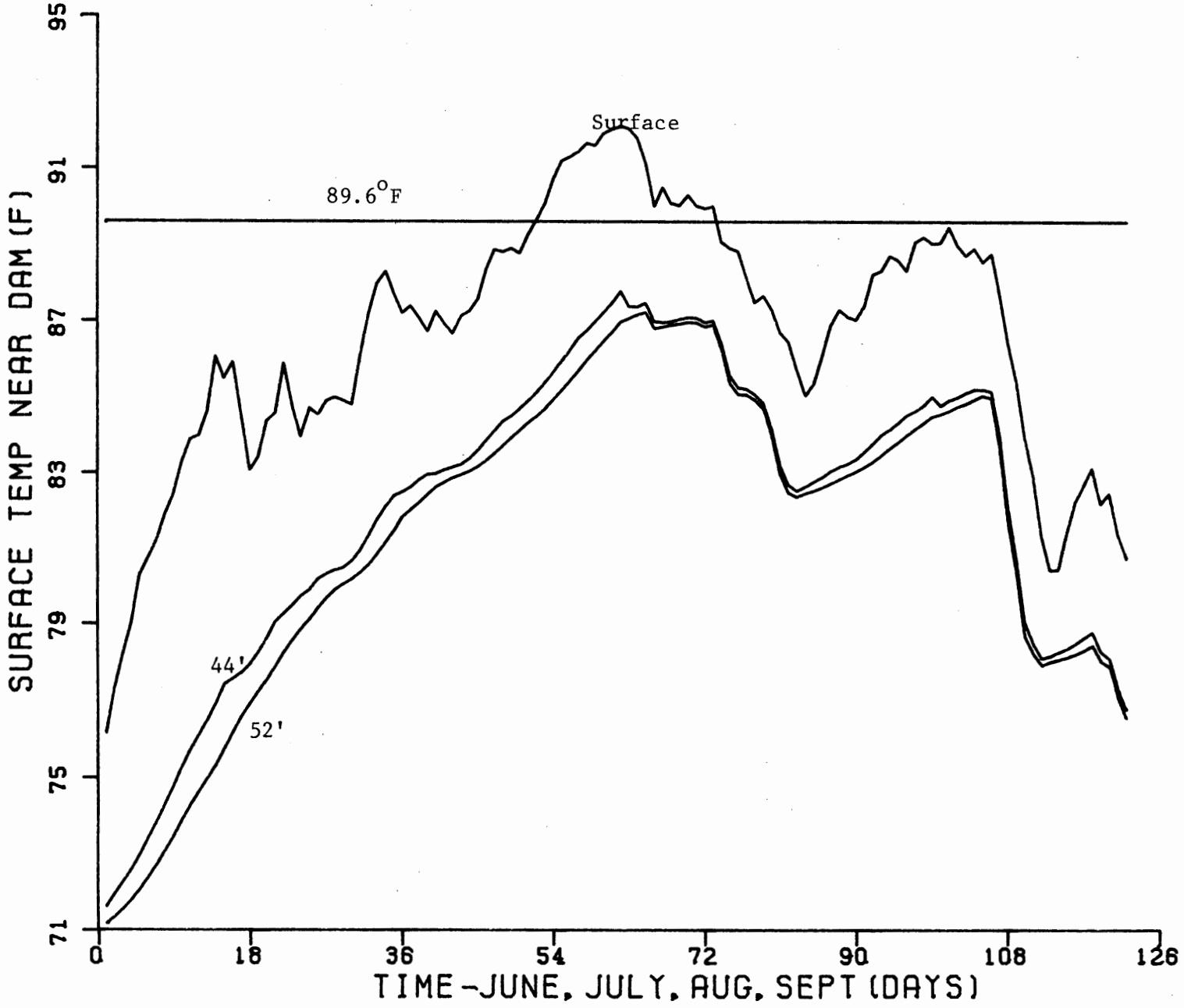

Figure 6.3e: 1961

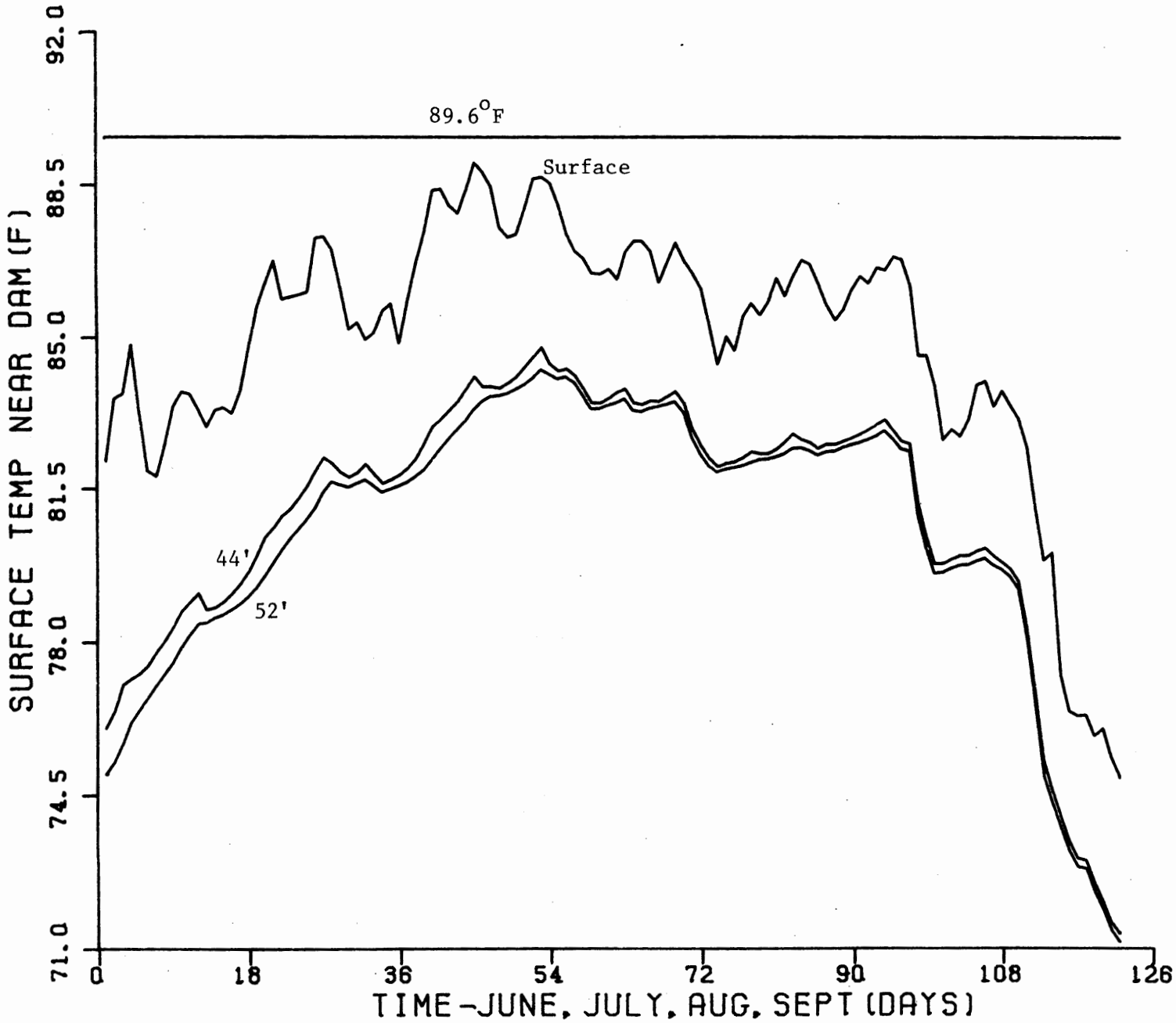

Figure 6.3f: 1962

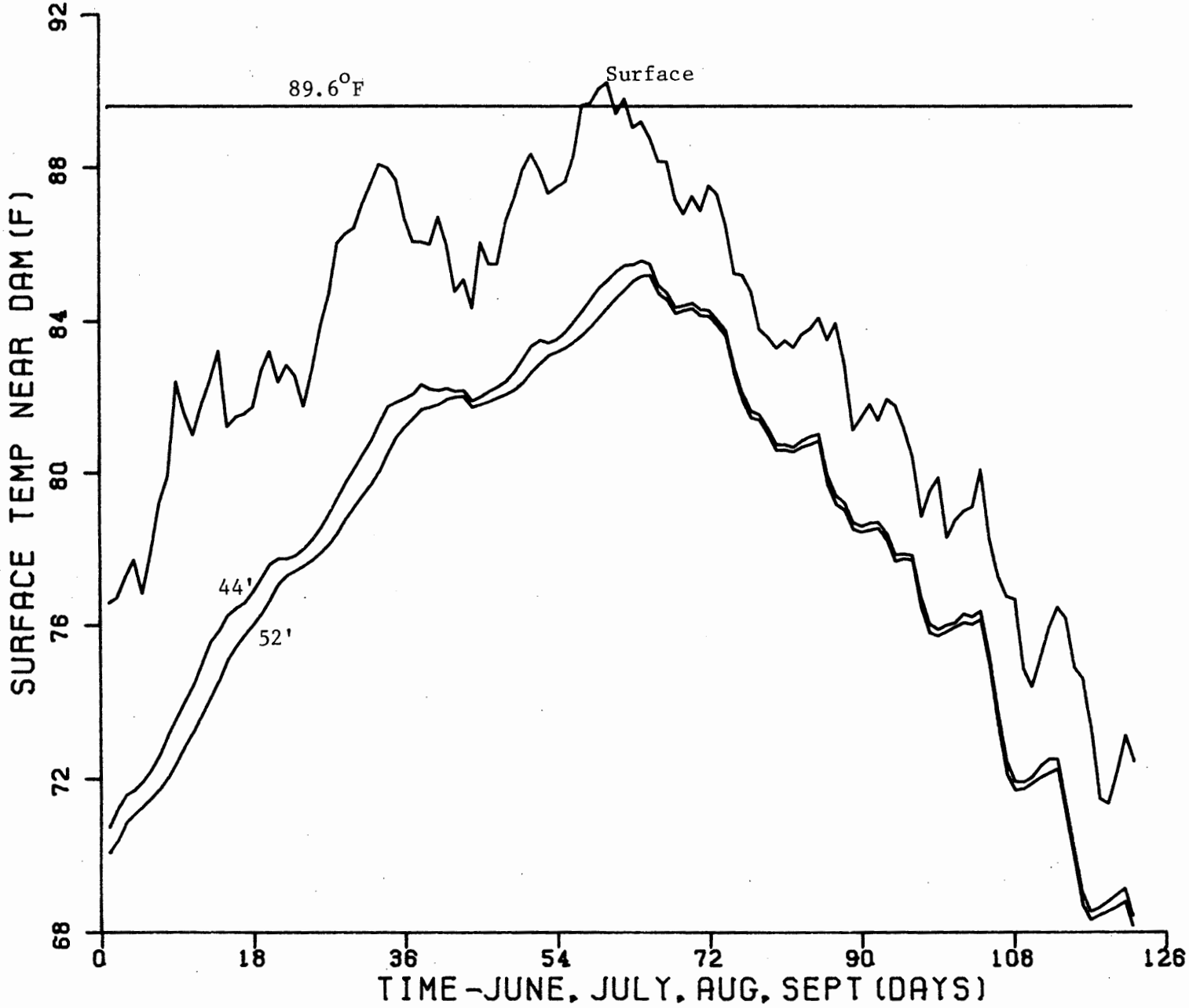

Figure 6.3g: 1963

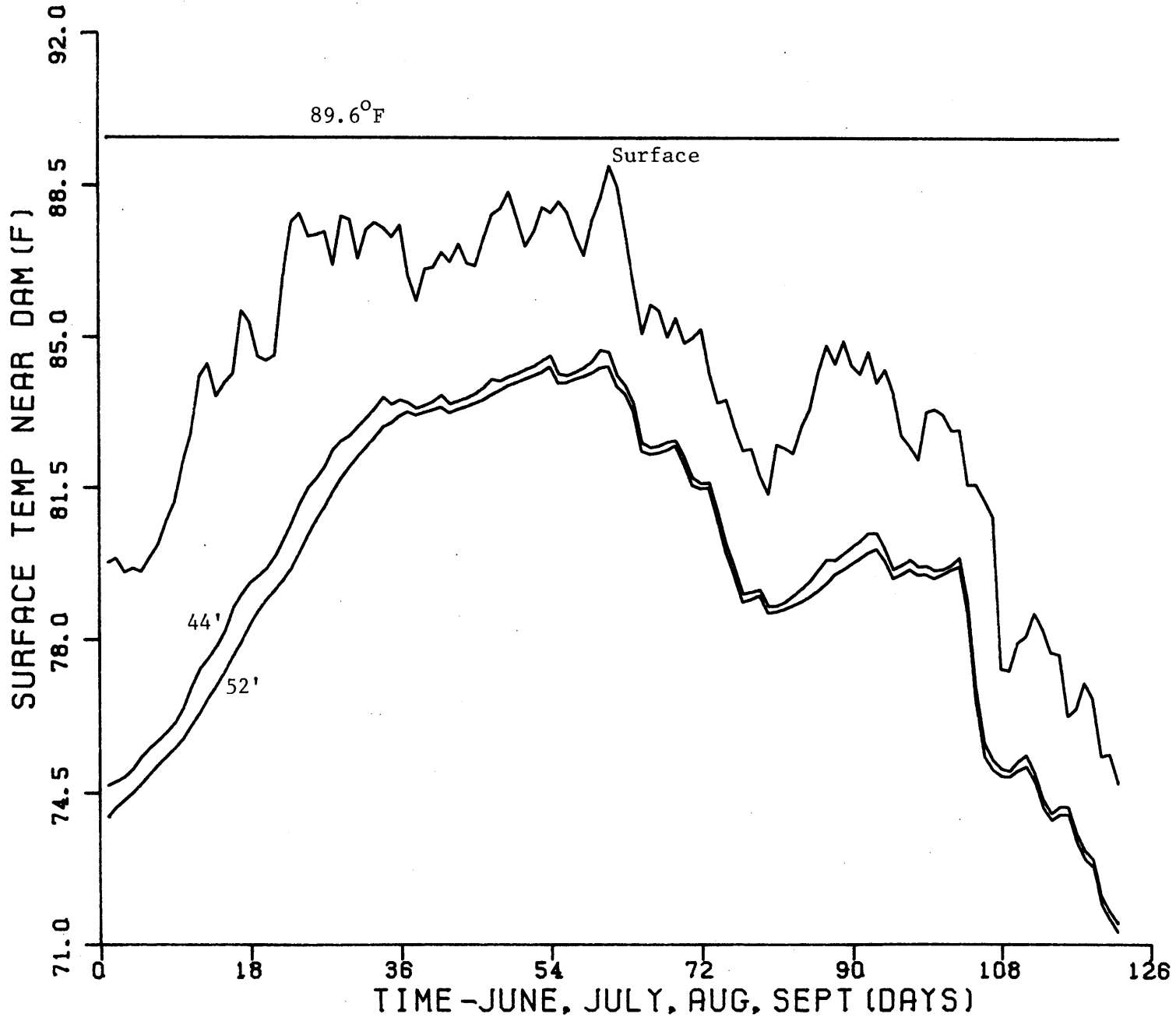

Figure 6.3h: 1964

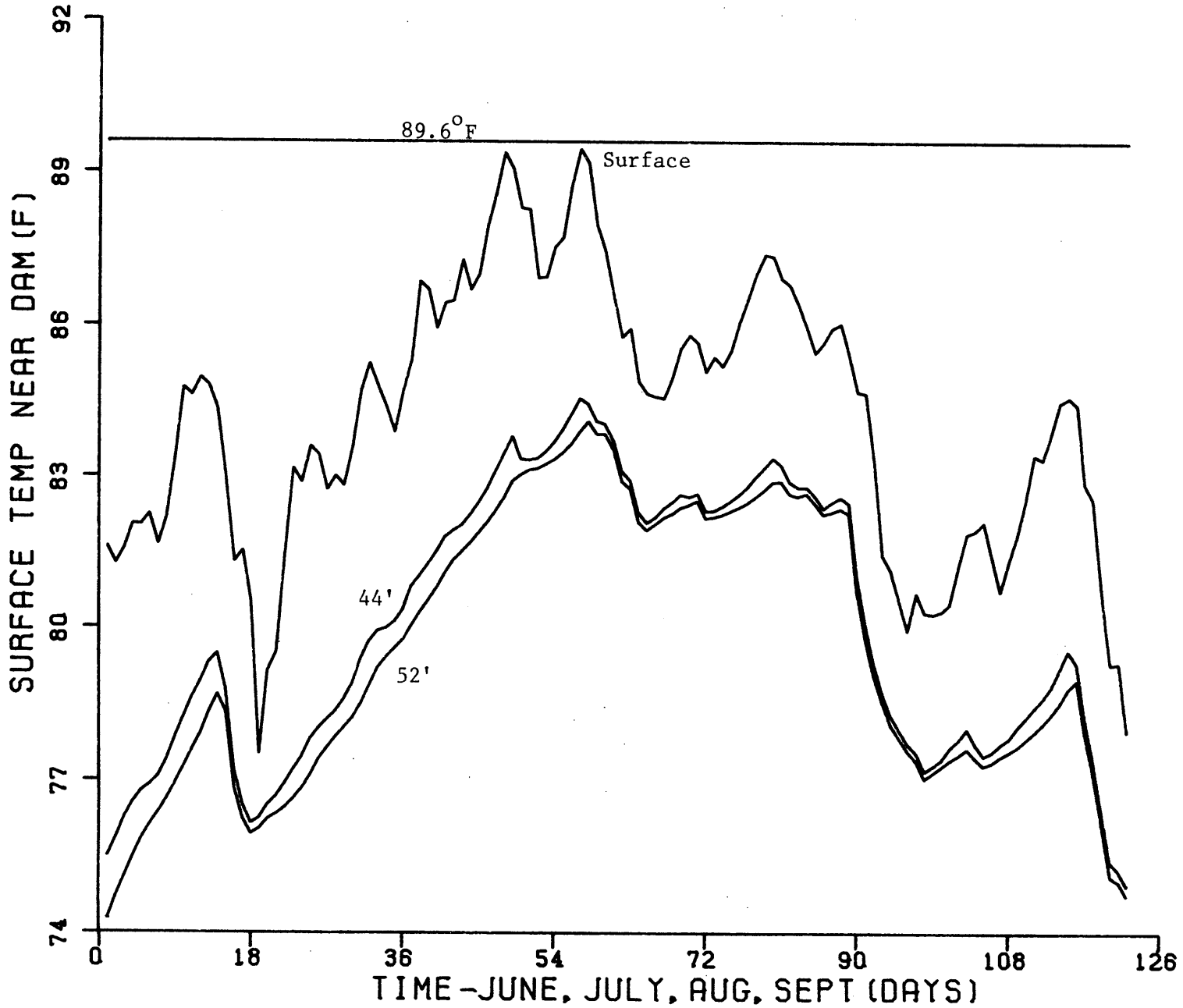

Figure 6.3i: 1965

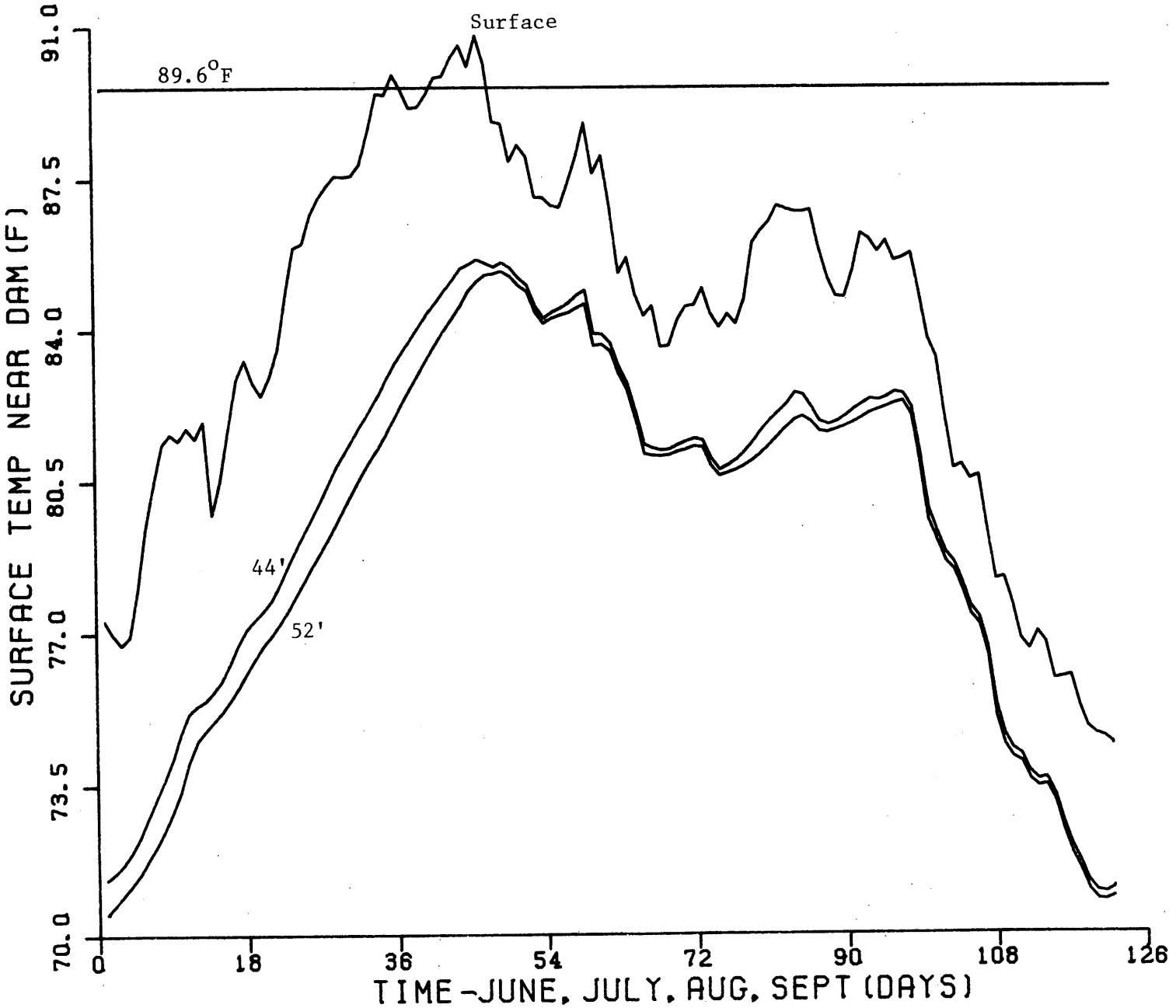

Figure 6.3j: 1966

the surface, and (3) a depth of 52 feet below the surface. Also plotted is a constant reference temperature of 32°C (89.6°F). These plots provide a qualitative indication of (1) the frequency with which the temperature of 89.6°F would be exceeded at the surface near the dam (and thus downstream in the North Anna River since the dam release is from the near surface) and (2) the temperature of cooler hypolimnetic water which could be used to mitigate temperatures downstream by means of mixing surface and hypolimnetic waters. (See Section 7.2.5 with regard to the siphon analysis.)

6.2 Vertical Temperature Profiles in the Main Lake

Figure 6.4 shows representative vertical profiles for two years - 1959, 1962 - during four dates (April 20, July 20, September 20 and January 20) for 1, 2 and 3-unit operation. The significant difference in hypolimnetic temperature among profiles for 1, 2 and 3 units reflects the use of a vertical diffusion coefficient which is strongly dependent on plant flow rate.

6.3 Surface Temperature Decay in the Lake Anna System

Figure 6.5 shows the monthly average surface temperature decay from the discharge to the end of the lake (the upstream end of the main lake side arm) in areal segments for July 1959, an extreme meteorological year. Results are shown for 1, 2 and 3 units.

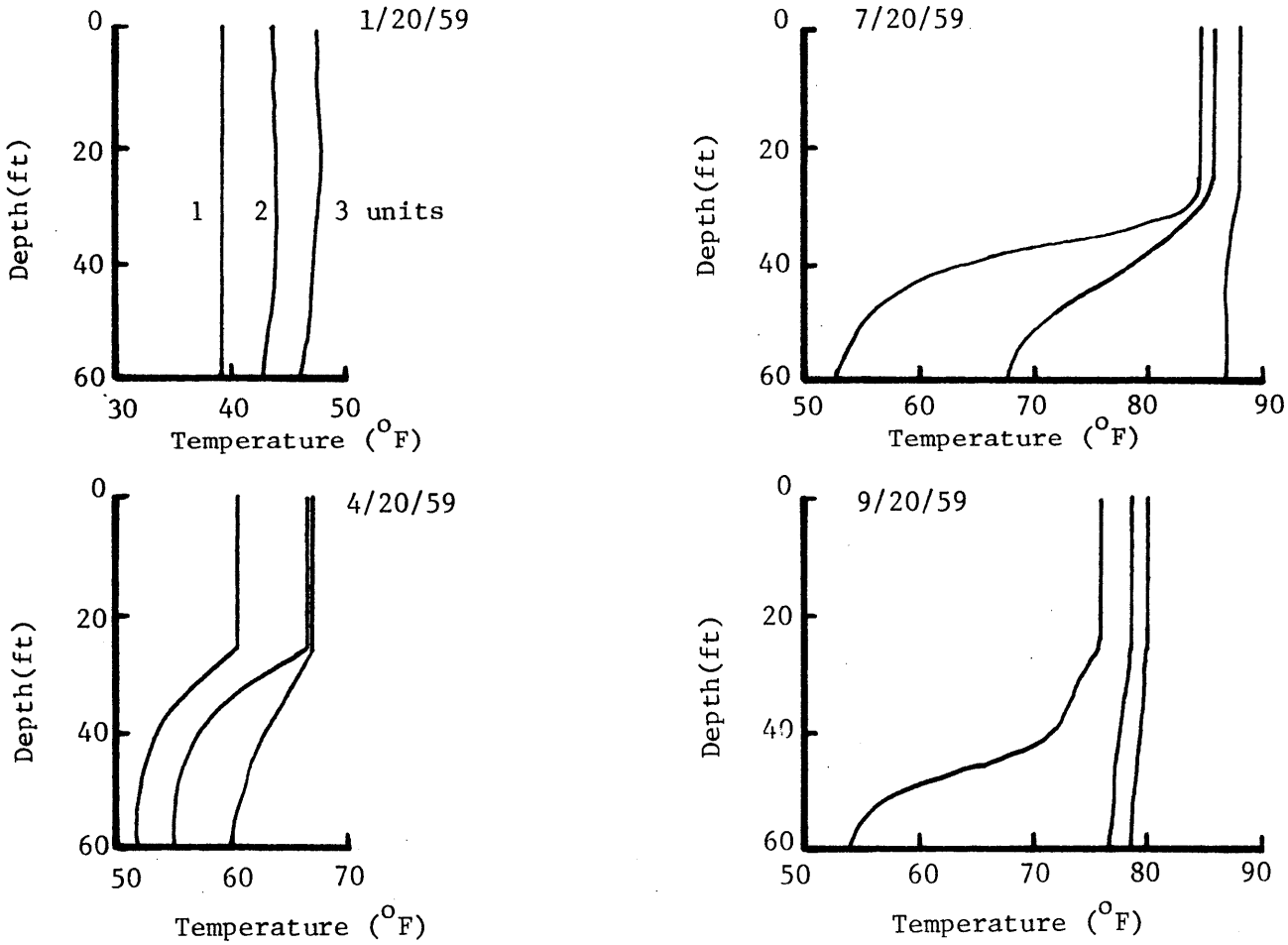

Figure 6.4a: Vertical Temperature Profiles in Main Lake for 1959 for 1,2,3 Units.

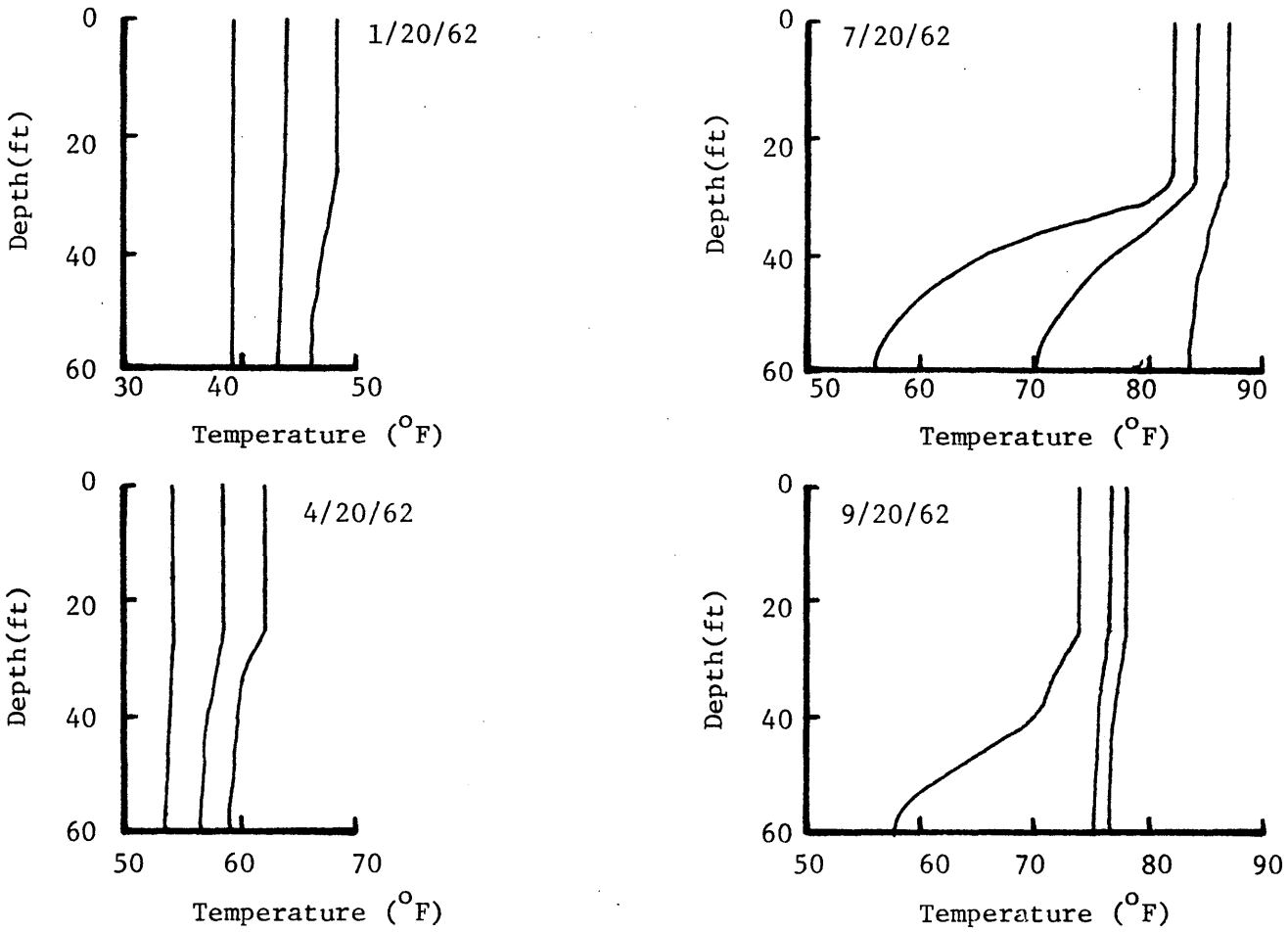

Figure 6.4b: Vertical Temperature Profiles in Main Lake for 1962 for 1, 2, 3 Units.

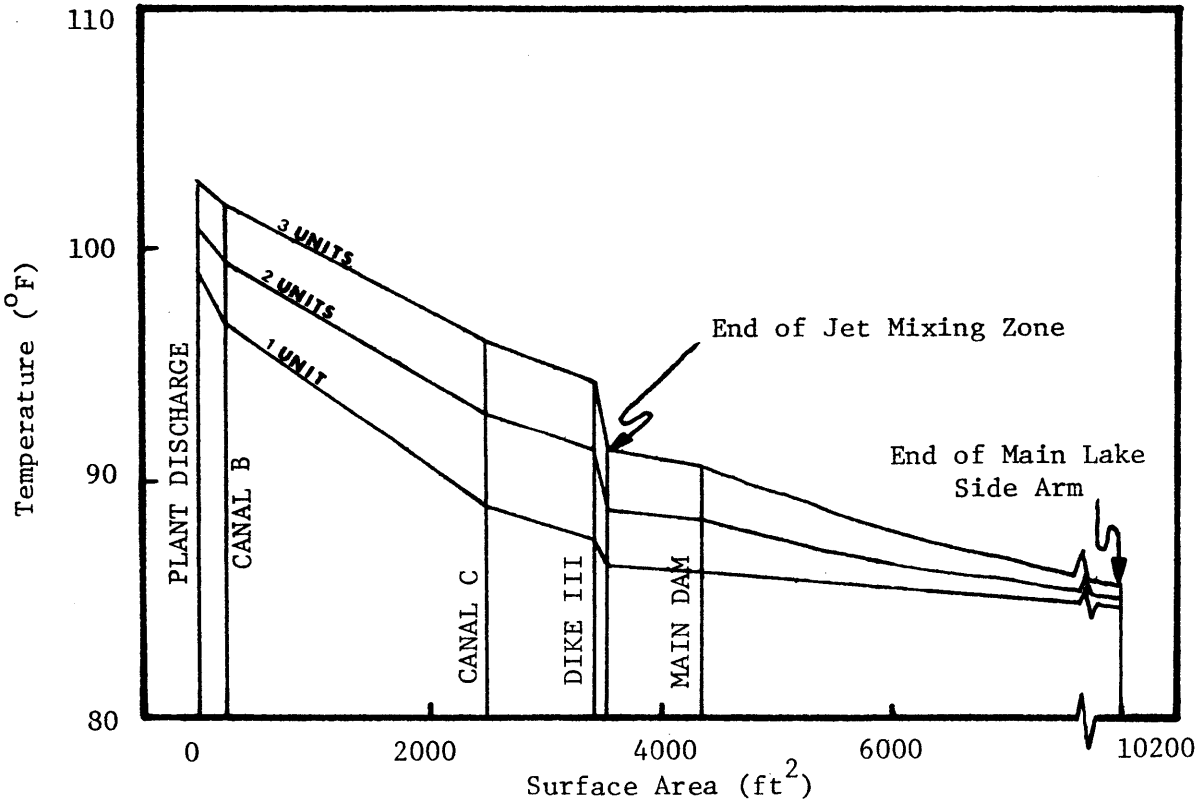

Figure 6.5: Average Surface Temperature Decay in the Complete North Anna Cooling System for July 1959 for 1,2,3, Units.

Table 6.1 compares average July surface temperatures at the North Anna Dam for the ten year historical period with similar temperatures from the uncalibrated model (Jirka et al, 1977). It is noted that the calibrated model temperature predictions were generally about $1^{o}F$ warmer in the month of July.

Table 6.1 Comparison of Calibrated and Uncalibrated Model Predictions of Average Surface Temperatures Near the Dam (see Table 6.1 in Jirka et al, 1977)

Number of Nuclear Units	10 Year Average Temperatures (^{o}F) in July	
	Calibrated Model	Uncalibrated Model
1	84.0	83.2
2	86.1	85.3
3	88.6	87.5

7. STRATEGIES TO REDUCE EXCESS TEMPERATURE IN THE LAKE ANNA ENVIRONMENT

During extreme meteorological conditions, the surface temperatures near the dam in the main lake sometimes exceeded the temperature standard of 32°C (89.6°F). An analysis was undertaken to determine how far this exceedance extended in the river downstream and to evaluate mitigation strategies to reduce this temperature.

7.1 Temperatures in N. Anna River

The temperature history of the dam has been shown in Figures 6.1-6.3. A simple model was developed to analyse the resulting downstream temperature distribution.

7.1.1 River Model

At a typical low flow of 40 cfs, the N. Anna River has the following characteristics (Mr. Jud White, VEPCO, personal communication): average depth h of 0.6m (2 ft.) and average width b of 26m (86 ft.). A steady-state one-dimensional temperature equation can be written

$$u \frac{\partial T}{\partial x} = E_L \frac{\partial^2 T}{\partial x^2} + \frac{\phi_n}{\rho c_p h} \qquad (7.1)$$

where x is the downstream coordinate, u is the advective velocity, E_L is a longitudinal dispersion coefficient and ϕ_n is net heat flux across the air-water surface. Appropriate boundary conditions for Equation 7.1 are

(i) $\frac{dT}{dx} \to 0$ as $x \to \infty$,

and

$$\text{(ii)} \quad uT_o = uT(x=0) - E_L \left.\frac{dT}{dx}\right|_{x=0} \tag{7.2}$$

where T_o is the temperature of the dam discharge. Linearizing the surface heat transfer (i.e., $\phi_n = -K(T-T_E)$),the solution to Equation 7.1 subject to Equation 7.2 is

$$T(x) = \frac{T_o - T_E}{\left[1-\left(\frac{1}{2} - \sqrt{\frac{1}{4} + \frac{E_L K}{\rho c_p h u^2}}\right)\right]} \exp\left[x\left(\frac{u - \sqrt{u^2 + \frac{4E_L K}{\rho c_p h}}}{2E_L}\right)\right] + T_E \tag{7.3}$$

The dispersion coefficient, E_L, in Equation 7.3 can be evaluated from an equation by Fischer (1967) :

$$E_L = 0.01 \frac{u^2 b^2}{h\, u_*} \tag{7.4}$$

where u_* = shear velocity. During low flow summertime conditions in the N. Anna River, E_L is on the order of 100 ft^2/s, and the term $4E_L K/\rho c_p h u^2$ is of order 0.1 or significantly less than unity; during other seasons with higher flows, the term would be smaller. Thus, the role of dispersion may be neglected resulting in the temperature decay for plug flow:

$$T(x) = T_E + (T_o - T_E) \exp(-Kx/\rho c_p uh) \tag{7.5}$$

Note that the use of Equation 7.5 in place of 7.3 is conservative in regards to temperatures near the dam because one effect of dispersion is to make $T(x=0) < T_o$.

7.1.2 River Model Historical Simulation

In order to compute downstream temperatures from Equations 7.3 or 7.5, flow rates, surface temperatures at the dam, and meteorological variables were required from the historical time period. As discussed in Section 3.5, flow rates were determined by Equation 3.4 with the stipulation that an in-stream minimum flow of 40 cfs would be maintained. An equation describing the depth of the N. Anna River as a function of the flow rate was derived, based on channel characteristics at a low flow of 40 cfs and consistent with Manning's equation for an open channel with constant width:

$$(\frac{h}{2}) = (\frac{Q}{40})^{0.6} \qquad (7.6)$$

where Q = flow rate in cfs

h = average depth of N. Anna River in feet.

Unfiltered equilibrium temperatures and a constant value of K (205 $Btu/ft^2/day\ ^oF$) were used with surface temperatures at the dam to represent surface heat transfer.

Equation 7.5 may be inverted to solve for the distance x downstream at which the temperature standard of 32°C (89.6°F) could be met. Table 7.1 presents summertime statistics of this persistence for the year 1959.

Note that these results are conservative in the following respects: (i) the model neglected longitudinal dispersion which would reduce, slightly, temperatures near the dam, (ii) the model did not account for lateral inflows (approximately 22% of the flow at Doswell,

Table 7.1 Average Summer (J,J,A,S) 1959 N. Anna River Temperature Analysis

Number of Nuclear Units	Number of Days (out of 122) During 1959 Summer that $T_o > 89.6$ and TEQ < 89.6	Average Distance Downstream at which T=89.6°F from Eq. 7.5 (miles)
1	1	0.3
2	14	0.3
3	66	1.4

23.6 miles downstream) which would further cool the river temperature, and (iii) during periods of high throughflow, all of the water from Lake Anna was assumed to be released from the epilimnion when, in reality, the radial gates would start releasing cooler water at a depth of about 31 feet below the surface.

7.2 Temperature Mitigation Strategies

Section 2.2.3 discussed three modifications to the structure of the WHTF and the operation of N. Anna Nuclear Power Station which were designed to reduce thermal impact on the main lake and on N. Anna River downstream from the dam. These options included reduced mixing (characterized by a dilution D_s=1.5) at the entrance to the three WHTF reaches, rerouting of flow in the WHTF through the two major side-arms and increases to 16°F and 18°F in the condenser temperature rise, ΔT_c, through a proportional decrease in condenser flow rate Q_c. For the summer time situation studied in the July 1977 report, temperatures at the dam could be reduced by 0.2°F through reduced entrance mixing, 0.4°F through re-routing and 0.4 and 0.8°F by increasing ΔT_c to 16°F and 18°F respectively. Based on recent model and data analysis, the effectiveness of these options is discussed briefly below.

Recently, additional options have also been discussed: (i) use of bubble aerators in the main lake near the dam to destratify the lake, thus lowering the surface and downstream temperatures in the summer, and (ii) use of a siphon to blend cooler hypolimnetic water with warmer epilimnetic water to maintain downstream temperatures below

prescribed standards and (iii) use of cooling towers to remove a portion of the heat load to the lake. The use of aerators is discussed briefly while a detailed analysis of the siphon option is given below. Cooling towers are not addressed in the present study.

7.2.1 Dilution Reduction

Strong entrance mixing is generally detrimental to cooling lake performance. By minimizing entrance mixing, heat transfer efficiency can be increased due to the higher water temperatures in the initial reaches of the WHTF. By carefully diffusing the outlet sections of each interconnecting canal, entrance mixing in each reach was to be minimized and thus cooling efficiency maximized.

In the analysis presented in Section 2.2.3, a dilution, D_s, of 1.5 was suggested as a practical minimal value to enhance the heat loss. However, according to Section 4.3.2, effective dilutions even lower than that are now often being observed. Thus it is doubtful if even the 0.2°F improvement could be obtained.

7.2.2 Rerouting

Temperatures in the side arms are lower than in the rest of the WHTF because of the absence of throughflow. Consequently less heat flux takes place. If flow was rerouted through the two major side arms of the WHTF (Elk Creek and Millpond Creek), somewhat greater thermal efficiency could be obtained; previous analysis suggests that in the summer temperatures would decrease by about 0.4°F if this modification

were enacted.

The analysis in Section 4.3.3 of measured side arm flow data suggested that the observed side-arm flows were only about 50% of their originally computed value. This would suggest greater improvements in thermal efficiency if the flow were rerouted. However, the temperature decay in each side arm was inversely correlated with side arm flow rate so that reduced side arm flow resulted in greater heat loss per unit of flow. On this basis it was estimated that rerouting would only result in about 0.5°F reduction in temperature at the dam.

7.2.3 Reduction in Q_c

Previous analysis suggested that a 2°F increase in condenser temperature would lead to a 0.4°F decrease in temperature at the dam while a 4°F increase in condenser temperature rise could lead to a 0.8°F decrease at the dam. It is doubtful if these numbers would change significantly as the result of recent model calibrations.

7.2.4 Analysis of Bubble Aerators

The use of bubble aerators to destratify the main lake would allow for lower downstream temperatures while increasing the dissolved oxygen in the less oxygen-rich hypolimnetic water. In contrast with the siphon (see Section 7.2.5) such a system has the advantage of lowering temperatures in the main lake as well as the N. Anna River, but a disadvantage is that it is less precisely operated. Inevitably

more bottom water would be brought to the surface than needed. Questions also remain as to the chemical and biological effects of mixing hypolimnetic water with surface water.

To be more effective, such a system would have to be controlled in a transient manner - i.e., only when needed to reduce warm surface temperatures. Such operation would be easy to control in practice but would be rather complicated to simulate in a model. Continuous year round use of a bubbler could be easily simulated (e.g., by allowing the upper mixed layer in the main lake to extend to the bottom); however this practice would be ineffective since it would only delay the response of the upper layer water temperatures. Under this arrangement, peak temperatures near the end of summer would not be affected significantly and temperatures during fall would be higher due to the increase in heat stored near the bottom. A moderately effective approach, which could be simulated, might be to initiate aeration during summer when the first temperature peak began and to assume complete vertical mixing for the remainder of the summer. Such a simulation is proposed if this option is ever seriously considered.

7.2.5 Hypolimnetic Siphon Analysis

A schematic of a possible siphon arrangement is shown in Figure 7.1. The siphon would mix cool hypolimnetic water with the warmer surface water in order to bring the N. Anna River temperature down to a particular target - e.g., 32°C. A siphon was considered as an efficient system to utilize the colder water since it could be operated merely

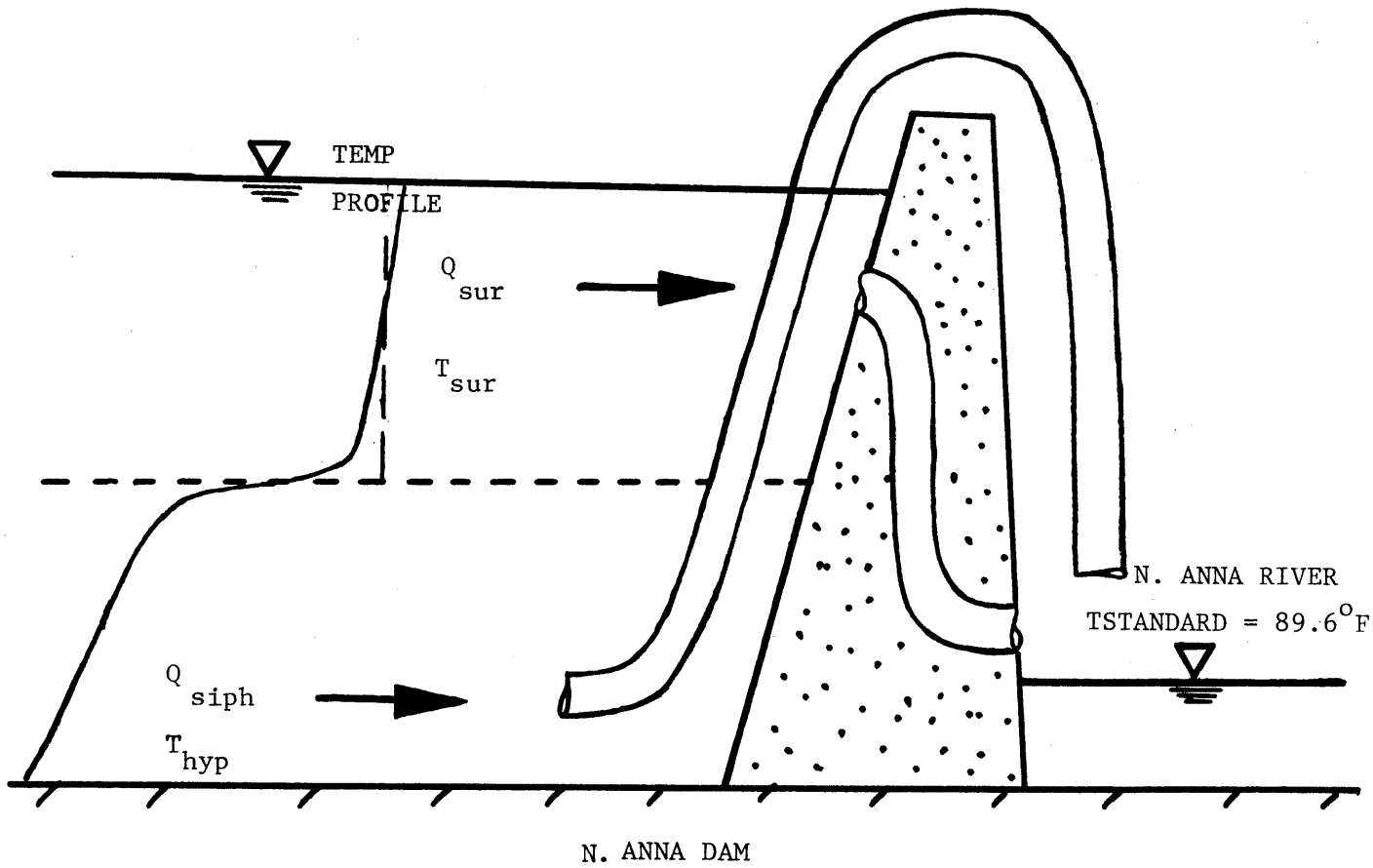

Figure 7.1: Schematic for Hypolimnetic Siphon Analysis at N. Anna Reservoir.

when required to mitigate temperatures downstream of the dam.

7.2.5.1 Strategy of Siphon Operation

The North Anna River is required to maintain an in-stream flow minimum of 40 cfs, which is usually done by using near-surface skimmers (except during flood flow). With an hypolimnetic siphon, a new operating policy was assumed such that the total flow passing through the dam (from existing skimmers plus proposed siphon) was unchanged. A heat balance at the point of mixing suggests

$$T_{sur}Q_{sur} + T_{hyp}Q_{siph} = (Q_{sur}+Q_{siph})T_{std} \qquad (7.7)$$

where subscripts sur and siph denote surface and siphon and T_{std} refers to a downstream target temperature. The siphon would be used only during times when the surface temperature at the dam exceeded the temperature standard, and then the surface flow and the siphon flow would be proportioned such that the mixed flow temperature would not exceed the standard.

7.2.5.2 Historical Predictions of Required Siphon Flows

Historical predictions were made over the 1957-1966 period for 3 unit operation in order to determine the amount of hypolimnetic volume required to lower the temperature in the N. Anna River to 32°C. Surface temperatures at the dam, hypolimnetic temperatures (at two possible depths: 44 ft. and 52 ft. below the surface), and corrected flow rates from Equation 3.4 were utilized to solve for Q_{siph} required for the siphon at 44 ft. or at 52 ft. Since the amount of

water required by the siphon turned out to be very small, the Lake Anna temperature model was not re-run. Instead it was assumed that temperatures at 44 and 52 ft. were the same as without the siphon.

Figures 7.2-7.11 detail the siphon flows required at the two possible depths for 3 unit operation and the surface flow over each summer period from 1957-1966. Table 7.2 summarizes the hypolimnetic volumes of water required for the siphon each summer. Note that the worst case occurs in 1959 when maximum flow rates of 177 cfs and 164 cfs were required for depths of 44 and 52 ft. The corresponding volumes of water were 4132 and 3903 acre-ft or approximately 7.8% and 7.2% of the lake volume between depths of 30 and 60 feet.

7.2.5.3 Surcharge Capability of Lake Anna

The calculations described above assumed that the combined outflow from skimmer and siphon at the dam equals the N. Anna River inflow to the reservoir. As such, the reservoir elevation remains constant at 250 ft. MSL. If the reservoir elevation were allowed to rise slightly during periods of strong summer inflows, both the maximum siphon flow rate and the volume of hypolimnetic water required could be reduced.

Figure 7.12 examines the required storage (maximum water level) to meet a downstream target temperature of 32°C for 3 unit operation during the summer of 1959 using siphons which deliver maximum flow rates of Q_{max} = 10, 25 and 50 cfs. In preparing Figure 7.12, the siphon flow rate Q_{siph} was computed according to Equation 7.7 if it was less than Q_{max}. If not, Q_{siph} was set equal to Q_{max} and Q_{sur} was computed so that

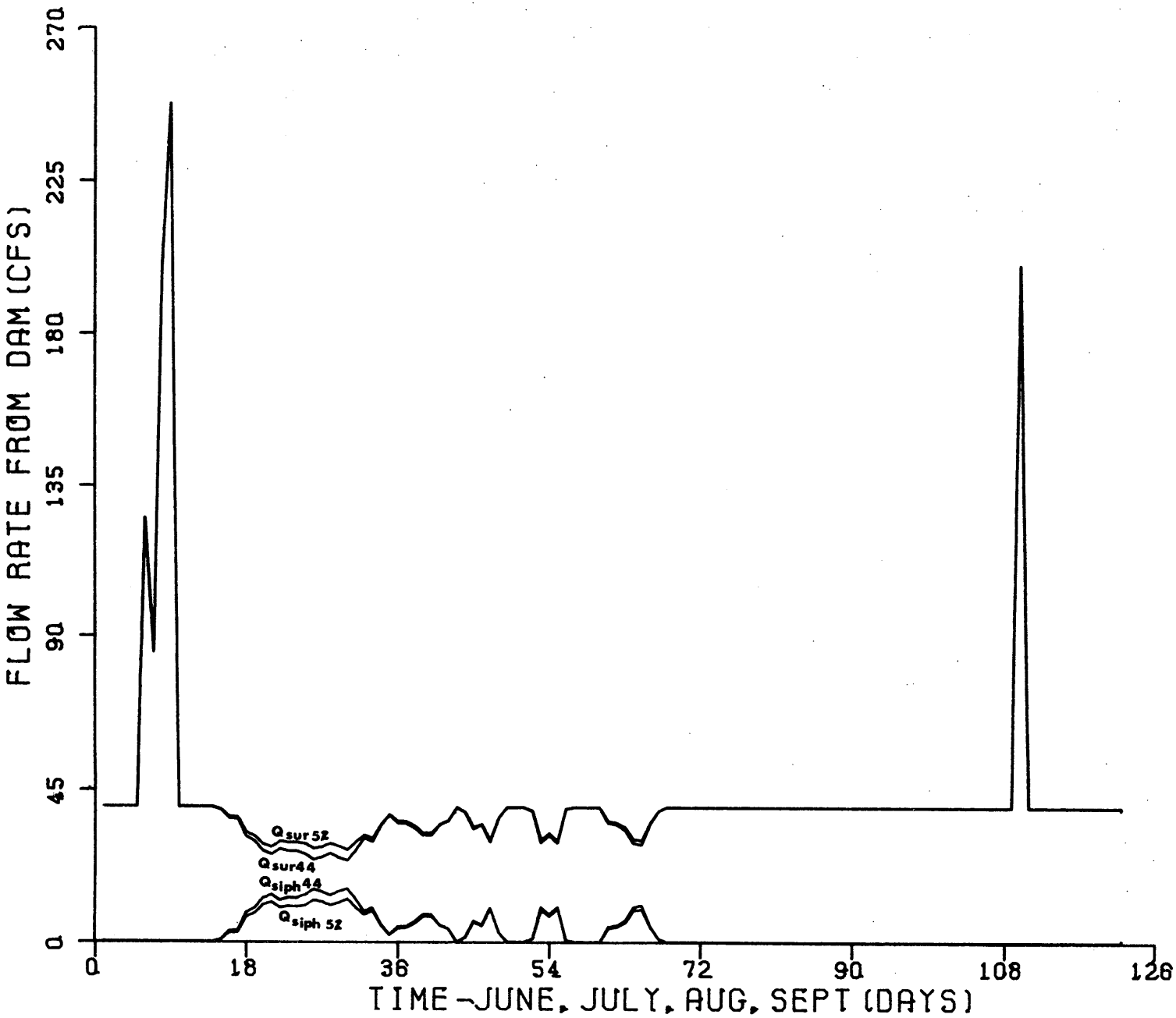

Figure 7.2 Required Flows From the Surface and Siphon located at a depth of 44 and 52 feet for Summer of 1957, 3 Unit Operation

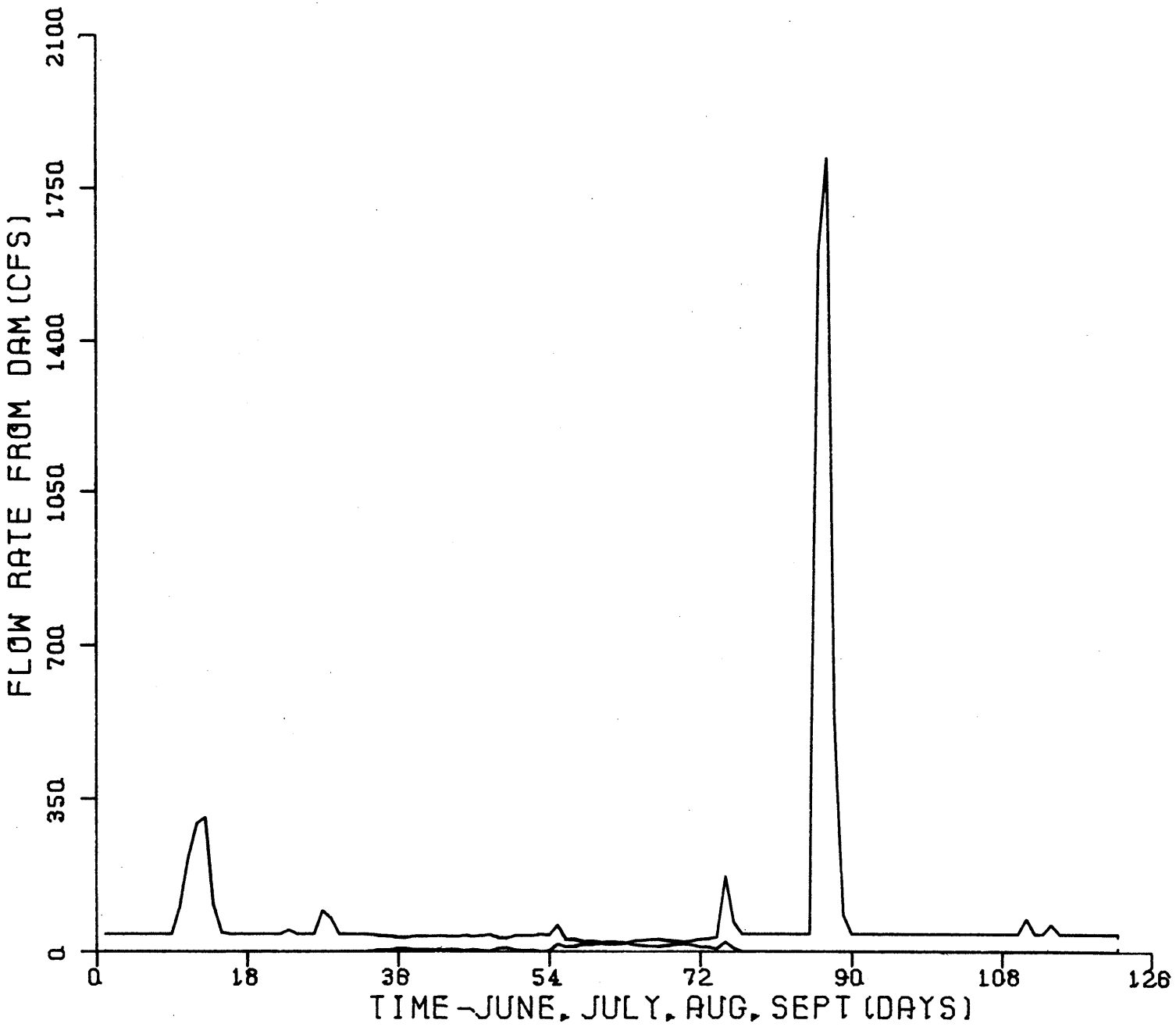

Figure 7.3 Surface and Siphon Flows Required for 1958, 3 Unit Operation

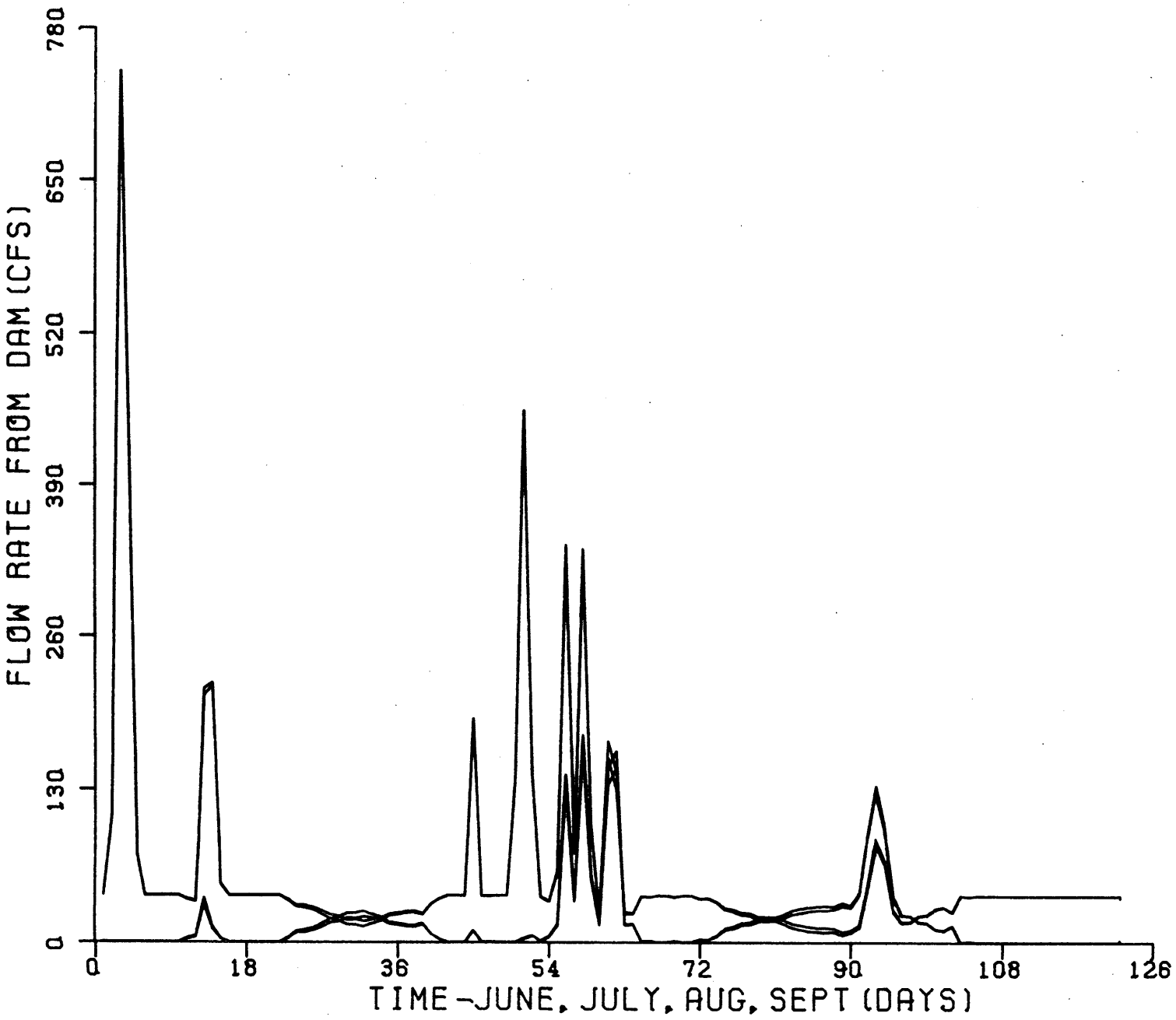

Figure 7.4 Surface and Siphon Flows Required for 1959, 3 Unit Operation

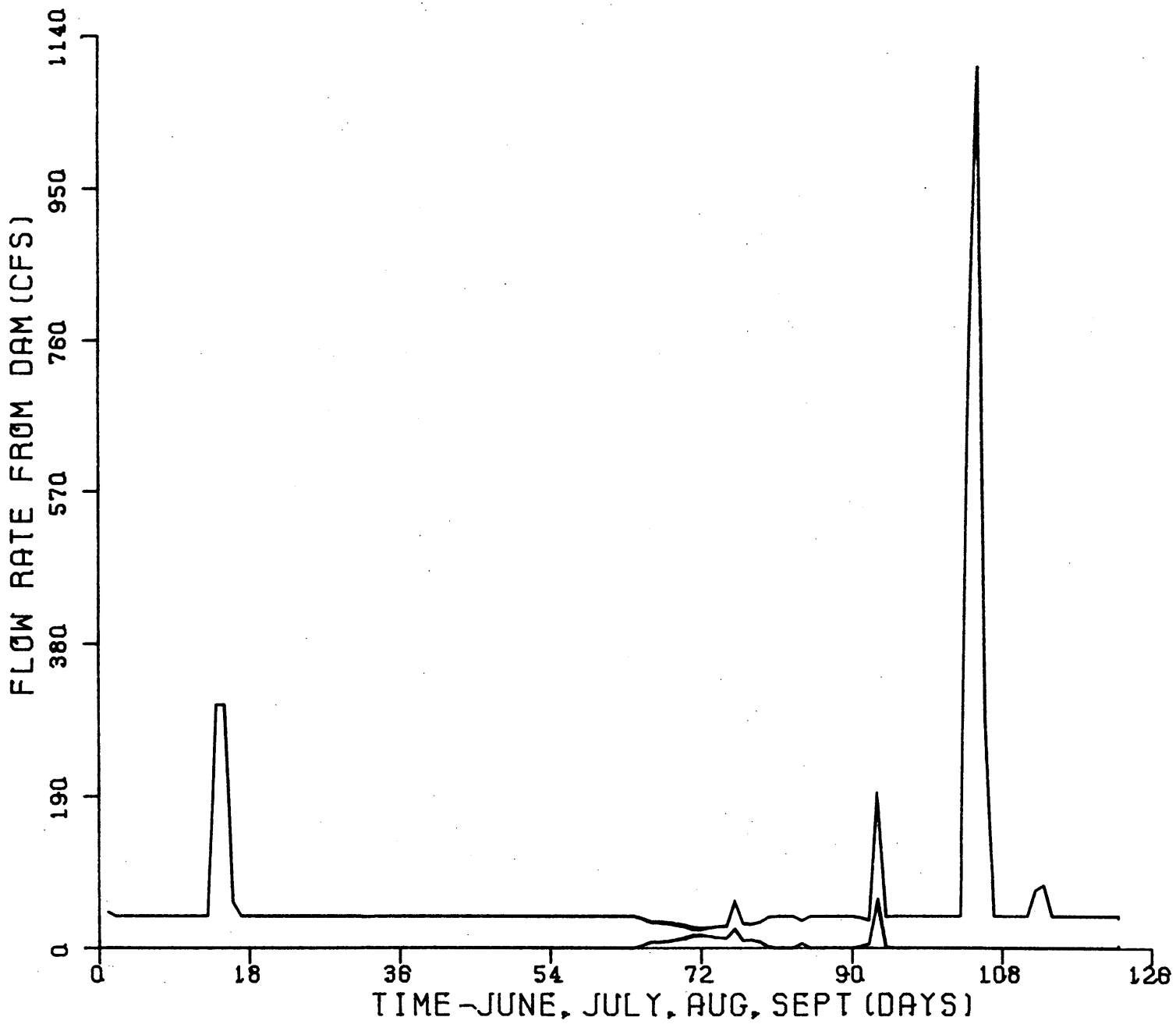

Figure 7.5 Surface and Siphon Flows Required for 1960, 3 Unit Operation

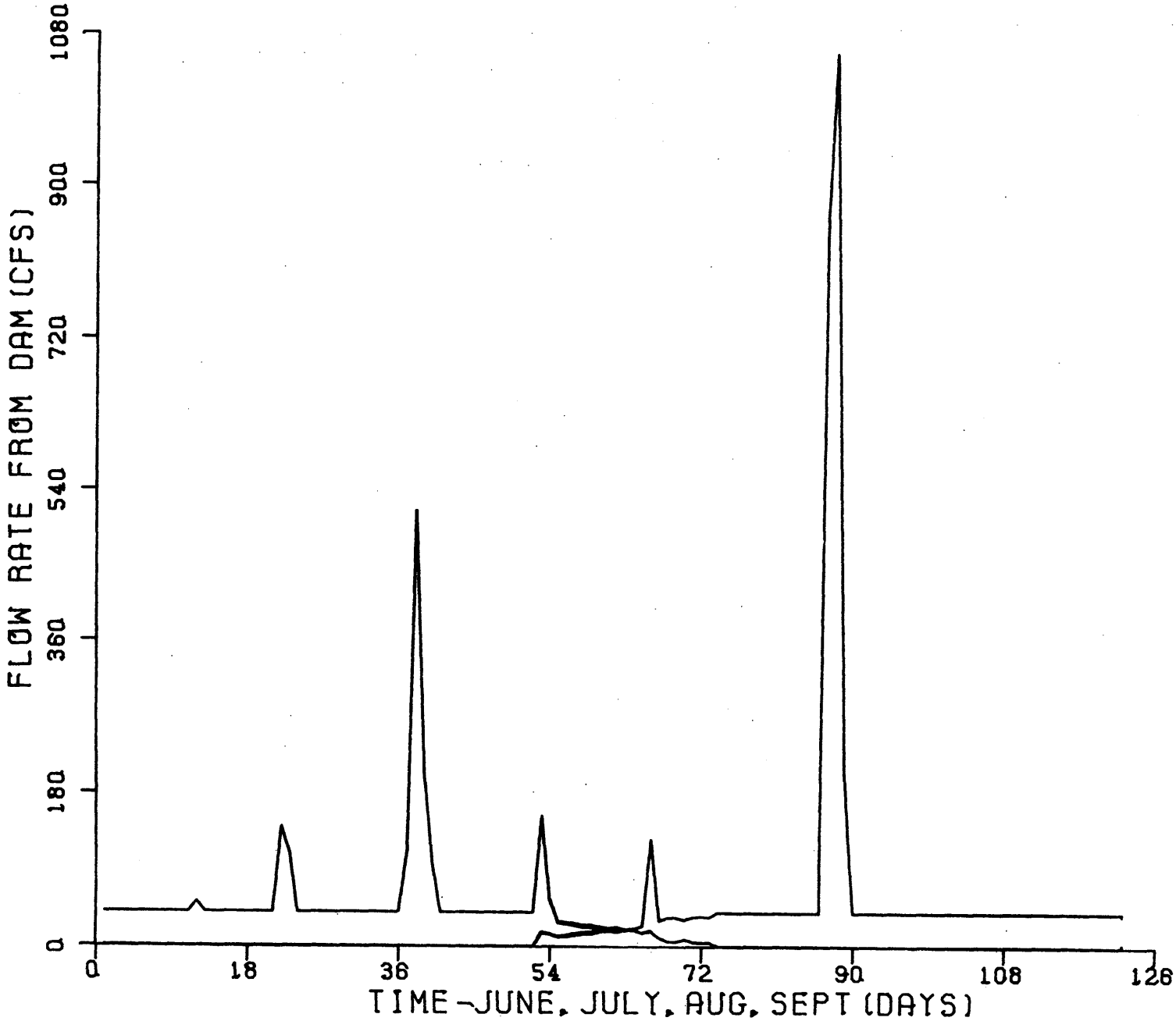

Figure 7.6 Surface and Siphon Flows Required for 1961, 3 Unit Operation

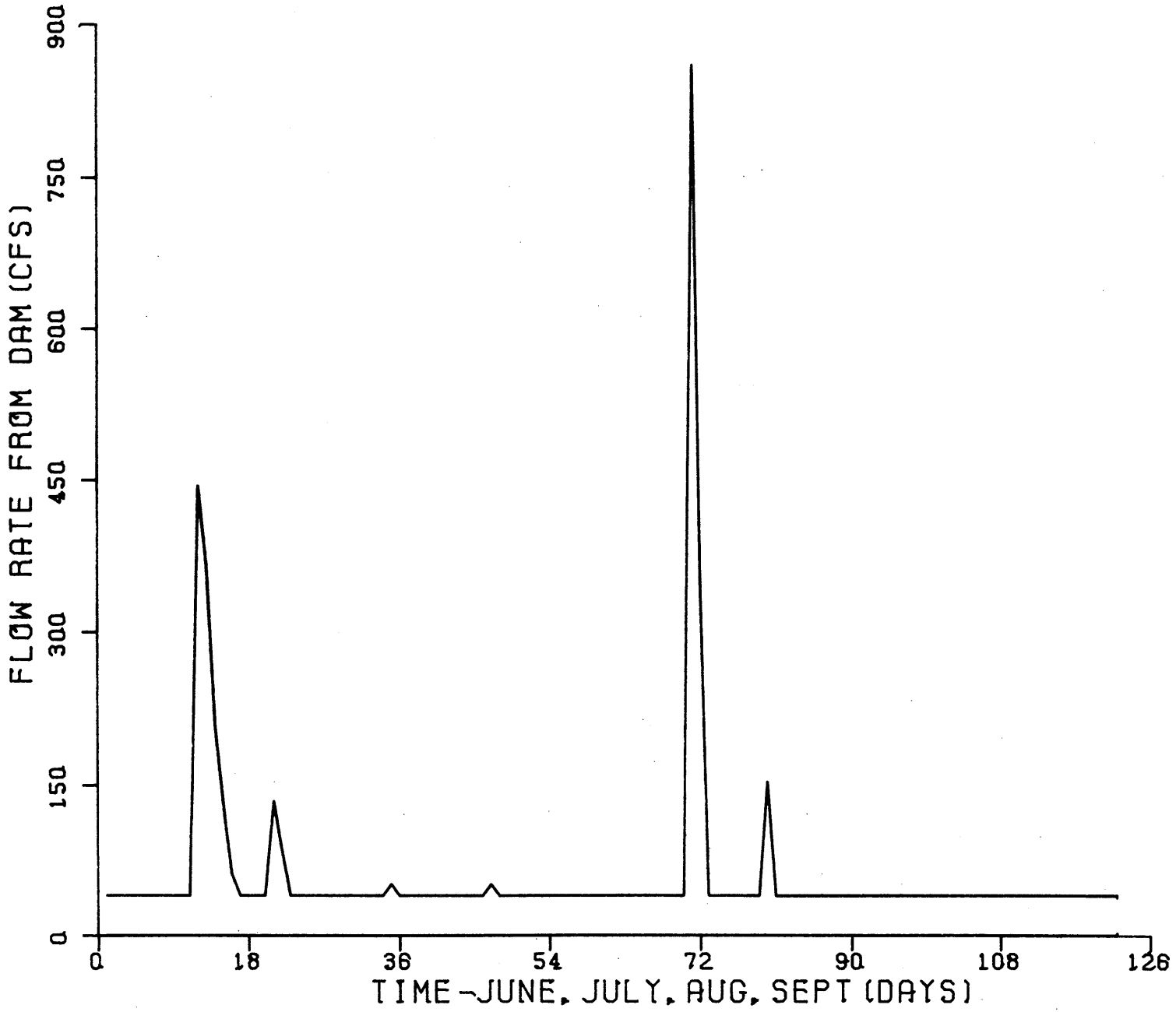

Figure 7.7 Surface Flow for 1962 (No siphon flow was required)

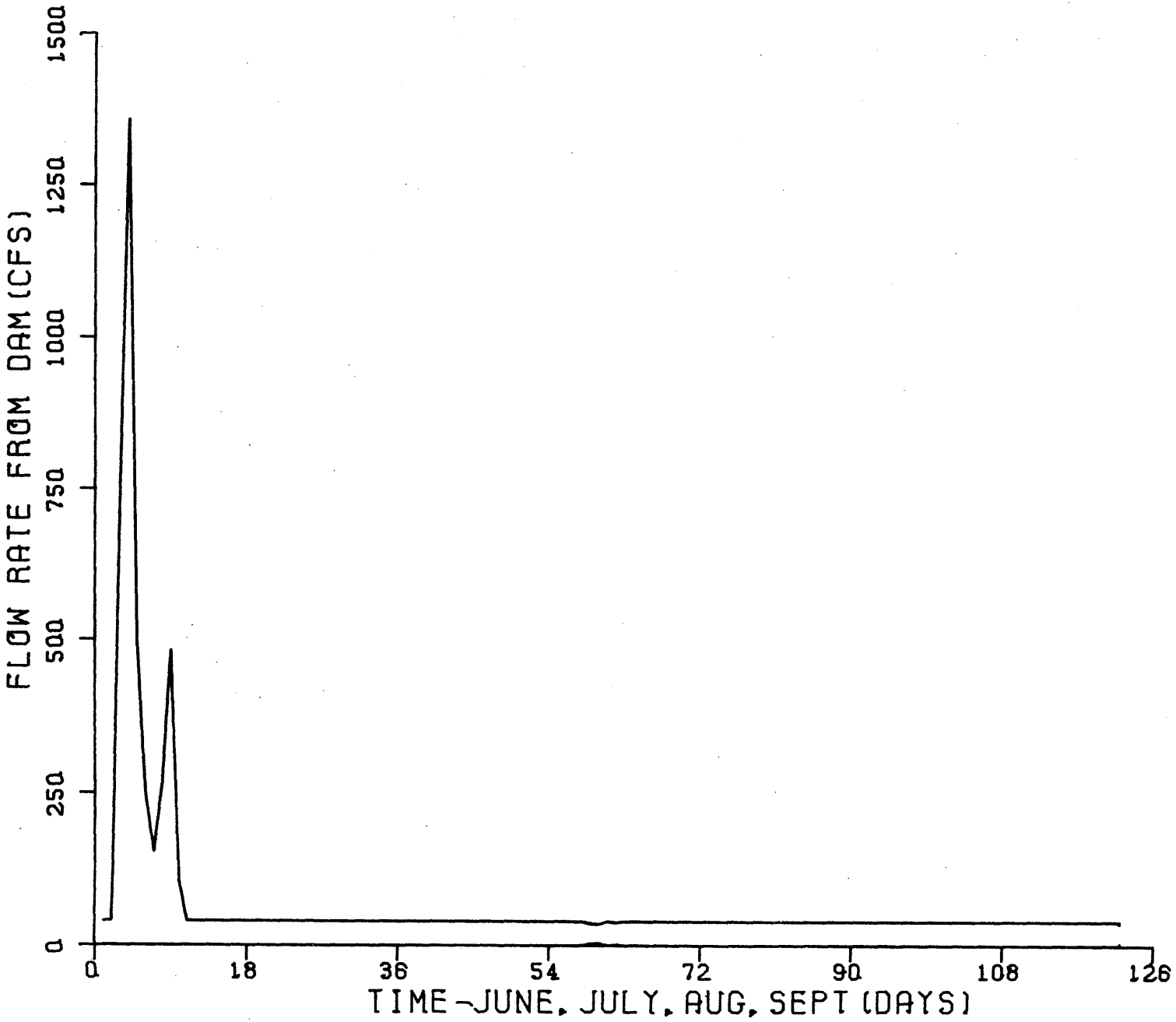

Figure 7.8 Surface and Siphon Flows Required for 1963, 3 Unit Operation

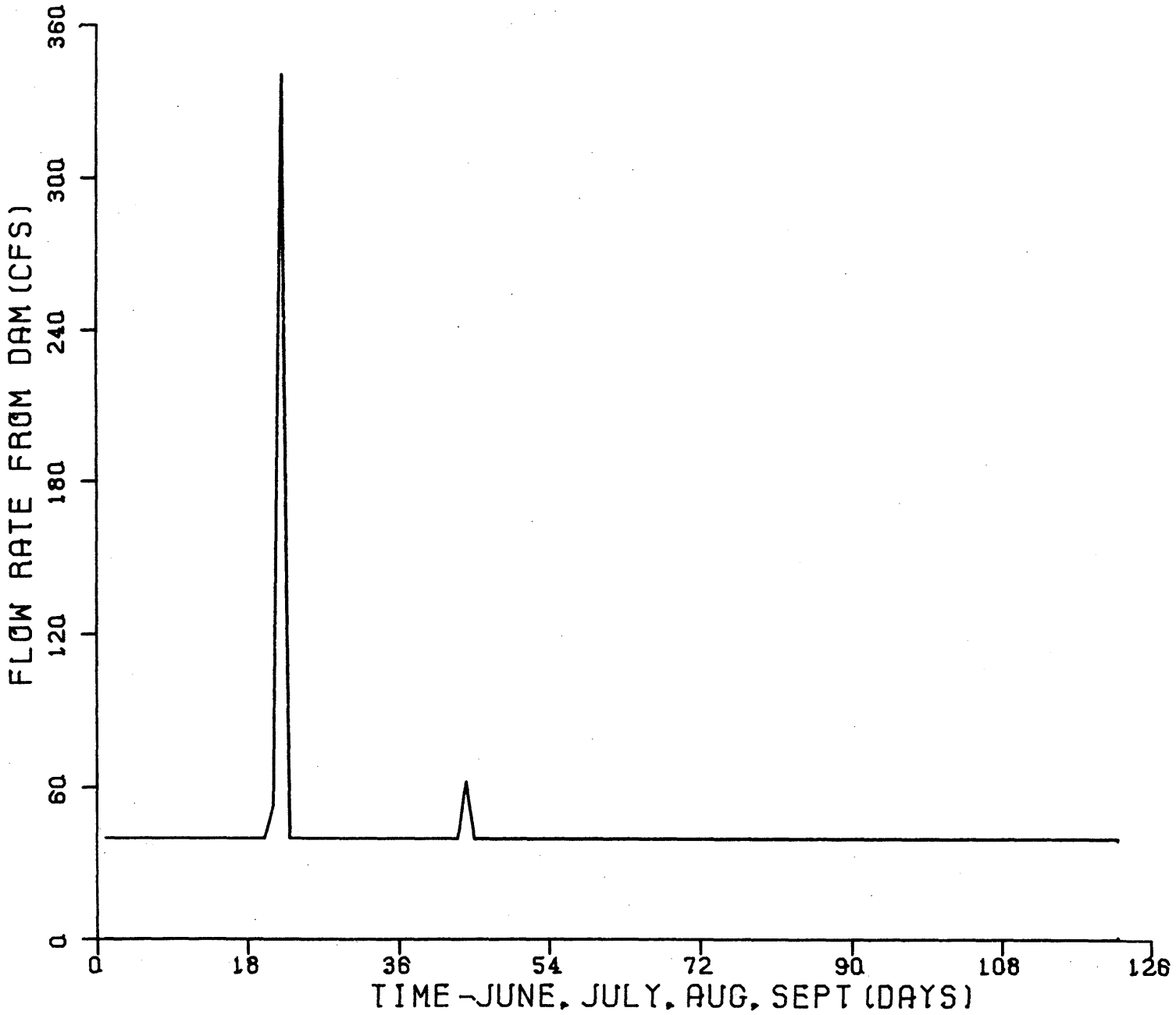

Figure 7.9 Surface Flow for 1964 (No siphon flow was required)

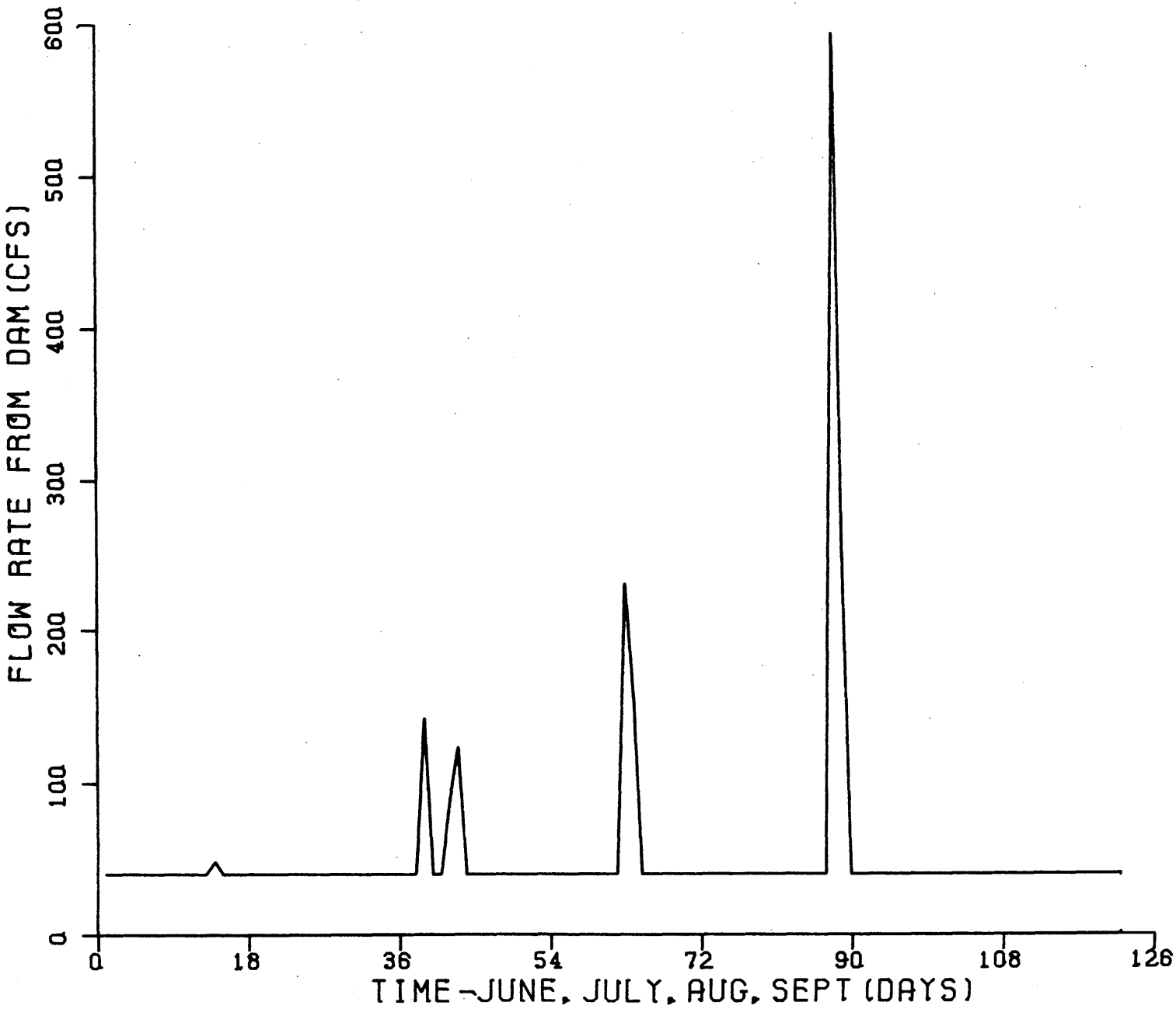

Figure 7.10 Surface Flow for 1965 (No siphon flow was required)

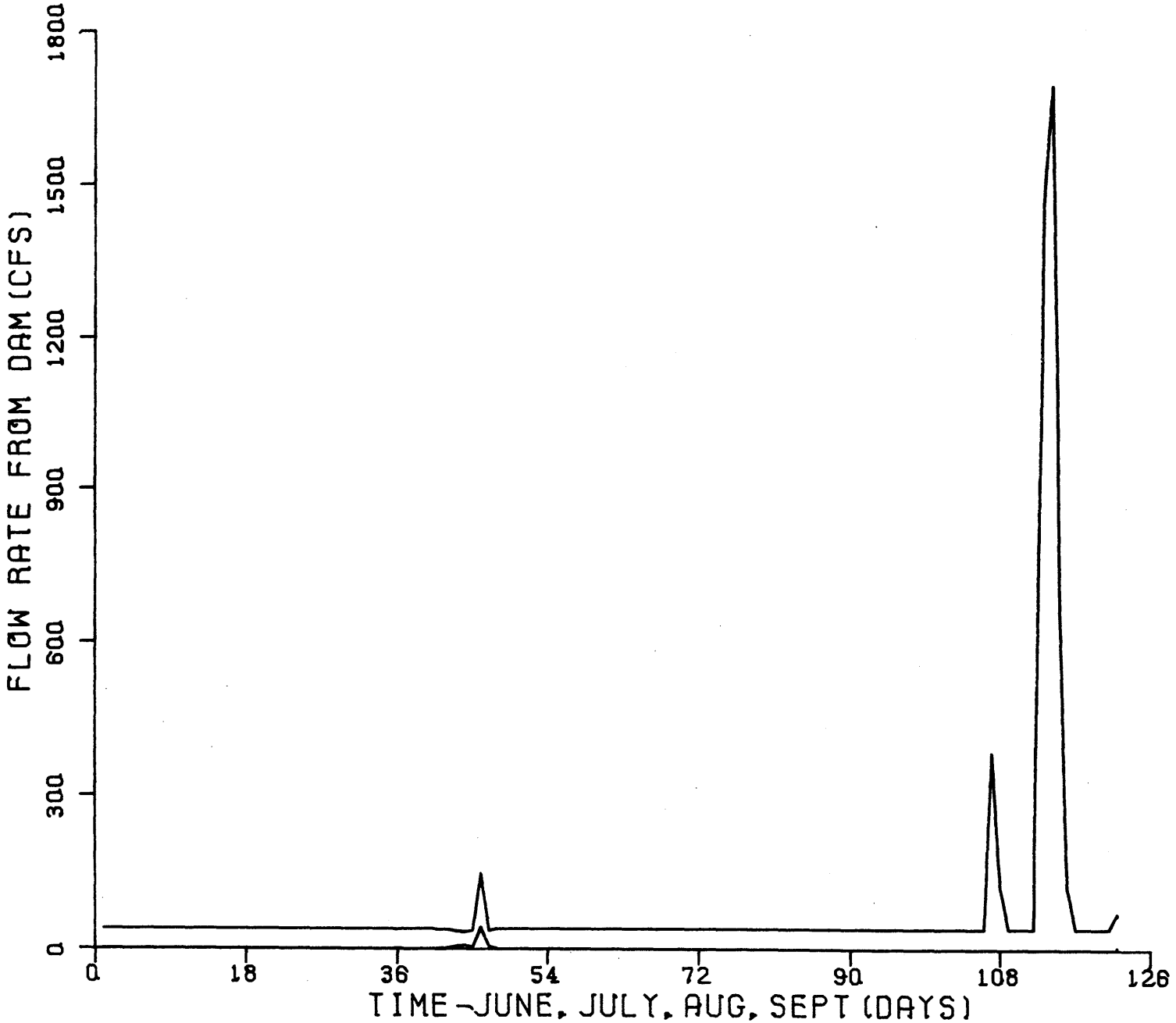

Figure 7.11 Surface and Siphon Flows Required for 1966, 3 Unit Operation

Table 7.2 Siphon Historical Calculations for 3 Units

	Siphon at 44'			Siphon at 52'		
Year	Max. Daily (cfs)	Volume Req'd. (ft^3)	% of Total Hypolimnetic Available Volume	Max. Daily (cfs)	Volume Req'd (ft^3)	% of Available Volume
1957	16	3.1×10^7	1.3	13	2.7×10^7	1.2
1958	24	3.8×10^7	1.6	22	3.5×10^7	1.5
1959	177	1.8×10^8	7.8	164	1.7×10^8	7.2
1960	62	2.2×10^7	1.0	23	2.1×10^7	0.9
1961	23	2.6×10^7	1.1	20	2.3×10^7	1.0
1962	0	0	0	0	0	0
1963	5	9.7×10^5	0.04	4	8.5×10^5	0.04
1964	0	0	0	0	0	0
1965	0	0	0	0	0	0
1966	44	6.2×10^6	0.3	40	5.5×10^6	0.2

(Note: Volume available below the 30' depth was $2.3 * 10^9$ ft^3)

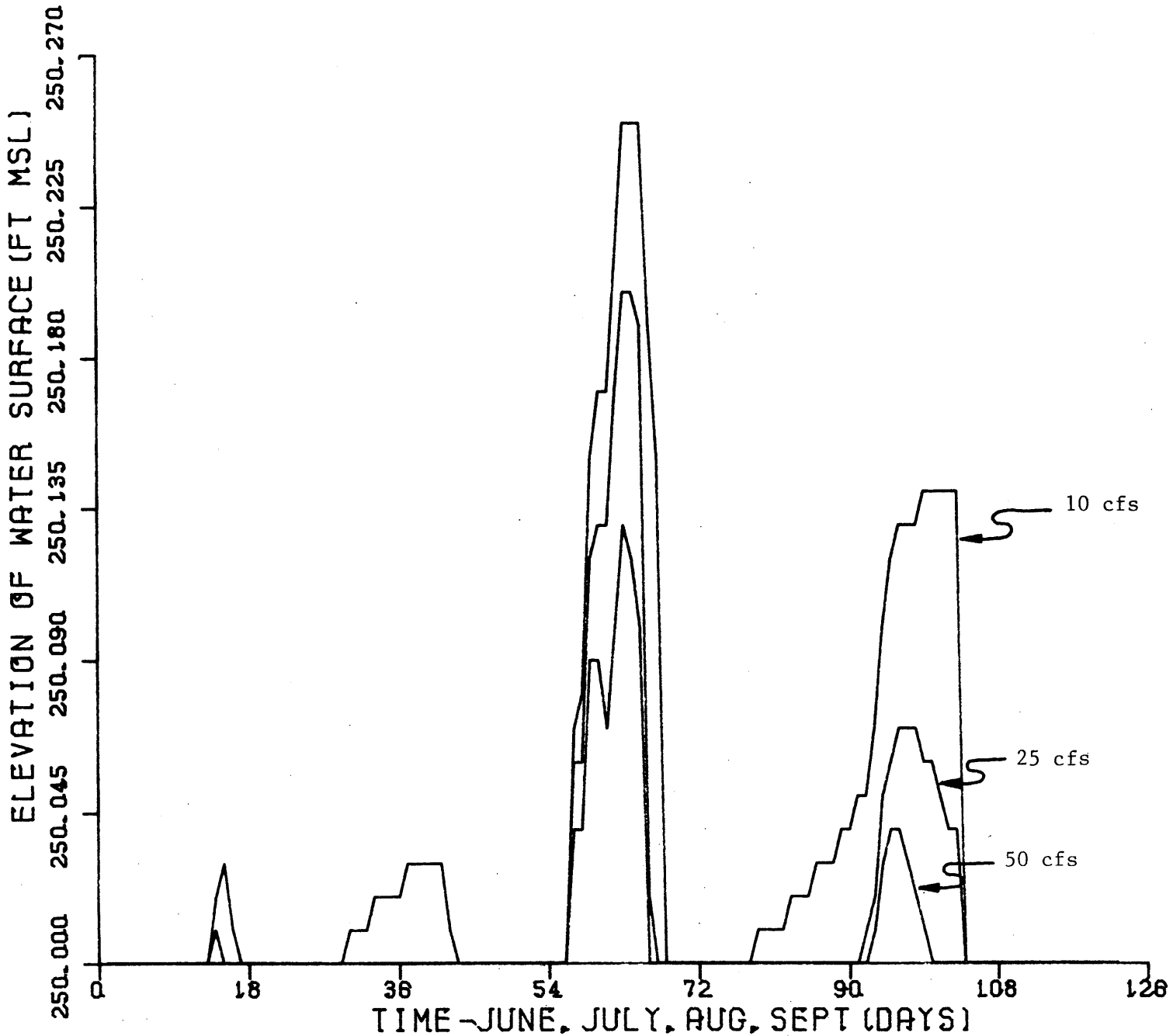

Figure 7.12 Surcharge Required for 1959 with 3 Units to Reduce Termperatures with a 10 cfs, 25 cfs, and 50 cfs Siphon.

the target T_{std} could be met. The difference between the river inflow and the sum of $Q_{sur} + Q_{siph}$ resulted in a change in elevation. This procedure was continued as the inflow subsided until the original elevation of 250 ft. MSL was reached. To show how this management scheme might work, Figure 7.13 details Q_{sur} and Q_{siph} as a function of time for the constraint Q_{max} = 25 cfs based on a target temperature of 32°C and with 3 units operational in the summer of 1959.

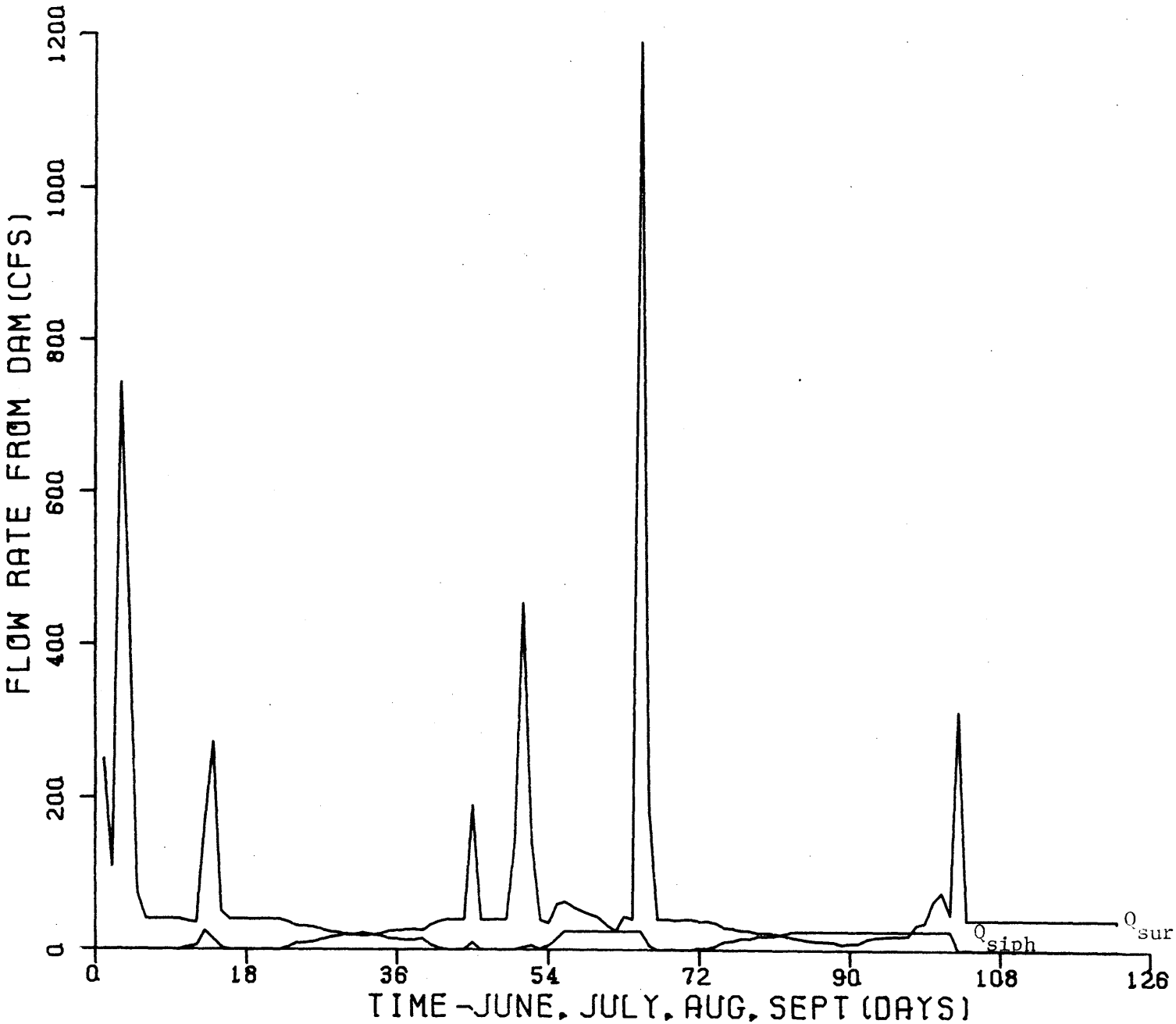

Figure 7.13: Surface and Siphon Flow Rates Utilizing a Siphon of 25 cfs for 3 unit 1959 Summer Conditions

8. SUMMARY AND CONCLUSIONS

A predictive mathematical model was developed for the North Anna Power Station operated by Virginia Electric and Power Company. This model was used to analyze the effect of waste heat from the plant's condenser system on the thermal structure of the Lake Anna system formed by a dam on the North Anna River.

The Lake Anna system is complex,consisting of a deep lake (Lake Anna) downstream from a series of lagoons, interconnecting reaches and dead-end side arms which form the Waste Heat Treatment Facility. Because of this complexity, different mathematical models were developed for each section and linked together in a segmented model. Initial calibration of the model was performed based on natural conditions in the Lake for the period 1974-1976. Long-term simulations were then performed for one, two, three, and four units using synthetic meteorological records for the years 1957-66. The synthetic meteorological data were generated by means of "regionalization," i.e. utilizing historical regional meteorological data and regressing that regional data with a shorter record of site specific data. A description of the mathematical model development, verification against natural conditions and the initial historical simulationswas contained in Jirka, (1977).

Unit 1 began commercial operations in June, 1978. Unit 2 began commercial operations in December 1980. Unit 3 is scheduled for 1989 and Unit 4 has been cancelled.

Beginning with the summer of 1978, data collection efforts were

intensified in order to calibrate and verify the model under operating conditions. The data collected included hourly and half-hourly temperature measurements at selected points, longitudinal and vertical temperature profiles at weekly or monthly intervals, continuous point measurements and approximately monthly profile measurements of side arm velocity, surveys of spatial variation in meteorological variables, and detailed plant operation records. As a result of calibration, changes were made in the model with regard to several components of surface heat exchange, side arm flow calculations, lagging and filtering of meteorological variables in the WHTF, the mixed-layer depth calculation in the main lake, and the representation of vertical diffusion below the surface layer in the main lake.

The model was verified against three years of field data (July 1978-September 1981). Graphical and statistical comparisons between prediction and observations show generally excellent agreement. Mean errors at various locations within the Lake Anna systems ranged from about $+0.87\ ^{o}F$ to about $-0.40\ ^{o}F$ while standard deviations ranged from about $2.8^{o}F$ to $1.8\ ^{o}F$. In general, a slight seasonal bias was observed with mean predicted temperatures slightly higher than measurements in the summer and slightly lower in winter. Thus with regards to the prediction of maximum (summertime) temperatures in Lake Anna and downstream in North Anna River, the model is conservative.

The ten-year set of historical simulations was re-run for one, two and three nuclear units with the calibrated model, and both expected surface temperatures at the dam and vertical profiles in the main lake were shown for a wide spectrum of meteorological conditions. During

summers of extreme meteorological conditions, temperatures sometimes exceeded the state temperature standard of 32°C. A simple plug-flow temperature model was developed to predict the persistence of elevated temperatures downstream in the North Anna River.

Several temperature mitigation strategies were explored including reduced dilution within the WHTF reaches, rerouting of flow through the major WHTF side arms, reduction in the condenser flow rate, bubble aerators in the main lake, and a hypolimnetic siphon in the main lake. The siphon alternative presented the most efficient means to lower temperatures in the North Anna River. The maximum withdrawal rate and the annual hypolimnetic volume required to meet the temperature standard were analyzed for the 10 year simulation for several combinations of siphon intake elevation and allowable lake surcharge (if any) above normal operating level of 250 ft MSL.

In summary, the mathematical model described herein has been shown to be highly accurate in describing the thermal structure of Lake Anna under conditions of one and (part-time) two unit operation providing confidence for its use with three units. The use of the model in a predictive mode to analyze the effects of the waste heat under 1, 2 and 3 units has been demonstrated during the long term historical simulations, and management decisions based on these results can now be made. The alternatives to mitigate temperatures in Lake Anna were clearly delineated, with the siphon alternative seemingly the optimum choice. Further validation of the model would benefit from additional field data collected during the summer with full two unit operation. In this regard, particular attention should be paid to possible refinements in the vertical

diffusion within the hypolimnion. Evidence to-date indicates that hypolimnetic mixing is strongly dependent on the number of units in operation and the summertime operation of a siphon is critically dependent on hypolimnetic temperature. It is also recommended that chemical and biological effects of mixing hypolimnetic and epilimnetic water be explored —both in Lake Anna and in N. Anna river downstream.

REFERENCES

Adams, E.E. and Koussis, A.D., "Transient Analysis for Shallow Cooling Ponds," Journal of the Energy Division, ASCE, Vol. 106, No. EY2 pp. 141-153, October (1980).

Bachmann, R.W. and Goldman, C.R., "Hypolimnetic Heating in Castle Lake, California," Limnology and Oceanography, Vol. 10, No. 2, pp. 233-239, April (1965).

Bedford, K.W. and Babajimopoulos, C., "Vertical Diffusivities in Areally Averaged Models," Journal of the Environmental Engineering Division, ASCE, Vol. 103, No. EE1, pp. 113-125, February (1977).

Bella, D.A., "Dissolved Oxygen Variations in Stratified Lakes," Journal of the Sanitary Engineering Division, ASCE, Vol. 96, No. SA5, pp. 1129-1146, October (1970).

Bloss, S. and Harleman, D.R.F., "Effect of Windmixing on the Thermocline Formation in Lakes and Reservoirs," R.M. Parsons Laboratory, Department of Civil Engineering, M.I.T., Technical Report No. 249, (1979).

Fischer, H.B., "The Mechanics of Dispersion in Natural Streams," Journal of the Hydraulics Division, ASCE, Vol. 93, No. HY6, pp. 187-216, November (1967).

Helfrich, K.R., "Evaluation of Models for Predicting Evaporative Water Loss in Cooling Impoundments," M.S. Thesis, Dept. of Civil Engineering, MIT, (1981)

Henderson-Sellers, B., "Role of Eddy Diffusivity in Thermocline Formation," Journal of the Environmental Engineering Division, ASCE, Vol. 102, No. EE3, pp. 517-531, June (1976).

Hicks, B.B. and Weseley, M.L., "An Examination of Some Bulk Formulae Used for Assessing the Performance of Industrial Cooling Ponds," in 1975 Annual Report of Radiological and Environmental Research Division, Argonne National Laboratory, ANL-75-60, Part IV, (1975).

Holley, E.R., Harleman, D.R.F., and Fischer, H.B., "Dispersion in Homogeneous Estuary Flow," Journal of the Hydraulics Division, ASCE, Vol. 96, No. HY8, pp. 1691-1709, August (1970).

Idso, S.B. and Jackson, R.D., "Thermal Radiation from the Atmosphere," Journal of Geophysical Research, Vol. 74, No. 23, October (1969).

Imberger, J., Patterson, J., Hebbert, B. and Loh, I., "Dynamics of Reservoir of Medium Size," Journal of the Hydraulics Division ASCE, Vol. 104, No. HY5, pp. 725-743, May (1978).

Jirka, G.H., Brocard, D.N., Hurley, K.O., Watanabe, M. and Harleman, D.R.F., "Analysis of Cooling Effectiveness and Transient Long-Term Simulations of a Cooling Lake," R.M. Parsons Laboratory, Department of Civil Engineering, MIT, Technical Report No. 232 (1977).

Jirka, G.H., Adams, E.E., and Stolzenbach, K.D., "Buoyant Surface Jets," Journal of the Hydraulics Division, ASCE, Vol. 107, No. HY11, November, (1981).

Koh, R.C.Y. and Chang, Y.C., "Mathematical Model for Barged Ocean Disposal of Wastes," EPA, No. 660/2-73-029, Washington, D.C. (1973).

Lick, W., "Numerical Models of Lake Currents," EPA, No. 600/3-76-020, Duluth, Minnesota (1976).

Linsley, R.K., Kohler, M.A., and J.L. Paulhaus, Hydrology for Engineers, McGraw-Hill, New York (1975).

Octavio, L.H., Jirka, G., and Harleman, D.R.F., "Vertical Heat Transport Mechanisms in Lakes and Reservoirs," R.M. Parsons Laboratory, Department of Civil Engineering, M.I.T. Technical Report No. 227 (1977).

Okubo, A., "Horizontal and Vertical Mixing in the Sea" in Impingement of Man on the Oceans edited by D.W. Hood, John Wiley and Sons, New York (1971).

Pareek, N.K., Discussion of "Role of Eddy Diffusivity in Thermocline Formation," Journal of the Environmental Engineering Division, ASCE, Vol. 103, No. EE4, pp. 749-750, August (1977).

Powell, T. and Jassby, A., "The Estimation of Vertical Eddy Diffusivities below the Thermocline in Lakes," Water Resources Research, Vol. 10, No. 2, pp. 191-198, April (1974).

R.M. Parsons Laboratory, "Analysis of Possible Design Modification in the Waste Heat Treatment Facility for the North Anna Power Station," Department of Civil Engineering, M.I.T., June (1977a).

R.M. Parsons Laboratory, "Supplementary Data Report to 'Analysis of Cooling Effectiveness and Transient Long-Term Simulations of a Cooling Lake with Application to the N. Anna Power Station'," Department of Civil Engineering, M.I.T., November (1977b).

Ryan, P.J. and Harleman, D.R.F., "Prediction of the Annual Cycle of Temperature Changes in a Stratified Lake or Reservoir: Mathematical Model and User's Manual," R.M. Parsons Laboratory, Department of Civil Engineering, M.I.T., Technical Report No. 137 (1971).

Ryan, P.J. and Harleman, D.R.F., "An Analytical and Experimental Study of Transient Cooling Pond Behavior," R.M. Parsons Laboratory, Department of Civil Engineering, M.I.T., Technical Report No. 161 (1973).

Ryan, P.J., Harleman, D.R.F. and Stolzenbach, K.D., "Surface Heat Loss from Cooling Ponds," Water Resources Research, Vol. 10, No. 5, pp. 930-938, October (1974).

Stefan, H. and Ford, D., "Temperature Dynamics in Dimictic Lakes," Journal of the Hydraulics Division, ASCE, Vol. 101, No. HY1, pp. 97-114, January (1975).

Stolzenbach, K. and Harleman, D.R.F., "An Analytical and Experimental Investigation of Surface Discharges of Heated Water," R.M. Parsons Laboratory, Department of Civil Engineering, M.I.T., Technical Report No. 135 (1971).

Sundaram, T.R. and Rehm, R.G., "The Seasonal Thermal Structure of Deep Temperate Lakes," Tellus, Vol. 25, No. 2 (1973).

Sundaram, T.R. and Rehm, R.G., "Formation and Maintenance of Thermoclines in Temperate Lakes," American Institute of Aeronautics and Astronautics Journal, Vol. 9, No. 7 (1971).

Swinbank, W.C., "Longwave Radiation from Clear Skies," Quarterly Journal of the Royal Meteorological Society of London, Vol. 89, July, (1963).

Thackston, E.L., "Effect of Geographical Variation on Recirculating Cooling Ponds," EPA, No. 660/2-74-085 (1974).

Watanabe, M., Harleman, D.R.F., and Connor, J.J., "Finite Element Model for Transient Two-Layer Cooling Pond Behavior," R.M. Parsons Laboratory, Department of Civil Engineering, MIT, Technical Report No. 202 (1975).

Wells, S.A., "A Three-Dimensional Field Evaluation and Analysis of Water Quality in Two Reservoirs," M.S. Thesis, Tennessee Technological University, Cookeville, Tennessee (1980).

White, Jud, Personal Communication, 1977.

APPENDIX A

SURFACE HEAT FLUX CALCULATIONS

SURFACE HEAT FLUX CALCULATIONS

The equation given by Ryan, Harleman, and Stolzenbach (1974) was utilized in the surface heat flux analysis in the model:

$$\phi_n = \phi_r - \{4 \times 10^{-8}(T_s+460)^4 + f(W)[(e_s-e_a) + 0.255(T_s-T_a)]\} \quad (A.1)$$

where

ϕ_n = net heat influx (Btu/ft^2/day),

$\phi_r = \phi_{sn} + 1.16 \times 10^{-13}(460+T_a)^6(1 + 0.17C^2)$,

$f(W) = 22.4(\Delta\theta_v)^{1/3} + 14\ W_2$,

e_s = saturated vapor pressure in mm of Hg of air at the average water surface temperature, T_s(°F),

e_a = actual vapor pressure in mm of Hg of the ambient air temperature, T_a(°F),

C = cloud cover (0 to 1),

W_2 = wind velocity (mph) measured at height of 2m above water surface,

ϕ_{sn} = net incident solar radiation (Btu/ft^2/day),

$\Delta\theta_v = T_{sv} - T_{av}$,

$T_{sv} = (T_s + 460)/(1-0.378\ \frac{e_s}{p}) - 460$,

$T_{av} = (T_a + 460)/(1-0.378\ \frac{e_a}{p}) - 460$,

p = atmospheric pressure in mm of Hg.

The net heat flux, ϕ_n, can be linearized with respect to an equilibrium temperature, T_E, defined as the water surface temperature for which, given a set of meteorological conditions, the net surface

heat flux is zero. This can be written as

$$\phi_n = -K(T_s - T_E) \tag{A.2}$$

where K = surface heat exchange coefficient.

The prefered method of determining T_E is an iterative solution based on its definition (i.e., $\phi_n = 0$):

$$4 \times 10^{-8}(T_E+460)^4 + F(W)[(e_E - e_a) + .255(T_E - T_a)] = \phi_r \tag{A.3}$$

The value of K is found explicitly from Equation A.2.

LIST OF FIGURES

LIST OF TABLES